Caractérisation physico-chimique et optique de miroirs multicouches pour le domaine EUV

Minhui Hu

▶ To cite this version:

Minhui Hu. Caractérisation physico-chimique et optique de miroirs multicouches pour le domaine EUV. Chimie-Physique [physics.chem-ph]. Université Pierre et Marie Curie - Paris VI, 2011. Français. NNT : . tel-00641198

HAL Id: tel-00641198
https://theses.hal.science/tel-00641198

Submitted on 15 Nov 2011

HAL is a multi-disciplinary open access archive for the deposit and dissemination of scientific research documents, whether they are published or not. The documents may come from teaching and research institutions in France or abroad, or from public or private research centers.

L'archive ouverte pluridisciplinaire **HAL**, est destinée au dépôt et à la diffusion de documents scientifiques de niveau recherche, publiés ou non, émanant des établissements d'enseignement et de recherche français ou étrangers, des laboratoires publics ou privés.

Caractérisation physico-chimique et optique de miroirs multicouches pour le domaine EUV

Thèse de l'Université Pierre et Marie Curie

présentée par Minhui HU

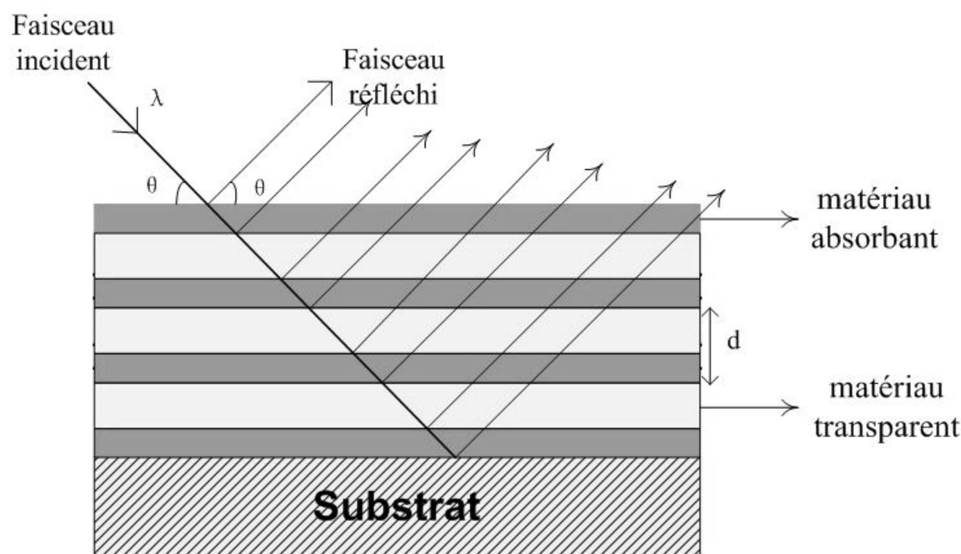

Octobre 2011

THÈSE

Présentée pour obtenir le grade de

DOCTEUR DE L' UNIVERSITE PARIS VI – PIERRE ET MARIE CURIE

par

Minhui HU

Sujet de la thèse :

Caractérisation physico-chimique et optique de miroirs multicouches pour le domaine EUV

École doctorale :
CHIMIE PHYSIQUE CHIMIE ANALYTIQUE

Soutenue le 12 octobre 2011 devant le jury composé de :

Mme. Lydia TCHANG-BRILLET	**Présidente**
M. Omar JBARA	**Rapporteur**
M. Chouki ZERROUKI	**Rapporteur**
Mme. Anny MICHEL	**Examinateur**
M. Philippe JONNARD	**Directeur de thèse**

Remerciements

Ce travail a été réalisé d'Octobre 2008 à Septembre 2011. Il a été effectué au Laboratoire de Chimie Physique-Matière et Rayonnement (LCPMR) à Paris.

Je tiens tout d'abord à remercier Alain Dubois, directeur du laboratoire LCPMR, pour avoir accepté de m'accueillir au sein de son laboratoire.

Mes plus vifs remerciements s'adressent à mon directeur de thèse, Philippe Jonnard, sans qui cette thèse ne serait pas ce qu'elle est. Je le remercie pour m'avoir montré ce qu'était le monde de la recherche, pour sa patience et son encouragement, pour m'avoir appris à être plus autonome tout au long de ce travail de recherche; pour ses précieux conseils, sa disponibilité et sa confiance quant à ce travail; pour son enseignement et sa gentillesse que j'ai pu apprécier pendant ces trois années. Ce fut un réel plaisir pour moi d'avoir travaillé avec lui. Je lui adresse ici le témoignage de mon plus profond respect et de ma plus vive reconnaissance.

Je tiens tout particulièrement à remercier, Jean-Michel André, pour avoir su me guider avec attention et gentillesse pendant ces trois années. Ses qualités scientifiques et humaines ont largement contribué à l'aboutissement de cette thèse. Qu'il trouve ici l'expression de ma profonde gratitude.

J'adresse mes sincères remerciements à Karine Le Guen, pour ses qualités humaines, son efficacité, ses connaissances et l'aide qu'elle m'a apportée dans la réalisation de cette thèse. Elle a toujours été là quand j'avais des difficultés qu'elles fussent théoriques ou expérimentales. J'exprime ma plus profonde sympathie et lui souhaitons beaucoup de bien.

Je remercie les rapporteurs de cette thèse Chouki Zerrouki et Omar Jbara pour la rapidité avec laquelle ils ont lu mon manuscrit et l'intérêt et l'attention qu'ils ont portés à mon travail. Merci également aux autres membres du jury qui ont accepté de juger ce travail: Lydia Tchang-Brillet et Anny Michel qui a également participé très activement au début de ce travail. Je leur exprime toute ma gratitude pour leur travail et pour toutes les remarques constructives qu'ils ont apportées à mon manuscrit.

Je tiens également à remercier toutes les personnes avec qui j'ai eu des collaborations fructueuses, sans qui je n'aurais pu présenter autant de résultats.

Je voudrais exprimer ma gratitude à Zhanshan Wang, de l'IOPE (Institute of Precision Optical Engineering, Université Tongji, Shanghai, Chine), qui a collaboré pour une grande part à ce travail sur l'étude des multicouches Mg/Co. Qu'il trouve ici l'expression de ma

profonde reconnaissance et de mon plaisir d'avoir travaillé avec lui. Je remercie également Jingtao Zhu d'avoir pris part à ce travail.

Merci également à l'équipe Composants X-UV du laboratoire Charles Fabry de l'Institut d'Optique de Palaiseau. Un grand merci en particulier à Frank Delmotte, Evgueni Meltchakov, Christophe Hecquet, pour le collaboratoire sur les multicouches Al/SiC, point essentiel de ce manuscrit.

Je remercie également Christian Mény, de l'Institut de Physique et Chimie des Matériaux de Strasbourg, pour la gentillesse qu'il a eue de m'avoir initié de la RMN, pour ses encouragements constants et pour les discussions enrichissantes que nous avons eues.

A Anouk Galtayries du Laboratoire de Physico-Chimie des Surfaces de l'ENSCP, merci pour la mise à disposition de ToF-SIMS, XPS et le temps qu'elle m'ont accordé durant ces mesures.

Je tiens à exprimer le plaisir que j'ai eu de travailler avec Angelo Giglia, Nicola Mahne et Stefano Nannarone de l'équipe de la ligne BEAR du synchrotron Elettra à Trieste, pour leur disponibilité et leur assistance technique.

Merci éисточ à Imène Machouk, de l'Institut de Minéralogie et de Physique des Milieux Condensés, pour m'avoir fourni les nombreux échantillons préparés par FIB.

Ma gratitude va également à Michaël Walls, du Laboratoire de Physique des Solides d'Orsay, qui n'a pas ménagé son temps pour effectuer les expériences de STEM-EELS.

Je souhaite remercier Patrick Ochin du Centre d'Etudes de Chimie Métallurgique, pour son aide sur la préparation des échantillons.

Je ne remercierai jamais assez tout le personnel du Laboratoire de Chimie Physique Matière et Rayonnement avec qui j'ai eu un grand plaisir de travailler dans une ambiance chaleureuse et conviviale.

Ma reconnaissance s'adresse également aux nouveaux docteurs et actuels doctorants : Hélène, Nicolas, Grégory,Cécilia, Jérôme, Wei, Cédric...... A toutes celles et ceux qui m'ont accordé leur confiance. Les moments passés ensembles resteront inoubliables.

Je souhaite remercier particulièrement Daniel Bertrand, professeur de l'Institut de Mathématiques à l'Université Pierre et Marie Curie. Merci pour tes excellents conseils et pour avoir su m'orienter lorsque j'en avais besoin. Merci églement à Erwan Brugallé.

Enfin, je souhaite exprimer toute ma reconnaissance à ma famille, plus particulièrement à mes parents et aussi a Sheng, pour leur soutien constant et leur patience. Merci à tous mes amis qui m'ont soutenus et fait partager de grands moments personnels.

Merci a tous pour votre soutien et votre compréhension sans limite.

Table des matières

Introduction **5**

Chapitre 1 : Les performances des miroirs multicouches pour le domaine EUV

1.1 Le rayonnement EUV ***7***

1.2 Les performances des miroirs multicouches ***11***

1.2.1 Principe 11

1.2.2 Méthodes de dépôts des multicouches 14

1.2.3 Optimisation de la réflectivité 15

1.2.4 Les performances des miroirs multicouches 17

Chapitre 2 : Méthodes expérimentales

2.1 La spectroscopie d'émission X (XES) ***19***

2.1.1 Principe 20

2.1.2 L'appareillage IRIS 22

2.2 La réflectométrie dans le domaine des rayons X durs (XRR) ***25***

2.2.1 Principe 25

2.2.2. Ajustement des courbes des réflectivités 26

2.3 La réflectométrie EUV sur BEAR ***28***

2.3.1 Description de la ligne BEAR 28

2.3.2 Mesure de la réflectivité 30

2.4 La spectroscopie de résonance magnétique nucléaire (spectroscopie RMN) ***31***

2.4.1 Principe 31

2.4.2 Description de l'appareillage utilisé 32

2.5 La spectrrométrie de masse d'ions secondaires par temps de vol (ToF-SIMS) ***33***

2.5.1 Principe 33

2.5.2 Description de l'appareillage utilisé 34

2.6 La spectroscopie de photoélectrons X (XPS) ***36***

2.6.1 Principe de la photoémission 36

2.6.2 Description de l'appareillage utilisé 37

2.7 La faisceau d'ions focalisés (FIB) ***39***

2.7.1 Principe 39

2.7.2 Préparation d'échantillons pour MET par le FIB 40

2.7.3 Description de l'appareillage utilisé 42

2.8 La microscopie électronique à balayage en transmission (STEM) et la spectroscopie de perte d'énergie des électrons (EELS) ***44***

2.8.1 Principe de la STEM 44

2.8.2 Principe de la EELS 44

2.8.3 Description de l'appareillage utilisé 45

Chapitre 3 : Etude des multicouches Mg/Co, Mg/B_4C/Co et Mg/Co/Zr

3.1 Introduction ***47***

3.2 Principales publications ***51***

3-[1] Co/Mg/X multilayer mirrors for the EUV range 53

3-[2] Development and interfacial characterization of Co/Mg periodic multilayers for the EUV range 56

3-[3] Comparison of Mg-based multilayers for solar He-II radiation at 30.4 nm Wavelength 63

3-[4] Investigation on the thermal stability of Mg/Co periodic multilayers for EUV applications 67

3-[5] Introduction of Zr in nanometric periodic Mg/Co multilayers 82

3-[6] Observation of an asymmetrical effect when introducing Zr in Mg/Co multilayers 91

Chapitre 4 : Etude des multicouches Al/SiC, Al/W/SiC et Al/Mo/SiC

4.1 Introduction ***95***

4.2 Principales publications ***98***

4-[1] Optical, chemical and depth characterization of Al/SiC periodic multilayers 99

4-[2] Structural properties of Al/Mo/SiC multilayers with high reflectivity for extreme ultraviolet light 108

Conclusion et perspectives **119**

Références **123**

Annexes : Autres publications **127**

A-[1] Thermal properties, optical and interface characterization of Mg/Co multilayers for the EUV range 129

A-[2] Introduction of Zr in Mg/Co nanometric periodic multilayers 133

A-[3] Optical, chemical, depth and magnetic characterization of Mg/Co-based nanometric periodic multilayers 138

A-[4] Thermal stability of Mg/Co multilayer with B_4C, Mo or Zr diffusion barrier layers 145

A-[5] Nanometer designed Al/SiC periodic multilayers: characterization by a multi-technique approach 151

A-[6] Characterization of EUV periodic multilayers 156

Introduction

Dans ce travail de thèse, nous allons présenter les spécificités du domaine du rayonnement extrême ultraviolet (EUV), compris entre le rayonnement X et le rayonnement ultraviolet. Le rayonnement EUV offre de grandes possibilités scientifiques et technologiques. Il trouve de nombreuses applications en photolithographie, en astrophysique, en spectrométrie de photoélectron, etc. En effet, de nombreux miroirs multicouches sont développés pour fonctionner dans ce domaine spectral, qui joue un rôle important pour les applications optiques.

Dans ce contexte, l'objectif de ce travail était de concevoir, réaliser, caractériser et proposer des multicouches. Puis le but est d'appliquer une méthode capable de distinguer entre interdiffusion et rugosité géométrique afin de corréler les performances optiques de la multicouche à leur qualité structurale. Nous proposons de caractériser les miroirs multicouches périodiques dans les domaines EUV, en employant une méthodologie combinant plusieurs techniques. La combinaison de ces méthodes permet d'obtenir une description chimique et structurale de l'empilement multicouche et de comprendre les phénomènes prenant place aux interfaces. Il est en effet important de connaître les phénomènes interfaciaux, comme la formation de composés ou le développement de la rugosité, car ils gouvernent les propriétés optiques des multicouches. Afin de comprendre comment se développe la rugosité et se forment les composés interfaciaux aux interfaces des multicouches nous avons également entrepris des études en fonction du recuit.

Ce manuscrit de thèse est construit de la façon suivante. Dans le chapitre 1, nous présenterons brièvement la physique du rayonnement EUV, les performances des miroirs multicouches et les applications du domaine EUV. Dans un second temps, nous intéresserons à la caractérisation des multicouches et des méthodes de dépôts. Puis, nous ferons un rappel sur le calcul théorique de la réflectivité du rayonnement EUV par les multicouches. Nous présenterons, dans le chapitre 2, les méthodes expérimentales utilisés pour concevoir, réaliser et caractériser les multicouches dans ce travail. Le chapitre 3 sera consacré à la description des travaux effectués et des principaux résultats obtenus des multicouches Mg/Co, Mg/B_4C/Co et Mg/Co/Zr, particuliérement intéressants à la longueur d'onde autour de 25 nm. Ce nouveau type de structure périodique a été conçu, réalisé et évalué. Le chapitre 4 présente

des résultats obtenus sur les multicouches Al/SiC, Al/W/SiC et Al/Mo/SiC entre 15 et 35 nm. Enfin, nous conclurons et donnerons les perspectives de ce travail.

Chapitre 1 :

Les performances des miroirs multicouches pour le domaine EUV

1.1 Le rayonnement EUV

Le rayonnement électromagnétique est classé par longueur d'onde (ou énergie) en ondes radio, micro-ondes, infrarouge, visible, ultraviolet, rayons X et rayons gamma, Figure 1.

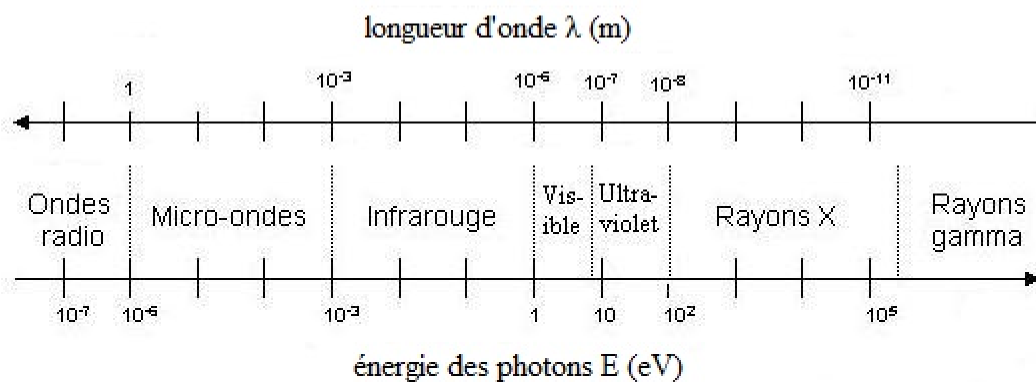

Figure 1. Le spectre électromagnétique.

Le rayonnement ultraviolet (UV) est un rayonnement électromagnétique d'une longueur d'onde entre le visible et les rayons X. La gamme spectrale EUV (Extreme ultraviolet, 121 nm – 10 nm) est une sous division de l'X-UV. Dans notre travail, nous allons présenter les spécificités du domaine du rayonnement EUV. L'EUV est naturellement produite par la couronne solaire et artificiellement par certains émissions caractéristiques, les sources de plasma et synchrotron. Dans l'EUV, les systèmes optiques doivent être utilisés sous vide car l'air absorbe fortement le rayonnement.

Le rayonnement EUV offre de grandes possibilités scientifiques et technologiques. Il trouve de nombreuses applications en astrophysique, en photolithographie, en spectrométrie de photoélectron, etc.

L'imagerie solaire dans le domaine EUV pour des études astrophysiques est une application des miroirs multicouches. Le développement de l'imagerie solaire a connu un grand succès au travers de plusieurs missions, par exemple: SOHO (Solar and Heliospheric, en 1995), STEREO (Solar Terrestrial Relations Observatory, en 2006) et SDO (Solar

Dynamics Observatory, en 2010). Ces missions ont contribué et contribuent à une meilleure compréhension des relations Soleil-Terre en étudiant les mécanismes de dissipation d'énergie dans les couches externes du Soleil, les processus de chauffage de la couronne, d'accélération du vent solaire et le transfert de l'énergie vers l'espace. Sur le satellite SOHO, l'EIT (Extreme ultraviolet Imaging Telescope) à été le premier instrument utilisant des multicouches en incidence normale pour obtenir les images haute résolution de la couronne solaire. L'instrument EIT est sensible à quatre longueurs d'onde différentes: 17,1, 19,5, 28,4 et 30,4 nm, correspondant à la lumière produite par les ions Fe XI/X, Fe XII, Fe XV et He II, respectivement. Le satellite SDO est le plus récent observatoire solaire dont le lancement a eu lieu le 11 février 2010. SDO est un satellite d'observation solaire avec au cœur de ses objectifs scientifiques la variabilité de l'activité solaire et ses conséquences sur l'environnement spatial. Ainsi, la mission SDO consiste à développer notre connaissance du Soleil, en particulier ses caractéristiques qui affectent la Terre et l'espace proche de celle-ci et les changements de son activité. Il doit permettre de comprendre comment et pourquoi le champ magnétique du Soleil change. Les détails de la dynamique de la surface et de l'atmosphère solaire à très petite échelle temporelle (10 secondes) et dans une large gamme de températures seront désormais accessibles 24 h sur 24 par le spectro-imageur AIA (Atmospheric Imaging Assembly). La Figure 2 représente les images du soleil à la longueur d'onde de 30,4 nm (l'émission He II) dans le cadre de la mission SoHO/EIT et SDO/AIA. AIA permettra ainsi d'obtenir des images avec un champ similaire à EIT, mais avec une cadence bien plus élevée.

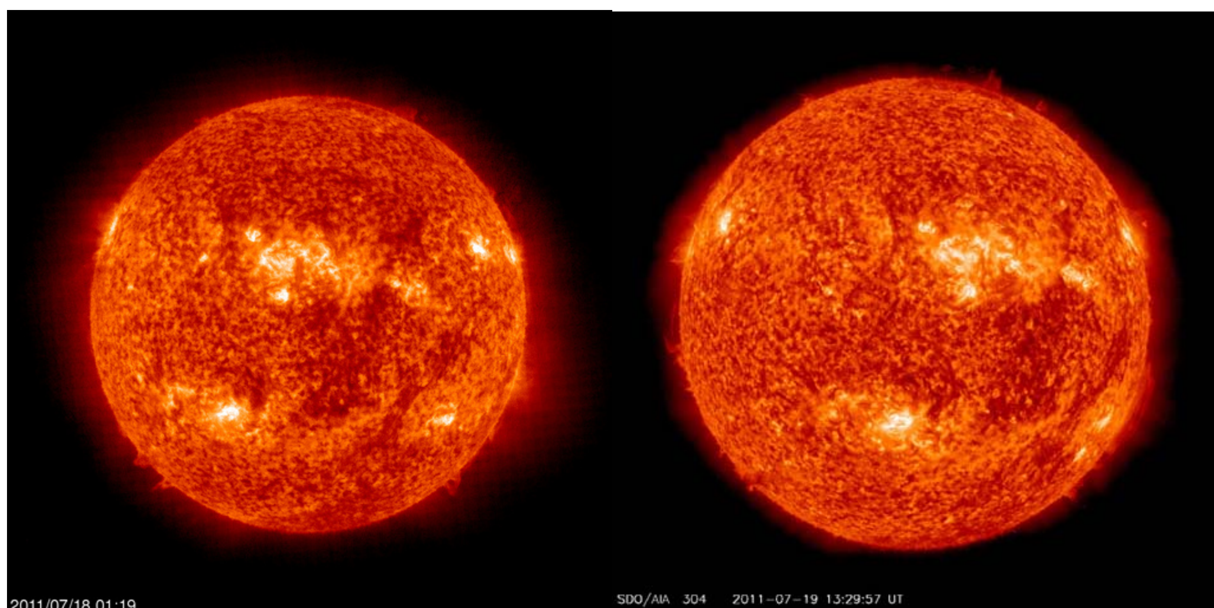

Figure 2. Images du soleil obtenue de la mission SOHO/EIT (gauche) et SDO/AIA (droite).

Chapitre 1 : Les performances des miroirs multicouches pour le domaine EUV

La photolithographie est une technique permettant de projeter à l'aide d'une source lumineuse, une image au travers d'un certain nombre d'objectifs sur un support photosensible afin de l'y imprimer. La photolithographie EUV est un procédé qui utilise un rayonnement EUV d'une longueur d'onde de 13,5 nm. Elle diffère des autres procédés classiques de photolithographie car elle utilise une série de miroirs de précision rétrécissant situés sur le chemin optique après un masque en réflexion, sur lequel est dessiné le motif du circuit à graver. Elle permet la fabrication des composants électroniques à partir de semi-conducteurs, de développer des techniques pour augmenter la capacité des puces tout en réduisant les coûts de production. Cette technologie est très prometteuse mais elle est aussi très jeune, il reste encore beaucoup de chemin avant de pouvoir intégrer la lithographie EUV dans les chaînes de production industrielles de processeurs. La Figure 3 présente un schéma de système de la lithographie EUV. Les multicouches Mo/Si permettent l'obtention des meilleures réflectivités en incidence normale pour les longueurs d'onde autour de 13,5 nm.

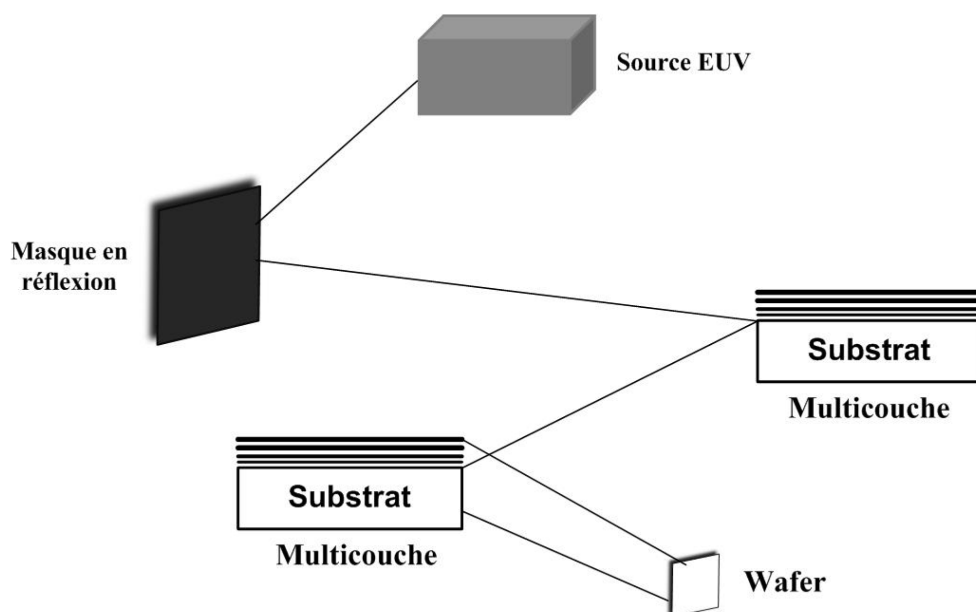

Figure 3. Système de la lithographie EUV.

Une autre application dans le domaine EUV est la spectrométrie de photoélectron excité par UV (UPS). La UPS implique la mesure des spectres de photoélectrons induits par des photons UV. Elle est utilisée pour étudier les niveaux d'énergie de la couche de valence et les liaisons chimiques, surtout le caractère liant des orbitales moléculaires. Vers 1956 Kai Siegbahn développe la spectrométrie photoélectronique X (XPS) pour l'analyse chimique des surfaces solides. La méthode UPS a été développée originellement pour des molécules en phase gazeuse en 1962 par David W. Turner. La UPS est utilisée pour l'étude des gaz et des

surfaces de solides. La méthode est sensible à la région superficielle. Comme source de photons, une lampe à décharge He II peut être utilisée. La spectrométrie de photoélectron excité par EUV est située entre l'XPS et l'UPS. Comme l'UPS, elle est généralement utilisée pour évaluer la structure de bande de valence. Comparée à l'XPS elle donne une meilleure résolution en énergie et par rapport à l'UPS des électrons éjectés sont plus rapides, résultant en un meilleur signal.

1.2 Les performances des miroirs multicouches

1.2.1 Principe

Une multicouche est formée par une alternance de couches minces de matériaux, respectivement absorbant et transparent au rayonnement incident, déposées sur un substrat plan (en silicium, silice, ...). Le matériau absorbant est généralement un élément métallique lourd, le matériau transparent est un matériau léger.

Dans les années 1980, les multicouches ont été fabriquées pour obtenir une périodicité nanométrique dans une dimension de manière à produire des miroirs pour l'optique X. Depuis les années 1990, la recherche sur les multicouches est devenue plus pratique. Elles sont désormais largement utilisées dans la gamme de la lithographie EUV, l'observation astronomique, les télescopes et microscopes à rayons X, etc. Dans certains autres domaines d'application, par exemple, Albert Fert a eu en 2007 le prix Nobel de physique pour avoir en 1988 réalisé des multicouches avec des matériaux ferromagnétiques Fe/Cr qui ont la propriété d'avoir une magnétorésistance géante.

Les ondes réfléchies par un miroir multicouche sont décrites par l'interférence constructive des réflexions sur toutes les interfaces. Une multicouche a un maximum de réflectivité quand les réflexions aux interfaces sont en phase pour chaque alternance de couche et donc interfèrent constructivement. Cela conduit à satisfaire la loi de Bragg :

$$2d \sin\theta = m\lambda$$

où d est la période de la multicouche, θ est l’angle de Bragg, m est l’ordre de diffraction (nombre entier) et λ est longueur d’onde du rayonnement. Pour un angle de Bragg fixé, on fabrique une multicouche avec une période d de manière à sélectionner la longueur d’onde souhaitée. Ainsi, pour un angle de Bragg donné, la longueur d’onde sélectionnée dépend directement de la période des couches et inversement. La figure 4 représente une coupe schématique d’une multicouche.

1.2 Les performances des miroirs multicouches

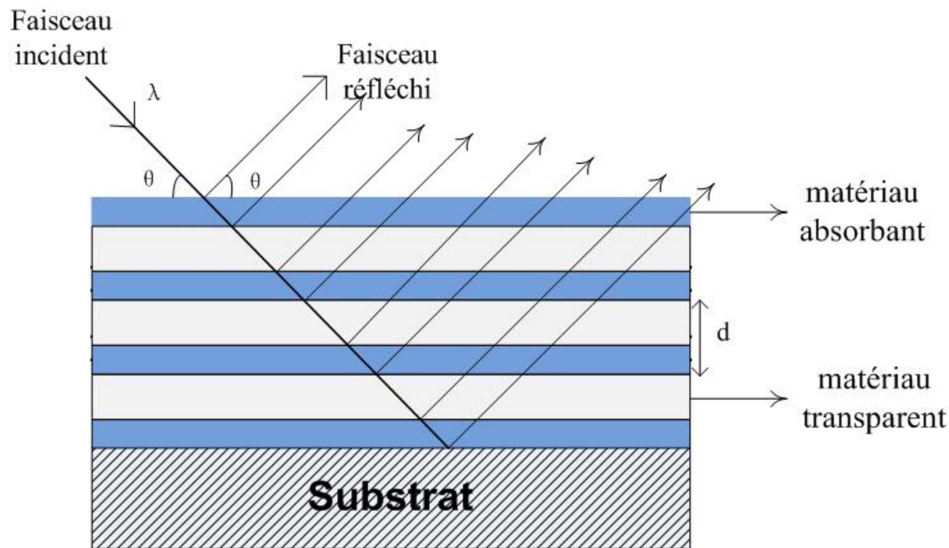

Figure 4. Coupe schématique d'une multicouche.

Si on tient compte des effets de réfraction aux interfaces, la loi de Bragg devient :

$$2d\sin\theta\sqrt{1-\frac{2\overline{\delta}}{\sin^2\theta}} = m\lambda$$

où $\overline{\delta}$ est le décrément à l'unité de l'indice optique moyenné sur une période :

$$\overline{\delta} = \Gamma\delta_{lourd} + (1-\Gamma)\,\delta_{léger}$$

où Γ est le rapport des épaisseurs de la couche contenant l'élément lourd sur la période du miroir multicouche :

$$\Gamma = \frac{d_{lourd}}{d_{lourd} + d_{leger}}$$

La réflectivité du miroir peut être optimisée en choisissant les épaisseurs et la nature des deux matériaux dans une période. Spiller [3] a proposé un critère de sélection des matériaux pour l'EUV. Il recommande de choisir d'abord le matériau transparent puis de choisir un deuxième matériau de manière à maximiser le coefficient de réflexion à l'interface entre les matériaux.

Pour le système Mg/Co, notre stratégie pour le choix des matériaux est d'abord de fixer le premier élément (une couche que nous avons déjà bien étudiée ou choisie pour l'analyse spéciale), puis d'essayer de simuler toutes les paires possibles de cet élément et un autre en utilisant le logiciel IMD [4] et retenir les meilleures. Nous étudions des structures en ajoutant un troisième ou quatrième matériau dans la période. Comme nous venons de le voir

pour les applications destinées à l'EUV à 15-35 nm, le choix s'est porté sur des multicouches Mg/Co, $Mg/B_4C/Co$, Mg/Zr/Co.

Le logiciel IMD a permis la conception et l'optimisation des travaux présentés. C'est un programme informatique pour la modélisation des fonctions optiques (réflexion, transmission, absorption, etc.) des multicouches et films minces. Aussi, il peut être utilisé pour ajuster les données expérimentales des mesures de la réflectométrie des rayons X (XRR) des multicouches, afin de déterminer l'épaisseur de film, les densités, les rugosités et les constantes optiques que nous présenterons en 2.1.

Les calculs des fonctions optiques d'une multicouche par l'IMD sont basés sur les équations de Fresnel (voir 1.2.3), modifiées pour tenir compte des imperfections de l'interface, qui décrivent la réflexion et la transmission d'une onde incidente à une interface entre deux matériaux différents. IMD inclut une base de données des constantes optiques pour plus de 150 matériaux. Les fonctions optiques peuvent être calculées non seulement par en fonction des longueurs d'onde ou des énergies, mais aussi en fonction des paramètres de chaque matériau (les épaisseurs, les rugosités, les densités, etc.) ou du faisceau incident (polarisation, l'angle d'incidence, etc.). Avec IMD, il est possible d'utiliser simultanément jusqu'à huit variables indépendantes lors du calcul des fonctions optiques.

Pour modéliser un système multicouche, au début, il est nécessaire de décrire une multicouche composée d'une structure périodique, elle-même composée de deux ou plusieurs couches de matériau. Puis nous donnons les informations de la simulation: l'environnement, le substrat, la longueur d'onde, la résolution spectrale, la polarisation et l'angle du rayonnement incident, etc. Enfin, nous donnons les paramètres d'optimisation du matériau: la rugosité, la densité, l'épaisseur et l'indice de réfraction, etc. Avec toutes ces informations, IMD permet le calcul des coefficients de réflexion ou de transmission d'ondes électromagnétiques rencontrant la multicouche.

Les multicouches Mg/Co sont les nouveaux matériaux pour l'optique X autour de 25 nm. Les multicouches Al/SiC, Al/Mo/SiC et Al/W/SiC sont conçues pour les optiques de sources «attoseconde».

1.2.2 Méthodes de dépôts des multicouches

Les systèmes de dépôt utilisés lors de ces études sont basés sur la pulvérisation cathodique magnétron à l'Institut d'Optique [5] et l'Université Tongji [6]. La pulvérisation cathodique est une technique consistant à recouvrir la surface d'un substrat par des atomes provenant du bombardement d'une cible (cathode), constituée du matériau à déposer, par des ions énergétiques (en général Ar^+) issus d'un plasma.

On applique un champ magnétique autour de la cible, qui modifie la trajectoire des électrons. Les électrons suivent des trajectoires hélicoïdales autour des lignes de champ magnétique subissant plus de collisions ionisantes avec les éléments neutres gazeux près de la surface de cible. On peut alors utiliser un plasma avec une pression moins élevée. Ainsi les atomes du substrat ont moins de possibilité d'être déviés par une particule se trouvant entre le substrat et la cible. On distingue deux différents types de pulvérisation : courant continu DC et radio fréquence RF.

La technique DC est utilisée pour les dépôts de couches minces conductrices. Dans ce procédé, une tension négative est appliquée entre la cible et le substrat. La cible est fixée sur l'électrode portée à une tension négative. Le substrat sur lequel on désire réaliser le dépôt est relié à la masse. Une partie des collisions électron-atome sont inélastiques et se traduisent par un transfert partiel de l'énergie à l'atome. Au cours du dépôt, la cible est chargée positivement sous l'impact des ions positifs, si cette cible est isolante, la charge positive qui y apparaît ne peut s'écouler. Par conséquent, le plasma s'éteint et le dépôt ne peut plus se produire, ce qui explique la restriction de l'utilisation de la pulvérisation DC aux dépôts des conducteurs.

La technique RF est utilisée pour les dépôts de conducteurs ainsi que ceux de couches minces isolantes et semiconductrices. En effet le problème rencontré dans le cas d'une cible isolante en pulvérisation DC peut être évité, puisque la tension appliquée aux bornes des électrodes est alternative. Le plasma contenant autant d'ions que d'électrons, la polarisation alternative de la cible fait que pendant l'alternance négative, la cathode attire les ions qui la pulvérisent, en la chargeant positivement. Pendant l'alternance positive, elle attire les électrons qui la déchargent.

Dans notre travail, les multicouches Al/SiC et Al/Mo/SiC ont été préparées à l'Institut d'Optique. Le mode DC a été utilisé pour le dépôt de Mo et le mode RF a été utilisé pour SiC et Al. Tous les échantillons sont déposés sur silicium. Le gaz de pulvérisation est l'argon utilisé sous une pression de 0,27 Pa. Les cibles de pulvérisation (99,95% de pureté ou mieux) sont Mo, SiC et Al (avec 1,5 % de Si). Les multicouches Mg/Co avec ou sans les couches Zr, Mo et B_4C ont été préparés en utilisant le système de pulvérisation cathodique magnétron (JGP560C6, SKY Inc, Chine) avec des cibles de Co (pureté 99,95 %) et Mg (pureté 99,98 %). Le gaz de pulvérisation est l'argon (99,999%). La pression de base a été 10^{-4} Pa et la pression de travail a été de 0,13 Pa. La puissance appliquée sur les cibles de Co et Mg a été fixée à 25 et 15 W. Toutes les multicouches ont été déposées sur des substrats silicium de 30 mm × 30 mm ayant une rugosité de 0,3 nm.

Pour déposer les multicouches, il existe cependant d'autres méthodes comme l'évaporation, la pulvérisation par faisceau d'ions, l'ablation laser, etc. L'évaporation a été la première méthode employée pour déposer des multicouches. La pulvérisation par faisceau d'ions est utilisée pour fabriquer les multicouches destinées à la lithographie EUV. Par rapport à la pulvérisation cathodique magnétron, cette technique permet de réduire les défauts dans le dépôt du fait d'une plus basse pression de travail. L'ablation laser reste marginale. Par rapport à ces méthodes, les avantages de la pulvérisation cathodique magnétron sont : dépôts de tous types de matériaux et sur n'importe quel substrat; couche déposée plutôt homogène; pression de travail réduite; vitesse de dépôt grande; risques de contamination réduits; meilleure structure des films et bonne adhésion au substrat.

1.2.3 Optimisation de la réflectivité

On distingue deux types de réflexion: la réflexion spéculaire et la réflexion diffuse. Les lois géométriques de la réflexion ne s'appliquent qu'à la réflexion spéculaire. La réflexion spéculaire se produit uniquement sur des surfaces lisses. Quand la taille des défauts de l'interface est plus petite que la longueur d'onde de la lumière incidente, la totalité de la lumière est réfléchie de manière spéculaire, c'est-à-dire que l'angle de réflexion de la lumière est égal à son angle d'incidence. Ce type de réflexion est régi par les lois de Snell-Descartes : le rayon réfléchi est symétrique au rayon incident par rapport à la normale à la surface réfléchissante. Sur le Figure 5, l'angle du rayonnement incident θ_i est donc le symétrique de

celui du rayonnement réfléchi θ_f par rapport à la normale. k_i et k_f sont les vecteurs d'onde respectifs de l'onde incidente et de l'onde réfléchie :

$$|k_i| = |k_f| = k = \frac{2\pi}{\lambda}$$

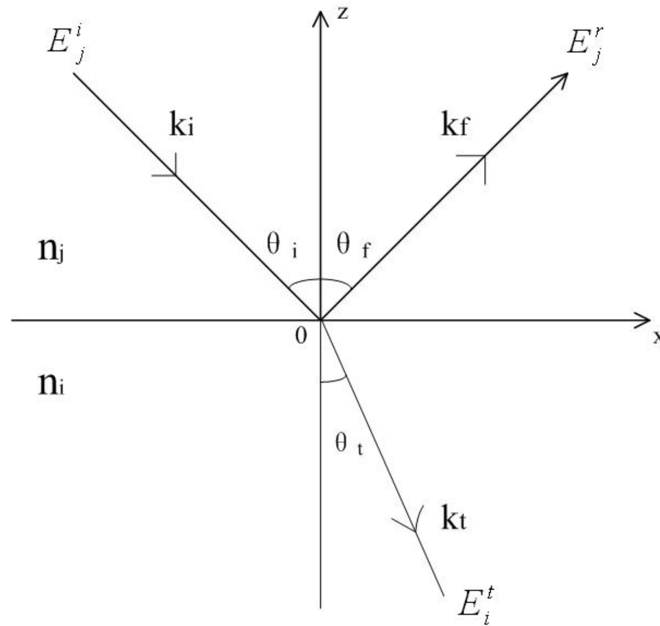

Figure 5. Schéma de la réflexion et transmission d'une onde plane.

On considère une onde électromagnétique plane rencontrant une interface parfaite entre deux milieux d'indices complexes n_j et n_i. Les coefficients de Fresnel expriment les liens entre les amplitudes des ondes réfléchies $r_{j,i}$ et transmises $t_{j,i}$ par rapport à l'amplitude de l'onde incidente :

$$\frac{|E_j^r|}{|E_j^i|} = \frac{n_j - n_i}{n_j + n_i} = r_{j,i}$$

$$\frac{|E_i^t|}{|E_j^i|} = \frac{2n_j}{n_j + n_i} = t_{j,i}$$

où E_i, E_r et E_t sont les amplitudes associées respectivement au champ électrique incident, réfléchi et transmis.

Pour la multicouche constituée de plusieurs couches d'indices différents, on peut définir des coefficients de Fresnel globaux. Sur la Figure 6, nous considérons un empilement de N couches minces. Et nous noterons j et i deux couches successives. d_i est l'épaisseur de la

couche i. $r_{j,i}$ est le coefficient de réflexion entre la couche j et i. Une relation de récurrence permet de calculer le coefficient de réfléxion R_i en supposant que l'empilement s'arrête à la couche i à partir de l'amplitude réfléchie à l'étape précédente R_j :

$$R_i = \frac{r_{j,i} + R_j e^{2ikn_i d_i}}{1 + r_{j,i} R_j e^{2ikn_i d_i}}$$

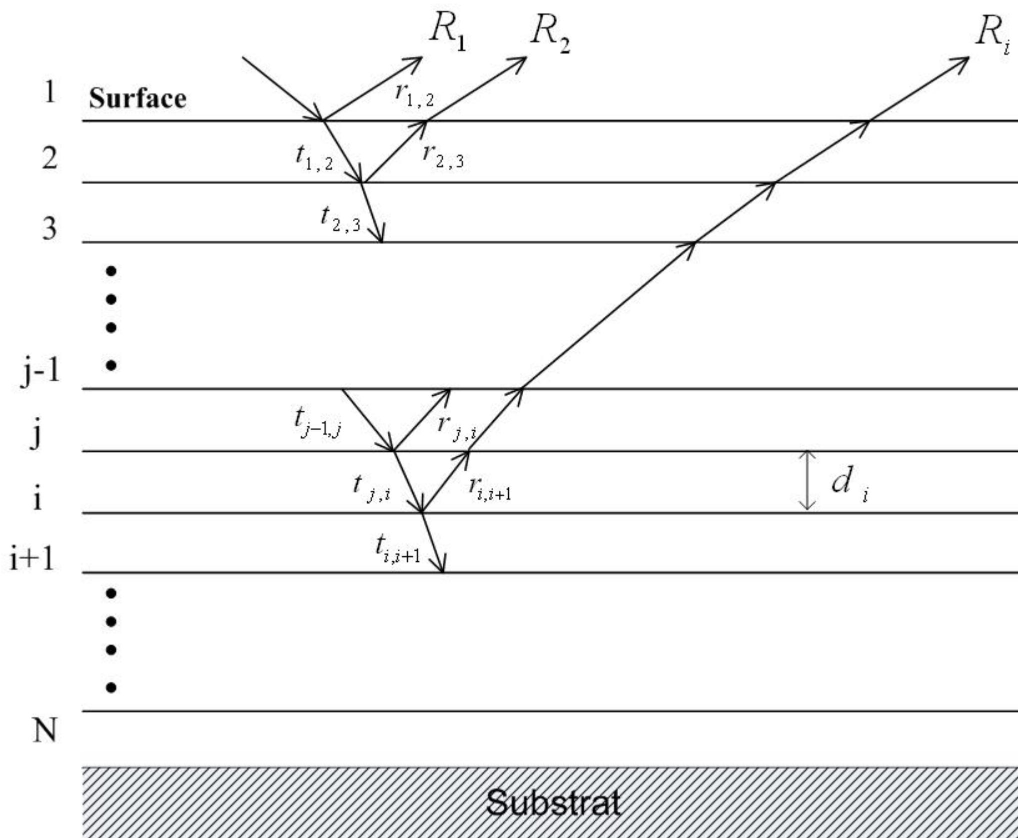

Figure 6. Schéma de la réflexion et transmission d'un empilement multicouche.

1.2.4 Les performances des miroirs multicouches

La qualité des multicouches est liée à leurs propriétés physico-chimiques. Des multicouches idéales seraient constituées de couches parfaitement lisses et continues. Mais à cause du procédé de dépôt ou des propriétés des matériaux, il existe deux types de rugosité dans une multicouche, la rugosité chimique et la rugosité géométrique. La rugosité chimique représente le cas d'une interdiffusion des deux matériaux conduisant à la formation d'interphases aux interfaces. La rugosité géométrique représente le cas d'une rugosité

interfaciale en raison de la nature intrinsèque des matériaux tels que les variations d'épaisseur, la densité des matériaux, la structure cristalline, etc.

Le but de ce travail est d'étudier les performances optiques des multicouches en distinguant l'interdiffusion et la rugosité géométrique [7]. Pour les applications spatiales ou d'autres applications comme lithographie EUV, optique X, … , la durée de vie et la résistance à la chaleur des multicouches sont nécessaires. La stabilité temporelle et la stabilité thermique sont donc deux propriétés importantes pour l'étude des multicouches. Par exemple, le système Si/B_4C dispose d'une bonne réflectivité, mais la stabilité temporelle et thermique sont mauvaises, et le système Si/SiC a une bonne stabilité temporelle et thermique, mais la valeur de la réflectivité est seulement de 16% autour 30.4 nm [8].

Pour ces objectifs, nous avons utilisé plusieurs méthodes de mesure que nous présenterons en détail dans le chapitre 2.

Chapitre 2 :

Méthodes expérimentales

2.1 La spectroscopie d'émission X (XES)

Depuis 1895, date de la découverte des rayons X par le physicien allemand Wilhelm Röntgen (Prix Nobel 1901), les nombreuses études sur le rayonnement X et son interaction avec la matière ont conduit au développement de méthodes analytiques performantes utilisées dans la recherche en laboratoire. William Lawrence Bragg et William Henry Bragg (Prix Nobel 1914), ont été les pionniers en développant la spectroscopie d'émission X (XES). Ils ont mesuré les longueurs d'onde des rayons X de beaucoup d'éléments avec une grande précision.

La XES (x-ray emission spectrometry) consiste à analyser la distribution en énergie des photons émis par les atomes d'un échantillon lorsque ceux-ci sont bombardés par des particules ionisantes. L'analyse des rayons X renseigne sur l'environnement physico-chimique (type et nombre de liaisons chimiques, nature des atomes voisins, phase cristalline, présence de défauts, etc.) des atomes émetteurs. En choisissant convenablement l'énergie des particules incidentes, il est possible d'obtenir cette information physico-chimique dans l'échantillon massif, à sa surface ou bien à une interface solide-solide (lieu de contact entre deux solides). Cette méthode expérimentale permet également de faire de l'analyse quantitative élémentaire.

Nous faisons notre travail par la XES induite par électrons, une technique d'analyse non destructive, qui permet de sonder en profondeur la composition physico-chimique des matériaux. La profondeur analysée dépend de la pénétration des électrons incidents, conditionnée par leurs interactions élastiques (qui dévient les électrons de leur trajectoire sans leur faire perdre d'énergie) et inélastiques (entraînant un transfert d'énergie des électrons incidents à la cible conduisant à l'émission de particules secondaires, tels les rayons X) dans le milieu. Les analyses sont réalisées sur l'appareillage IRIS [9] (Instrument de Recherche sur les Interfaces et les Surfaces).

2.1 La spectroscopie d’émission X (XES)

2.1.1 Principe

Un spectre d'émission typique présente un fond continu, c’est-à-dire qu'il y a eu émission de photons correspondant à une large gamme d'énergie. Lorsqu'un électron arrive au voisinage d'un noyau, sa trajectoire est déviée et il subit une accélération due à la force attractive d'origine électrostatique. Il s'avère qu'une particule décélérée (freinée) rayonne de l'énergie. L'énergie émise sous forme de rayons X est prélevée sur l'énergie cinétique de l'électron qui poursuit sa trajectoire avec une énergie cinétique plus faible. C'est la raison pour laquelle ce rayonnement porte le nom de rayonnement continu de freinage ou Bremsstrahlung.

Sur le fond continu, se superposent des raies ou des pics qui correspondent à une émission importante de photons d'énergies caractéristiques. C’est la conséquence d'une réorganisation du cortège électronique. Lorsque un électron énergétique arrive sur un atome de la cible, une lacune est créée en couche profonde (Figure 7). Ce processus est l’ionisation d’un niveau de cœur. L’émission X caractéristique provient de la décroissance radiative de l'état ionisé en couche interne d’un atome. L'énergie d'une émission X caractéristique est égale à la différence d'énergie entre les états initial et final, c’est-à-dire à la différence d’énergie de liaison des deux sous-couches impliquées dans la transition.

Selon que la réorganisation du cortège électronique prend place à partir d’un niveau de cœur ou de la bande de valence (Figure 7), on observe respectivement une raie atomique (prend place entre deux niveau de cœur) ou une bande d’émission (à partir d’un niveau appartenant à la bande de valence). Toutes les transitions entre les niveaux ne sont pas permises. Elle sont imposées par des règles de sélection qui font intervenir les nombres quantiques l et j de l'électron : $\Delta l=\pm 1$; $\Delta j=0, \pm 1$ (0 – 0 interdit).

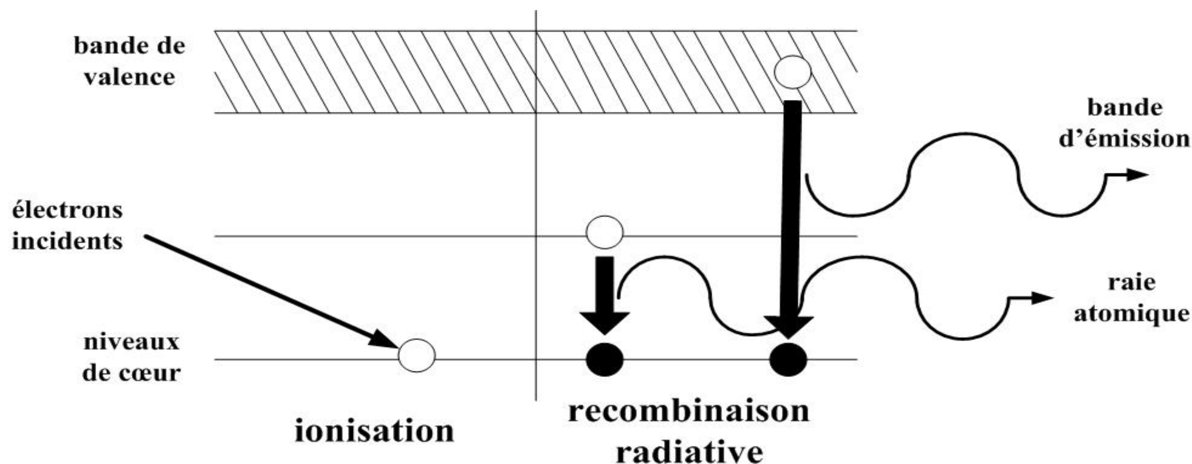

Figure 7. Schéma de principe de l'émission X induite par électrons.

La distribution des électrons dans la bande de valence est quelconque et large de plusieurs eV. Il en résulte que si la largeur naturelle de la sous-couche vers laquelle a lieu la transition est faible devant la largeur de la bande de valence, alors la distribution en énergie des photons émis décrit la distribution des états de valence. Dans ce cas, la largeur de la sous-couche de cœur intervient comme un simple élargissement de la distribution des états de valence qui s'ajoute à l'élargissement instrumental. Les électrons de valence étant les moins liés à l'atome, leur distribution en énergie est très sensible à l'environnement physico-chimique de l'atome. Par conséquent, la forme et la largeur de la bande d'émission reflètent les liaisons chimiques formées par l'atome émetteur.

Dans le cadre de ce travail, nous avons étudié les émissions Co $L\alpha\beta$ (transitions 3d - $2p_{3/2}$ et 3d - $2p_{1/2}$), Mg $K\beta$ (transition Mg 3p - 1s), Si $K\beta$ (transition Si 3p - 1s) et Al $K\beta$ (transition Al 3p - 1s).

Le choix de l'énergie des électrons incidents détermine l'épaisseur émissive, c'est-à-dire l'épaisseur du matériau que l'on désire sonder. Nous avons utilisé le programme Monte-Carlo CASINO [10] qui permet de simuler la distribution en profondeur des ionisations dans un matériau soumis à un bombardement électronique et aussi déterminer l'épaisseur sondée. Un modèle de l'émission étudiée est créé et nous permet de choisir l'angle et l'énergie adéquats des électrons incidents.

2.1.2 L'appareillage IRIS

Le montage expérimental IRIS comporte trois chambres principales. La Figure 8 montre la structure principale de l'instrument.

- **Chambre de préparation:** La chambre est équipée d'emplacements pour insérer des dispositifs pour la préparation de couches minces. Il est équipé pour l'évaporation thermique des métaux, pour le recuit, le nettoyage ou le décapage des échantillons. La chambre est reliée à une autre chambre où trois échantillons peuvent être stockés.

- **Chambre source:** Dans la chambre source se trouve un canon à électrons et l'échantillon qui constitue la source du rayonnement. L'angle d'incidence du faisceau d'électrons influe sur la profondeur de pénétration des électrons dans l'échantillon et sur l'absorption des photons sortant de l'échantillon. La valeur de l'angle d'inclinaison de l'échantillon est le résultat d'un compromis entre la maximisation de l'épaisseur sondée et la minimisation du phénomène de réabsorption. L'énergie cinétique des électrons peut varier de 0 à 10 keV. Le canon à électrons utilisé est de type Pierce. Nous travaillons avec une haute tension de focalisation qui permet de régler la dimension du faisceau émis sur l'échantillon. La densité de courant d'électrons peut être réglée de 0 à 10 mA/cm^2. Un porte-échantillon refroidi à l'eau est utilisé.

- **Chambre du spectromètre:** La chambre sert à analyser le rayonnement polychromatique X produit sous l'effet du bombardement électronique. Elle est équipée d'un spectromètre à dispersion de longueur d'onde à cristal courbé fonctionnant en réflexion. Le spectromètre à focalisation est de type Johann [11], dont le principe est schématisé en Figure 9. Dans cette figure, le rayonnement réfléchi par le cristal courbé sous un rayon 2R est focalisé sur un cylindre de rayon R, appelé cylindre de focalisation. Un compteur à flux gazeux assure la détection des rayons X. Les déplacements relatifs du cristal et du détecteur sont mécaniquement les mêmes que ceux rapportés dans la référence [12]. Le cristal tourne d'un angle θ alors que le détecteur se déplace d'un angle 2θ. Le rayonnement provenant d'une source étendue de rayons X est dispersé par un cristal courbe suivant la loi de Bragg (voir 1.2). Le rayon de courbure 2R est de 500 mm. Le détecteur, placé derrière une fente réglable, est un compteur à flux gazeux (90% Ar et 10% CH_4) fonctionnant dans le domaine de Geiger.

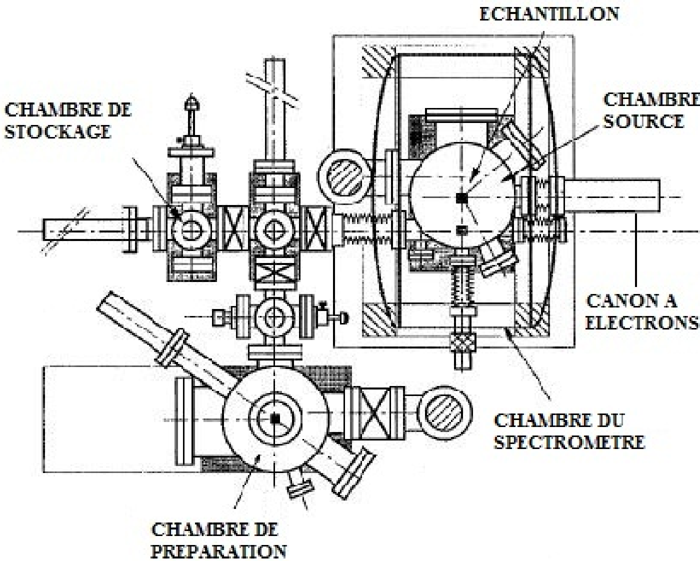

(a)

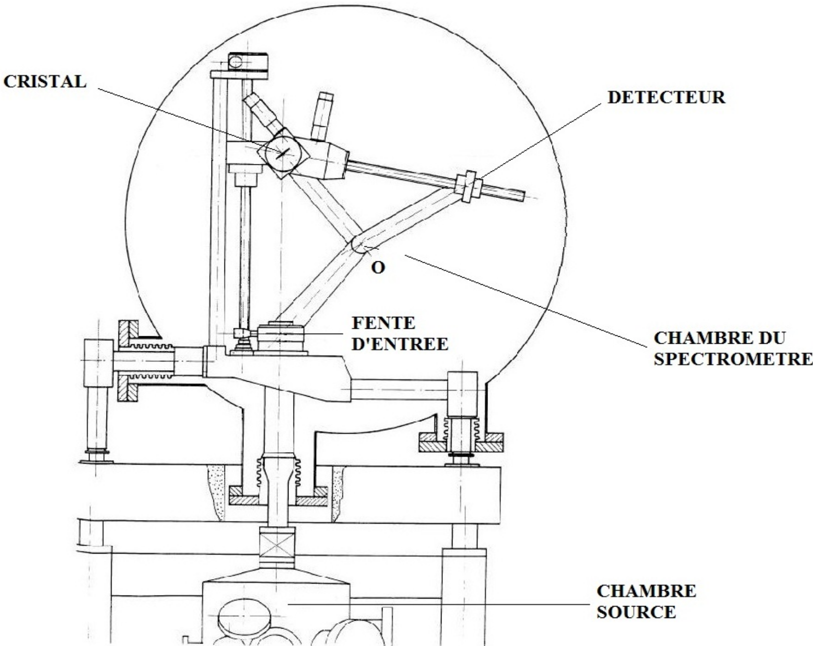

(b)

Figure 8. Schéma de l'appareillage IRIS: (a) vue de dessus (b) vue de face.

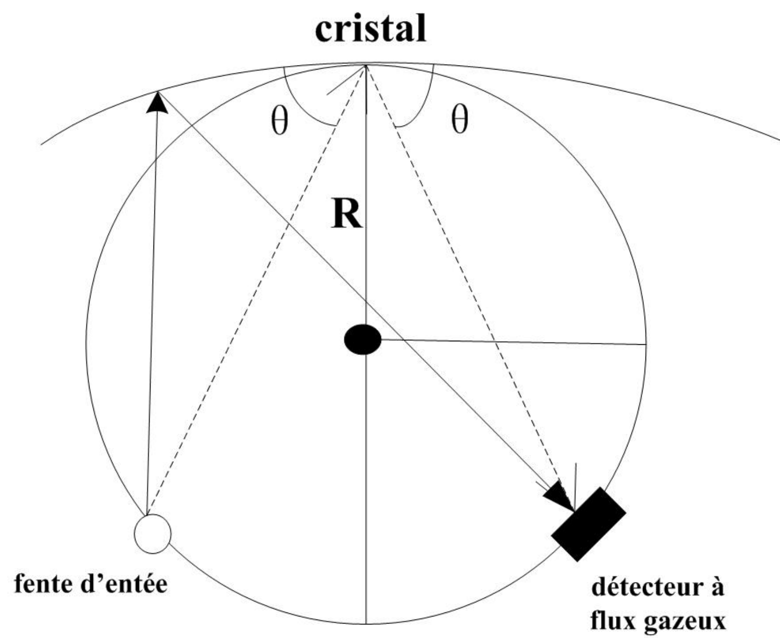

Figure 9. Schéma de la géométrie du spectromètre.

2.2 La réflectométrie dans le domaine des rayons X durs (XRR)

La caractérisation des miroirs multicouches est réalisée par la réflectométrie dans le domaine des rayons X durs. La période de la multicouche peut être calculée à partir des courbes de réflectivité expérimentales en utilisant la loi de Bragg corrigée. L'ajustement des courbes de réflectivité permet de déterminer l'épaisseur, la densité, la rugosité et l'indice optiques complexes de chaque couche.

2.2.1 Principe

La réflectométrie dans le domaine des rayons X durs est une technique non-destructive. Elle consiste à étudier la réflexion d'un faisceau X rasant. Dans notre travail, les mesures XRR des multicouches Al/SiC, Al/Mo/SiC et Al/W/SiC ont été réalisées à l'Institut d'Optique [1]. La Figure 10 représente le principe du réflectomètre XRR. Il est composé d'une source de rayons X, d'un système de fentes, d'un porte-échantillon, d'un goniomètre $\theta/2\theta$, d'un monochromateur et d'un détecteur. Pendant la mesure, la source de rayons X est fixe, l'échantillon bouge d'un angle θ et le détecteur d'un angle 2θ. La source est un tube à rayons X à anode de cuivre produisant une longueur d'onde de 0,154 nm (E=8048 eV, raie d'émission Kα du cuivre). La source est alimentée par un générateur haute-tension délivrant une tension de 40 kV et une intensité de 25 mA. Le monochromateur en carbone graphite est placé entre l'échantillon et le détecteur. Le détecteur est un compteur proportionnel à gaz (Argon/Méthane). Un ordinateur de contrôle permet d'acquérir les courbes de réflectivité donnant l'intensité mesurée en fonction de l'angle du détecteur.

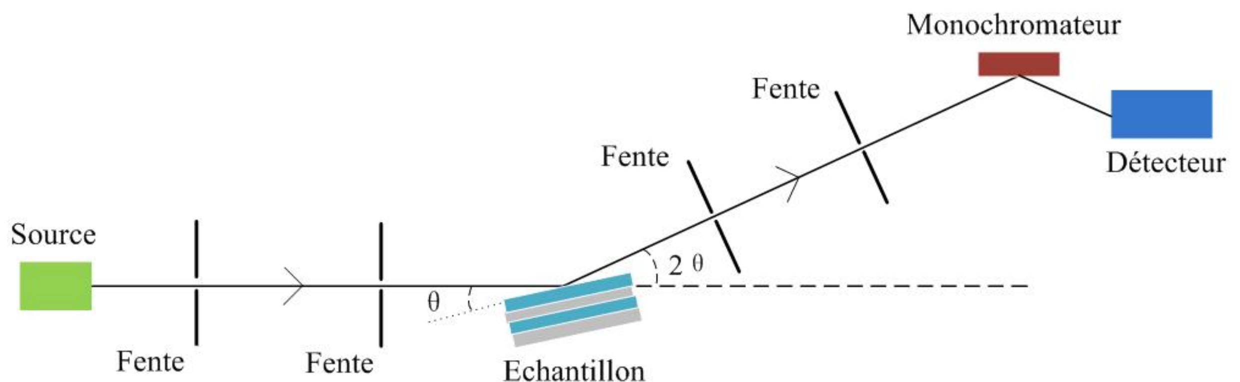

Figure 10. Schéma de principe du réflectomètre XRR.

2.2 La réflectométrie dans le domaine des rayons X durs (XRR)

Pour les multicouches Mg/Co, Mg/B_4C/Co, Mg/Zr/Co, les mesures ont été réalisées à l'Université Tongji à Shanghai avec un réflectomètre D1 système, Bede Ltd.

Pour les courbes des réflectivités, lorsque les rayons X sont incidents sur l'échantillon aux angles inférieurs à l'angle critique θc, on observe un plateau de réflectivité dû à la réflexion totale (Figure 11). On observe ensuite une série de pics de Bragg. L'intensité des pics de Bragg est fortement liée au contraste d'indice entre les deux matériaux constituant la période mais aussi à la rugosité des interfaces. Une diminution de l'intensité des pics de Bragg et de l'enveloppe de la courbe renseigne donc sur la qualité des interfaces de l'empilement. L'élargissement éventuel des pics de Bragg permet de mettre en évidence une variation des épaisseurs le long de la multicouche.

L'échantillon peut être caractérisé en ajustant la courbe expérimentale à la courbe théorique par une méthode essai-erreur [2] en utilisant le programme IMD [3]. Lorsque nous utilisons IMD pour modéliser les courbes expérimentales de XRR, les valeurs des paramètres sont estimées automatiquement, en utilisant la méthode des moindres carrés. L'estimation des paramètres est basée sur le test du χ^2 afin de déterminer un certain nombre de paramètres qui décrivent la multicouche. Cependant pour utiliser cette méthode, un modèle approximatif de l'empilement doit être connu ainsi que l'ordre de grandeur des épaisseurs et de la rugosité pour pouvoir fixer les conditions initiales. Cet ajustement permet de déterminer en plus de la période, l'épaisseur, la densité et la rugosité de chaque couche.

2.2.2 Ajustement des courbes des réflectivités

Un exemple de mesure de réflectivité XRR à 0.154 nm avec son ajustement correspondant illustré dans la Figure 11. Il concerne une multicouche de Mg/Co. Nous pouvons constater que la position des pics de Bragg et des extinctions sont en bon accord avec la simulation. La courbe de meilleur ajustement dans la Figure 11 a été obtenue en ajustant six paramètres : les épaisseurs, les rugosités, les densités des deux couches Mg et Co. Afin de s'adapter à la courbe, nous avons varié manuellement les six paramètres, jusqu'à ce que la courbe de réflectance calculée coïncide avec la courbe mesurée.

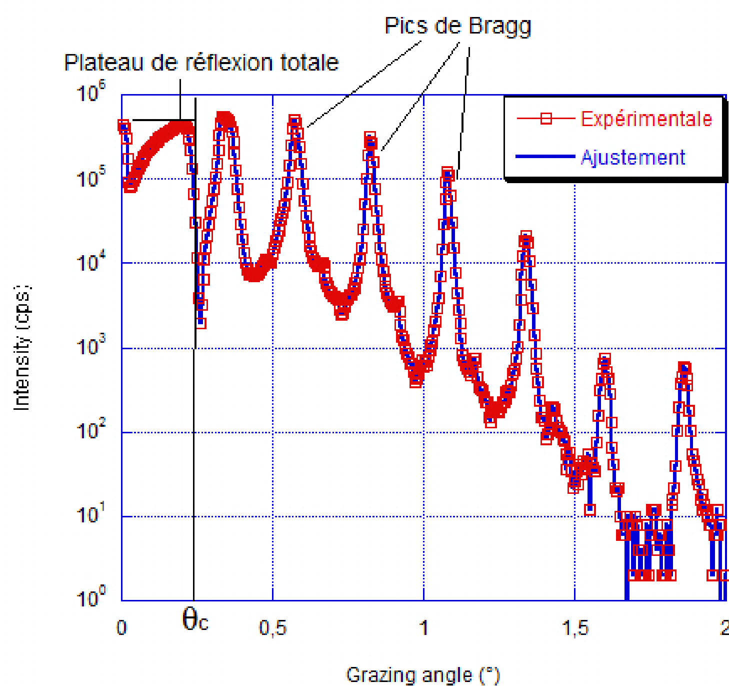

Figure 11. Spectre XRR avec l'ajustement d'un multicouche Mg/Co.

A titre d'exemple, les paramètres ajustés de la multicouche Mg/Co sont présentés dans le Tableau 1. Dans le tableau, le rapport de densité (%) est la densité de la couche divisée par la densité du matériau massif. La densité de la couche est proche de celle du matériau massif et la rugosité σ de la couche d'interface est d'environ 0,4 nm. L'épaisseur de la multicouche préparée coïncide avec celle de la conception. L'accord entre l'expérience et la simulation est bon.

Tableau 1. Paramètres de la multicouche Mg/Co obtenus par ajustement à la courbe expérimentale. de XRR.

Multicouche	d_{Mg} (nm) d_{Co} (nm)	σ_{Mg} (nm) σ_{Co} (nm)	Rapport de densité (%) Mg Co
Mg/Co	14,1 2,63	0,40 0,40	100,7 102,2

2.3 La réflectométrie EUV sur BEAR

La réflectométrie dans le domaine EUV permet de caractériser les performances optiques des miroirs multicouches à la longueur d'onde d'utilisation. Plusieurs sources EUV peuvent être utilisées pour effectuer les mesures. Dans ce travail, toutes les mesures de réflectivité ont été réalisées au synchrotron.

Le synchrotron désigne un grand instrument destiné à l'accélération à haute énergie de particules élémentaires. Le rayonnement synchrotron est une lumière émise par des électrons qui tournent dans un anneau de stockage à une vitesse proche de la vitesse de la lumière. Il est obtenu par des dispositifs magnétiques qui courbent la trajectoire des électrons ou les font osciller, soient des aimants de courbures, soient des onduleurs. Le rayonnement synchrotron a été observé pour la première fois en 1947 par Herb Pollock et Robert Langmuir sur le synchrotron de 70 MeV qu'ils avaient construit au laboratoire de recherche de la General Electric à Shenectady (New York). L'utilisation du rayonnement synchrotron concerne un très large ensemble d'activités de recherche, que ce soit en recherche fondamentale pour la chimie, la physique et les sciences de la matière, ou en recherche appliquée. Il y a de nombreux synchrotrons en fonctionnement dans le monde entier, par exemple Soleil (France), ESRF (France), BESSY (Allemagne), APS (USA), Spring-8 (Japan), etc.

Nous avons mesuré les réflectivités à la ligne BEAR du rayonnement synchrotron d'Elettra à Trieste, Italie. Le synchrotron d'Elettra est une machine de troisième génération qui date des années 1990 et se caractérise par une émission synchrotron non seulement dans les aimants de courbure mais aussi dans les onduleurs et les "wigglers" insérés dans les sections droites de l'anneau de stockage. L'intensité maximale du courant présent dans l'anneau est de 300 mA. L'énergie des électrons dans l'anneau est de 2 GeV.

2.3.1 Description de la ligne BEAR

La ligne BEAR (Bending magnet for Emission Absorption and Reflectivity) que nous avons utilisée travaille dans la gamme spectrale de 4eV à 1400 eV. Un système optique contrôle la position du faisceau et sélectionne la longueur d'onde et la polarisation. La ligne est terminée par deux chambres: la chambre de préparation et la chambre expérimentale (Figure 12) [13], qui sont maintenues sous ultravide de 10^{-8} Pa (10^{-10} mbar). Un sas et une

canne de transfert permettent d'introduire l'échantillon et de passer d'une chambre à l'autre. Le faisceau arrive dans la chambre expérimentale où sont effectuées les mesures comme la réflectivité, l'absorption, la diffusion, la photoémission, etc. La polarisation de la lumière arrivant sur l'échantillon peut être sélectionnée en faisant tourner la chambre autour de l'axe optique de la ligne de lumière.

La ligne BEAR est équipée de trois monochromateurs. Leurs caractéristiques sont présentés dans le Tableau 2. Pour nos études, nous avons utilisés les longueurs d'onde comprises entre 15 nm et 40 nm. Alors nous avons utilisé les monochromateurs G1200 pour réaliser les mesures de réflectivité.

Tableau 2. Caractéristiques des monochromateurs de la ligne BEAR.

Monochromateur	Incidence	Domaine
GNIM	Normale	4 – 40 eV (310– 31 nm)
G1200	Rasante	40 – 600 eV (31 – 2,0667 nm)
G1800	Rasante	600 – 1400 eV (2,0667 – 0,8857 nm)

Le goniomètre compte 10 degrés de liberté. Les rotations du détecteur et l'échantillon sont dans la gamme 0-360° et la résolution angulaire est de 0,001°. Ils permettent de positionner l'échantillon et le détecteur à la position désirée.

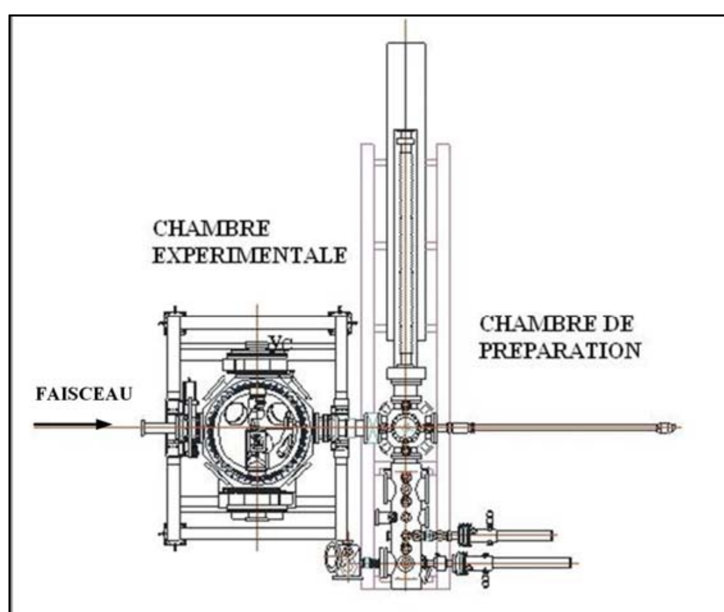

Figure 12. Schéma des chambres de mesure et de préparation de la ligne de BEAR.

2.3.2 Mesure de la réflectivité

Pour les mesures de la réflectivité, les flux photoniques incident et réfléchi sont mesurés par une photodiode en silicium reliée à un picoampéremètre. Une grille de tungstène permet de mesurer en continu le flux incident après le monochromateur. La mesure de la réflectivité peut être réalisée à angle constant en faisant varier l'énergie. On peut également la réaliser à énergie constante en faisant varier l'angle.

D'abord, on mesure le courant correspondant au faisceau direct incident sur la photodiode (Id_1) et le courant des électrons dans la grille de tungstène (Id_2). Puis on mesure le courant correspondant au faisceau réfléchi incident sur la photodiode (Ir_1) et le courant des électrons dans la grille (Ir_2). La réflectivité absolue est calculée par le rapport des deux courants du faisceau direct et réfléchi normalisés au courant de grille :

$$R = \frac{\dfrac{I_{r1} - I_{rb1}}{I_{r2} - I_{rb2}}}{\dfrac{I_{d1} - I_{db1}}{I_{d2} - I_{db2}}}$$

où Ir_b et Id_b correspondent au bruit de fond moyen de la chaîne de mesure.

L'erreur sur la valeur de la réflectivité absolue est de ±1%. Nos mesures sont réalisées uniquement en polarisation s.

2.4 La spectroscopie de résonance magnétique nucléaire (spectroscopie RMN)

2.4.1 Principe

La spectroscopie RMN est une technique qui exploite les propriétés magnétiques de certains noyaux atomiques, basée sur le phénomène de résonance magnétique nucléaire. Le phénomène de RMN a été observé pour la première fois en 1946 par Felix Bloch et Edward Mills Purcell. Ils ont reçu pour cette invention le prix Nobel de physique en 1952. Depuis cette date, la technique a connu un développement spectaculaire dans différents domaines comme en physique, en chimie organique, en biologie structurale et en médicine, etc.

Le principe de la spectroscopie RMN est l'absorption résonante d'un photon qui permet la transition entre les niveaux d'énergies nucléaires adjacents dont la dégénérescence est levée par un champ magnétique (effet Zeeman). La fréquence de résonance est reliée par le rapport gyromagnétique du noyau étudié à la valeur du champ magnétique. Le champ local vu par les noyaux n'est pas exactement le champ appliqué et la fréquence de résonance dépend de l'environnement dans lequel se trouve l'atome sondé.

Dans les matériaux ferromagnétiques, deux techniques de mesures sont possibles. La première est la RMN sous champ dans laquelle l'aimantation des matériaux étudiés est saturée par un champ magnétique extérieur. La deuxième est la RMN en champ nul, c'est la technique que nous avons utilisée pour caractériser nos multicouches. Elle se distingue pricipalement de la RMN conventionnelle par l'absence d'un aimant pour produire un champ magnétique externe. Dans un matériau ferromagnétique l'alignement interne des moments magnétiques électroniques est à l'origine d'un champ magnétique interne qui est appelé le champ hyperfin.

La spectroscopie RMN représente des signaux de résonance émis par certains noyaux atomiques de l'échantillon et fournit les résultats sous forme de spectres (nombre d'atome en fonction de la fréquence de résonance). La fréquence de résonance correspond à un environnement particulier. Cette méthode d'analyse est ainsi utilisée pour l'analyse structurale des échantillons. Dans le cas de matériaux ferromagnétiques elle permet également d'obtenir des informations sur les propriétés magnétiques des échantillons en caractérisant leur dureté magnétique (inverse de leur susceptibilité magnétique).

2.4 La spectroscopie de résonance magnétique nucléaire (spectroscopie RMN)

Dans notre travail, nous cherchons essentiellement à obtenir des informations sur les multicouches Mg/Co. Cette méthodologie a été plus particulièrement appliquée à l'analyse de multicouches magnétiques à base de Co. Elle permet de déterminer la structure cristallographique du Co : les fréquences sont différentes selon sa phase cristalline, cfc, hc ou cc. Elle est également sensible à l'environnement chimique du Co et permet donc de déterminer le mélange aux interfaces de multicouches à base de Co. Cela a enfin permis d'établir des corrélations entre d'une part la structure des échantillons et leurs propriétés magnétiques et d'autre part les procédés de fabrication.

2.4.2 Description de l'appareillage utilisé

Dans notre cas, toutes les expériences de spectroscopie RMN décrites dans ce travail sont menées à l'IPCMS (Institut de Physique et Chimie des Matériaux de Strasbourg). Le spectromètre RMN a été fabriqué à l'IPCMS. La RMN est souvent associée aux diffractions X et électronique et à la magnétométrie pour étudier la structure et les interfaces des multicouches métalliques, les vannes de spin pour la magnéto-électronique, l'ordre chimique à courte distance, les nanocomposites, les métaux granulaires en matrice métallique ou les oxydes, l'interface métal/oxyde magnétique et le couplage d'échange. Dans notre travail, nous utilisons maintenant le caractère essentiellement magnétique de la technique pour l'étude des corrélations entre la nanostructure de systèmes composites et leurs propriétés magnétiques locales dans les multicouches.

A l'IPCMS, les échantillons sont analysées par la spectroscopie RMN à champ nul à 4,2 K en utilisant un spectromètre large bande (20-750 MHz) conçu pour l'étude des systèmes ferromagnétiques [14,15]. Les spectres RMN représentent la distribution des atomes en fonction de leur fréquence de résonance, c'est-à-dire du champ hyperfin. La sensibilité de l'équipement permet d'observer une couche atomique de Cobalt.

2.5 La spectrrométrie de masse d'ions secondaires par temps de vol (ToF-SIMS)

2.5.1 Principe

La spectrométrie de masse d'ions secondaires à temps de vol (ToF-SIMS) est une technique d'analyse physico-chimique de l'extrême surface de tous types de matériaux compatibles avec l'utlra-vide. Elle est basée sur la détection des ions secondaires produits sous l'effet d'un bombardement d'ions primaires incidents. Cette technique d'analyse peut être considérée comme destructive de la couche de surface sur une zone de quelques centaines de μm^2. Les applications du ToF-SIMS sont nombreuses : analyse élémentaire et moléculaire, profil en profondeur, identification de contaminants de surface, imagerie ionique, etc.

En 1910, J.J.Thomson découvrit l'émission de particules secondaires de métaux bombardés par des rayons cathodiques [16]. En 1949, Herzog et Viehböck firent les premières expériences de SIMS. Au début des années 60, deux projets d'instruments SIMS avec un analyseur magnétique ont été développés par la NASA et l'université d'Orsay [17]. Au début des années 70, des instruments SIMS statique ont été développés par Alfred Benninghoven à l'Université de Münster et K. Wittmack dans la région de Munich. Au début des années 80, à l'Université de Münster des analyseurs à temps de vol (ToF) ont été intégrés à des instruments SIMS.

Pendant l'analyse SIMS, la surface d'un échantillon est bombardée dans une enceinte sous l'utlra-vide par un faisceau d'ions primaires (typiquement de Ga^+ ou Bi^+). Le Figure 13 présente un schéma du bombardement ionique sur un multicouche. L'énergie des ions primaires à l'origine des émissions secondaires est de quelques keV. Les particules secondaires émises sous forme d'ions négatifs et positifs, créés par le bombardement d'ions primaires, sont accélérées par un champ électrostatique pour avoir une même énergie cinétique, puis séparées et détectées en masse, grâce à un secteur magnétique ou par leur temps de vol. Le temps de parcours des particules dans l'analyseur étant proportionnel à la racine carrée de la masse de ces particules, le temps de parcours de chaque ion permet la détermination de sa masse.

2.5 La spectrrométrie de masse d'ions secondaires par temps de vol (ToF-SIMS)

L'intensité du faisceau d'ions primaires définit deux types d'analyse : le SIMS dynamique et le SIMS statique, le SIMS dynamique utilisant des densités de courant de l'ordre de quelques mA/cm^2, il correspond à une analyse en volume. Inversement, le SIMS statique utilisant des densités de courant primaires qui n'excèdent pas quelques nA/cm^2. Il est donc très sensible à l'analyse de la surface de l'échantillon car les particules émises proviennent d'un ou deux nanomètres de l'extrême surface.

Le SIMS permet de déterminer la composition élémentaire et la structure chimique des couches supérieures de l'échantillon. Les profils de concentrations en profondeur sont obtenus par alternance entre temps d'analyse et temps d'érosion. La résolution en profondeur est inférieure à 1 nm.

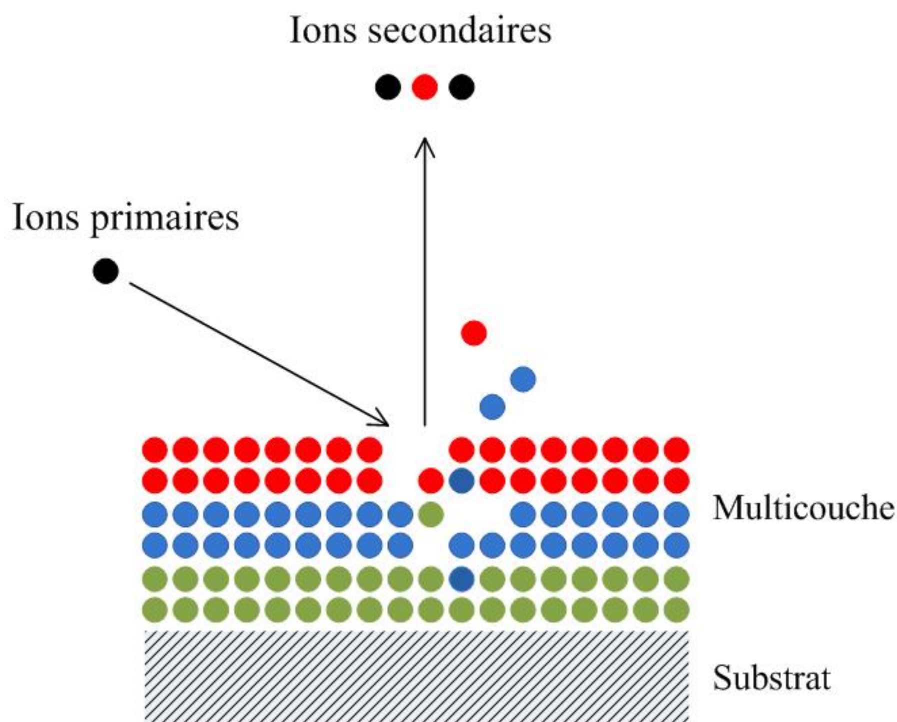

Figure 13. Schéma de principe de la méthode SIMS.

2.5.2 Description de l'appareillage utilisé

Dans notre cas, toutes les expériences ToF-SIMS décrites dans ce travail sont menées sur l'appareillage ToF-SIMS 5 (ION-TOF GmbH à Münster, Allemagne) du LPCS (Laboratoire de physicochimie des surfaces) de l'ENSCP. Les parties principales d'un appareillage ToF-SIMS 5 sont présentées sur la Figure 14.

Le système est composé de la source d'ions, l'analyseur à temps de vol avec un réflectron et le détecteur. Au sommet de l'analyseur à temps de vol se trouve un réflectron. En renvoyant les ions vers le détecteur. Ensuite, les ions sont post-accélérés pour finalement tomber sur le détecteur, qui enregistre le temps de parcours d'un ion secondaire de la particule et le transforme en signal digital. Il en résulte un spectre.

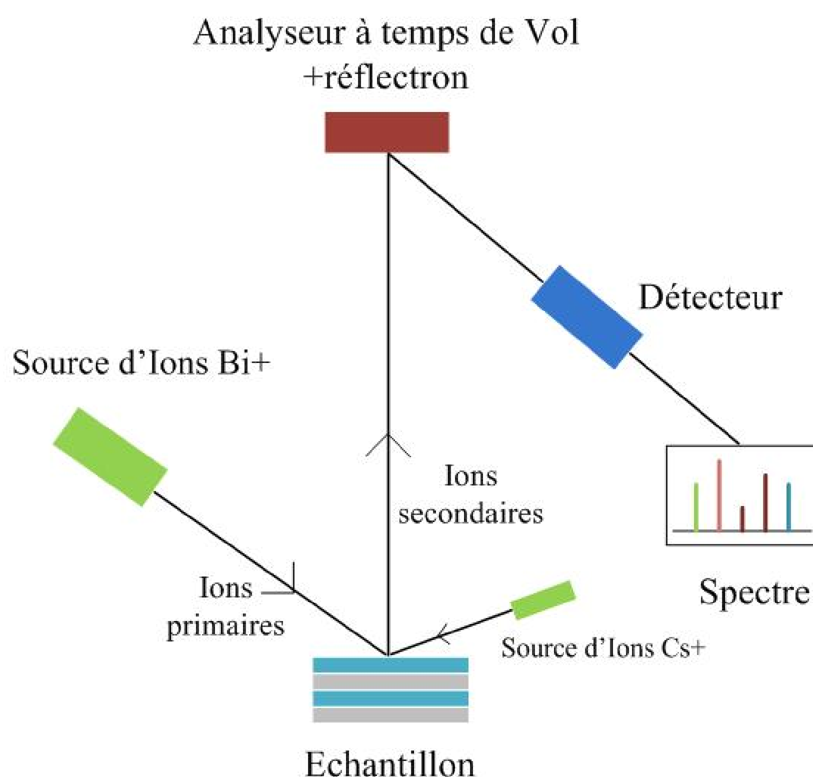

Figure 14. Schéma l'appareillage ToF-SIMS 5.

L'échantillon est introduit dans une chambre d'analyse et mis sous vide. La pression de travail dans la chambre est autour de 10^{-8} Pa. La surface érodée est de 500 µm x 500 µm, et seule la surface centrale (100 µm x 100 µm) est analysée. Les spectres de masse sont obtenus en érodant par faisceau d'ions césium (Cs^{+}), à une énergie d'impact de 1 keV et un courant de 50nA et en utilisant des ions primaires bismuth (Bi^{+}), à une énergie d'impact de 25 keV et un courant de 15nA, pour l'analyse. L'angle d'incidence du faisceau primaire avec la normale à la surface est de 45°. La dose totale d'ions primaires est inférieure à 10^{12} ions/cm^{2} de manière à assurer des conditions statiques. Les deux spectres d'ions positifs et négatifs sont enregistrés. Le spectre d'ions positifs est dominé par les espèces électropositives et le spectre d'ions négatifs par les espèces électronégatives.

2.6 La spectroscopie de photoélectrons X (XPS)

2.6.1 Principe

La spectroscopie de photoélectrons X (XPS) est une méthode physique d'analyse chimique. Le principe de l'XPS consiste à mesurer l'énergie cinétique les électrons émis lors de l'irradiation par un faisceau monoénergétique de photons X.

L'XPS a été développé dans les années 1960 par K. Siegbahn, physicien suédois, prix Nobel de physique en 1981. Elle est basée sur l'effet photo-électrique exposé par Einstein en 1905 où le concept du photon a été utilisé pour décrire l'éjection d'électrons d'une surface excitée par des photons.

L'XPS permet de mesurer le nombre d'électrons émis dans un intervalle d'énergie en fonction de l'énergie de liaison des électrons. Le diagramme énergétique du phénomène est représenté par la Figure 15.

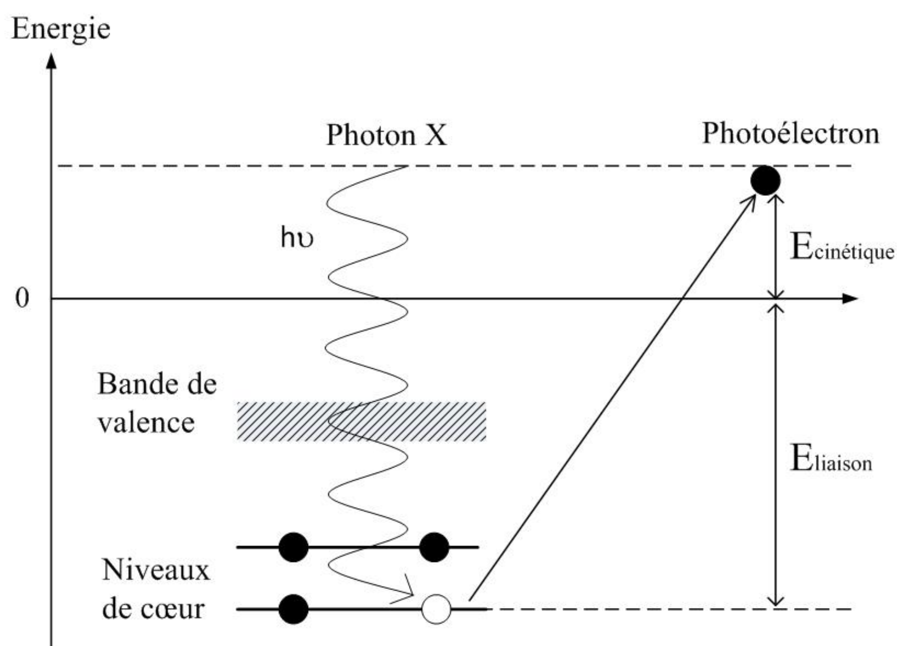

Figure 15. Principe de l'effet photoélectrique et de la spectroscopie de photoélectrons.

L'énergie de liaison $E_{liaison}$ caractérisant un électron d'un niveau électronique donné peut être déterminée par la relation d'Einstein :

$$E_{liaison} = h\upsilon - E_{cinétique}$$

où $h\upsilon$ est l'énergie des photons X incidents et $E_{cinétique}$ l'énergie cinétique du photoélectron.

Un spectre de photoélectrons est obtenu par l'enregistrement du nombre d'électrons détectés, exprimé en coups par seconde, en fonction de leur énergie de liaison. L'XPS permet d'obtenir la composition chimique de surface, les éléments présents en surface et les états chimiques de ces éléments d'un matériau sur une profondeur de quelques nm. La profondeur d'analyse dépend de l'énergie cinétique des photoélectrons émis. Il est aussi possible de mesurer l'épaisseur d'une couche mince et des éléments de contamination. Tous les éléments sauf l'hydrogène et l'hélium sont détectables. Cette technique d'analyse est non destructive.

2.6.2 Description de l'appareillage utilisé

Un appareillage XPS comprend trois composantes principales présentées sur la Figure 16 : une source de photons qui provoquera l'excitation, un analyseur qui permettra de séparer les photoélectrons émis en fonction de leur énergie cinétique et un système de détection et de comptage associé à une informatique d'acquisition.

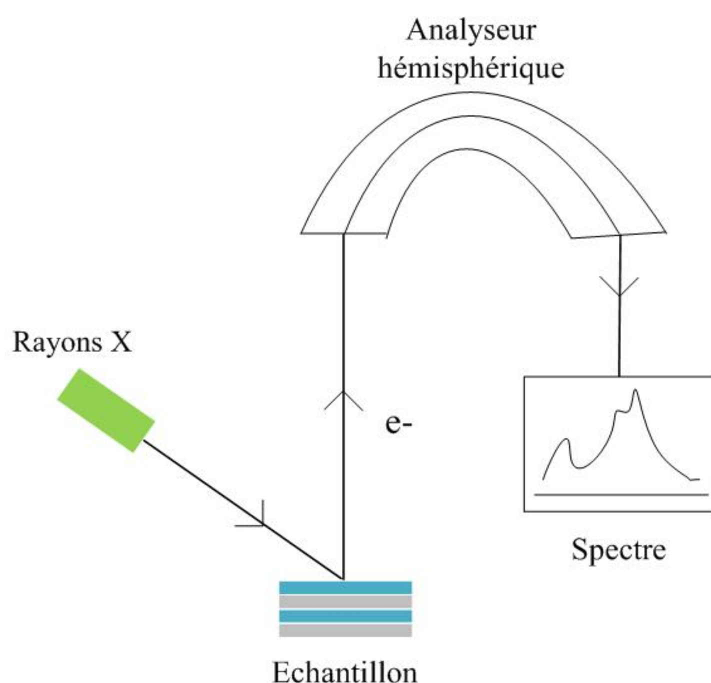

Figure 16. Schéma de principe d'un appareillage XPS.

Dans notre cas, toutes les expériences XPS décrites dans ce travail sont menées sur l'appareillage ESCALAB 250 du LPCS (Laboratoire de physicochimie des surfaces) de l'ENSCP. Les échantillons ont été mis en place dans la chambre d'analyse sous ultra-vide de l'ordre de 10^{-10} mbar. La source d'excitation est un rayonnement Al Kα (1486,6 eV)

monochromatique. La calibration en énergie est effectuée avec le signal de l’hydrocarbure de contamination à 285,0 eV. Les échantillons ont été analysés avec un angle entre l'analyseur et la surface égal à 90°. Les électrons émis par l’échantillon sont collectés et focalisés par une série de lentilles électrostatiques de type hémisphérique vers l’entrée de l’analyseur du spectromètre. Il est formé de deux hémisphères aux bornes desquelles est appliquée une différence de potentiel. Les spectres ont été traités avec le programme Avantage, fourni par Thermo Electron Corporation. A partir des intensités obtenues par décomposition des pics principaux de niveaux de cœur des éléments, les épaisseurs des couches détectées et la composition chimique de surface de la multicouche Al/Mo/SiC ont été estimées.

2.7 Le faisceau d'ions focalisés (FIB)

2.7.1 Principe

Le faisceau d'ions focalisés (FIB) est un instrument, développé initialement pour les besoins de l'industrie de la micro-électronique. Il étend de manière considérable les possibilités d'étude ainsi que le nombre d'échantillons observables. Les principaux domaines d'applications du FIB sont la science des matériaux, la microfabrication, le semi-conducteur et le circuit intégré, etc. La préparation de coupes ultraminces des échantillons constitue une étape cruciale des études par microscopie électronique en transmission (MET). Dans les instruments FIB dédiés à la microfabrication, il y a toujours une possibilité de visualiser l'échantillon usiné par microscopie à balayage. Ce peut être tout simplement la sonde ionique qui est utilisée pour générer les électrons secondaires, ou même la chambre sous vide peut être équipée d'une colonne électronique ou plus généralement, la colonne FIB est montée en accessoire d'un microscopie électronique à balayage (MEB). C'est ce qu'on appelle double faisceau (*Dual Beam).*

Le FIB *Dual Beam* est équipé de deux canons : un canon ionique et un canon électronique. Le but de cette technique est d'une part, d'usiner la matière à l'échelle nanométrique et d'autre part, de faire une image électronique ou ionique pour contrôler l'usinage. Le canon de FIB utilise une source de métal liquide, généralement du gallium (Ga), pour creuser l'échantillon. En général, le Ga est placé en contact avec une pointe de tungstène (W) et chauffé, provoquant une ionisation et une émission par effet de champ. Les ions extraits de la source sont accélérés et ensuite focalisés par des lentilles électrostatiques. En même temps, le MEB utilise un faisceau d'électrons focalisés pour faire l'image d'un échantillon. Les images en électrons secondaires fournissent une information sur la topographie et la structure du matériau au point d'impact du faisceau primaire. Comme la Figure 17 le montre, le faisceau d'ions primaire Ga^+ frappe la surface de l'échantillon et arrache une petite quantité des ions secondaires (i^+ ou i^-), des atomes neutres (n^0) ou des électrons secondaires (e^-).

2.7 Le faisceau d'ions focalisés (FIB)

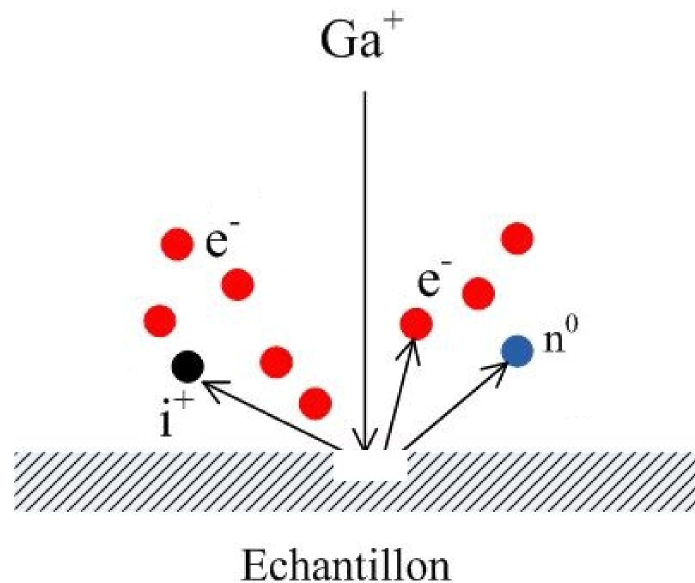

Figure 17. Schéma de principe du FIB.

La technique FIB est destructive. Quand des ions Ga de haute énergie sont projetés sur un échantillon, ils pulvérisent les atomes de la surface de l'échantillon. En même temps, les atomes de Ga sont implantés dans les premiers nanomètres de la surface de l'échantillon.

2.7.2 Préparation d'échantillons pour MET par le FIB

Une application importante du FIB est la préparation d'échantillons pour la Microscopie électronique en transmission (MET), car la MET nécessite des échantillons très minces. La préparation ne sera visible que dans l'observation "haute résolution". La gravure ionique est suivie in situ par le microscope électronique. Après la sélection de la zone intéressante de l'échantillon, il est impératif de placer sur sa surface un film métallique (platine, tungstène, ...) ou un film de carbone par une source d'évaporation métallique pour la protéger pendant la préparation.

L'usinage ionique est effectué d'abord avec un faisceau d'ions en incidence normale. Deux tranchées déterminent les faces extérieures des deux côtés de la zone d'intérêt. La largeur et la profondeur de ces tranchées sont généralement d'une dizaine de microns. Elles délimitent une lamelle d'épaisseur micrométrique. Ensuite, l'échantillon est incliné pour effectuer l'amincissement final. Cette étape permet d'éliminer la couche amorphe formée au

cours de l'usinage. La Figure 18 présente l'image MEB de nos multicouche Mg/Co en cours d'amincissement par le FIB.

Puis on extrait la lame mince et on la dépose sur une grille de MET. La méthode d'extraction consiste à souder, à l'aide d'un micromanipulateur, la lame mince sur un support spécial. Le micromanipulateur coupe les côtés de la lame et sa base, pour libérer la lame mince. Puis l'échantillon est transféré sur la grille MET (Figures 19 et 20).

Ensuite, l'échantillon est aminci et poli par l'avant, puis il est tourné de 180° et l'arrière de l'échantillon est aminci et poli sous le contrôle du MEB quand l'épaisseur désirée est atteinte. L'épaisseur des lames minces obtenues en routine est d'environ 50 - 100 nm.

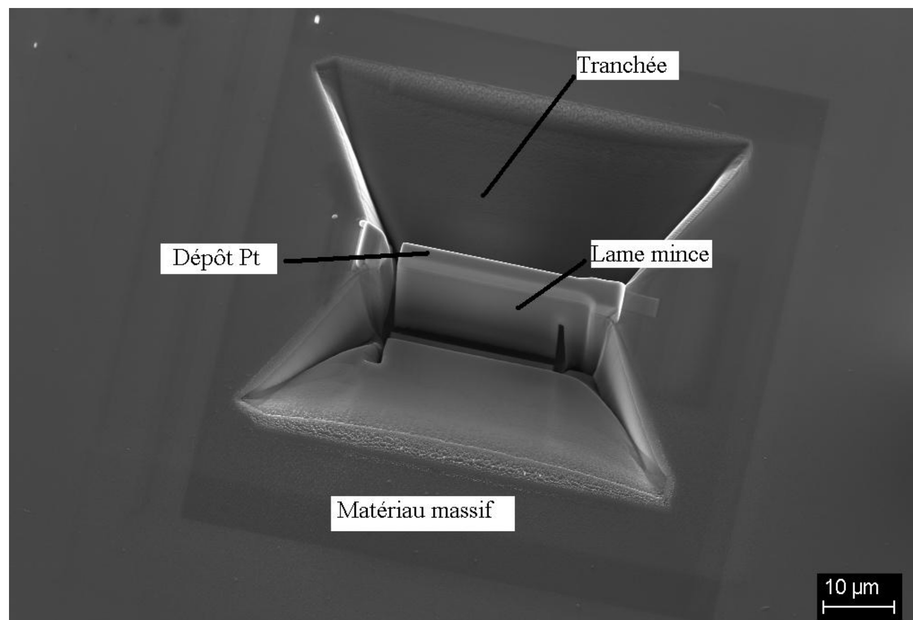

Figure 18. L'échantillon est découpé par le FIB et prêt à être extrait.

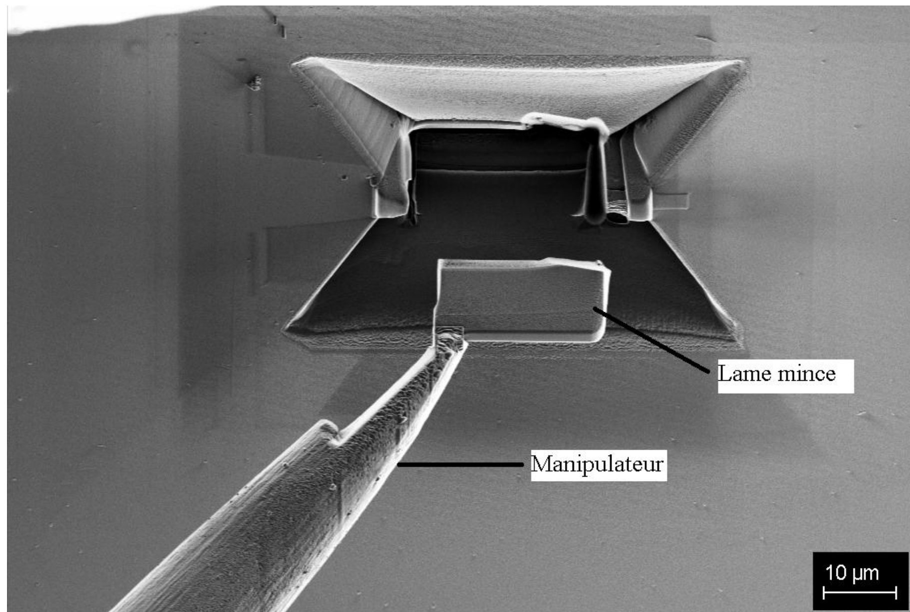

Figure 19. L'échantillon est retiré par un manipulateur.

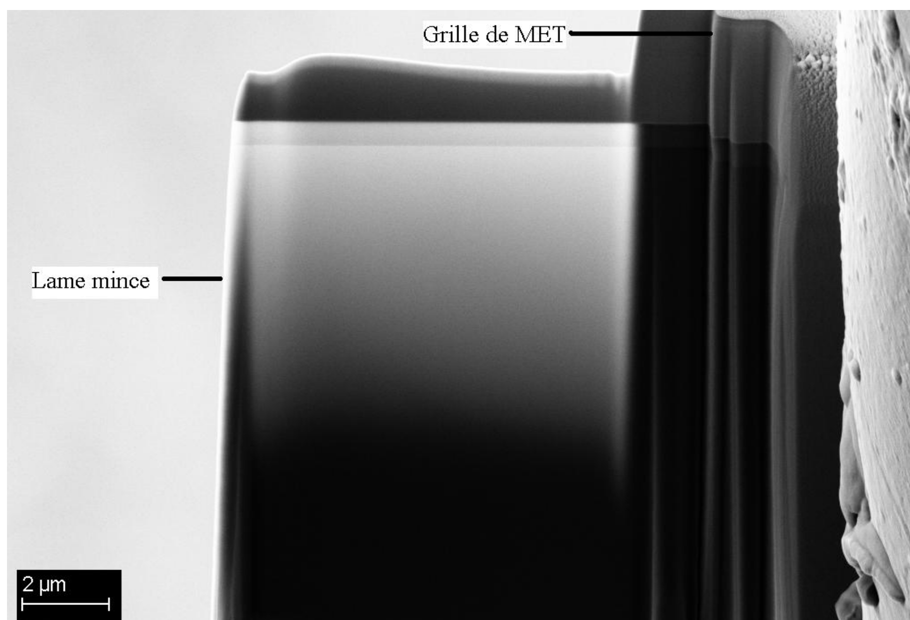

Figure 20. L'échantillon est transféré et déposée sur une grille de MET.

2.7.3 Description de l'appareillage utilisé

Dans notre travail, nous avons utilisé la FIB pour préparer l'échantillon pour la MET. Dans notre cas, toutes les expériences FIB décrites dans ce travail sont menées sur l'appareillage NEON 40 EsB (FIB/MET CrossBeam®, Carl Zeiss) de l'IMPMC (institut de minéralogie et de physique des milieux condensés). L'appareillage comprend trois composantes principales présentées sur la Figure 21: un canon à ions Ga pour la fonction FIB,

un canon à électrons pour la fonction MEB et un détecteur. La résolution du faisceau d'ions est de 7 nm à 30 kV. Le canon à ions est à un angle de 54° et le canon à électrons est monté sur le dessus de la chambre. Les ions Ga^{+} extraits de la source sont accélérés à une énergie de 30 keV. La taille du faisceau d'électrons est de 1,1 à 2,5 nm pour des tensions comprises entre 1 et 20 kV. L'appareillage est équipé d'une injection de gaz de platine et de carbone etc.

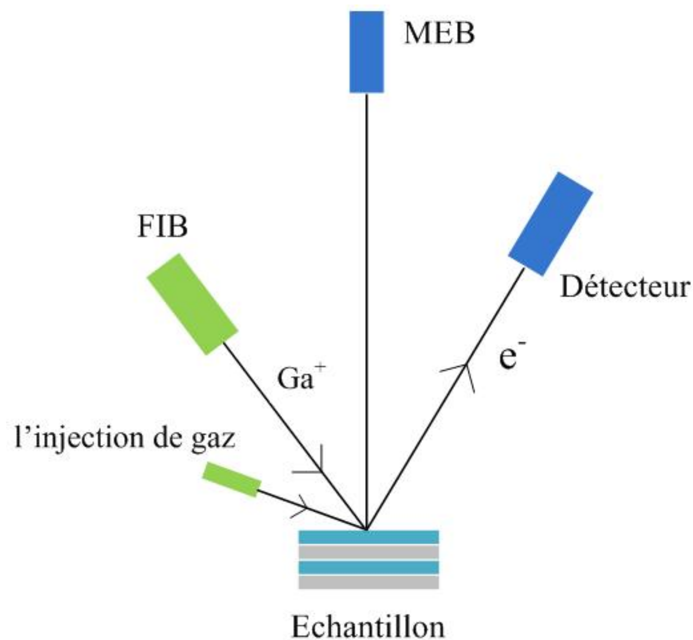

Figure 21. Schéma de principe d'un appareillage FIB/MET CrossBeam®.

2.8 La microscopie électronique à balayage en transmission (STEM) et la spectroscopie de perte d'énergie des électrons (EELS)

2.8.1 Principe de la STEM

La microscopie électronique à balayage par transmission (STEM) est un type de microscope électronique dont le principe combine des aspects du microscope électronique à balayage (MEB) et du microscope électronique en transmission (MET). Elle utilise un faisceau d'électrons rapides pour former l'image d'un échantillon mince (moins de 500 nm) par transmission.

Cette technique consiste à focaliser le faisceau électronique en une sonde électronique aussi petite que possible et à donner à cette sonde un mouvement de balayage. Un système de lentilles magnétiques permet à ce faisceau de balayer la surface de l'échantillon à analyser. Le signal diffusé à partir du nanovolume d'interaction est intégré sur un détecteur. Une image est acquise séquentiellement en balayant la sonde à la surface de l'échantillon. Les observations peuvent se faire en champ clair ou en champ sombre.

En STEM le volume d'interaction est faible, étant donné que l'échantillon est mince. En connaissant le facteur de grandissement, la STEM permet de mesurer l'épaisseur de chaque couche, d'observer la formation de cristaux dans les couches et l'interdiffusion entre les couches. Plus spécifiquement, dans notre travail, nous nous focaliserons sur l'étude de coupes transverses de multicouches car nous pouvons voir la qualité des différentes couches métalliques. Une information sur la cristallinité des couches nous intéresse aussi car la transition amorphe-cristallin entraine souvent une augmentation de la rugosité interfaciale dans ces structures.

2.8.2 Principe de la EELS

Dans le STEM, les électrons émis par le filament du microscope interagissent avec les atomes de l'échantillon. Ces interactions peuvent conduire les électrons incidents à perdre de l'énergie. La spectroscopie de perte d'énergie des électrons (EELS) étudie la distribution en énergie des électrons ayant traversé l'échantillon. C'est une technique d'analyse dans laquelle

le matériau à analyser est exposé à un faisceau d'électrons dont l'énergie cinétique est située dans une plage relativement étroite. Certains de ces électrons seront soumis à des interactions inélastiques avec l'échantillon, ce qui signifie qu'ils perdront de l'énergie et que leurs trajectoires subiront une déflection faible et aléatoire.

Le principe de l’EELS est de former un spectre avec les électrons sortant de l’échantillon. En observant le spectre des pertes en énergie, on peut déduire des informations sur la structure de bande et analyser chimiquement la zone éclairée, afin d'appréhender les propriétés électroniques ou optiques de nanostructures. Plus on peut focaliser finement le faisceau électronique, plus l’analyse chimique peut être locale. Dans notre cas, en observant quel est le spectre du EELS on peut déterminer la composition élémentaire de l'échantillon, les informations chimiques et structurales des divers éléments. Les différents signaux observés résultent donc de processus d'excitation différents et mettent en jeu différentes catégories de populations d'électrons du solide. Ces observations EELS permettront d’établir une stratégie de préparation des multicouches afin d’optimiser leurs performances optiques.

2.8.3 Description de l’appareillage utilisé

Dans notre travail, toutes les expériences STEM-EELS sont menées sur l’appareillage STEM ULTRASTEM NION du LPS (Laboratoire de Physique des Solides d’Orsay). Il fonctionne à 100 kV et sous ultra-vide. Il utilise un canon de type émission de champ froid. Un faisceau d'électrons est focalisé sur la surface d'un échantillon en utilisant différentes lentilles magnétiques. Typiquement la largeur naturelle du faisceau incident est de 0,3 eV. La taille de la sonde corrigée des aberrations sphériques est d'environ 0,1 nm. Les images sont générées par la numérisation du faisceau focalisé sur l'échantillon. Un ensemble de détecteurs permet de détecter une partie des composantes élastiques et inélastiques du faisceau diffusé à différents angles par l'échantillon. Son avantage le plus important est la possibilité de collecter simultanément les images du EELS et de fond noir annulaire à grand-angle (High-angle annular dark-field, HAADF). Ainsi on peut caractériser les matériaux morphologiquement et chimiquement à l'échelle nanométrique. Nous utilisons une sonde à angle de convergence de 35 mrad et un angle de collecte pour le spectromètre EELS de 50 mrad. Les spectres EELS sont acquis avec une dispersion de 1 eV par canal.

2.8 La microscopie électronique à balayage en transmission (STEM) et la spectroscopie de perte d’énergie des électrons (EELS)

Chapitre 3 :

Etude des multicouches Mg/Co

3.1 Introduction

Comme présenté dans le chapitre 1, les multicouches périodiques nanométriques sont utilisées comme composants optiques dans le domaine EUV, pour des applications telles que les télescopes spatiaux, les microscopes X, la photolithographie EUV ou les lignes de lumière synchrotron. Leurs performances optiques dépendent de la qualité des interfaces entre les différentes couches de l'empilement. L'interdiffusion et la rugosité géométrique affectent les propriétés optiques à la longueur d'onde d'application et peuvent amoindrir la réflectance. Le but de ce travail est de proposer une méthode capable de distinguer entre interdiffusion et rugosité géométrique afin de corréler les performances optiques de la multicouche à sa qualité structurale.

L'équipe a déjà étudié le système Mg/SiC [18]. Des simulations indiquent en effet que la structure multicouche idéalement optimisée pour la longueur d'onde de 30,4 nm, avec la polarisation s de la lumière incidente à 20°, présente une réflectivité théorique de 60 %. Cependant, les mesures de réflectivité à 30,4 nm montrent que la grande valeur de la rugosité interfaciale ($\geq$ 1 nm) est directement responsable de la limitation des performances optiques : la réflectance n'est que de 40%. Cet exemple nous a motivés à explorer la combinaison d'autres matériaux alliant faible rugosité et haute réflectivité.

Pour les applications à l'optique des rayons X-EUV, un nouveau système Mg/Co est proposé en raison de son potentiel dans le domaine spectral 25 - 30 nm. La nécessité de ces multicouches avec une forte réflectance est ressentie dans de nombreux domaines d'application tels que l'imagerie solaire ou la microscopie en photoémission, utilisant la raie d'émission He II (30,4 nm). Mais en raison de son étude encore récente, le système Mg/Co n'a été que peu caractérisé. Dans ce chapitre, une série de multicouches Mg/Co sont étudiés selon trois axes principaux. Le premier porte sur l'étude des multicouches Mg/Co et en combinant différentes techniques. Le deuxième concerne l'étude de la résistance thermique de Mg/Co lors de recuit jusqu'à 400°C. Le troisième examine l'effet de l'introduction d'un

troisième matériau, par exemple Zr, dans la structure de Mg/Co en termes de gain ou de perte de réflectivité.

Tout d'abord, nous avons créé le système Mg/Co et ses possibles tri- ou quatre-couches par simulations (article **3-[1]**). Les simulations effectuées pour une multicouche idéale sans interaction entre les couches et aucune rugosité interfaciale montrent que, avec la polarisation s de la lumière incidente à 45°, la reflectance atteint une valeur maximale égale à 56,5% autour de 25 nm de longueur d'onde (photons de 50 eV), proche du seuil d'absorption de Mg $L_{2,3}$. L'introduction d'une couche de Zr, Y ou B_4C améliore notablement la valeur de la réflectivité : 58, 61 et 63% respectivement. La valeur de réflectivité simulée se compare favorablement avec celle des autres multicouches conçu pour la même longueur d'onde telles que Se/Si, Ni/Ba, Co/Cd, Ni/Ca et Sc/Ni [19]. Les multicouches Mg/Co ont des applications potentielles à condition que l'interaction entre les couches Mg et Co soit minime.

Pour vérifier si la multicouche Mg/Co est efficace pour les applications dans la gamme EUV, certaines des multicouches simulées ont été préparées par pulvérisation magnétron. Nous avons appliqué notre méthodologie alliant réflectométrie X et EUV, XES, RMN, ToF-SIMS, XPS, FIB et STEM-EELS pour étudier les multicouches.

Nous avons d'abord étudié les multicouches Mg/Co pour la longueur d'onde de 25 nm (article **3-[2]**). La mesure de réflectivité à la longueur d'onde de 25 nm est de 46%. Les épaisseurs des couches de Mg et Co déduites des ajustements des mesures XRR correspondent à celles de la structure simulée pour la multicouche Mg/Co. Les densités de couche sont équivalentes à celle du matériau massif et la rugosité superficielle est inférieure à 0,5 nm. L'état chimique des atomes de Mg est étudié par XES et l'état chimique des atomes de Co est examiné par RMN. D'après les mesures XES et RMN, les interfaces ne présentent pas d'interdiffusion et la seule rugosité géométrique explique la différence entre les valeurs de réflectance simulée et mesurée. La bonne qualité de la structure périodique est mise en évidence dans l'image STEM d'une lamelle excavée à partir de Mg/Co en utilisant le FIB.

Ensuite, nous avons étudié les multicouches Mg/Co pour la longueur d'onde de 30,4 nm (longueur d'onde proche de celle de la raie He-II). Le mesure de réflectivité à la longueur d'onde de 30,4 nm est de 40% et une largeur d'interface n'est que de 0,5 nm (article **3-[3]**). Les

résultats expérimentaux indiquent que la multicouche Mg/Co est prometteuse pour l'imagerie solaire dans le domaine EUV à la longueur d'onde 30,4 nm.

Pour les applications spatiales ou d'autres applications comme lithographie EUV, optique X, … , l'étude de la durée de vie et de la résistance à la chaleur des multicouches sont nécessaires. La stabilité temporelle et la stabilité thermique sont donc deux propriétés importantes pour l'étude des multicouches. La stabilité temporelle des multicouches Mg/Co est vérifiée sur une période d'environ huit mois et ne révèle aucun changement significatif de la réflectivité dans le domaine des rayons X durs ainsi que du signal de RMN (article **3-[2] et A-[6]**). Afin de comprendre comment se développe la rugosité et se forment les composés interfaciaux aux interfaces des multicouches Mg/Co, nous avons entrepris une étude en fonction du recuit jusqu'à 400°C (article **3-[4], A-[1] et A-[4]**). Les mesures de réflectivité dans la gamme EUV montrent que la valeur de réflectivité augmente jusqu'à 45,0% dans le cas de Mg/Co recuit à 280°C. Ensuite, la valeur de réflectivité diminue à 26,2% à 305°C et à 400°C la réflectivité est nulle. L'ajustement des courbes de réflectivité EUV indique que l'épaisseur de la couche et la rugosité reste constante jusqu'à 280°C, alors que de 305°C les valeurs varient fortement. Les images MEB montrent que les multicouches ne résiste pas à des températures supérieures à 305°C. L'analyse de la RMN montre qu'à partir de 305°C, les atomes de Co se regroupent en grains. Donc toutes les mesures montrent que la stabilité thermique de Mg/Co jusqu'à 305°C. A partir de 305°C, un fort changement dans la morphologie de l'échantillon se produit et explique la perte de réflectivité.

Nous nous attendions à une interdiffusion possible, afin d'améliorer les performances optiques des systèmes Mg/Co, nous avons introduit une couche de B_4C (article **3-[2] et A-[6]**) ou Zr (article **3-[5] et A-[2]**) à une interface comme barrière de diffusion. Les expériences montrent que l'introduction de B_4C dans la multicouche dégrade considérablement, la réflectivité dans le domaine EUV, conduisant à une valeur de moins de 1%. À partir de mesures XES et RMN, la faible réflectance est due à une forte interdiffusion aux interfaces. Nous avons étudié l'introduction de couches de Zr dans la structure Mg/Co. Les multicouches Mg/Zr/Co, Mg/Co/Zr et Mg/Zr/Co/Zr ont été conçues. Les mesures montrent que Mg/Co/Zr est plus efficace (50% de réflectivité) que Mg/Zr/Co et Mg/Zr/Co/Zr (~40%). Pour comprendre ce comportement asymétrique, nous avons étudié la qualité de l'interface par ToF-SIMS et RMN (article **3-[6]**). Le ToF-SIMS montre que la forme du profil est symétrique pour Mg/Co et Mg/Co/Zr et asymétrique pour Mg/Zr/Co et Mg/Zr/Co/Zr. La

multicouche Mg/Co/Zr présente les meilleurs profils en termes de symétrie et de contraste. Au contraire, pour les multicouches Mg/Zr/Co et Mg/Zr/Co/Zr, nous avons attribué cette différence à un processus d'interdiffusion où les couches Co sont déposés sur des couches Zr. Ceci est en bon accord avec les performances optiques de Mg/Co/Zr, Mg/Zr/Co et Mg/Zr/Co/Zr. Les spectres RMN montrent que les couches Co de Mg/Co/Zr sont bien définies. Et il n'y a plus de couches de Co pur dans les multicouches Mg/Zr/Co et Mg/Zr/Co/Zr à cause de l'interdiffusion à l'interface Zr-sur-Co. La stabilité thermique de Mg/Co/Zr a également été étudiée (article **3-[5] et A-[4]**), les résultats montrent que la réflectivité atteint 51% quand il a été recuit à 200 °C.

Comme les systèmes Mg/Co avec les couches de Zr, les simulations des multicouches avec des couches de Mo donnent dans tous les cas (tri- et quadri-couches) des valeurs élevées de réflectivité (> 60%). Donc les multicouches Mg/Mo/Co, Mg/Co/Mo et Mg/Mo/Co/Mo ont été conçues. Les mesures de réflectivité dans le domaine EUV montrent que Mg/Co/Mo est plus efficace (44% de réflectivité) que Mg/Mo/Co (42% de réflectivité) et Mg/Mo/Co/Mo (33% de réflectivité). La stabilité thermique de Mg/Co/Mo a également été étudiée, les résultats montrent que la réflectivité atteint 45% quand il a été recuit à 100°C. Ce résultat présente une grande différence avec les simulations. Pour comprendre cette différence, nous avons étudié la qualité de l'interface par XES et RMN. D'après les mesures XES et RMN, les interfaces ne présentent pas d'interdiffusion. Le système est moins réactif que celui avec Zr et cependant est moins bon optiquement (article **A-[4]**). Dans ce cas, des mesures supplémentaires devraient être faites sur ce système. Nous pouvons envisager de refaire des échantillons et des mesures sur ce système.

3.2 Principales publications

3-[1]

M.–H. Hu, K. Le Guen, J.-M. André, P. Jonnard, S. K. Zhou, H. Ch. Li, J. T. Zhu, Z. S. Wang : **Co/Mg/X multilayer mirrors for the EUV range,** *X-RAY OPTICS AND MICROANALYSIS：AIP Conference Proceedings, Volume 1221, pp. 56-58 (2010)*

3-[2]

K. Le Guen, M.-H. Hu, J.-M. André, P. Jonnard, S. K. Zhou, H. Ch. Li, J. T. Zhu, Z. S. Wang, C. Meny : **Development and interfacial characterization of Co/Mg periodic multilayers for the EUV range,** *The Journal of Physical Chemistry C (ACS Publications), 114 (14), pp 6484–6490 (2010)*

3-[3]

J. T. Zhu, S. K. Zhou, H. Ch. Li, Q. Sh. Huang, Z. S. Wang, K. Le Guen, M.-H. Hu, J.-M. André, P. Jonnard : **Comparison of Mg-based multilayers for solar He-II radiation at 30.4 nm wavelength,** *Applied Optics, Vol. 49, No. 20, pp. 3922-3925 (2010)*

3-[4]

M.-H. Hu, K. Le Guen, J.-M. André, S. K. Zhou, H. Ch. Li, J. T. Zhu, Z. S. Wang, C. Meny, N. Mahne, A. Giglia, S. Nannarone, I. Estève, M. Walls, P. Jonnard : **Investigation on the thermal stability of Mg/Co periodic multilayers for EUV applications,** *Appl Phys A: Materials Science & Processing, in press (2011)*

3-[5]

K. Le Guen, M.-H. Hu, J.-M. André, P. Jonnard, S.K. Zhou, H.C. Li, J.T. Zhu, Z.S. Wang, N. Mahne, A. Giglia, S. Nannarone : **Introduction of Zr in nanometric periodic Mg/Co multilayers,** *Appl Phys A: Materials Science & Processing, Volume 102, Number 1, 69-77 (2011)*

3.2 Principales publications

3-[6]

K. Le Guen, M.-H. Hu, J.-M. André, S. K. Zhou, H. Ch. Li, J. T. Zhu, Z. S. Wang, C. Meny, A. Galtayries and P. Jonnard : **Observation of an asymmetrical effect when introducing Zr in Mg/Co multilayers**, *Applied Physics Letters, 98, 251909 (2011)*

Co/Mg/X Multilayer Mirrors For the EUV Range

M.-H. Hu[1], K. Le Guen[1], J.-M. André[1], P. Jonnard[1], S. K. Zhou[2], H. Ch. Li[2], J. T. Zhu[2], Z. S. Wang[2]

[1] Laboratoire de Chimie Physique-Matière et Rayonnement, Université Pierre et Marie Curie, CNRS UMR 7614, 11 rue Pierre et Marie Curie, F-75231 Paris Cedex 05, France
[2] Institute of Precision Optical Engineering, Department of Physics, Tongji University, Shanghai 200092, CHINA

Abstract. A new material combination namely Co/Mg multilayer designed for optics applications in the EUV range, is reported. Simulations show that reflectivity value of the Co/Mg multilayer can reach a reflectivity of 55% at 25.2 nm (49.2 eV), when the grazing incidence angle is set to 45° and s polarization is considered. The introduction of additional materials, e.g., Y and Zr can improve the reflectivity to 61%. Co/Mg and Co/Mg/B_4C multilayers have been deposited following the parameters deduced from the simulations. The introduction of a B_4C barrier layer would in principle increase the multilayer reflectivity to 61%. In fact the reflectivity measurements at 0.154 nm show that the introduction of B_4C does not improve the structural quality of the multilayers.

Keywords: multilayer, x-ray reflectivity, cobalt, magnesium
PACS: 68.65.Ac, 42.79.e

INTRODUCTION

Periodic multilayers are widely used nowadays in many fields such as X-ray space telescopes, extreme ultraviolet (EUV) lithography or X-ray laser facilities. To verify if the periodic Co/Mg multilayers would be efficient mirrors for applications in the EUV range, we search by simulation what are the optimum values of the multilayer period d and the Γ ratio ($\Gamma = d_{Co} / (d_{Co} + d_{Mg})$, where d_{Co} is the thickness of the high absorption layer Co and d_{Mg} is the thickness of the low absorption layer Mg) that give the best value of reflectivity. Others multilayers have experimentally shown to be efficient in the same wavelength range such as B_4C/Si (R=30% at 23.6 nm wavelength), Zr/Al (R=28% at 25.8 nm), C/Si (R=23% at 25.6 nm and R=20% at 28.3 nm) [1] and Mg/SiC (R=56% at 30.4 nm and 10° incidence angle).

Starting from the Co/Mg optimized parameters, we also perform reflectivity simulations of multilayer stacks by introducing a thin metal layer at the interfaces. The various metals considered are from period 5 and 6 of the periodic table. The introduction of a thin B_4C interfacial layer is also considered.

Two samples, Co/Mg and Co/Mg/B_4C, are prepared with the stack parameters deduced from the simulations. Their reflectivity is measured at 0.154 nm (8048 eV) to determine the thickness, roughness and density of the layers.

SIMULATIONS

The simulation of the reflectivity of the Co/Mg multilayers is obtained from computations performed using the IMD software [2], modelling the optical properties (reflectance, transmittance, absorptance, etc.) of multilayer films. We consider "ideal" multilayers, without interfacial roughness or interdiffusion with Co near the substrate Si and Mg near the surface, made of 100 periods. The grazing incidence angle is set to 45° and s polarization is considered. The aim is to determine the parameters leading to the best reflectivity in the EUV and soft x-ray ranges.

The multilayer period and the Γ ratio are varied from 2 to 19 nm and from 0.1 to 0.9, respectively. The reflectivity reaches a maximum equal to 54.9% at 25.2 nm (49.2 eV) when d is equal to 17 nm and Γ to 0.15 (Table 1). This yields $d_{Co} = 2.55$ nm and $d_{Mg} = 14.45$ nm. These thicknesses are compatible with available deposition processes. Let us remark that the reflectivity is maximum close to the Mg L_3 edge where absorption is minimal within the multilayer.

Starting from the Co/Mg design optimized parameters, the effect on reflectivity of the introduction of a third material is considered. We perform reflectivity simulations of stacks by introducing a 1.5 nm thick metal layer at the Co-on-Mg, Mg-on-Co and both interfaces. The various metals considered in our study are from periods 5 and 6 of the periodic table (Z = 39-47 and 72-79). The simulations show that, with respect to the Co/Mg system, the reflectivity values are maximum with two metals: Y and Zr. With Y and Zr metal layers introduced at the Co-on-Mg interface, the reflectivity values are 61 and 58%, respectively. When the Y or Zr metal is introduced at the Mg-on-Co interface, the reflectivity decreases, the values being 51 and 52%, respectively. For the case of introducing the Y and Zr metal at both

CP1221, X-ray, Optics and Microanalysis, Proceedings of the 20th International Congress
Edited by M. Denecke and C. Walker
©2010 American Institute of Physics 978-0-0764-0/10/30 $30.00

Co-on-Mg and Mg-on-Co interfaces, the reflectivity values become 53 and 49%, respectively. Table 2 summarizes the simulated values of the reflectivity and the corresponding wavelength. Other metals give reflectivity values similar to the Co/Mg system.

TABLE 1. The simulated reflectivity of the Co/Mg multilayer with the multilayer period d, Co thickness d_{Co}, Mg thickness d_{Mg} and the Γ ratio.

Multilayer	d (nm)	d_{Co} (nm)	d_{Mg} (nm)	Γ	λ (nm)	R (%)
Co/Mg	17.00	2.55	14.45	0.15	25.2	55

To prevent possible interdiffusion at the interfaces of the Co/Mg system, a 0.9 nm thick B_4C layer, is added at the Co-on-Mg, Mg-on-Co and both interfaces. We find that this material should in principle improve the optical properties: the reflectivity values of Co/Mg/B_4C or Co/B_4C/Mg/B_4C increase to 61 and 58%, respectively, whereas that of Co/B_4C/Mg decreases to 51% (Table 2). In the same time, the addition of the B_4C barrier layer would also have some effect on the conditions of the layers growth and the interface formation.

TABLE 2. The simulated values of reflectivity with the multilayer period d for some Co/Mg multilayers with interfacial metal or B_4C layers.

Multilayer	d (nm)	λ (nm)	R (%)
Co/Mg/Y	18.5	26.3	61
Co/Y/Mg	18.5	26.3	51
Co/Y/Mg/Y	20.0	27.7	53
Co/Mg/Zr	18.5	26.3	58
Co/Zr/Mg	18.5	26.3	52
Co/Zr/Mg/Zr	20.0	27.5	49
Co/Mg/B_4C	17.9	25.8	61
Co/B_4C/Mg	17.9	25.8	51
Co/B_4C/Mg/B_4C	18.8	26.7	58

Because Co and Mg atoms react easily with oxygen atom, it could be necessary to protect the multilayer against surface oxidation. Some relatively inert materials could be used as capping layer. A B_4C capping layer is chosen here. When the B_4C thickness is varied, the simulations show that increasing the B_4C thickness up to 5 nm slightly enhances the reflectivity but also increases the background under the Bragg peak. A 2% reflectivity increase of the reflectivity is achieved with a 3 nm B_4C capping layer, especially in the case of Co/Mg (57%), Co/Mg/B_4C (63%) and Co/B_4C/Mg/B_4C (60%) systems.

SAMPLE PREPARATION AND CHARACTERIZATION

Following the multilayer design using reflectivity simulations, the Co/Mg (Table 1) and Co/Mg/B_4C (Table 2) multilayers are chosen to be deposited. They are deposited onto Si polished wafers using an ultrahigh vacuum direct current magnetron sputtering deposition system (JGP560C6, SKY Inc.). The purity of Co, Mg and B_4C targets are 99.95%, 99.98% and 99.5%, respectively. The base pressure of this sputtering system reaches 10^{-4} Pa. The working gas is argon (99.999% purity) at the constant pressure of 0.2 Pa. The number of periods is 30. Both multilayers are deposited with a 3.5 nm thick B_4C capping layer.

The reflectivity curve of the deposited multilayers is measured at 0.154 nm (Cu Kα emission at 8048 eV) with a small angle x-ray diffractometer (D1 system, Bede Ltd.) working in the θ-2 θ mode. The angular resolution is 5/1000°. The reflectivity curves of the Co/Mg and Co/Mg/B_4C samples are presented in Figure 1. The Bragg peaks are narrow and well-defined. For the Co/Mg/B_4C multilayers, 9 Bragg peaks are seen up to 2.5°, whereas 11 Bragg peaks are observed up to 3° for the Co/Mg multilayers. The Bragg peaks are more intense for Co/Mg with respect to Co/Mg/B_4C. It is also observed that the decrease of the background is much steeper for Co/Mg/B_4C with respect to Co/Mg. From these curves, it appears that the structural quality of Co/Mg is better than that of Co/Mg/B_4C. The comparison of the reflectivity curves, with and without B_4C layers, gives evidence that the introduction of B_4C does not improve the structural quality of the multilayers. This is probably due to an interaction between the B_4C layers and the metal layers.

The Co/Mg reflectivity curve is fitted in order to determine the parameters of the stack: the thickness, roughness and density of the various layers. They are collected in Table 3. In the table, the density ratio (%) is the density of the layer divided by the density of the bulk. We do not fit the reflectivity of Co/Mg/B_4C. It is too difficult to do because of the large number of parameters and the possible interaction of the B_4C layers with the metal layers.

The fitting results indicate that the prepared multilayer coincides with the design one. The density of layer is close to the bulk material and the roughness of the layer interface is about 0.4 nm. If these values are used in the simulation in the EUV range, the reflectivity of the Co/Mg multilayer is 53.3% at

CP1221, X-ray, Optics and Microanalysis, Proceedings of the 20th International Congress
Edited by M. Denecke and C. Walker
©2010 American Institute of Physics 978-0-0764-0/10/30 $30.00

25.2 nm (49.2 eV). This confirms that the periodic Co/Mg multilayers would be efficient mirrors for applications in the EUV range.

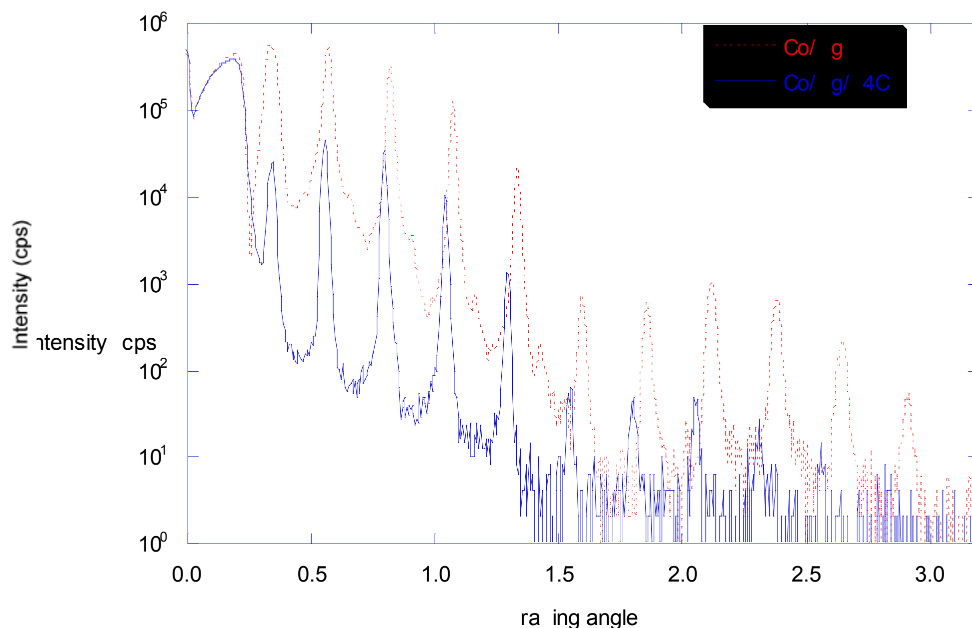

FIGURE 1. X-ray reflectivity curves measured at 0.154 nm for the multilayers.

TABLE 3. Fitting parameters of the reflectivity curve of the Co/Mg sample measured at 0.154 nm. σ is the interfacial roughness.

Multilayer	d_{Co} (nm) d_{Mg} (nm)	σ_{Co} (nm) σ_{Mg} (nm)	Density ratio Co (%) Density ratio Mg (%)
Co/Mg	2.63 14.1	0.40 0.40	102.2 100.7

CONCLUSION

The simulated reflectivity value of the perfect Co/Mg multilayers is equal to 54.9% at 25.2 nm (49.2 eV). This wavelength is close to that of the He-II radiation (30.4 nm), which plays an important role in the EUV range. Then, the Co/Mg multilayer could have potential applications provided the interaction between the Co and Mg layers is minimal. The introduction of additional materials at Co-on-Mg interfaces, e.g., Y and Zr could increase the reflectivity to 61%. The addition of thin B_4C layers at Co-on-Mg interfaces, makes the reflectivity value increase to 61%. Two samples are elaborated using magnetron sputtering and their optical performances are characterized by reflectivity in the hard x-ray range. It appears that the structural quality of Co/Mg is better than that of Co/Mg/B_4C.

We plan in the future to deposit more samples for example with addition of Y or Zr metal. The analysis of all these samples will be performed by means of X-ray emission spectroscopy and nuclear magnetic resonance to determine the chemical state of the Mg and Co atoms present within the multilayers. Reflectivity measurements at the application wavelength in the EUV range will also be performed. The details will be presented in a forthcoming paper.

REFERENCES

1. PXRMS multilayer survey: http://henke.Uol.gov/cgi-bin/mldata.pl
2. D. L. Windt, Comp. Phys. 12, 360 (1998)

CP1221, X-ray, Optics and Microanalysis, Proceedings of the 20th International Congress
Edited by M. Denecke and C. Walker
©2010 American Institute of Physics 978-0-0764-0/10/30 $30.00

Development and Interfacial Characterization of Co/Mg Periodic Multilayers for the EUV Range

K. Le Guen,* M.-H. Hu, J.-M. André, and P. Jonnard

Laboratoire Chimie Physique - Matière Rayonnement, University Pierre et Marie Curie Paris 06, CNRS UMR 7614, 11 rue Pierre et Marie Curie, F-75231 Paris cedex 05, France

S. K. Zhou, H. Ch. Li, J. T. Zhu, and Z. S. Wang

Institute of Precision Optical Engineering, Department of Physics, Tongji University, Shanghai 200092, People's Republic of China

C. Meny

Institut de Physique et Chimie des Matériaux de Strasbourg, CNRS UMR 7504, 23 rue du Loess, BP 43, F-67034 Strasbourg cedex 2, France

Received: November 23, 2009; Revised Manuscript Received: February 3, 2010

We propose a new system, namely the periodic Co/Mg multilayer system, for optics applications in the EUV range. Close to the Mg L edge, i.e., around a wavelength of 25 nm or a photon energy of 50 eV, a reflectivity of about 43% is measured at 45° for s-polarized radiation. Moreover, it appears that this system is stable over a period of time of three months. The introduction of thin boron carbide interfacial layers proves disastrous contrary to simulations that show this could be beneficial. We combine X-ray reflectivity in the hard X-ray range, X-ray emission spectroscopy, and nuclear magnetic resonance to determine the thickness and roughness of the Co and Mg layers as well as the chemical state of the Co and Mg atoms at the interfaces. This reveals that in the Co/Mg system the interfaces are abrupt and there is no interdiffusion between the Co and Mg layers. Then the difference between the experimental and simulated reflectivities is ascribed to the interfacial roughness of the order of 0.4 nm. In the Co/Mg/B_4C system, evidence of a large mixing of the Co and B_4C layers is presented and explains the poor reflectance of this system.

1. Introduction

Periodic multilayers made of alternating nanometric thin films nowadays play an important role for optical applications from the extreme ultraviolet (EUV) to the hard X-rays.[1,2] The performances of these structures in terms of reflectance and bandwidth strongly depend on the quality of interfaces between the different layers, i.e. the value of the interfacial roughness and the interdiffusion. Thus the development of optimized stacks relies on the characterization of the layers, determination of their thickness, roughness, and density, as well as the comprehension of the interfacial phenomena, atomic diffusion, or formation of compounds.

In this paper we propose a new system, namely Co/Mg, for applications in the EUV range close to the Mg L edge, that is to say around 25 nm wavelength or 50 eV photon energy. In view of a possible application as monochromator, the simulated reflectivity obtained with the IMD software[3] and assuming an s-polarized light incoming at 45° is calculated. It shows a maximum of 56.5% given an "ideal" multilayer with no interaction between the layers and no interfacial roughness.[4] Because we suspect a possible interdiffusion and the formation of compounds at the metal–metal interfaces, we consider the introduction of boron carbide at one interface. This kind of barrier layer has proved its efficiency for numerous multilayer systems devoted to optics applications.[5,6] For the ideal Co/Mg/B_4C multilayer a maximum reflectance of 53.5% is calculated.[4]

For comparison, in the case of the Mg/SiC system, simulations of an "ideal" multilayer indicate a reflectance of about 60% at 30.4 nm and 20° off normal incidence using s-polarized light. But, reflectivity measurements at 30.4 nm demonstrate that the large value of the rms interfacial roughness (≥1 nm) is directly responsible for the limitation of the optical performances (*R* is only 40%).[7] This example has motivated us to explore other optimum material combinations, even systems where simulations predict a reflectance slightly lower than that of Mg/SiC provided that (i) the measured roughness remains moderate and (ii), as a consequence, the discrepancy between simulated and measured reflectance values is lower than in the case of Mg/SiC. Indeed, at 30.4 nm and near normal incidence, the Co/Mg system gives experimental performances of the same order of magnitude as the Mg/SiC system: 40% reflectivity and 1.3 nm bandwidth for Co/Mg; 45% reflectivity and 1.7 nm bandwidth for Mg/SiC.[8] In the same conditions, the Al/SiC and Mo/Si systems reach reflectance of only 17% and 22%, respectively,[9] and B_4C/Mo/Si reaches 32%.[10]

Multilayers are fabricated by magnetron sputtering and tested in the EUV range. They are characterized by X-ray reflectivity (XRR) in the hard X-ray range after their preparation to determine the thickness, roughness, and density of their layers. The introduction of thin boron carbide layers is also considered. The time stability of these structures is also studied over a duration of about 3 months. To determine if some interaction

* To whom correspondence should be addressed. Phone: 33 1 44 27 66 08. Fax: 33 1 44 27 62 26. E-mail: karine.le_guen@upmc.fr.

10.1021/jp911119z © 2010 American Chemical Society
Published on Web 03/19/2010

TABLE 1: Designed Structure of the Co/Mg and Co/Mg/B_4C Multilayers

multilayer	sample name	period d (nm)	d_{Co} (nm)	d_{Mg} (nm)	d_{B4C} (nm)	simulated reflectivity
Co/Mg	CoMg_1	8.00	2.55	5.45	–	–
	CoMg_2	17.00	2.55	14.45	–	56.5% @ 25.2 nm
Co/Mg/B_4C	CoMgB_4C_1	8.90	2.55	5.45	0.90	–
	CoMgB_4C_2	17.90	2.55	14.45	0.90	53.5% @ 25.8 nm

takes place between the layers, we look to the chemical state of the Mg and Co atoms present within the multilayer, by using X-ray emission spectroscopy (XES) and nuclear magnetic resonance (NMR). If there is some interdiffusion between the layers, the chemical state of the atoms of the interfacial layer is different from that of the atoms at the center of the layer. In this case, at least two chemical states of Mg and Co should be observed. The interest of combining XES and NMR is to obtain the information from both sides of the interface.

2. Experimental Section

2.1. Sample Preparation. The studied periodic Co/Mg and Co/Mg/B_4C multilayers were prepared by using a calibrated ultrahigh vacuum direct current magnetron sputtering system (JGP560C6, SKY Inc., China) with targets of Co (purity 99.95%), Mg (purity 99.98%), and B_4C (purity 99.5%) in Ar gas (99.999%). The targets are 100 mm in diameter. The base pressure was 10^{-4} Pa and the working pressure was 0.13 Pa of Ar gas. The power applied on the Co, Mg, and B_4C targets was set to 25, 15, and 80 W, respectively. The multilayers were all deposited onto 30 mm × 30 mm ultrasmooth polished Si substrates with rms surface roughness of 0.3 nm.

The description of the designed structure of each multilayered sample is summarized in Table 1. Each sample is made of 30 bilayers. The first layer on the substrate is the cobalt one. A 3.50-nm-thick capping layer made of B_4C is deposited at the surface of each sample in order to prevent oxidation: in the sample where 0.90-nm-thick B_4C layers enter in the composition of the periodic structure, the thickness of the capping layer is reduced to 2.60 nm.

The samples named CoMg_1 and CoMgB_4C_1, both characterized by a short period (8.00 and 8.90 nm, respectively), are dedicated to the X-ray emission spectroscopy analysis. Indeed, to be able to identify by means of XES the formation of an interfacial layer at the interface between two successive layers, the thickness of this interfacial layer should be comparable to that of the layer of the emitting atoms (Co layer for the Co L$\alpha\beta$ emissions and Mg layer for the Mg Kβ emission). The two remaining samples (namely CoMg_2 and CoMgB_4C_2) are designed to lead to the highest reflectivity value at the application wavelength. Thus, these two samples are analyzed by means of XRR in the EUV range. Moreover, the four samples have been studied by NMR spectroscopy in order to study the chemical state of the (magnetic) Co atoms.

2.2. X-ray Reflectivity at 0.154 nm. The structural quality of all these multilayers and the agreement between the aimed and effective thicknesses have been checked by using X-ray reflectivity at 0.154 nm (Cu Kα emission at 8048 eV). The measurements are made with use of a grazing incidence X-ray reflectometer (D1 system, Bede Ltd.) working in the $\theta-2\theta$ mode. The angular resolution is 5/1000°. Bragg law corrected for refraction was used to determine the multilayer period. The fit of the XRR curves performed with Bede Refs software (genetic algorithm)[11] was used to determine individual layer thickness, roughness, and layer density.

2.3. EUV Reflectivity. The measurement of the reflectivity curves in the EUV domain is performed on the BEAR beamline[12] at the Elettra synchrotron center using s-polarization. The photon energy is carefully calibrated by using the Pt $4f_{7/2}$ feature and the Si L edge. The goniometer angular resolution is 1/100°. Impinging and reflected photon intensities are measured by using a solid state photodiode. Incident intensities are monitored with an Au mesh inserted in the beam path whose drain current is used for normalization. The overall accuracy on the absolute reflectivity values is estimated to be about 1%.

2.4. X-ray Emission Spectroscopy. The X-ray emission analysis is performed in a high-resolution wavelength dispersive soft X-ray spectrometer.[13] The Mg Kβ and Co L$\alpha\beta$ emission coming from the magnesium and cobalt atoms present in the Co/Mg and Co/Mg/B_4C multilayered samples are analyzed. These emissions correspond to the Mg 3p−1s and Co $3d-2p_{3/2}$ and $3d-2p_{1/2}$ transitions respectively and are related to the occupied valence states having the Mg 3p and Co 3d character. These emissions are sensitive to the physicochemical state of the magnesium and cobalt atoms, respectively.[7,14]

The Mg 1s and Co 2p core holes are created by an electron beam coming from a Pierce gun. The energy of the incident electrons was chosen to be higher than the threshold of the studied emission (1303.4 and 778.8 eV for the Mg 1s and Co $2p_{3/2}$ binding energies, respectively). In the present case, the electron energy was 7.5 keV for the Mg Kβ emission and 3.5 keV for the Co L$\alpha\beta$ emissions. Following the ionization of the atoms present in the sample, characteristic X-rays are emitted,[15,16] then dispersed by a $(10\bar{1}0)$ beryl (for Mg Kβ emission) or TlAP (001) (for Co L$\alpha\beta$ emission) bent crystal and detected in a gas-flux counter working in the Geiger regime. The current density of the electrons reaching the sample is set to less than 1 $mA \cdot cm^{-2}$ to ensure that the shape and intensity of the studied emission remain constant throughout the measurements.

In the following, each presented emission spectrum is normalized with respect to its maximum and a linear background corresponding to the Bremsstrahlung contribution is subtracted. To determine the composition of the multilayers (especially to identify possible interfacial compounds), their emission spectrum is compared to that of reference compounds. This methodology is now routinely used to study complex materials.[6,17–24]

In the Co−C binary phase diagram, no compound arising from the reaction of the two materials is mentioned.[25] The region for the solubility of graphite in cobalt is limited to the 0−1% C range. On the contrary, the Co−B and Co−Mg binary phase diagrams exhibit the Co_3B, Co_2B, and CoB[27] and $MgCo_2$[27] compounds, respectively. In the Mg−B binary phase diagram, the MgB_2, MgB_4, and MgB_7 compounds are reported.[28] To our knowledge, the Co−B−C ternary diagram is not available in the literature. Among all these compounds, only MgB_2 was easily available: its Mg Kβ emission spectrum will be compared to that of the Co/Mg/B_4C multilayer. For the same emission, we have also considered as references a MgO single crystal cleaved along the (100) plane and a MgZn (Zn 1 wt %) dilute alloy. For that latter sample, we have carefully checked that its Mg Kβ emission spectrum is very close to that of the Mg metal.[29] In the case of the Co L$\alpha\beta$ emissions, a Co thin film deposited by magnetron sputtering is used as reference.

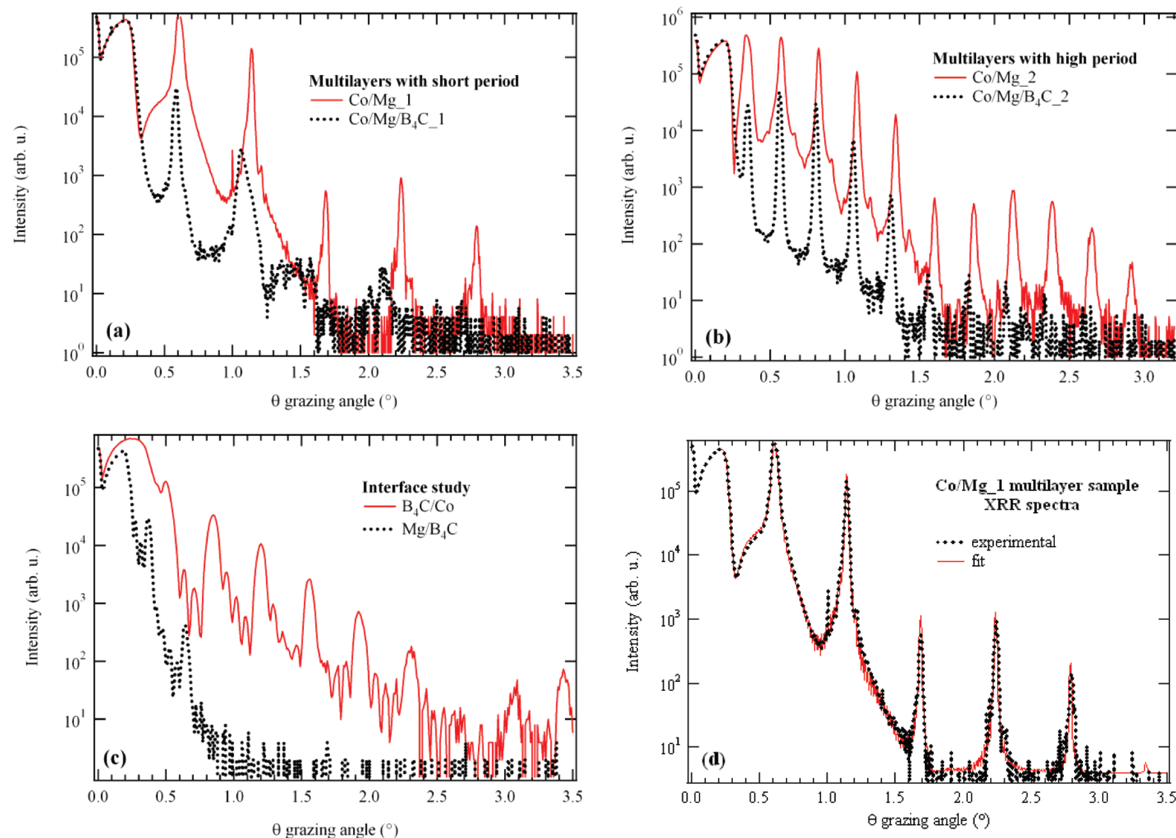

Figure 1. X-ray reflectivity curves measured at 0.154 nm: (a) Co/Mg_1 and Co/Mg/B_4C_1 samples; (b) Co/Mg_2 and Co/Mg/B_4C_2 samples; (c) B_4C/Co and Mg/B_4C multilayers deposited for thickness calibration purposes; and (d) fit of the reflectivity curve in the case of the Co/Mg_1 sample.

The Mg Kβ spectrum of the Mg_2CoH_5 compound has been observed.[30] We expect the electronic structure (and hence the X-ray spectrum) of a magnesium-rich Mg−Co compound to be close to that of this hydride. However, it is not easy to compare this measured spectrum to ours owing to a discrepancy concerning the photon energy calibration and a problem of oxidation of the sample.

2.5. Nuclear Magnetic Resonance Spectroscopy. Zero field NMR has been performed with a homemade automated broadband NMR spectrometer. For the sake of sensitivity all the samples were measured at 4.2 K since the NMR signal increases as the inverse of the measurement temperature. All spectra have been recorded for different values of radio frequency field strengths allowing for correcting the NMR intensities with a frequency dependent enhancement factor. Therefore the NMR spectra represent the distribution of Co atoms versus their resonance frequency (i.e. the hyperfine field experienced by their nuclei).[31,32] The NMR resonance frequency is sensitive to the local environment of the probed atoms: nearest neighbor local structure and/or local chemical environment.

Bulk reference samples consisting of 1% B and 1% Mg into Co have been measured to check the influence of the B and Mg neighborhood on the Co resonance frequency (hyperfine field). NMR lines at 117 and 170 MHz have been observed, respectively. According to the Co−B and Co−Mg phase diagrams, B and Mg do not mix easily with Co, therefore the observed NMR lines are likely to arise from Co_3B and Co_2Mg phases embedded into bulk Co.

3. Results and Discussion

3.1. X-ray Reflectivity at 0.154 nm. The reflectivity curves of the Co/Mg and Co/Mg/B_4C multilayers are presented in Figure 1 on a logarithmic scale. In Figure 1a, five well-defined and narrow Bragg peaks are observed for the CoMg_1 sample up to 3°; on the contrary, in the case of the CoMgB_4C_1 sample, up to 3°, only the first Bragg peak is narrow and well-defined while the three following Bragg peaks are large and not intense for the two last ones. In Figure 1b, all the Bragg peaks are narrow and well-defined. For the Co/Mg/B_4C_2 sample, nine Bragg peaks are seen up to 2.5°, whereas eleven Bragg peaks are observed up to 3° for the Co/Mg_2 sample. The Bragg peaks are more intense for Co/Mg_2 with respect to Co/Mg/B_4C_2. It is also observed, Figure 1a and b, that the intensity of the background decreases more rapidly for Co/Mg/B_4C samples with respect to Co/Mg samples. From these curves, it appears that the structural quality of Co/Mg multilayers is better than that of Co/Mg/B_4C multilayers. The comparison of the reflectivity curves, with and without B_4C layers, gives evidence that the introduction of B_4C does not improve the structural quality of the multilayers. This is probably due to an interaction between the B_4C layers and the metal layers.

For the CoMg_1 and CoMgB_4C_1 samples, the position of the Bragg peaks leads to a period value equal to 7.92 and 8.40 nm, respectively (see Table 2). The correction for refraction is taken into account in the calculation. For the CoMg_2 and CoMgB_4C_2 samples, the position of the Bragg peaks corresponds to a period value equal to 16.70 and 17.13 nm, respectively (see Table 2). In the case of the Co/Mg_1 and Co/Mg_2 samples, a good agreement exists between the aimed and experimental period values (difference of about 1%). On the contrary, for the CoMgB_4C_1 and CoMgB_4C_2 samples, the difference between the aimed and experimental values becomes significant (between 5 and 6%). The introduction of a B_4C layer within the multilayer structure decreases the period

TABLE 2: Variation over 108 Days of the Period Values Calculated Using the Refraction Corrected Bragg Law and Parameter Values Extracted from the Fit of the Co/Mg_2 Reflectivity Curve Measured at 0.154 nm[a]

sample	d (nm) period[b] $t = 0$	d (nm) period[b] $t = 108$ days	XRR fit d_{Co} (nm); d_{Mg} (nm)	XRR fit d(nm)	XRR fit σ_{Co} (nm); σ_{Mg} (nm)	XRR fit density ratios: Co (%); Mg (%)
CoMg_1	7.92	7.95	2.51; 5.44	7.95	0.56; 0.54	91 ± 5; 105 ± 5
CoMgB$_4$C_1	8.40	8.46	–	–	–	–
CoMg_2	16.70	16.71	2.63; 14.10	16.73	0.40; 0.40	102 ± 5; 100 ± 5
CoMgB$_4$C_2	17.13	17.17	–	–	–	–

[a] σ stands for the interfacial roughness. Corrected for refraction. [b] The period is calculated using the Bragg law corrected from refraction.

value (period contraction) due to a reaction between the B$_4$C layer and the metal layer.

To identify which interface, B$_4$C/Co or Mg/B$_4$C, is responsible for the poor reflectivity of the Co/Mg/B$_4$C stack, we compare in Figure 1c the reflectivity curves of the B$_4$C/Co and Mg/B$_4$C multilayers made of only 5 or 10 periods and the designed period was 15 nm for both samples. These two multilayers were prepared in a preliminary batch by using nonoptimized conditions to calibrate the deposited thicknesses. It is clearly seen that the Mg/B$_4$C system leads to a very low reflectivity, only two very weak Bragg peaks being observed. The first Bragg peaks of the B$_4$C/Co system are also weak with respect to the plateau before the total reflection. The number of bilayers of B$_4$C/Co is 10 while that of Co/Mg is 30 and as a consequence, all the Bragg peaks of the B$_4$C/Co multilayer are about three times broader, Figure 1c, than those of Co/Mg and Co/Mg/B$_4$C multilayers, Figure 1a and b. These observations indicate that the optical qualities of both B$_4$C/Co and Mg/B$_4$C are low, the Mg/B$_4$C interface being the worse one. Therefore, interface imperfections, including roughness and/or diffuseness, greatly limit the final Co/Mg/B$_4$C multilayer reflectivity.

To estimate the time stability of these samples, we have checked the reproducibility of the reflectivity measurements over a period of 108 days: the corresponding periods are also presented in Table 2. The different period values coincide within the experimental uncertainty demonstrating the good time stability of the Co/Mg stack. It would be necessary to measure the reflectivity of the multilayers over even a larger period of time because applications require stability over a few years.

To improve the description of the multilayer, the Co/Mg_1 and Co/Mg_2 reflectivity curves are fitted in order to estimate the values of the structural parameters of the stack: the thickness, roughness, and density of the various layers. The roughness deduced from the fit is an overall roughness including the contributions from both geometrical roughness and interdiffusion. These values are collected in Table 2. In that table, the density ratio (%) is defined as the density of the layer divided by the density of the bulk. As an illustration, Figure 1d shows the comparison between the experimental and fitted XRR curve in the case of the Co/Mg_1 sample. We do not fit the reflectivity of the CoMgB$_4$C_1 and CoMgB$_4$C_2 samples because of the large number of parameters and the probable reaction of the B$_4$C layer with the metal layer.

The values of the Co and Mg layer thickness are those of the designed structure for CoMg_1 while for CoMg_2, a slight difference exists between these values: compared to the design, the Co layer is about 3% thicker and the Mg layer about 3% thinner. In both cases, the period values are close to that calculated with the Bragg law corrected for refraction. For a given sample, the roughness values at both interfaces are comparable. The density values are given within a 5% uncertainty. For both samples, the layers are as dense as the bulk materials, except in the CoMg_1 sample where the Co layer is less dense than in the bulk. As a summary, the fitting results indicate that the deposited multilayered samples coincide in a satisfactory manner with those expected in the preparation step.

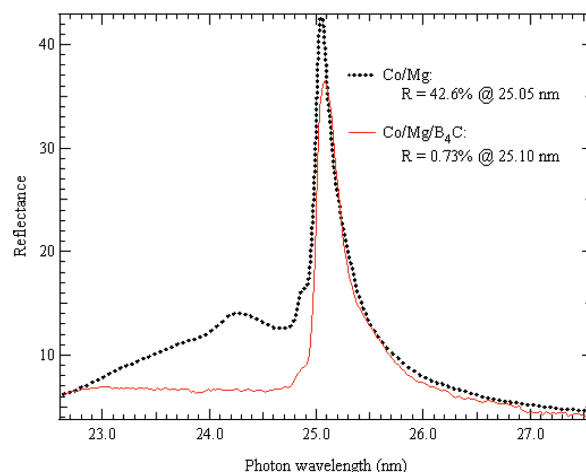

Figure 2. EUV reflectivity curves of the Co/Mg and Co/Mg/B$_4$C multilayers measured at 45°. The Co/Mg/B$_4$C curve is amplified 50 times.

3.2. EUV Reflectivity. The reflectivity curves of the Co/Mg_2 and Co/Mg/B$_4$C_2 multilayer samples measured at 45° and around the photon energy of 50 eV are presented in Figure 2 on a linear scale. The asymmetric shape of the two reflectivity curves is due to the presence of the Mg L edge (L$_2$ and L$_3$ edges at 49.78 and 49.50 eV respectively). Contrary to the CoMgB$_4$C_2 sample where, preceding the maximum value, the reflectivity remains constant, in the case of the CoMg_2 sample an additional structure centered around 24.3 nm (or 51 eV) is present.

The maximum of the CoMg_2 reflectivity curve is equal to 42.6% at 25.05 nm whereas that of the CoMgB$_4$C_2 sample is only 0.73% at 25.10 nm. In the case of the CoMg_2 sample, the measured value has to be compared to the simulated value (56.5% at 25.2 nm given an "ideal" multilayer: no interaction and no roughness at the interfaces). That is to say that the experimental value represents 75% of the simulated value, which is higher than in the case of the Mg/SiC system.[7] Moreover, for comparison, using the parameter values extracted from the fit of the CoMg_2 XRR curve measured at 0.154 nm (see Table 2) for reflectivity simulations in the EUV range, the reflectivity of this multilayer is calculated to be 27% at 25.2 nm at 45° of grazing incidence. The absence of agreement between this latter value and the measured value reflects the fact that, in the fitting procedure, the values retained for the structural parameters (thickness, roughness, and density of the layers) are not correctly optimized.

In the case of the CoMgB$_4$C_2 sample, the measured reflectivity curve demonstrates the poor quality of the multilayer in terms of optical performances. The introduction of a B$_4$C material at the Co-on-Mg interface does not contribute at all to

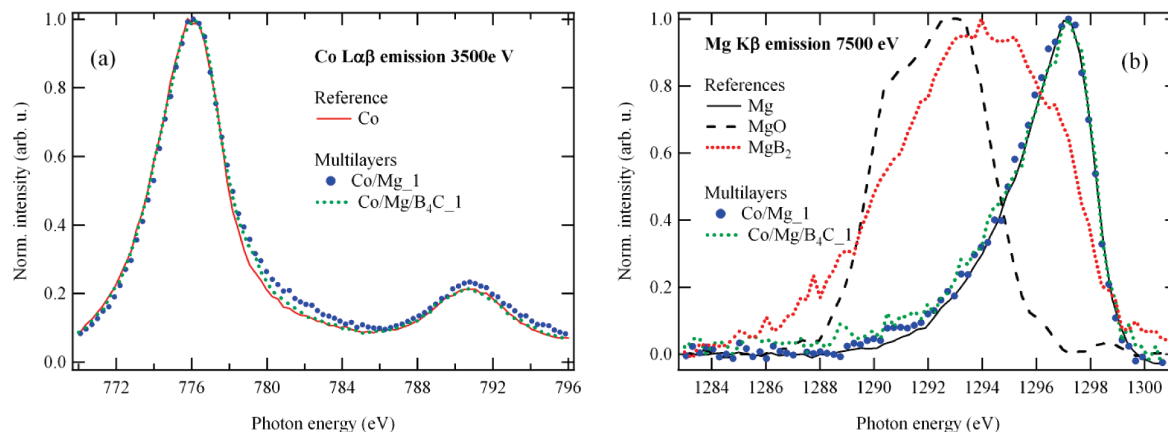

Figure 3. (a) Co L$\alpha\beta$ and (b) Mg Kβ emission bands originating from the references (Co (a) and Mg, MgO, and MgB_2 (b)) compared to those of the Co/Mg_1 and Co/Mg/B_4C_1 multilayer samples.

improve the quality of the interfaces, in contrast with the IMD simulations for an "ideal" multilayer (see Table 1). A reaction between the B_4C layer and the metallic layers could be responsible for this drastic drop of the reflectivity with respect to the Co/Mg system.

3.3. XES Analysis. The Co L$\alpha\beta$ emission spectrum originating from the Co reference is compared to that of the CoMg_1 and CoMgB_4C_1 multilayer samples in Figure 3a while the Mg Kβ emission spectrum originating from the references (Mg, MgO, and MgB_2) is compared to that of the CoMg_1 and CoMg/B_4C_1 multilayer samples in Figure 3b.

Concerning the Co L$\alpha\beta$ emission, Figure 3a, the spectra of the multilayers is close to that of the Co reference sample. From one sample to the other, the position of the Co Lα maximum does not vary by more than 0.3 eV. The position of the Co Lβ maximum remains constant for the three samples. The intensity ratio determined with the values of the maximum of the Co Lα and Lβ emission bands remains of the order of 0.2 for the three samples. As a consequence, the Co L$\alpha\beta$ emission band shapes are not sufficiently different from each other to enable us to discuss the formation of interfacial compounds between successive layers within the multilayers. The Co L$\alpha\beta$ emission is not sensitive enough to the physicochemical environment surrounding the emitting Co atoms. Our XES analysis will be essentially based on Mg Kβ experimental data.

For the Mg Kβ emission, Figure 3b, the multilayers spectra are rather similar to that of the Mg reference. Thus, this result allows us to say that, within the CoMg_1 and CoMgB_4C_1 samples, the Mg atoms are in a physicochemical state close to that of Mg atoms in the Mg metallic state. Nevertheless, we can try to gain further insight into the comparison of these spectra. In the high photon energy side, the multilayer spectra are both close to that of the Mg reference. On the contrary, in the low photon energy side, the shape of the multilayer spectra slightly differs from that of the Mg reference: a kind of tail is observed in the region where the respective maxima of the MgO and MgB_2 Mg Kβ emission spectra are present (1293 eV for MgO and 1294 eV for MgB_2). To infer the possible oxidation of the Mg atoms present within the multilayer, it is advisible to decrease the energy of the incident electrons: the analyzed depth becomes thinner and information about the layers close to the surface is provided.

In Figure 4 we study in the case of the CoMg_1 sample the change, as a function of the electron energy, of the shape of the Mg Kβ emission band. For an electron energy equal to 4.5 keV, the analyzed depth is estimated, using CASINO software,[33] to correspond to the 20 first Mg layers in Co/Mg, and recovers

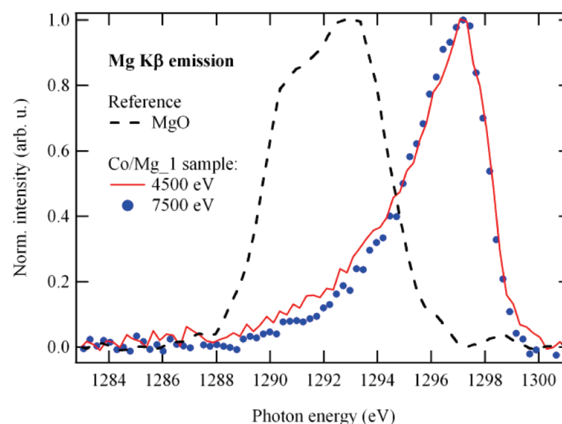

Figure 4. Change, as a function of the electron energy, of the shape of the Mg Kβ emission band originating from the Co/Mg_1 sample, compared to that of the MgO reference.

the all 30 Mg layers at 7.5 keV of electron energy. The tail observed in the Mg Kβ emission spectrum is more intense with electrons of energy equal to 4.5 keV. The same effect is also observed in the CoMgB_4C_1 sample (not shown). Thus the Mg atoms present within the two multilayers are slightly oxidized. In the case of the CoMgB_4C_1 sample, this result does not allow us to exclude that the Mg atoms can also slightly react with B atoms to form the MgB_2 compound.

Another explanation for the tail observed in the spectrum of the CoMg_1 sample could be that a Co−Mg compound forms at the interfaces of the multilayer. Indeed the experimental spectrum of $MgCo_2$ is not published and one could imagine that its maximum appears in the same region of the tail as that of MgO. We present in Figure 5 the Mg Kβ spectrum of the Mg and $MgCo_2$ compounds calculated from the first principles using the Wien2k software[34] compared to the experimental one originating from the Mg reference sample. The calculated spectrum is obtained from the Mg 3p density of states weighed by the transition probability and convoluted by a Lorentzian function to take into account the natural width of the Mg 1s level and by a Gaussian function to take into account the experimental broadening. The comparison for Mg metal shows that the calculation reproduces quite accurately the experiment. All the spectra are presented on an energy scale relative to the position of the Fermi level. The energy position of the maximum of the $MgCo_2$ emission band is about 0.4 eV higher than that of the Mg spectrum. More striking is the large width of the Mg emission band with respect to that of $MgCo_2$. From these calculations, we can affirm that, within our sensitivity, the

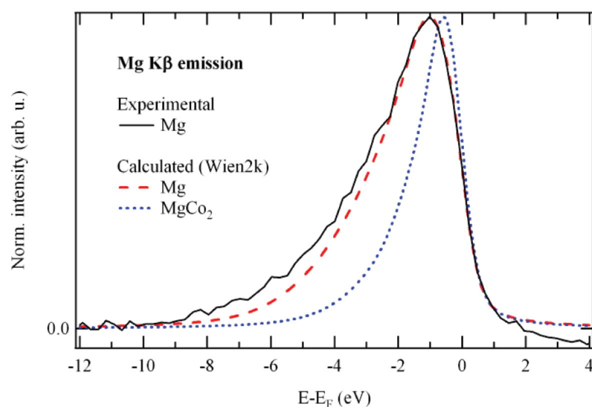

Figure 5. Comparison of the Mg Kβ emission band calculated for the Mg and $MgCo_2$ compounds by using Wien2k with that measured at 7500 V for the Mg reference sample. The energy scale refers to the position of the Fermi level E_F.

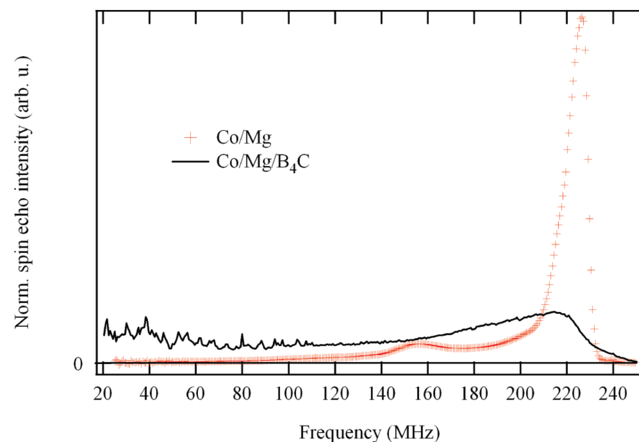

Figure 6. NMR spectra of Co/Mg and $Co/Mg/B_4C$ multilayers. The spectra surface areas are normalized to the same area.

possible formation of the $MgCo_2$ compound at the interfaces of the CoMg_1 and CoMgB4C_1 samples is not confirmed by XES. From comparison with transition metal silicides,[35] the same kind of narrow bandwidth spectrum is expected for other possible Co−Mg compounds that could form out of equilibrium: CoMg[36,37] or $CoMg_2$.[37,38]

3.4. NMR Analysis. NMR spectra obtained for the Co/Mg and $Co/Mg/B_4C$ multilayers are presented in Figure 6. To compare the shape of the spectra, their total surface area is normalized to one. The thickness of the Mg layers has no influence on the NMR spectra (neither in shape nor in intensity) and therefore on the sample structure; fore the sake of clarity one spectrum only of each type of sample is shown.

As can be seen, the shape of the spectra of the two kinds of samples is very different. The Co/Mg samples show a well-defined line at 226 MHz that is the fingerprint of bulk hcp Co. The Co atoms are mainly situated in pure Co layers and the intermixing at the Co/Mg interfaces is limited. An additional line is observed at 156 MHz. This line is at a frequency significantly different from the one observed for the CoMg1% reference sample (170 MHz) and has very probably a different origin. Actually the shape of the low-frequency part of the spectrum (below 210 MHz) looks very similar to the shape observed in multilayers with sharp interfaces,[31,32] but this interpretation is difficult to ascertain because of the lack of appropriate reference samples. However a tentative simulation with the step interface model[39] that is appropriate for samples with sharp interfaces is presented in Figure 7. The model

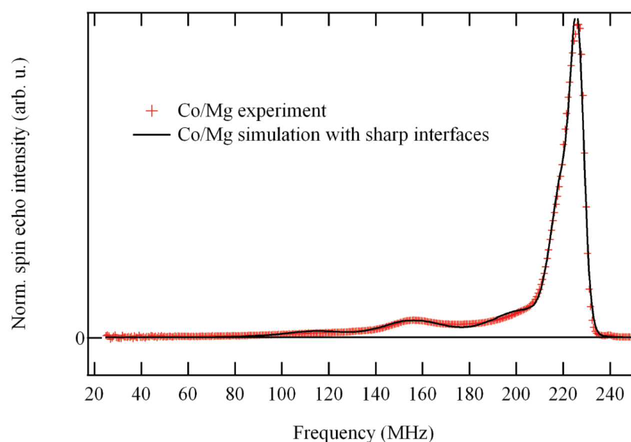

Figure 7. Simulation of the Co/Mg multilayer spectrum with a sharp interface model.

reproduces closely the experimental spectrum. It must be noted that in this model the ratio between the intensities of the interfacial part of the spectrum and the bulk part of the spectrum is not an adjusted parameter, but is fixed from the thickness of the deposited Co layers. This gives us confidence in our interpretation and suggests strongly that the Co/Mg multilayers present sharp interfaces.

In contrast, the shape of the $Co/Mg/B_4C$ spectra is very different. No Co bulk line is observed anymore. This shows that the Co layers are not pure but that alien atoms (Mg, B, or C) are mixed with Co. Since the Co/Mg multilayers show sharp interfaces the mixing is likely to originate from the Co/B_4C interfaces. The intermixing in the $Co/Mg/B_4C$ is more important than the one depicted by the change in spectra shape since the absolute integral intensity of the $Co/Mg/B_4C$ spectra is 3 times smaller than the intensity of the Co/Mg spectra. This means that two-thirds of the total Co atoms included in these samples are not observed in the $Co/Mg/B_4C$ NMR spectra. These Co atoms are most probably situated into non-ferromagnetic phases (and therefore give no NMR signal) with a large content of Mg, B, or C atoms. This confirms the large mixing observed by XRR in the $Co/Mg/B_4C$ samples.

The samples have been analyzed after a period of three months where they were stocked in a desiccator. No significant variation of the NMR signal is detected for both Co/Mg and $Co/Mg/B_4C$ systems. This confirms the reflectivity measurement in the hard X-ray range after 108 days for the Co/Mg multilayer.

4. Conclusion

The Co/Mg multilayers are promising for applications in the EUV range around 25 nm. A reflectivity of 46% at 45° angle is measured representing three-quarters of the ideal reflectivity, i.e. for a perfect multilayer without roughness and interdiffusion. This experimental value can be improved by increasing the number of bilayers within the stack and also by optimizing the deposition conditions and the capping layer. Thus, it is important to characterize in detail these kinds of nanometric multilayers. This was done in the present work by using X-ray reflectivity in the hard and soft X-ray ranges, X-ray emission spectroscopy, and nuclear magnetic resonance spectroscopy. The reflectivity measurements and their fit enable us to establish that the thicknesses of the various deposited layers are close to the aimed ones during the preparation. It was also deduced from these measurements that the interfacial roughness is less than 0.5 nm. XES and NMR spectra permit the determination of the chemical state of the Mg and Co atoms, respectively, at the interfaces.

They reveal no compound formation and abrupt interfaces. Thus the difference between the experimental and simulated reflectivity values can be ascribed to the interfacial roughness.

The introduction of thin boron carbide interfacial layers into the stack considerably degrades the EUV reflectance, leading to a poor value of less than 1%. From XES and NMR measurements, it is observed that it is the Co atoms that react with the B or C atoms of the carbide layers to form an interfacial compound while the Mg atoms seem undisturbed. It has not been possible to determine this compound due to the lack of reference compounds. We have shown that the Mg/B_4C system is worse (in terms of optical qualities) than the Co/B_4C system. From this simple fact, we could have deduced that within the trilayer, the Mg/B_4C interfaces were responsible of the very low reflectivity. However, this is not the case. From XES and NMR, we determine that it is the Co/B_4C interfaces that lead to the deterioration of the reflectivity. In fact within the multilayer, there is a competition between the Co and Mg atoms to react with the atoms of the B_4C layers and it appears that in the stack, the Co atoms are more reactive than the Mg ones. Thus, it is not possible to infer the properties of a trilayer system from the properties of bilayer systems.

The temporal stability of the Co/Mg and Co/Mg/B_4C multilayers has been checked over a period of about three months and reveals no significant deterioration of the reflectivity in the hard X-ray range as well as of the NMR signal. For applications, this stability has to be checked over longer periods of time. The thermal stability must be verified because the multilayers can be subjected to high thermal loads. In this case, it probably will be necessary to consider the introduction of an efficient diffusion barrier. This will be addressed in a forthcoming paper.

Acknowledgment. S. Nannarone, A. Giglia, and N. Mahne from the BEAR beamline at the ELETTRA synchrotron are thanked for their help during the measurements of EUV reflectivity. The authors from Tongji University are indebted to the National Natural Science Foundation of China (Granted No. 10825521).

References and Notes

(1) Yanagihara, M.; Yamashita, K. X-ray Optics. In *X-Ray Spectrometry: Recent Technological Advances*; Tsuji, K., Injuk, J., van Grieken, R., Eds.; John Wiley & Sons: Chichester, UK, 2004.

(2) PXRMS Multilayer Survey Results, http://henke.lbl.gov/cgi-bin/mldata.pl.

(3) Windt, D. L. *Comput. Phys.* **1998**, *12*, 360.

(4) Hu, M.-H.; Le Guen, K.; André, J.-M.; Jonnard, P.; Zhou, S. K.; Li, Ch.; Zhu, J. T.; Wang, Z. S. *AIP Conf. Proc.* 1221 (ICXOM 20, 2009).

(5) Braun, S.; Mai, H.; Moss, M.; Scholtz, R.; Leson, A. *Jpn. J. Appl. Phys.* **2002**, *41*, 4074.

(6) Maury, H.; Jonnard, P.; André, J.-M.; Gautier, J.; Roulliay, M.; Bridou, F.; Delmotte, F.; Ravet, M.-F.; Jérome, A.; Holliger, P. *Thin Solid Films* **2006**, *514*, 278.

(7) Maury, H.; Jonnard, P.; Le Guen, K.; André, J.-M.; Wang, Z.; Zhu, J.; Dong, J.; Zhang, Z.; Bridou, F.; Delmotte, F.; Hecquet, C.; Mahne, N.; Giglia, A.; Nannarone, S. *Eur. Phys. J. B* **2008**, *64*, 193.

(8) Windt, D. L.; Bellotti, J. A. *Appl. Opt.* **2009**, *48*, 4932.

(9) Zhu, J.; Zhou, S.; Li H.; Huang, Q.; Wang, Z.; Le Guen, K.; Hu, M.-H.; André, J.-M.; Jonnard, P. *Opt. Express*. Submitted for publication.

(10) Gautier, J.; Delmotte, F.; Roulliay, M.; Bridou, F.; Ravet, M.-F.; Jérome, A. *Appl. Opt.* **2005**, *44*, 384.

(11) Wormington, M.; Panaccione, C.; Matney, K.; Bowen, D. *Phil. Trans. R. Soc. London, Part A* **1998**, *357*, 2827.

(12) Nannarone, S.; Borgatti, F.; DeLuisa, A.; Doyle, B. P.; Gazzadi, G. C.; Giglia, A.; Finetti, P.; Mahne, N.; Pasquali, L.; Pedio, M.; Selvaggi, G.; Naletto, G.; Pelizzo, M. G.; Tondello, G. *AIP Conf. Proc.* **2004**, *708*, 450.

(13) Bonnelle, C.; Vergand, F.; Jonnard, P.; André, J.-M.; Staub, P. F.; Avila, P.; Chargelègue, P.; Fontaine, M.-F.; Laporte, D.; Paquier, P.; Ringuenet, A.; Rodriguez, B. *Rev. Sci. Instrum.* **1994**, *65*, 3466.

(14) Jonnard, P.; Vergand, F.; Bonnelle, C.; Orgaz, E.; Gupta, M. *Phys. Rev. B: Condens. Matter Mater. Phys.* **1998**, *57*, 12111.

(15) Azaroff, L. V. *X-ray Spectroscopy*; McGraw-Hill Inc.: New York, 1974.

(16) Bonnelle, C. *Annu. Rep. Prog. Chem., Sect. C: Phys. Chem.* **1987**, *84*, 201.

(17) Iwami, M.; Kusaka, M.; Hirai, M.; Tagami, R.; Nakamura, H.; Watabe, H. *Appl. Surf. Sci.* **1997**, *117*, 434.

(18) Kurmaev, E. Z.; Galakhov, V. R.; Shamin, S. N. *Crit. Rev. Solid State Mater. Sci.* **1998**, *23*, 65.

(19) Miyata, N.; Ishikawa, S.; Yanagihara, M.; Watanabe, M. *Jpn. J. Appl. Phys. Part 1* **1999**, *38*, 6476.

(20) Jarrige, I.; Jonnard, P.; Frantz-Rodriguez, N.; Danaie, K.; Bosseboeuf, A. *Surf. Interface Anal.* **2002**, *34*, 694.

(21) Galakhov, V. R. *X-Ray Spectrom.* **2002**, *31*, 203.

(22) Salou, M.; Rioual, S.; Ben Youssef, J.; Dekadjevi, D. T.; Pogossian, S. P.; Jonnard, P.; Le Guen, K.; Gamblin, G.; Rouvellou, B. *Surf. Interface Anal.* **2008**, *40*, 1318.

(23) Le Guen, K.; Gamblin, G.; Jonnard, P.; Salou, M.; Ben Youssef, J.; Rioual, S.; Rouvellou, B. *Eur. Phys. J.: Appl. Phys.* **2009**, *45*, 20502.

(24) Maury, H.; André, J.-M.; Le Guen, K.; Mahne, N.; Giglia, A.; Nannarone, S.; Bridou, F.; Delmotte, F.; Jonnard, P. *Surf. Sci.* **2009**, *603*, 407.

(25) Ohtani, H.; Hasebe, M.; Nishizawa, T. *Trans. Iron Steel Inst. Jpn.* **1984**, *24*, 857.

(26) Faria, M. I. S. T.; Leonardi, T.; Coelho, G. C.; Nunes, C. A.; Avillez, R. R. *Mater. Charact.* **2007**, *58*, 358.

(27) *Landolt-Börnstein*, New Series IV/5, subvolume C; Springer-Verlag: New York, 1993.

(28) Nayeb-Hashemi, A. A.; Clark, J. B. *Phase Diagrams of Binary Magnesium Alloys*; ASM International: Metals Park, OH, 1988; pp 43–46.

(29) Jonnard, P.; Le Guen, K.; Gauvin, R.; Le Berre, J.-F. *Microsc. Microanal.* **2009**, *15*, 36.

(30) Belin, E.; Gupta, M.; Zolliker, P.; Yvon, K. *J. Less-Common Met.* **1987**, *130*, 267.

(31) Meny, C.; Panissod, P. *Modern Magnetic Resonance*; Webb, G., Ed.; Springer: Heidelberg, Germany, 2006.

(32) Panissod, P.; Meny, C. *Appl. Magn. Reson.* **2000**, *19*, 447.

(33) Hovington, P.; Drouin, D.; Gauvin, R. *Scanning* **1997**, *19*, 1. Drouin, D.; Hovington, P.; Gauvin, R. *Scanning* **1997**, *19*, 20. Hovington, P.; Drouin, D.; Gauvin, R.; Joy, D. C.; Evans, N. *Scanning* **1997**, *19*, 29.

(34) Schwarz, K.; Blaha, P. *Comput. Mater. Sci.* **2003**, *28*, 259.

(35) Jarrige, I.; Capron, N.; Jonnard, P. *Phys. Rev. B* **2009**, *79*, 035117.

(36) Yoshida, M.; Bonhomme, F.; Yvon, K.; Fischer, P. *J. Alloys Compd.* **1993**, *190*, L45.

(37) Gennari, F. C.; Castro, F. J. *J. Alloys Compd.* **2005**, *396*, 182.

(38) Wang, Y. J.; Aizawa, T.; Nishimura, C. *Mater. Trans.* **2006**, *47*, 1052.

(39) Meny, C.; Panissod, P.; Loloee, R. *Phys. Rev. B* **1992**, *45*, 12269.

JP911119Z

Comparison of Mg-based multilayers for solar He II radiation at 30.4 nm wavelength

Jingtao Zhu,[1] Sika Zhou,[1] Haochuan Li,[1] Qiushi Huang,[1] Zhanshan Wang,[1,*] Karine Le Guen,[2] Min-Hui Hu,[2] Jean-Michel André,[2] and Philippe Jonnard[2]

[1]Institute of Precision Optical Engineering, Department of Physics, Tongji University, Shanghai 200092, China

[2]Laboratoire de Chimie Physique—Matière et Rayonnement, Université Pierre et Marie Curie, CNRS, UMR 7614, 11 rue Pierre et Marie Curie, F-75231 Paris Cedex 05, France

*Corresponding author: wangzs@mail.tongji.edu.cn

Received 16 March 2010; revised 14 June 2010; accepted 17 June 2010; posted 18 June 2010 (Doc. ID 125536); published 6 July 2010

Mg-based multilayers, including SiC/Mg, Co/Mg, B_4C/Mg, and Si/Mg, are investigated for solar imaging and a He II calibration lamp at a 30.4 nm wavelength. These multilayers were fabricated by a magnetron sputtering method and characterized by x-ray reflection. The reflectivities of these multilayers were measured by synchrotron radiation. Near-normal-incidence reflectivities of Co/Mg and SiC/Mg multilayer mirrors are as high as 40.3% and 44.6%, respectively, while those of B_4C/Mg and Si/Mg mirrors are too low for application. The measured results suggest that SiC/Mg, Co/Mg multilayers are promising for a 30.4 nm wavelength. © 2010 Optical Society of America

OCIS codes: 310.1620, 230.4170, 040.7480, 340.6720, 350.6090.

1. Introduction

The development of normal-incidence multilayer mirrors in the extreme ultraviolet (EUV) spectral region has enabled various applications in space observation, such as the construction of a new instrumentation relying on imaging optics for solar physics [1–7]. Such systems have been successfully used in a series of missions, such as the SOHO-EIT and TRACE satellites [8,9]. The multilayer mirrors for solar imaging are required to provide high reflectance of spectral line emissions from the solar corona, such as Fe IX (17.1 nm), Fe XII (19.5 nm), Fe XV (28.4 nm), and He II (30.4 nm) [5,7,10]. A narrow bandpass is also required in order to eliminate spectral interference in the resultant image.

In the EUV region, the Mo/Si material combination is widely used at wavelengths just longer than the Si L-edge near 12.4 nm. With high quality and excellent stability, Mo/Si multilayers have been successfully used in several satellite instruments for solar physics over the past two decades [5,8,9], However, the peak reflectance of Mo/Si falls gradually and the spectral bandpass becomes relatively wide, with the increasing absorption of Si at a longer wavelength range than Si L-edge. The reflectance of Mo/Si is only about 20% at 30.4 nm. Moreover, a Mo/Si multilayer has a high-intensity second-order reflectance peak, thus inducing spectral contamination [11]. Therefore, new high-reflectance multilayer mirrors are required for research at the wavelength of 30.4 nm.

Mg-based multilayers based on a combination of Mg layers and layers of another material can provide high reflectance only at wavelengths longer than the Mg L-edge at 25.2 nm. This has been confirmed by a Mg/SiC multilayer, with reflectance as high as 44% at 31.2 nm and a 10° incident angle [12,13]. Here we present results of some Mg-based multilayer reflective mirrors working at 30.4 nm, including Co/Mg, SiC/Mg, B_4C/Mg, and Si/Mg. All these multilayers were fabricated by direct-current magnetron sputtering technology, and characterized by grazing incident x-ray reflection (GIXR) and near-normal-incident EUV reflection.

0003-6935/10/203922-04$15.00/0
© 2010 Optical Society of America

2. Design and Calculation

After Mg was chosen as a spacer layer, some candidate materials were proposed as an absorbing layer. Based on Spiller's selection theorem [14], in the EUV region, SiC/Mg, B_4C/Mg, and Si/Mg combinations can provide high theoretical reflectance at 30.4 nm. Since the extinction coefficient of Co is larger than that of the other three materials, the reflectance of a Co/Mg multilayer is relatively low. But Co/Mg has also been researched for its smooth interface and quite excellent thermal stability [15,16]. Mg-based multilayers, including SiC/Mg, Co/Mg, B_4C/Mg, and Si/Mg, were designed for the He II emission line at 30.4 nm. Calculated reflection curves and layer thicknesses are shown in Fig. 1 and Table 1, respectively. The optical constants were obtained from the Center for X-Ray Optics website [17]. All the periodic multilayers are considered as ideal interface structures without roughness or diffusion. A 3.5 nm thick B_4C capping layer was deposited onto the surface of each sample to prevent oxidation. All multilayers were calculated with 30 bilayers using IMD software [18].

In Fig. 1, the reflection curve of the Mo/Si multilayer is low and wide. Moreover, there is a high-intensity second-order peak at the wavelength near 16 nm. Those of Mg-based multilayers are much higher and narrower at 30.4 nm. The second-order reflective peak is suppressed owing to the Mg L-edge at 25.2 nm. SiC/Mg, B_4C/Mg, and Si/Mg multilayers have quite high peak reflectance, higher than 56%. The Co/Mg combination has a relatively low reflectance, of 44.25%. The full width at half-maximum (FWHM) of all Mg-based multilayers is less than 2.0 nm, narrower than that of Mo/Si multilayers.

3. Experimental

All multilayers were prepared by an ultrahigh vacuum direct-current magnetron sputtering system (Model JGP560C, SKY Technology, China). The vacuum chamber is pumped by a turbomolecular system, and the base pressure before deposition was 8.0E − 5 Pa. The sputtering gas is argon (99.9999% purity) at a constant pressure of 1.0 mTorr (0.13 Pa). Circular targets with 100 mm diameter were used. The sputtering cathodes work at a regulated power mode. The sputtering targets were Co (99.95% purity), SiC (99.5% purity), B_4C (99.5% purity), Si (99.999% purity), Mg (99.95% purity), and Mo (99.5% purity). All multilayers were deposited onto ultrasmooth polished silicon (100) wafers (20 mm × 30 mm). The surface roughness of the silicon substrate is 0.3 nm [root mean square (rms)]. Layer thicknesses were controlled by varying the time that the substrate stayed over the sputtering targets.

After deposition, grazing incident x-ray reflection measurements were made in the θ–2θ reflection geometry mode, using an x-ray diffractometer working at the Cu K-α line (0.154 nm). The Bragg law, modified to take into account the refraction, was used to calculate the multilayer period thickness. EUV reflectance measurements were made at a 10° incident angle, using the reflectometer at the Spectral Radiation Standard and Metrology Beamline and Station (beamline U26) at the National Synchrotron Radiation Laboratory in Hefei, China. The monochromator is a 600 lines/mm grating with a spectral resolution

Table 1. Calculated Peak Reflectance and FWHM ($\Delta\lambda$) of Mg-Based and Mo/Si Multilayers Shown in Fig. 1

Multilayer	Layer Thickness (nm)	Peak Reflectivity (%)	$\Delta\lambda$ (nm)
B_4C/Mg	4.22/11.61	58.22	1.93
Si/Mg	6.35/9.52	56.40	1.30
SiC/Mg	4.21/11.59	56.34	1.72
Co/Mg	2.67/13.01	44.25	1.42
Mo/Si	3.06/13.65	28.81	3.19

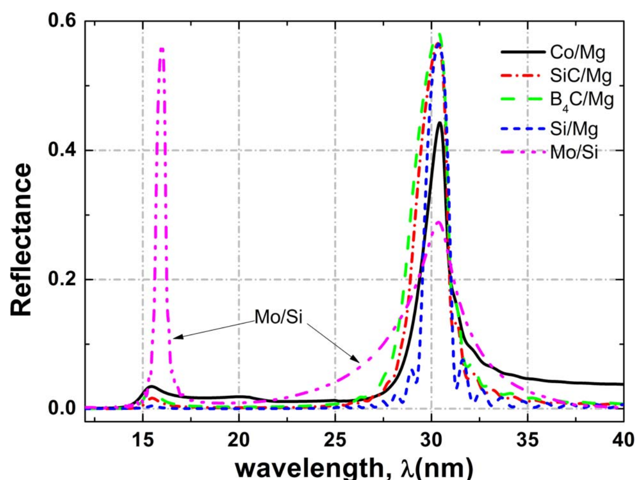

Fig. 1. (Color online) Calculated reflectance as a function of wavelength of Mg-based and Mo/Si multilayers designed for high reflectance at the He II ($\lambda = 30.4$ nm) emission line. (All calculations are made at 10° from normal incidence for 30 bilayer ideal multilayer structures.)

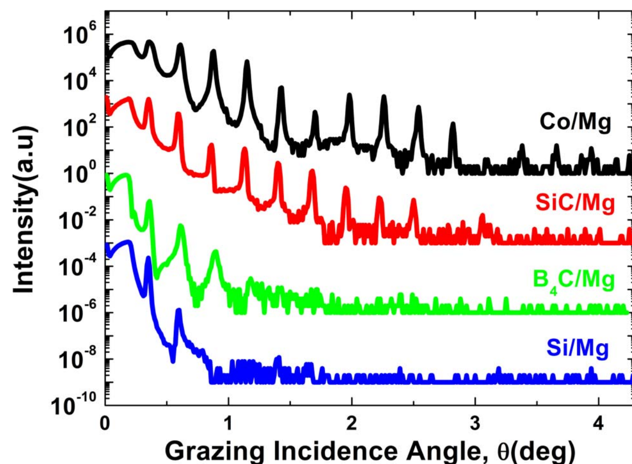

Fig. 2. (Color online) X-ray reflectance versus grazing incidence angle of Mg-based multilayers deposited according to the design in Table 1. Each curve shifted vertically by 3 orders of magnitude for better discrimination.

Table 2. Measured Peak Reflectance, Bandwidth, and Fitted Parameters of Mg-Based and Mo/Si Multilayers at 30.4 nm Shown in Fig. 3

Multilayer	Reflectance (%)	$\Delta\lambda$ (nm)	Periodic (nm)	$\Gamma_{Mg(Si)}$	σ (nm)	σ (nm)
SiC/Mg	44.6	1.74	15.98	0.66	$1.1(\sigma_{\text{Mg-on-SiC}})$	$1.3(\sigma_{\text{SiC-on-Mg}})$
Co/Mg	40.3	1.32	15.76	0.85	$0.5(\sigma_{\text{Mg-on-Co}})$	$0.5(\sigma_{\text{Co-on-Mg}})$
Si/Mg	5.6	1.35	15.72	—	—	—
B_4C/Mg	0.2	1.85	15.34	—	—	—
Mo/Si	23.7	3.11	16.46	0.84	$0.5(\sigma_{\text{Si-on-Mo}})$	$0.6(\sigma_{\text{Mo-on-Si}})$

($\lambda/\Delta\lambda$) higher than 192. A magnesium filter was inserted into the incident light beam.

4. Results and Discussion

Figure 2 shows the GIXR measurement curves of Mg-based multilayer mirrors. The curves have been shifted vertically for better comparison. Periodic thicknesses calculated from GIXR data are 15.8, 16.0, 15.3, and 15.7 nm for Co/Mg, SiC/Mg, B_4C/Mg, and Si/Mg, respectively. Co/Mg and SiC/Mg curves showing sharp Bragg peaks indicate clear interfaces of multilayer mirrors. However, the poor Bragg peaks of B_4C/Mg and Si/Mg curves cannot be considered as absolute evidence of poor interface structures, because comparison of GIXR curves (especially Bragg peak intensities and number of Bragg peaks) from multilayers consisting of high-density/low-density materials (such as Co/Mg and SiC/Mg) and low-density/low-density materials (such as B_4C/Mg and Si/Mg) is very complicated. For hard x-ray incidence onto a multilayer made of a low-density/low-density material combination, the Bragg peaks are weak because of the low contrast during hard x-ray interaction with low-density matter. So, the EUV reflectance measurements are required to further characterize the Mg-based multilayer mirrors.

The EUV reflectance measurements results are shown in Fig. 3 (the Mo/Si multilayer mirror was measured at the incident angle of 5°). As expected, the Mo/Si multilayer mirror gives a reflectance of 23.7% and the widest bandwidth of 3.11 nm. Although it has lower reflectance in theory, the Co/Mg multilayer mirror shows a rather high measured reflectance. The peak reflectance of Co/Mg is 40.3% at 30.5 nm. SiC/Mg has measured peak reflectance of 44.6% at 30.3 nm. The peak reflectance of the Si/Mg and B_4C/Mg multilayer mirrors are only 5.6% and 0.2%, respectively. Their poor reflectances absolutely indicate the poor interface structure in multilayer mirrors. We also investigated the interface structures of B_4C/Mg using x-ray emission spectroscopy and nuclear magnetic resonance spectroscopy measurement (not shown here). The results suggest no change of the chemical state of the Mg atoms and B_4C atoms in Mg/Co/B_4C multilayers [16]. The poor performance of B_4C/Mg and Si/Mg multilayer mirrors is probably due to their imperfect interface structures resulting from intermixing. This will be studied in the future. Calculated and experimental results show that SiC/Mg and Co/Mg multilayers are promising material combinations at the 30.4 nm wavelength.

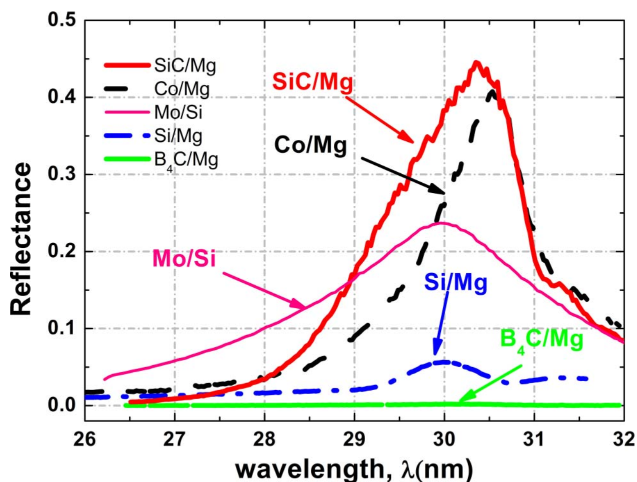

Fig. 3. (Color online) Measured reflectance versus wavelength of Mg-based multilayers at 10° incident angle by synchrotron radiation.

The measured reflectance curves were fitted by Levenberg–Marquardt algorithm using the IMD software [18] (fitted curves were not shown here). Fitting results are listed in Table 2. The imperfect interfaces of Si/Mg and B_4C/Mg multilayer mirrors are too severe to be fitted. The fitted period thickness of the Co/Mg multilayer is 15.76 nm, with a thickness ratio of $\Gamma_{Mg} = 0.85$ (Γ_{Mg} is defined here as d_{Mg}/d_{period}), and an interface width (σ) of 0.5 nm. For SiC/Mg, the fitted result suggests that the periodic thickness and Γ_{Mg} are 16.0 nm and 0.66, respectively. Interface widths (σ) are 1.1 nm for $\sigma_{\text{Mg-on-SiC}}$ and 1.3 nm for $\sigma_{\text{SiC-on-Mg}}$, which are much larger than those of the Co/Mg multilayer, resulting in a lower measured reflectance compared to the theoretical value. This indicates that the interface of Co/Mg is much better than that of SiC/Mg.

Only multilayer mirrors with great stability to heat can be used in outer space. Takenaka [13] studied the stability of SiC/Mg and concluded that the reflectance changed little to a temperature of 300 °C in an argon atmosphere. Reference [19] showed that SiC/Mg multilayer was thermally stable with no heating above 200 °C under their experimental condition. Space environment experiments will be carried out to investigate the stability of SiC/Mg and Co/Mg multilayer mirrors.

5. Summary

For solar observation by selecting the He II emission line, we designed, prepared, and characterized Co/Mg, SiC/Mg, B_4C/Mg and Si/Mg multilayer mirrors.

The Co/Mg multilayer provides measured reflectance of 40.3% and a sharp interface with a width of only 0.5 nm. The measured reflectance of the SiC/Mg multilayer is 44.6%. The interface widths (σ) are 1.1 nm for $\sigma_{\text{Mg-on-SiC}}$ and 1.3 nm for $\sigma_{\text{SiC-on-Mg}}$, worse than those of Co/Mg. Si/Mg and B_4C/Mg multilayer mirrors show a reflectance too low to be used in practice. The experimental results indicate that the Co/Mg and SiC/Mg multilayer mirrors are promising for EUV solar imaging at the 30.4 nm wavelength.

The authors are indebted to Hongjun Zhou and Tonglin Huo at National Synchrotron Radiation Laboratory, China, for their help in EUV reflectance measurements. This work is supported by the 863 Program of China (2006AA12Z139), the National Natural Science Foundation of China (NSFC) (10825521, 10905042, and 10876023), the Shanghai Commission of Science and Technology (SCST), China (09XD1404000, 07DZ22302, 09ZR1434300, and 0952nm06900), the Shanghai Municipal Education Commission, the Shanghai Education Development Foundation (Chen Guang 2008CG25), and the Young Talents Foundation of Tongji University.

References

1. M. Grigonis and E. J. Knystautas, "C/Si multilayer mirrors for the 25–30 nm wavelength region," Appl. Opt. **36**, 2839–2842 (1997).
2. L. Gardner, J. Kohl, S. Cranmer, S. Fineschi, L. Golub, J. Raymond, P. L. Smith, L. Strachan, R. Howard, D. Moses, D. Socker, D. Wang, R. R. Fisher, J. Davila, C. St. Cyr, G. Noci, M. Romoli, G. Tondello, G. Naletto, P. Nicolosi, and L. Poletto, "The advanced solar coronal explorer mission (ASCE)," Proc. SPIE **3764**, 134–146 (1999).
3. W. T. Thompson, "UV detectors aboard SOHO," Proc. SPIE **3764**, 196–208 (1999).
4. M. F. Ravet, F. Bridou, X. Zhang-Song, A. Jerome, F. Delmotte, R. Mercier, and M. Bougnet, "Ion beam deposited Mo/Si multilayers for EUV imaging application in astrophysics," Proc. SPIE **5250**, 99–108 (2004).
5. D. L. Windt, S. Donguy, J. Seely, B. Kjornrattanawanich, E. M. Gullikson, C. C. Walton, L. Golub, and E. DeLuca, "EUV multilayers for solar physics," Proc. SPIE **5168**, 1–11 (2004).
6. M. Suman, M. G. Pelizzo, D. L. Windt, and P. Nicolosi, "Extreme-ultraviolet multilayer coatings with high spectral purity for solar imaging," Appl. Opt. **48**, 5432–5437 (2009).
7. J. T. Zhu, Z. S. Wang, Z. Zhang, F. L. Wang, H. C. Wang, W. J. Wu, S. M. Zhang, D. Xu, L. Y. Chen, H. J. Zhou, T. L. Huo, M. Q. Cui, and Y. D. Zhao "High reflectance multilayer for He-II radiation at 30.4 nm," Appl. Opt. **47**, C310–C314 (2008).
8. http://umbra.nascom.nasa.gov/eit.
9. http://trace.lmsal.com.
10. T. Murachi, I. Yoshikawa, H. Takenaka, and S. Ichimaru, "Characteristics of SiC/Mg multilayer mirrors," Proc. SPIE **5900**, 59001A (2005).
11. E. N. Ragozin, K. N. Mednikov, A. A. Pertsov, A. S. Pirozhkov, A. A. Reva, S. V. Shestov, A. S. Ul'yanov, and E. A. Vishnyako, "Spectroscopic characterization of novel multilayer mirrors intended for astronomical and laboratory applications," Proc. SPIE **7360**, 73600N (2009).
12. H. Takenaka, S. Ichimaru, T. Ohchi, and E. M. Gullikson, "Soft-x-ray reflectance and heat resistance of SiC/Mg multilayer," J. Electron Spectrosc. Relat. Phenom. **144–147**, 1047–1049 (2005).
13. T. Ejima, A. Yamazaki, T. Banse, K. Saito, Y. Kondo, S. Ichimaru, and H. Takenaka, "Aging and thermal stability of Mg/SiC and Mg/Y_2O_3 reflection multilayers in the 25–35 nm region," Appl. Opt. **44**, 5446–5453 (2005).
14. E. Spiller, "Reflective multilayer coatings for the far UV region," Appl. Opt. **15**, 2333–2338 (1976).
15. N. Sato, "Structure and magnetism of transition-metal-magnesium thin films with an artificially layered structure," J. Appl. Phys. **64**, 4113–4122 (1988).
16. K. Le Guen, M.-H. Hu, J.-M. André, P. Jonnard, S. K. Zhou, H. Ch. Li, J. T. Zhu, and Z. S. Wang, "Development and interfacial characterization of Co/Mg periodic multilayers for the EUV range," J. Phys. Chem. C **114**, 6484–6490 (2010).
17. http://henke.lbl.gov/optical_constants/.
18. D. L. Windt, "IMD—software for modeling the optical properties of multilayer films computers in physics," Comput. Phys. **12**, 360–370 (1998).
19. H. Maury, P. Jonnard, K. Le Guen, J.-M. André, Z. Wang, J. Zhu, J. Dong, Z. Zhang, F. Bridou, F. Delmotte, C. Hecquet, N. Mahne, A. Giglia, and S. Nannaronne, "Thermal cycles, interface chemistry and optical performance of Mg/SiC multilayer," Eur. Phys. J. B **64**, 193–199 (2008).

Investigation of the thermal stability of Mg/Co periodic multilayers for EUV applications

M.-H. Hu[1], K. Le Guen[1], J.-M. André[1], S. K. Zhou[2], H. Ch. Li[2], J. T. Zhu[2], Z. S. Wang[2], C. Meny[3], N. Mahne[4], A. Giglia[4], S. Nannarone[4,5], I. Estève[6], M. Walls[7], P. Jonnard[1]

(1) Laboratoire Chimie Physique – Matière Rayonnement, UPMC Univ Paris 06, CNRS UMR 7614, 11 rue Pierre et Marie Curie, F-75231 Paris cedex 05, France

(2) Institute of Precision Optical Engineering, Department of Physics, Tongji University, Shanghai 200092, P.R. China

(3) Institut de Physique et Chimie des Matériaux de Strasbourg, CNRS UMR 7504, 23 rue du Loess, BP 43, F-67034 Strasbourg cedex 2, France

(4) CNR-IOM Laboratorio TASC, SS 14 km 163,5, I-34149 Basovizza, Trieste, Italy

(5) Università di Modenae R.E., Dipartimento Ingegneria Materiali, viaVignolese 905/a, Modena, Italy

*(6)*Institut de Minéralogie et de Physique des Milieux Condensés, Univ Paris 06 et 07, CNRS UMR 7590, 4 place Jussieu, F-75252 Paris Cedex 05, France

(7) Laboratoire de Physiques des Solides, CNRS UMR 8502, Univ Paris Sud, F-91405 Orsay, France

AUTHOR EMAIL ADDRESS philippe.jonnard@upmc.fr

TITLE RUNNING HEAD Thermal stability of Mg/Co multilayers

Accepted by : Appl Phys A: Materials Science & Processing, in press.

ABSTRACT

We present the results of the characterization of Mg/Co periodic multilayers and their thermal stability for the EUV range. The annealing study is performed up to a temperature of 400°C. Images obtained by scanning transmission electron microscopy and electron energy loss spectroscopy clearly show the good quality of the multilayer structure. The measurements of the EUV reflectivity around 25 nm (~49 eV) indicate that the reflectivity decreases when the annealing temperature increases above 300°C. X-ray emission spectroscopy is performed to determine the chemical state of the Mg atoms within the Mg/Co multilayer. Nuclear magnetic resonance used to determine the chemical state of the Co atoms and scanning electron microscopy images of cross sections of the Mg/Co multilayers reveal changes in the morphology of the stack from an annealing temperature of 305°C. This explains the observed

[1] Corresponding author: Dr. Philippe Jonnard, Laboratoire Chimie Physique – Matière et Rayonnement, tel: 33 1 44 27 63 03; fax: 33 1 44 27 62 26

reflectivity loss.

KEYWORDS annealing, interface, multilayer, Mg, Co, scanning transmission electron microscopy, electron energy loss spectroscopy, EUV reflectivity, nuclear magnetism resonance, x-ray emission spectroscopy, scanning electron microscopy

1. Introduction

In the extreme ultraviolet (EUV) range, highly efficient periodic multilayers are widely used in many fields such as X-ray space telescopes, EUV lithography or X-ray laser facilities. The previous measurements of the optical and interface properties of the Mg/Co multilayer [1, 2] show that this multilayer is promising for future applications in the wavelength range close to the Mg L edge around 25 nm (or a photon energy of 50 eV) and in particular for the observation of the 30.4 nm He II emission [3]. In the 25 nm range, a reflectivity of about 43% is measured at 45° for *s*-polarized radiation.

Another important property often required for multilayer devices is their thermal stability. In fact multilayers can be subject to high thermal loads, for example, when in use in space telescopes where they needs to withstand the high temperature space environment. Systems already investigated in this context include Mg/SiC [4, 5] which is thermally stable for applications only up to 200°C and also on more stable systems such as Mo/Si, Mo/C and Fe/Al, etc. [6-11] and more recntly Mo/B_4C [12].

The present work examines Mg/Co multilayers and their thermal stability by studying interdiffusion, interfacial compound formation and roughness development. From the phase diagram, the Mg-Co system is stable in the solid state up to a high temperature. The only possible compound is Co_2Mg. In this work, we study Mg/Co multilayer samples prepared by magnetron sputtering and then annealed up to 400°C, under ultra-high vacuum. Scanning transmission electron microscopy (STEM) images and electron energy loss spectroscopy (EELS) give direct evidence of the quality of the layers of the unannealed multilayer. The measurements of the EUV reflectivity around 25 nm (~49 eV) indicate the optical property of the multilayers. X-ray emission spectroscopy (XES) and nuclear magnetic resonance (NMR) are performed to determine the chemical state of the Mg and Co atoms within the Mg/Co multilayer, respectively. The interest of combining XES and NMR is to obtain the information from both sides of the interfaces. Scanning electron microscopy (SEM) checks the changes of the interface morphology as a function of the annealing temperature.

2. Experimental Section

2.1 Samples

Following the multilayer design resulting from simulations [13], we prepared two sets of Mg/Co

multilayers with different periods, Mg/Co_1 and Mg/Co_2 whose parameters are given in Table 1. They were both deposited onto ultra-smooth polished Si substrates (30 mm × 40 mm) by an ultrahigh vacuum direct current magnetron sputtering deposition system (Model JGP560C, SKY Technology, China) using Co (99.95% purity) and Mg (99.98% purity) targets. The sample preparation was done at a base pressure of 1×10^{-4} Pa. The working gas is argon (99.999% purity) at a constant working pressure 0.13 Pa. The number of periods is 30. In order to prevent oxidation, both multilayers are capped with a 3.5 nm thick B_4C layer. For Mg/Co_2, we cut the 15 mm × 15 mm sample into six small pieces of size 7.5 mm × 5 mm in order to do the annealing at different temperatures.

Table 1. Designed structures of the Mg/Co multilayers.

Sample name	Period d (nm)	d_{Co} (nm)	d_{Mg} (nm)	Simulated reflectivity	Size (mm^2)	Experimental	Annealing
Mg/Co_1	8.00	2.55	5.45	-	10×10 4×6	XES NMR	Yes Yes
Mg/Co_2	17.00	2.55	14.45	56.7% @ 25.2 nm	15×15 7.5×5 7.5×5	STEM / EELS EUV reflectivity SEM	No Yes Yes

We characterized the Mg/Co_2 unannealed multilayer after its preparation by measuring its the reflectivity at 0.154 nm of [1]. The structural parameters of the Mg/Co_2 multilayer, deduced from the fit of the reflectivity curve, show a good agreement between the aimed and effective thicknesses of the layers and an interfacial roughness of Co-on-Mg and Mg-on-Co layers which are 0.5 and 0.6 nm, respectively.

To investigate the thermal stability of Mg/Co periodic multilayers, all the Mg/Co multilayers were annealed at 280, 305 and 400°C for one hour centre in the preparation chamber of the BEAR beamline [14] at the Elettra synchrotron. The base pressure is 1×10^{-8} Pa. All samples were annealed for one hour. The EUV reflectivity measurements were made *in situ*, that is to say that the sample remained in a UHV environment. The XES, NMR and SEM measurements were done *ex situ* after transferring the samples in air.

The Mg/Co_2 unannealed sample is dedicated to the STEM / EELS (Table 1) analysis. The Mg/Co_2 annealing samples are dedicated to the reflectivity measurement in the EUV range and SEM studies in order to characterize the optical properties and the morphology of the multilayers,

respectively. Then the set of Mg/Co_1 annealing samples, which is characterized by a short period, is dedicated to the XES and NMR analysis in order to study the chemical state of the Mg and Co atoms, respectively. Indeed, to be able to identify the formation of an interfacial layer at the interface between two successive layers, the thickness of this interfacial layer should be comparable to that of the layer of the emitting atoms.

2.2 Scanning transmission electron microscope and electron energy loss spectroscopy

The lamella of the cross section of the unannealed Mg/Co_2 multilayer was examined by STEM and EELS. A Nion Ultrastem 100 operating at 100 kV and under ultra-high vacuum was used for these observations. The spherical aberration-corrected probe size was around 0.1 nm. The images are generated by scanning the focused beam over the lamella. Both energy-loss spectra and high angle annular dark field (HAADF) images can be collected simultaneously, which makes the STEM a good technique for materials morphological and chemical characterization at the sub-nanometer level. We used a probe convergence angle of 35 mrad and a collection angle for the EELS spectrometer of 50 mrad. Spectra were acquired with a dispersion of 1 eV per channel (with a 1024 channel camera) to have access simultaneously to the Co-L edge (779 eV) and the Mg K edge (1305 eV). The HAADF collection range was 75 to 200 mrad.

2.3 EUV reflectivity

The EUV reflectivity curves were measured on the BEAR beamline of the Elettra synchrotron facility using *s*-polarized light. The absolute uncertainty of the reflectivity values was about 1%. The photon energy was calibrated with respect to the Pt $4f_{7/2}$ and Si L with an accuracy of 0.1 eV. The intensities of incident and reflected radiation were measured with a solid state photodiode. The incoming photon flux was also monitored using an Au mesh inserted into the beam path, whose drain current was used for normalization.

2.4 Nuclear magnetic resonance spectroscopy

In order to probe the chemical state of the Co atoms within the multilayers, the samples have been analyzed by zero field NMR. The experiment was performed at 4.2 K using an automated frequency scanning broadband spectrometer with phase coherent detection [15]. The NMR spectra represent the distribution of Co atoms versus their resonance frequency [16]. The NMR frequency is strongly dependent on the number and nature of atoms in its neighborhood and also possibly on the symmetry of this neighborhood.

2.5 X-ray emission spectroscopy

We have performed XES with a high-resolution wavelength dispersive spectrometer [17] to identify the chemical state of the Mg atoms within the multilayers. Similar studies have already been performed by this method [18-26]. We observed the shape of the Mg Kβ emission band from the 3p–1s transition which describes the Mg 3p valence states. They are sensitive to the chemical state of the Mg atoms [27, 28]. The energy of the incident electrons used to produce the ionizations necessary to induce the electron transitions was set to 7.5 keV. The electron beam comes from a Pierce gun. Following the ionization of the atoms present in the sample, characteristic x-rays were emitted [29, 30], then dispersed by a (100) bent beryl crystal. The radiation was detected in a gas-flux counter working in the Geiger regime. The spectra of the multilayers were compared to the references, Mg metal and MgO.

2.6 Scanning electron microscopy and focused ion beam

Lamellae of the cross section of the Mg/Co_2 multilayers were prepared by FIB (Focused Ion Beam) / SEM CrossBeam® workstation NEON40EsB (Carl Zeiss). The FIB/SEM system, combination of a scanning electron microscope and a Ga^{+} ion beam, allowed a precise and located milling by sputtering of material with a simultaneous accurate observation. This FIB/SEM workstation is also equipped with an *in situ* gas injection system loaded with platinum gas precursor.

We first deposited a thin carbon rich platinum film (about 15 nm thick) with the electron beam to protect the sample surface against ion-beam damage. Then a 1 µm thick platinum layer was deposited with the ion beam. A first cross section of the multilayers is cut and observed by SEM. A lamella, whose size was approximately 10 µm × 4 µm with a thickness of 1 µm, was excavated, lifted-out *in situ* using a micromanipulator and glued to a copper half TEM grid. Finally, the lamella was polished to a thickness of 60 nm, giving the electron transparency needed for TEM. However, further thinning to about 30 nm in a Gatan PIPS system operating at 1 kV was found to be necessary for the high resolution imaging and EELS experiments.

3. Results and discussion

3.1 Samples without annealing

Figure 1 shows us the overall view of STEM images of the unannealed Mg/Co_2 multilayer as prepared by FIB. We can clearly distinguish the multilayer structures: from top to bottom are the substrate, the 30 periods multilayer and the Pt protection layer. The figure shows us the multilayer of good quality and the layers are smooth. The diffuse nature of the interfaces is probably mostly due to loss of resolution due to multiple scattering in the thicker parts of the TEM sample (which happens here

to be mainly in the lower part of the figure, in the layers nearest the substrate).

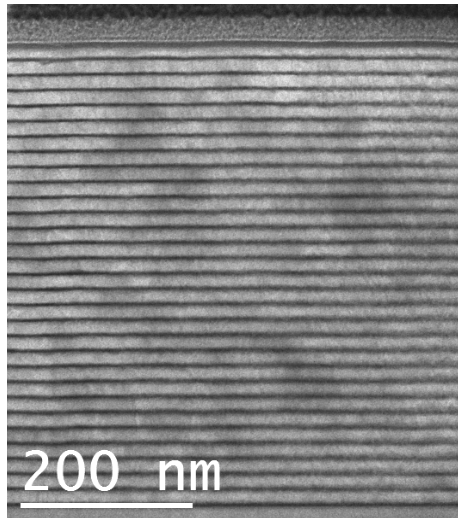

Figure 1. STEM BF image of the unannealed Mg/Co_2 multilayer.

To get a better impression of the quality of the layers we need to zoom onto a part thin enough (and well oriented enough) to allow visualisation of the crystal structure in the dense Co layers. Figure 2 shows a zoom onto the first two periods of the multilayer in the thinnest part of the sample. The horizontal fringes have spacings corresponding to those of the hexagonal planes in bulk magnesium and bulk cobalt in the appropriate regions. Lattice spacings are measured as 0.26 ± 0.01nm in the Mg layer (c/2 = 0.2605nm in bulk Mg) and 0.21nm ± 0.01nm in the Co layer (c/2 = 0.204nm in bulk Co). Other orientations are sometimes visible, but are probably due, in this thin region, to disordered and/or oxide layers at the outer surfaces of the STEM sample caused by to ion-beam damage and air exposure. (In most thicker regions, the hexagonal Mg fringes can be seen but not those of Co, which is too dense). The layers thus appear to be generally well-crystallised and somewhat epitaxial in nature. A poorly crystallised region is also seen between the substrate and the first Co layer. In order to determine the nature of this layer and to attempt a further check of the roughness of the layers some preliminary EELS spectrum-images have been acquired in this thinner region.

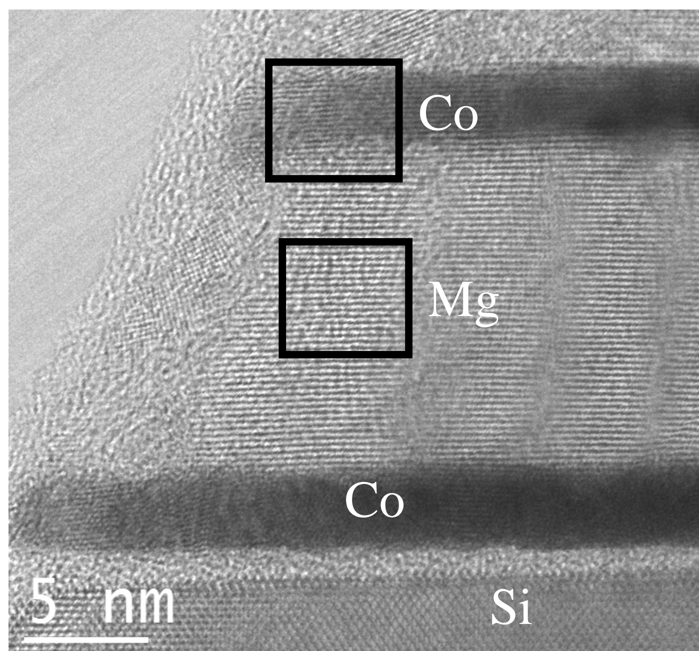

Figure 2. Close up of the thinnest part of the unannealed Mg/Co_2 multilayer.

Figure 3 shows Co, Mg, O EELS maps and the corresponding HAADF images from the first two bi-layers. The layers can be seen to be chemically well-ordered at this scale. A strong oxygen signal is detected, along with Mg in the poorly crystallised region mentioned above. This appears therefore to be an MgO layer. The oxygen signal is also slightly enhanced over the Mg layers, probably due to surface oxidation.

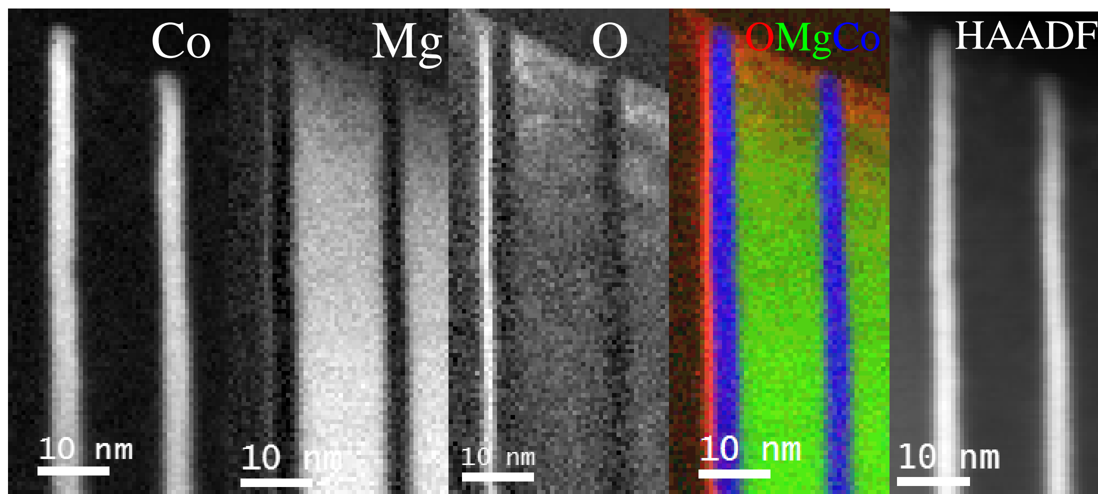

Figure 3. Co, Mg, O EELS maps and the corresponding HAADF images from the first two bi-layers.

Figure 4 shows a higher resolution set of EELS maps going across one Co layer. The vertical integrations in the dotted boxes give the interface width. The width of the interfaces on both sides is measured here as approximately 1 nm, *i.e.* almost twice as much as the figures found by reflectivity.

Convolution with the probe-size of around 0.1 nm cannot account for the entire discrepancy. EELS signals can suffer from delocalisation, *i.e.* excitation of an atom by a fast electron passing at a distance which can be several angstroms. However the effects would not be expected to be very large here, especially in the case of the high energy-loss Mg K edge. The broadening of the profiles is more likely to be due to non-negligible multiple elastic and inelastic scattering in the region where the data were acquired (~40 nm) which is still not ideally thin for 100 keV electrons and these materials, and the disordered layers seen to be present at the sample surface which almost certainly contain a mixture of Mg and Co. Further EELS experiments on thinner samples (or using higher acceleration voltages) and using higher energy resolution should provide further details of the structure and chemistry of the range of samples studied here.

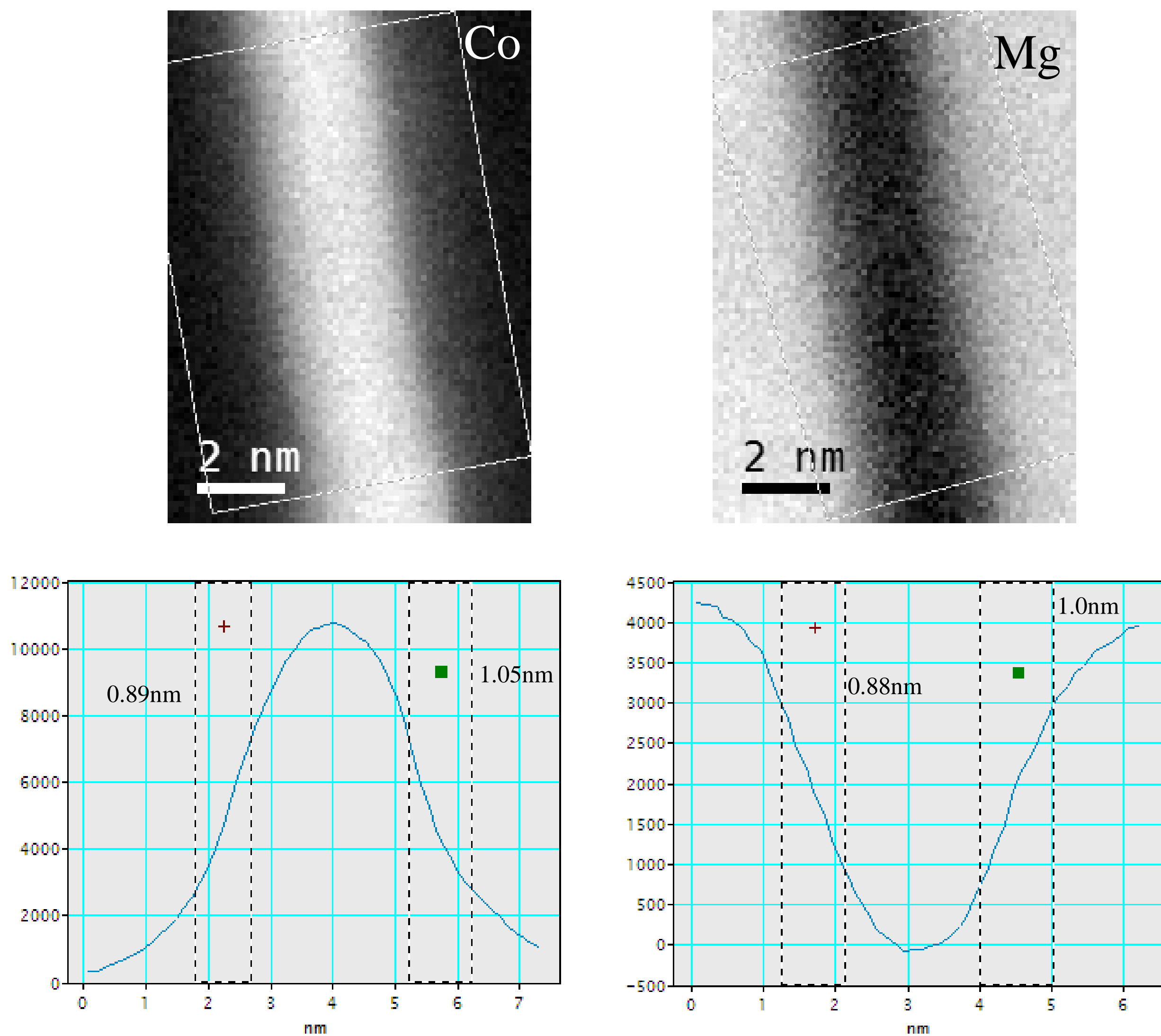

Figure 4. Higher resolution EELS maps (top) of Co (left) and Mg (right) across the second Co layer and the interface width profiles (bottom).

3.2 Samples with annealing

EUV reflectivity

We show in Figure 5 the reflectivity curves as a function of the annealing temperature, measured in the 45-55 eV energy range at 45° Bragg angle, angle for which the multilayer is designed, and in the 42-52 eV energy range at 50°. At 45° the maximum reflectivity is 42.4% at 49.3 eV, which is close to the Mg-L absorption edge at 49.50 eV for $2p_{3/2}$ and 49.78 eV for $2p_{1/2}$. This is rather too close to the Mg-L edge and we prefer to fit the reflectivity curves obtained at 50°. In the following, the position and maximum position of the Bragg peak will then be discussed for spectra recorded at 50° of grazing incidence.

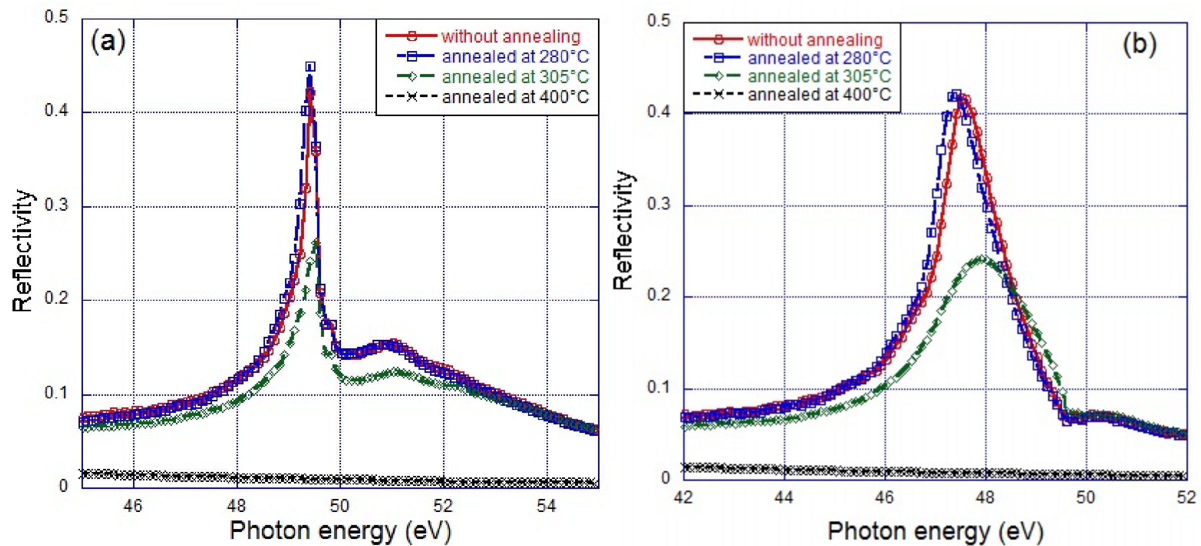

Figure 5. Evolution as a function of the annealing temperature of the Mg/Co_2 EUV reflectivity curves obtained at 45° (a) and 50° (b) Bragg angles.

The reflectivity slightly increases and the position of the Bragg peak of the Mg/Co_2 annealed at 280°C is slightly shifted (0.2 eV) towards lower photon energy with respect to that of the multilayer without annealing. At 305°C, a reflectivity drop of nearly 45% is observed as well as a peak shift (0.4 eV) towards higher photon energy. At 400°C, the reflectivity can be considered as zero. The structural parameters of the stack deduced from the fit of the reflectivity curves measured at 50° are collected in Table 2. The interfacial roughness and the thickness are stable for the unannealed and 280°C samples. However, the interfacial roughness increases quite a lot for the Mg/Co_2 annealed at 305°C and the fitted thicknesses vary drastically.

Table 2. Parameter values extracted from the fit to the Mg/Co_2 reflectivity curve measured at a Bragg

angle of 50° in the EUV range. σ stands for the interfacial roughness.

Multilayer Mg/Co_2	d (nm)	d_{co} (nm) d_{Mg} (nm)	σ (nm)
Without annealing	16.9	2.6 14.3	Co-on-Mg = 0.5 Mg-on-Co = 0.6
Annealed at 280°C	16.98	2.86 14.12	Co-on-Mg = 0.5 Mg-on-Co = 0.6
Annealed at 305°C	16.9	3.95 12.95	Co-on-Mg = 1.0 Mg-on-Co = 2.7

<u>NMR analysis</u>

NMR spectra obtained for the Mg/Co_1 multilayers as a function of the annealing temperatures are presented in Figure 7(a). As can be seen, the spectra shapes of the Mg/Co_1 multilayers after annealing at different temperatures show a well defined line at 226 MHz which corresponds to Co atoms lying in the bulk of the Co layers with an hcp structure. The Co atoms are thus mainly situated in pure Co layers (226 MHz) and the intermixing at the Mg/Co interfaces is limited. An additional line is observed at 156 MHz for the multilayer without annealing and for the sample annealed at 280°C in Figure 7(b). This line has been identified in our previous work with the Co atoms situated at perfect interfaces between Co and Mg atoms [1]. The overall shape of the spectrum after annealing at 280°C is very similar to that observed for the as deposited sample. It can be noticed that the Co interface line seems to be even better resolved after annealing at 280°C than in the spectrum of the as deposited sample. This observation would suggest that such low temperature annealing results in some sharpening of the Co/Mg interfaces.

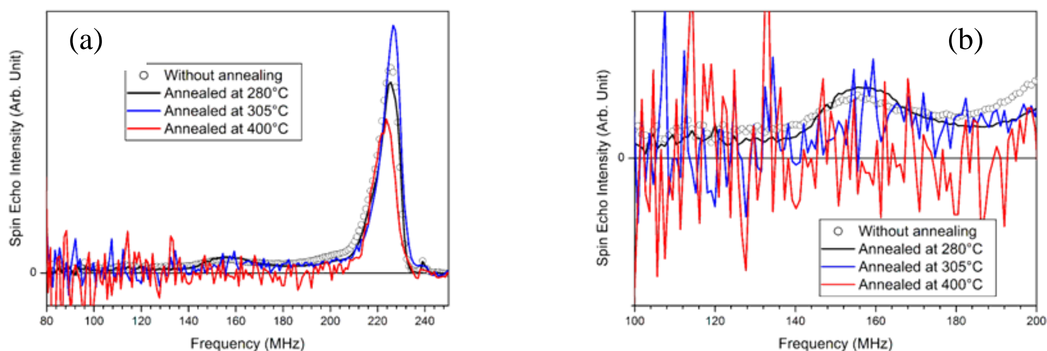

Figure 6. (a) NMR spectra of Mg/Co_1 multilayers as a function of the annealing temperatures; (b) zoom around 156 MHz.

The modification of the NMR spectra is much more significant for higher annealing temperatures (305 and 400°C). The most striking observation is that the contribution of the Co atoms at the Co/Mg interfaces (156 MHz) vanishes with increasing annealing temperature, Figure 7(b). This could be attributed to the formation of non magnetic interfacial alloys or compounds. However this is not consistent with the XES analysis and the observation that the total NMR intensity is not significantly reduced after annealing.

Additional details can be obtained from the magnetic information that is provided by the NMR experiments. Indeed NMR can also probe the magnetic stiffness of the samples [16]. This stiffness can have several origins and is described as a magnetic restoring field. The plot of this restoring field versus the annealing temperature is shown in Figure 8 (room temperature corresponding to 20°C). It can be seen that while the restoring field stays unchanged after the annealing at 280°C, it increases strongly for higher annealing temperatures. After the annealing at 400°C the restoring field is an order of magnitude higher than after the annealing at 280°C. This observation does not support the intermixing process since such a process usually leads to a decrease in the restoring field. However it shows that the magnetization processes are drastically modified by the annealing process.

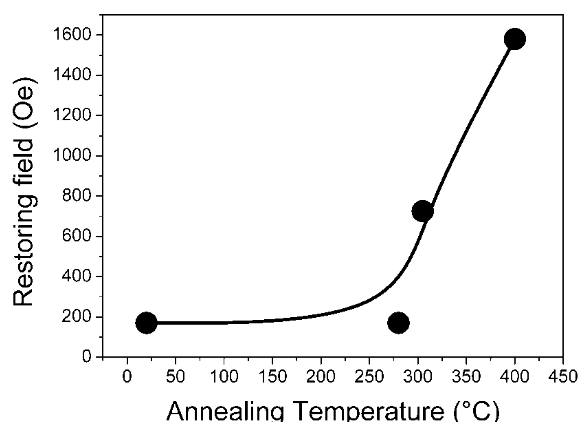

Figure 7. Magnetic restoring field versus the annealing temperature of Mg/Co_1 multilayers.

Actually the vanishing of the interfacial line as well as the increase in the restoring field with the annealing temperature can both be explained by the clustering of the Co layers into spheres or more probably into Co grains with pan cake like shapes. Indeed spherical grains would lead to a reorientation of the magnetization direction of the Co grains compared to the magnetization direction of the Co thin film. In such a case the NMR resonance frequency would shift from 226 MHz to 220 MHz [31], which

is not observed in the NMR spectra. The clustering of the Co atoms will result in Co particles for which the surface to volume ratio is much smaller than in the case for the as deposited multilayer shape. If the Co grains are large enough, the contribution of the surface Co atoms becomes so small that it is not measurable anymore. The magnetic properties of Co grains are also very different from those of Co films. In Co films extended domain wall (Neel walls) can develop, resulting in soft magnetic properties (small restoring fields in NMR) while in Co grains such domain walls if they exist will have a smaller mobility, resulting in hard magnetic properties (large restoring fields in NMR). Therefore the clustering of the Co films into large Co grains with increasing annealing temperature explains both the evolution of the NMR spectra and the evolution of the magnetic properties of the samples.

XES analysis

We present in Figure 8 the Mg Kß emission band of the Mg/Co_1 sample as a function of the annealing temperature and the comparison to the references Mg and MgO. The Mg Kß emission band of the Mg/Co multilayer without annealing is discussed in detail in Ref. [1].

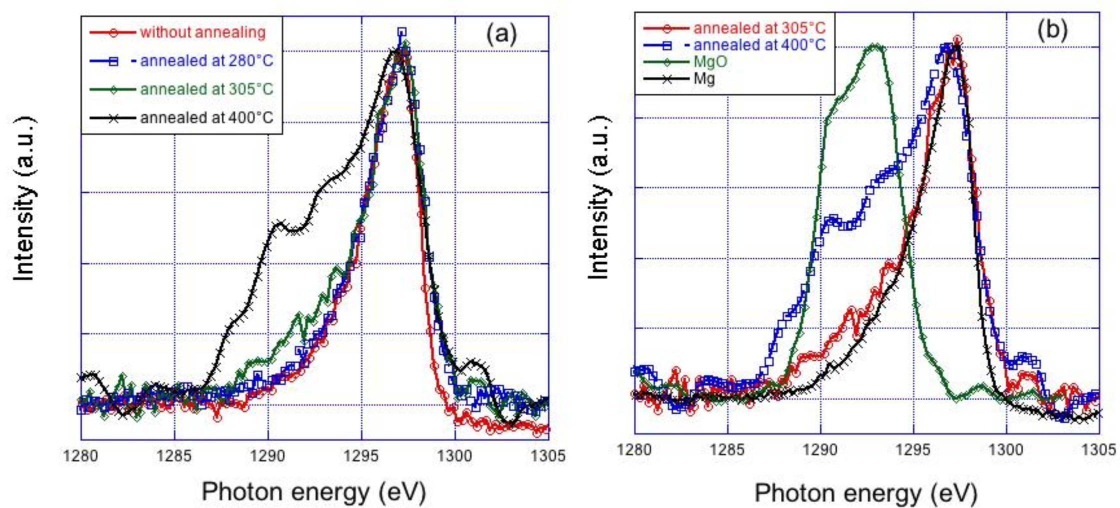

Figure 8. The Mg Kß emission band of sample Mg/Co_1 annealed at different temperatures (a) and its comparison with the Mg and MgO spectra (b).

The spectrum of the sample annealed at 280°C is close that obtained without annealing and close to that of Mg metal. We deduce that within the sample annealed at 280°C, the Mg atoms are in a physico-chemical state close to that of Mg atoms in the Mg metallic state and the interaction with the Co layers is limited. The spectra of Mg/Co_1 samples annealed at 305°C and 400°C differ from that of Mg/Co without annealing toward the low photon energies. A shoulder appears in the region of the MgO maximum (1288-1295 eV) whose intensity increases with temperature. Thus from 305°C an oxidation of the Mg layer takes place. Because of the annealing conditions, the oxidation takes place after the EUV measurements when the sample is returned to the air prior their XES analysis. Thus, whatever the

annealing temperature, the Mg atoms do not interact with the Co atoms, which is in agreement with the NMR result.

SEM analysis

From the SEM images of cross sections presented in Figure 9 we can see that the Mg/Co_2 multilayers without annealing and annealed at 280°C have clear multilayer structures. The cross section of the samples presents from top to bottom the Pt protection layer, the Mg/Co_2 multilayer and the Si substrate. For the sample annealed at 305°C, there exist some cracks between the multilayer and the substrate, the interface is no longer flat and there seems to be a loss of adherence. The sample annealed at 400°C has more serious changes compared to the sample annealed at 305°C: cracks and voids exist also between the layers. The change in the multilayer structure results from the change in the morphology of the Co layers deduced from NMR. The deformation of the Co layers generates mechanical stress that finally is discharged by the delamination of the multilayer and the formation of cracks. Because of these cracks, the multilayer is no longer flat and so its reflectivity decreases. Finally, the cracks facilitate the introduction of oxygen within the multilayer. This explains the oxidation of the Mg layers observed in XES.

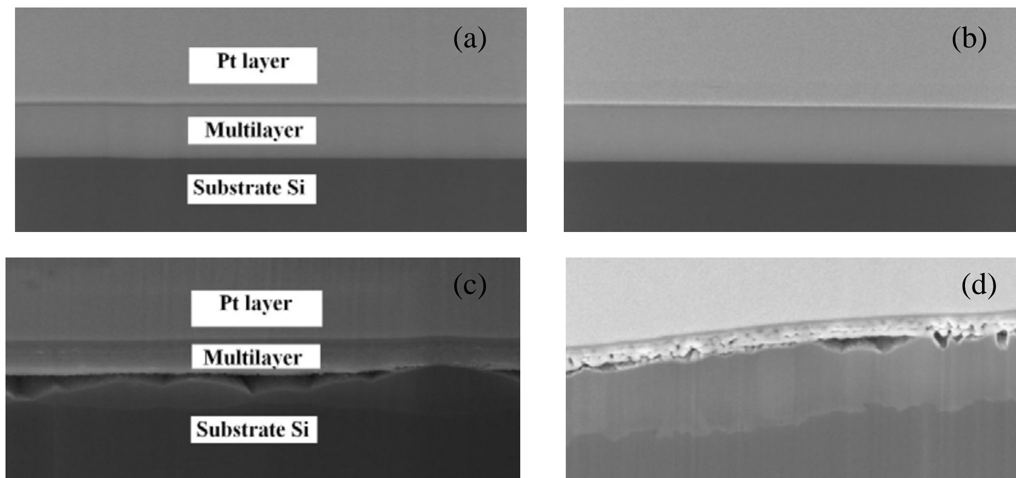

Figure 9. SEM images of Mg/Co_2 multilayer without annealing (a), annealed at 280°C (b), 305°C (c) and 400°C (d).

4. Conclusions

We have characterized a Mg/Co periodic multilayer and its thermal stability by using STEM / EELS, EUV reflectivity around 25 nm (~50 eV), NMR, XES and SEM. The multilayer is designed for optical application in the EUV range. STEM / EELS images show the good quality of the as-prepared multilayer and the crystallization of the Co and Mg layers. EUV reflectivity measurements

show that the reflectivity slightly increases with the temperature up to 280°C. Then, the reflectivity drops by nearly 45% at 305°C and vanishes at 400°C. The combination of the results obtained by the various used techniques allows us to explain this reflectivity variation: as a function of the annealing temperature the morphology of the Co layers changes; this generates some cracks within the multilayer and then a loss of its flatness; consequently the reflectivity decreases until the multilayer is destroyed.

ACKNOWLEDGMENT

The authors from Tongji University are indebted to the National Natural Science Foundation of China (Granted No. 10825521 and 11061130549). Part of this work was made within the framework of the French TEM and Atom-probe network (METSA) and the ANR project COBMUL (J10R069).

REFERENCES

[1] K. Le Guen, M.-H. Hu, J.-M. André, P. Jonnard, S. K. Zhou, H. Ch. Li, J. T. Zhu, Z. S. Wang, C. Meny: J. Phys. Chem. C, 2010, 114, 6484.

[2] K. Le Guen, M.-H. Hu, J.-M. André, P. Jonnard, S. K. Zhou, H. Ch. Li, J. T. Zhu, Z. S. Wang, N. Mahne, A. Giglia, S. Nannarone: Applied Physics A, 2011, 102, 69.

[3] J. Zhu, S. Zhou, H. Li, Q. Huang, Z. Wang, K. Le Guen, M.-H. Hu, J.-M. André, P. Jonnard: Appl. Opt., 2010, 49, 3922.

[4] H. Maury, P. Jonnard, K. Le Guen, J. M. André, J. Wang, J. Zhu, J. Dong, Z. Zhang, F. Bridou, F. Delmotte, C. Hecquet, N. Mahne, A. Giglia, and S. Nannarone: European Physical Journal B, 2008, 64, 193.

[5] H. Takenaka, S. Ichimaru, T. Ohchi, E.M. Gullikson: J. Elec. Spec. Rel. Phenom., 2005, 144, 1047.

[6] T. Djavanbakht, V. Carrier, J.-M. Andre, R. Barchewitz and P. Troussel: J. Phys. IV France, 2000, 10, 10-281.

[7] P. Mengucci, G. Majni, A. Di Cristoforo, R. Checchetto, A. Miotello, C. Tosello and G. Principi: Thin Solid Films, 2003, 433, 205.

[8] H. -J. Stock, U. Kleineberg, B. Heidemann, K. Hilgers, A. Kloidt, B. Schmiedeskamp, U. Heinzmann, M. Krumrey, P. Müller and F. Scholze: Appl. Phys A, 1994, 58, 371.

[9] U. Kleineberg, H.-J. Stock, A. Kloidt, B. Schmiedeskamp, U. Heinzmann, S. Hopfe and R. Scholz: physica status solidi (a), 1994, 145, 539.

[10] B. Heidemann, T. Tappe, B. Schmiedeskamp and U. Heinzmann: Z. Phys. B, 1995, 99, 37.

[11] R. Senderak, M. Jergel, S. Luby, E. Majkova, V. Holy, G. Haindl, F. Hamelmann, U. Kleineberg and U. Heinzmann : J. Appl. Phys., 1997, 81, 2229.

[12] M. Barthelmess, S. Bajt: Appl. Opt. 2011 50, 1610.

[13] M.-H. Hu, K. Le Guen, J.-M. André, P. Jonnard, S. K. Zhou, H. Ch. Li, J. T. Zhu, Z. S. Wang: AIP Conf. Proc., 2010, 1221, 56.

[14] S. Nannarone, F. Borgatti, A. DeLuisa, B. P. Doyle, G. C. Gazzadi, A. Giglia, P. Finetti, N. Mahne, L. Pasquali, M. Pedio, G. Selvaggi, G. Naletto, M. G. Pelizzo, G. Tondello: AIP Conference Proceedings, 2004, 708, 450.

[15] C. Meny, and P. Panissod: Modern Magnetic Resonance, G. Webb, Ed., Springer, Heidelberg, 2006.

[16] P. Panissod, and C. Meny: Applied Magnetic Resonance, 2000, 19, 447.

[17] C. Bonnelle, F. Vergand, P. Jonnard, J.-M. André, P. F. Staub, P. Avila, P. Chargelègue, M.-F. Fontaine, D. Laporte, P. Paquier, A. Ringuenet, B. Rodriguez: Review of Scientific Instruments, 1994, 65, 3466.

[18] H. Maury, P. Jonnard, J.-M. André, J. Gautier, M. Roulliay, F. Bridou, F. Delmotte, M.-F. Ravet, A. Jérome, P. Holliger: Thin Solid Films, 2006, 514, 278.

[19] M. Iwami, M. Kusaka, M. Hirai, R. Tagami, H. Nakamura, and H. Watabe: Applied Surface Science, 1997, 117, 434.

[20] E. Z. Kurmaev, V. R. Galakhov, and S. N. Shamin: Crit. Rev. Solid State Mater. Sci., 1998, 23, 65.

[21] N. Miyata, S. Ishikawa, M. Yanagihara, and M. Watanabe: Japanese Journal of Applied Physics Part 1-Regular Papers Short Notes & Review Papers, 1999, 38, 6476.

[22] I. Jarrige, P. Jonnard, N. Frantz-Rodriguez, K. Danaie, and A. Bosseboeuf: Surface and Interface Analysis, 2002, 34, 694.

[23] V. R. Galakhov: X-Ray Spectrometry, 2002, 31, 203.

[24] M. Salou, S. Rioual, J. Ben Youssef, D. T. Dekadjevi, S. P. Pogossian, P. Jonnard, K. Le Guen, G. Gamblin, and B. Rouvellou: Surface and Interface Analysis, 2008, 40, 1318.

[25] K. Le Guen, G. Gamblin, P. Jonnard, M. Salou, J. Ben Youssef, S. Rioual, and B. Rouvellou: European Physical Journal-Applied Physics, 2009, 45.

[26] H. Maury, J. M. André, K. Le Guen, N. Mahne, A. Giglia, S. Nannarone, F. Bridou, F. Delmotte, and P. Jonnard: Surface Science, 2009, 603, 407.

[27] P. Jonnard, F. Vergand, C. Bonnelle, E. Orgaz, and M. Gupta: Physical Review B (Condensed Matter), 1998, 57, 12111.

[28] P. Jonnard, K. Le Guen, R. Gauvin, J.-F. Le Berre: Microsc Microanal., 2009, 15, 36.

[29] L.V. Azaroff: “X-ray Spectroscopy”. McGraw-Hill Inc., 1974.

[30] C. Bonnelle: X-ray spectroscopy. Annu. Rep. Prog. Chem., Sect. C, Phys. Chem., 1987, 84, 201.

[31] M. Malinowska, C. Meny, E. Jedryka, P. J. Panissod: Phys.: Condens. Matter. 1998, 10, 4919.

Appl Phys A (2011) 102: 69–77
DOI 10.1007/s00339-010-6093-2

Applied Physics A
Materials Science & Processing

RAPID COMMUNICATION

Introduction of Zr in nanometric periodic Mg/Co multilayers

**K. Le Guen · M.-H. Hu · J.-M. André · P. Jonnard ·
S.K. Zhou · H.C. Li · J.T. Zhu · Z.S. Wang · N. Mahne ·
A. Giglia · S. Nannarone**

Received: 20 July 2010 / Accepted: 14 October 2010 / Published online: 27 October 2010
© Springer-Verlag 2010

Abstract We study the introduction of a third material, namely Zr, within a nanometric periodic Mg/Co structure designed to work as optical component in the extreme UV (EUV) spectral range. Mg/Co, Mg/Zr/Co, Mg/Co/Zr and Mg/Zr/Co/Zr multilayers are designed, and then characterized in terms of structural quality and optical performances through X-ray and EUV reflectometry measurements, respectively. For the Mg/Co/Zr structure, the reflectance value is equal to 50% at 25.1 nm and 45° of grazing incidence and reaches 51.3% upon annealing at 200°C. Measured EUV reflectivity values of tri-layered systems are discussed in terms of material order within a period and compared to the predictions of the theoretical model of Larruquert. Possible applications are pointed out.

1 Introduction

We are interested in the design, the development and the characterization of multilayered mirrors exhibiting high reflectance values in the extreme ultraviolet (EUV) range [1–4]. To that purpose, we explore different ways as for instance the introduction of a third material within a bi-layered structure and the effect of annealing. Multilayers made of more than two materials have already proven to be efficient optical systems [5–10].

Such multilayered mirrors can be used as optical components in various applications owing to the high peak reflectivity at the wavelength of interest, which is enhanced with respect to the neighboring wavelengths although the spectral purity is not ensured. They can be used as monochromators at 45° in synchrotron centres, in telescopes for imaging purposes even if telescopes are generally operated at normal incidence.

We have recently shown that Co/Mg multilayers exhibit a reflectance value equal to 42.6% at 25.1 nm [3]. To enhance the performance of this system, in the following we present the comparative analysis of the optical performances in the EUV spectral range of bi-, tri- and quadri-layered structures based on Mg, Co and Zr. X-ray and EUV reflectivity measurements are performed to access the structural parameters of the stack and estimate the EUV optical performances, respectively. Measured EUV reflectivity values of tri- and quadri-layered systems are discussed in terms of material order within the structure on the basis of the theoretical model of Larruquert [8, 11]. The effect of annealing up to 200°C on the reflectance of the Mg/Co and Mg/Co/Zr multilayers is also studied.

2 Experiment

2.1 Multilayer deposition

The studied periodic multilayers were prepared using a calibrated ultra-high vacuum direct current magnetron sputtering system (JGP560C6. SKY Inc. China) with targets of Mg

K. Le Guen (✉) · M.-H. Hu · J.-M. André · P. Jonnard
Laboratoire de Chimie Physique—Matière Rayonnement, UPMC Univ Paris 06, CNRS UMR 7614, 11 rue Pierre et Marie Curie, 75231 Paris cedex 05, France
e-mail: karine.le_guen@upmc.fr
Fax: +33-1-44276226

S.K. Zhou · H.C. Li · J.T. Zhu · Z.S. Wang
Institute of Precision Optical Engineering, Department of Physics, Tongji University, Shanghai 200092, P.R. China

N. Mahne · A. Giglia · S. Nannarone
Istituto Officina dei Materiali IOM-CNR Laboratorio TASC, S.S.14. km 163.5 in Area Science Park, 34012 Trieste, Italy

Table 1 Structure and simulated reflectance of the "aimed" multilayers. IMD reflectivity simulations are performed assuming an "ideal" structure (neither roughness nor interfacial compound)

Multilayer	Period d (nm)	d_{Mg} (nm)	d_{Co} (nm)	d_{Zr} (nm)	Simulated reflectivity $\theta_{grazing} = 45°$	Simulated reflectivity $\theta_{grazing} = 50°$
Mg/Co	17.00	14.45	2.55	–	56.7% @ 25.2 nm	54.0% @ 26.4 nm
Mg/Zr/Co	17.20	13.20	2.50	1.50	54.6% @ 25.2 nm	52.4% @ 26.5 nm
Mg/Co/Zr	17.20	13.20	2.50	1.50	62.7% @ 25.2 nm	58.3% @ 26.4 nm
Mg/Zr/Co/Zr	17.00	12.00	2.00	1.50	47.1% @ 25.2 nm	53.1% @ 26.0 nm

(purity 99.98%), Co (purity 99.95%), and Zr (purity 99.5%) in Ar gas (99.999%). The targets are 100 mm in diameter. The base pressure was 5×10^{-5} Pa and the working pressure was 1×10^{-1} Pa of Ar gas. The power applied on the Co, Mg and Zr targets was set to 20, 15 and 20 W, respectively. Multilayers were deposited onto 30 mm × 40 mm ultra-smooth polished Si substrates with *rms* surface roughness of 0.3 nm. Each sample is made of 30 periods. The first layer on the substrate is the first layer given in the sample name. A 3.50 nm-thick B_4C capping layer is deposited at the surface of each sample to prevent oxidation.

Materials and layer thicknesses are optimized to get the highest reflectance at 45° of incidence. At 45°, the Bragg peak is very close to the Mg L absorption edge (24.9 nm for $2p_{1/2}$ and 25.0 nm for $2p_{3/2}$) and consequently its shape is asymmetrical. That is why we consider, in addition to the 45° value, the 50° grazing angle in order to move the Bragg peak away from the Mg L edge. The spectra measured at 50° will be used for fitting purposes, while those measured at 45° will allow us to estimate the optical performance of the multilayer at the application angle and wavelength. The structure of each designed sample and the IMD simulated reflectivity of the "ideal" stack (neither roughness nor interfacial compound) are detailed in Table 1 [12].

From the results of the reflectivity simulations, conclusions on some general trends can be drawn:

- at 45° of grazing incidence, whatever the structure is, the reflectivity is maximum at 25.2 nm owing to the Mg L discontinuity;
- with respect to the bi-layered structure, the addition of a third material (Zr) to form tri- and quadri-layers does not systematically lead to a higher reflectance;
- among the tri-layered structures, the order of the material sequence seems to play an important role: here, the Mg/Co/Zr system leads to a higher reflectance value than that of Mg/Zr/Co.

2.2 X-ray reflectivity at 0.154 nm

The quality of the multilayers was controlled through X-ray reflectometry using the Cu Kα emission line (0.154 nm or 8048 eV). Measurements are made using a grazing incidence X-ray reflectometer (D1 system. Bede Ltd.) operated in the θ–2θ mode. The angular resolution is 5/1000°. Bragg law corrected for refraction was used to determine the multilayer period. The fit of the XRR curves performed with IMD was used to determine the thickness and roughness of the different layers in each structure and also to estimate their density. The roughness deduced from the fit is an overall roughness including the contributions from both geometrical roughness and interdiffusion.

2.3 EUV reflectivity

The measurement of the reflectivity curves in the EUV domain is performed on the BEAR beamline [13] at the Elettra synchrotron centre using s-polarized light. The photon energy is carefully calibrated using the Pt $4f_{7/2}$ feature and the Si L edge. The goniometer angular resolution is 1/100°. Impinging and reflected photon intensities are measured using a photodiode. Incident intensities are monitored using an Au mesh inserted in the beam path whose drain current is used for normalization. The overall accuracy on the absolute reflectivity values is estimated to be about 1%. A short (22.5–27.6 nm at 45° of grazing incidence and 23.8–29.5 nm at 50°) spectral range associated to a 0.1 nm step is used for the accurate measurement of the reflectance value while a wide (20.7–31.0 nm at both 45 and 50°) spectral range associated to a 0.2 nm step is considered for the estimation of the background.

3 Results and discussion

3.1 X-ray reflectivity at 0.154 nm

As an illustration, the X-ray reflectivity curves of the Mg/Co and Mg/Co/Zr multilayers measured at 0.154 nm are presented in Fig. 1 on a logarithmic scale. Within the entire probed angular range, up to 11 well-defined Bragg peaks are present, giving evidence for the good structural quality of the stacks. For Mg/Co, the seventh Bragg peak is almost extinguished as a consequence of the ratio of the Co thickness to the d period close to 1/7. It appears that, for all systems, the width of the measured Bragg peaks broadens as the

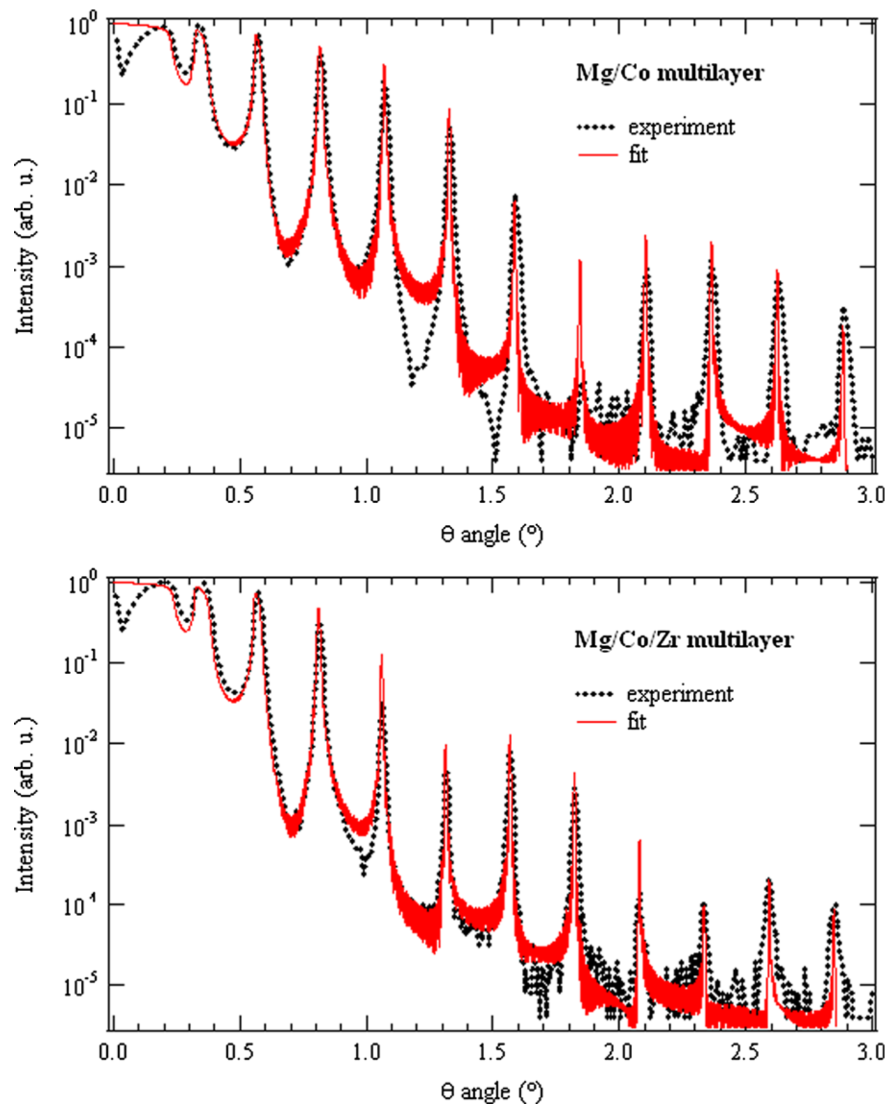

Fig. 1 Fit of the X-ray reflectivity curves of the Mg/Co and Mg/Co/Zr multilayers measured at 0.154 nm

grazing angle increases. This could be ascribed to a non homogeneity of the depth distribution of the layer thicknesses. The thickness, roughness and density values, deduced from the fit of the XRR curves, are collected in Table 2 where the density ratio (%) is defined as the density of the layer divided by the density of the bulk. The density values are given within a 5% uncertainty. For comparison, the value of the period is also calculated using the refraction corrected Bragg law.

The measured periods are in good agreement with the aimed values while the roughness values are of the same magnitude for all structures. Within the estimated uncertainty, the layer densities are close to those of the bulk materials.

3.2 EUV reflectivity

The EUV reflectivity spectra of the Mg/Co, Mg/Zr/Co, Mg/Co/Zr and Mg/Zr/Co/Zr multilayers measured in the short spectral range at 45 and 50° of grazing incidence are presented in Fig. 2. The asymmetric shape of the curves originates from the presence of the Mg L edge. For each multilayer, the Bragg peak stands onto a background corresponding to the total reflection and diffuse scattering. In the following, we will distinguish the values (in %) at the application wavelength of the peak reflectivity, the background and the net reflectivity, this latter being the difference between the two previous quantities. The background height at the application wavelength is estimated considering the wide (20.7–31.0 nm) spectral range.

At 45°, the reflectivity peaks are narrow due to the absorption at wavelengths shorter than the Mg L edge. At 50°, the peak bandwidth is about twice larger than at 45°. The values of the peak reflectivity and background measured at 45° of grazing incidence in the wide spectral range (20.7–31.0 nm) are collected in Table 3. At 45°, with respect to the bi-layered Mg/Co structure (42.4%), the addition of a third

Table 2 Structural parameters extracted from the fit of the XRR curves measured at 0.154 nm. For comparison, the period value is also calculated using the refraction corrected Bragg law

Multilayer	Bragg law corrected for refraction	XRR fitting procedure			
	Period d (nm)	d (nm)	d_{Co} (nm) d_{Mg} (nm) d_{Zr} (nm)	σ (nm)	Density ratio Co (%) Density ratio Mg (%) Density ratio Zr (%)
Mg/Co	16.88	16.9	Co: 2.6 Mg: 14.3 –	$\sigma_{Co/Mg} = 0.5$ $\sigma_{Mg/Co} = 0.6$	100 96 –
Mg/Zr/Co	17.28	17.3	Co: 2.3 Mg: 13.5 Zr: 1.5	$\sigma_{Co/Zr} = 0.6$ $\sigma_{Zr/Mg} = 0.6$ $\sigma_{Mg/Co} = 0.7$	96 100 94
Mg/Co/Zr	17.11	17.1	Co: 2.4 Mg: 13.2 Zr: 1.5	$\sigma_{Zr/Co} = 0.6$ $\sigma_{Co/Mg} = 0.6$ $\sigma_{Mg/Zr} = 0.7$	100 95 98
Mg/Zr/Co/Zr	17.03	17.0	Co: 2.0 Zr: 1.5 Mg: 12.0 Zr: 1.5	$\sigma_{Zr/Co} = 0.7$ $\sigma_{Co/Zr} = 0.7$ $\sigma_{Zr/Mg} = 0.5$ $\sigma_{Mg/Zr} = 0.6$	99 100 100 100

component in the stack leads to a higher peak reflectivity (50.0%) if Zr is introduced at the Mg–on–Co interface while a lower value (41.4%) is measured when Zr is introduced at the Co–on–Mg interface. The presently studied quadri-layer leads to the lowest reflectance (40.6%) as expected from the IMD simulations. The background value is the highest for the quadri-layered system. Among the tri-layered structures, although Mg/Co/Zr exhibits the highest background, its net reflectivity remains the best. We do not present the peak reflectivity and background detailed values in the case of the 50° grazing incidence since these multilayers are designed for a 45° application angle.

In spite of the relatively high background, since the reflectance at the wavelength of interest is enhanced with respect to the neighboring wavelengths, these multilayers (particularly Mg/Co/Zr) could be efficiently used for imaging purposes in astrophysics applications for instance. As an illustration, Mg-based multilayers (Co/Mg, SiC/Mg, B_4C/Mg and Si/Mg) operated at near normal incidence have been very recently developed for solar He-II radiation at 30.4 nm [4]. On the contrary, their use for spectroscopic purpose may be inadequate since in that case high spectral purity is required.

To refine the description of each stack, the thickness, roughness and density values deduced from the fit of the XRR curves are introduced as constrained parameters to simulate the EUV reflectivity curves. The result is presented in Fig. 3 for the Mg/Co, Mg/Zr/Co, Mg/Co/Zr and Mg/Zr/Co/Zr multilayers. It clearly appears that, for each multilayer, the simulated EUV peak reflectivity is systematically higher than the measured value. Three reasons can be proposed to explain this discrepancy:

- the optical constants of materials are obviously different at 0.154 nm and in the ∼25 nm range. Moreover, the EUV refractive indices are not known with accuracy and the reflectivity strongly depends on these parameters;
- in XRR measurements, the grazing angle is in the range 0–3° whereas it is 45 or 50° for the EUV measurements. Then, the discrepancy could be due to the different penetration depth or to the different power spectral densities of the interface roughness of the layer surface;
- the presence of highly reactive materials, as for example Mg, could induce the formation of interface compounds whose optical properties are also not well known. Concerning this latter argument, we have recently demonstrated that in Co/Mg the interfaces are abrupt [3].

Nevertheless, in agreement with the XRR measurements at 0.154 nm, the structural quality of the stack is high since the ratio of the experimental to simulated reflectances is around 80%.

To improve again the agreement between the measured and simulated EUV reflectivity curves, we propose the following procedure based on the fact that, as mentioned above, in the EUV domain the optical indices (and material densities) are not known with a high accuracy. We consider the Co, Mg and Zr refractive indices ($n + ik$) as independent parameters to adjust in the EUV reflectivity simulations. With respect to the values collected in the CXRO database [http://www-cxro.lbl.gov], we consider in Table 4 a global

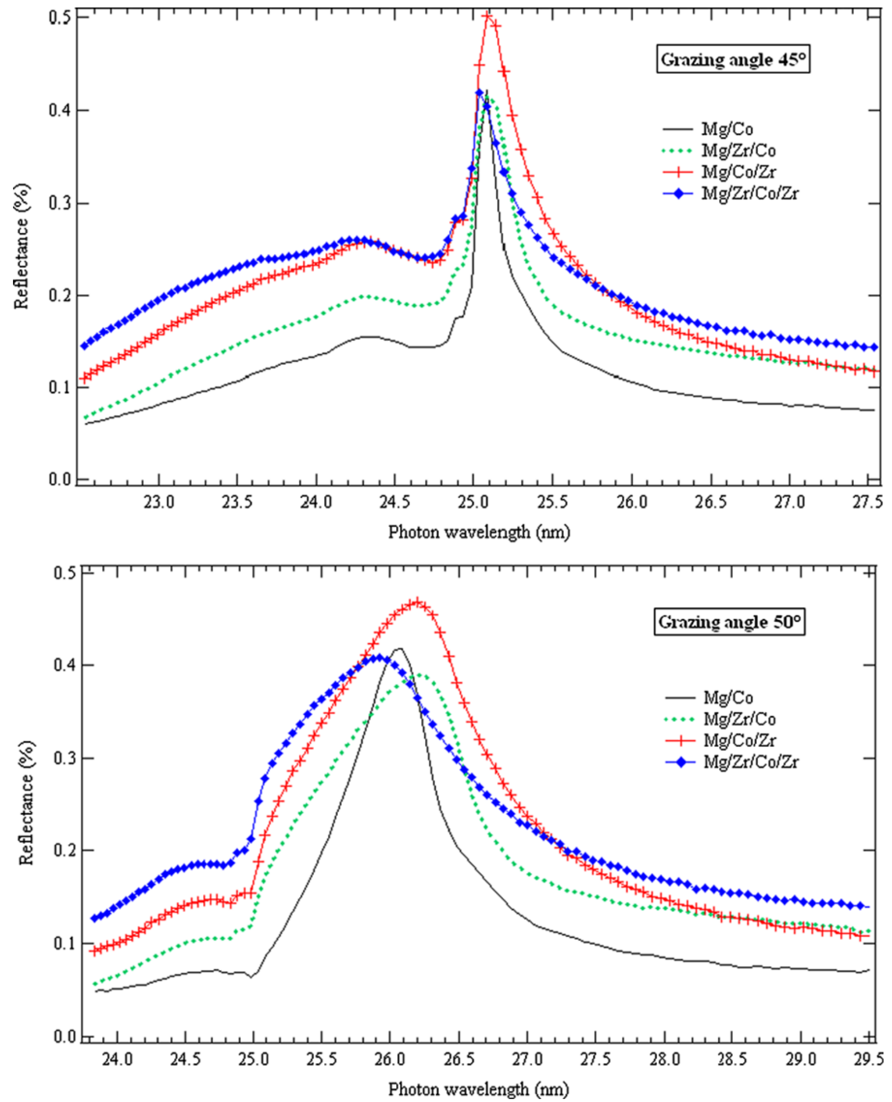

Fig. 2 EUV reflectivity spectra of the Mg/Co, Mg/Zr/Co, Mg/Co/Zr and Mg/Zr/Co/Zr multilayers measured at 45° (*top*) and 50° (*bottom*) of grazing incidence

Table 3 Reflectivity and background values measured at 45° of grazing incidence in the wide spectral range (20.7–31.0 nm). R_{exp} and R_{sim} stand for measured and simulated reflectance, respectively

Multilayer	λ (nm)	Peak reflectivity (%)	Background (%)	Net reflectivity (%)	$R_{\text{exp}}/R_{\text{simul}}$
Mg/Co	25.1	42.4	5.5	36.9	0.75
Mg/Zr/Co	25.1	41.4	5.2	36.2	0.76
Mg/Co/Zr	25.1	50.0	6.4	43.6	0.80
Mg/Zr/Co/Zr	25.1	40.6	6.9	33.7	0.86

variation (in %), independent increase or decrease of the real and imaginary parts. The values of thickness and roughness of each layer are kept constant to the values determined through the XRR fit (Table 2).

First, in the Mg/Co multilayer, with respect to the CXRO data, the real and imaginary parts have to be increased for Co while for Mg only the imaginary part has to be enhanced keeping almost constant the real part. Then, in the tri- and quadri-layered structures, the variations found for Co and Mg in Mg/Co are frozen and only the Zr indices are adjusted. The need for large variations reveals the lack of precise knowledge of the indices in the EUV range.

3.3 Comparison with the theoretical predictions

For tri- and quadri-layered structures, we consider the predictions of the theoretical model developed by Larruquert and devoted to the EUV reflectance enhancement in multilayer with more than two materials [8, 11, 14]. To ensure the highest reflectance, the model considers the largest possible refractive index contrast among the materials and ends up

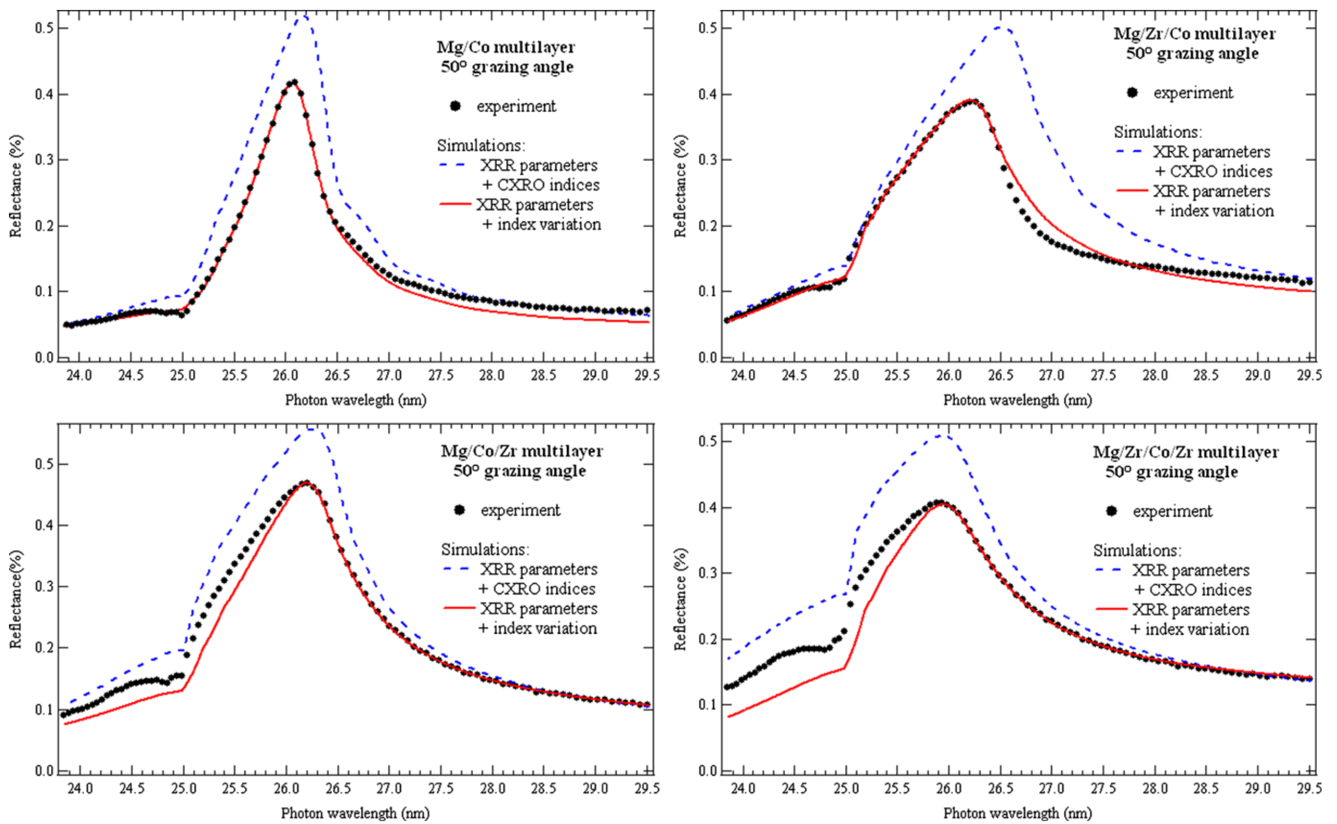

Fig. 3 Measured (*dotted line*) EUV reflectivity curves compared to simulations using the thickness and roughness from the XRR fit and the CXRO optical indices (*dashed line*) and simulations using the thickness and roughness of the XRR fit and the variation of the optical indices (*solid line*)

Table 4 Variations, with respect to the CXRO database, of the optical complex indices $n + ik$ of Co, Mg and Zr in order to fit the EUV reflectivity curves

Multilayer	n index variation (%) Co Mg Zr	k index variation (%) Co Mg Zr
Mg/Co	107	115
	99	115
	–	–
Mg/Zr/Co	107	115
	99	115
	83	100
Mg/Co/Zr	107	115
	99	115
	108	140
Mg/Zr(1)/Co/Zr(2)	107	115
	99	115
	Zr(1) 112	110
	Zr(2) 108	140

in a material selection rule within a period. Nevertheless, in his model, Larruquert has excluded the highly reactive materials such as alkaline and most alkalino-earth metals (Mg). In addition, given the Mg layer thickness (12 to 14.45 nm), we have to note that the presently studied multilayer are not sub-quarterwave multilayers.

Within the multilayer, we consider a period made of m thin films of different absorbing materials deposited onto the substrate and the outer medium is designated using the "inc" subscript. The letter i is chosen to identify a given layer within the stack: $i = 1$ corresponds to the outermost layer and $i = m + 1$ the substrate. For the tri-layered structure, m is equal to 3. For s-polarized incoming radiation, two conditions are required to lead to maximum reflectance [11]:

$$\begin{cases} \mathrm{Im}[(s\Delta N_1)/\cos\theta_1\} > 0 & \text{condition 1} \\ \mathrm{Im}[\Delta N_i/\Delta N_{i-1}] < 0 \quad i = 2, \ldots, m & \text{condition 2} \end{cases}$$

where $s = r^*_{\mathrm{inc},1}(1 - r^2_{\mathrm{inc},1})$ in which $r_{\mathrm{inc},1}$ stands for the amplitude reflectance given by the Fresnel coefficient at the interface with refractive indices N_{inc} and N_1 and $\Delta N_i = N_{i+1} - N_i$. In summary, to ensure an enhanced reflectivity, the condition 1 should lead to a positive value and the condition 2 to a negative value. Table 5 collects the values re-

Table 5 Application of conditions 1 and 2 developed by Larruquert [11] in the case of the Mg, Co and Zr materials. Optical constants originate from the CXRO database [http://www-cxro.lbl.gov]

Multilayer	Condition 1	Condition 2	
	–	$i = 2$	$i = 3$
Substrate/Zr/Mg/Co	+0.011	−0.221	−0.090
Substrate/Mg/Zr/Co	−0.016	+0.623	+0.090
Substrate/Mg/Co/Zr	+0.029	−0.623	−0.221

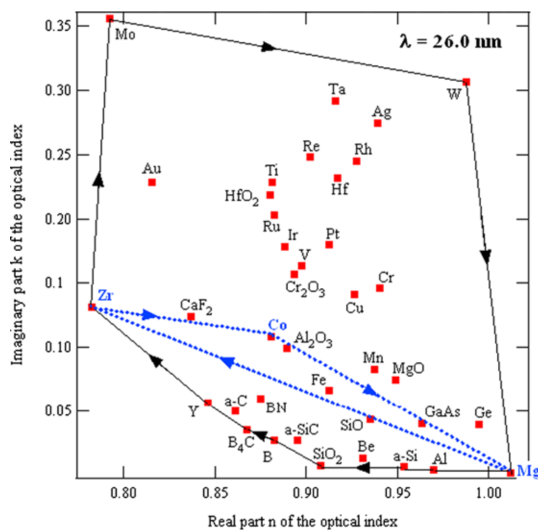

Fig. 4 Determination of the material order in the tri-layered structure applying the model of Larruquert [8] at $\lambda = 26.0$ nm

sulting from the calculation of conditions 1 and 2 in the case of the Mg, Co and Zr materials. We have successively considered 3 material sequences, namely Zr/Mg/Co, Mg/Zr/Co and Mg/Co/Zr where the first layer on the substrate is the first material given in the sample name. The Mg/Zr/Co/Zr quadri-layered structure is not taken into account since it is made of only three different materials.

From these results, the model predicts that the Mg/Co/Zr structure is the most suited in terms of enhanced EUV reflectivity. Indeed, it is the only structure fulfilling the two conditions.

An alternative way of using the theoretical model of Larruquert is to adopt a graphical method [8]. In Fig. 4, the optical constant values at $\lambda = 26.0$ nm of a large set of materials are plotted in the n–k plane the optical constants at $\lambda = 26.0$ nm of a large set of materials where the refractive index $N = n + ik$. Data are extracted from the CXRO database. According to [8], the "correct" material order leading to an enhanced reflectivity is as follows: clockwise rotation corresponds to the top layer to substrate sequence.

The so-called "minimum polygon" including all the materials, namely Zr/Mo/W/Mg/Al/SiO_2/B_4C/Y, is plotted in solid line and presents the largest circumference. The multilayer with an optimized film thickness distribution including all the materials of the minimum polygon will lead to a reflectance higher than the reflectance that can be obtained with a multilayer constructed with a subset of these materials. Nevertheless, an important assumption is considered: the interfaces are assumed to be smooth and abrupt, with no interdiffusion of the materials across the interface. The selection of a set of materials whose optical constants are inside the minimum polygon will lead to a lower reflectance regardless of the number of materials. As a consequence, in our case, the secondary polygon (dotted line), that is to say Zr/Co/Mg/Al/SiO_2/B_4C/Y, will be characterized by a lower reflectivity than that for the "minimum polygon" since its circumference is smaller. It appears that the substrate/Mg/Co/Zr sequence is more suited in terms of reflectivity than the substrate/Mg/Zr/Co combination.

From the secondary polygon, the Mg/Co/B_4C structure should also be pertinent according to the model. Nevertheless, in our recent study on Co/Mg/B_4C multilayers, nuclear magnetic resonance (NMR) spectroscopy has allow us to evidence a strong intermixing between Co atoms and B and/or C atoms from B_4C layers leading to a reflectivity of 0.7% at 25.1 nm [3].

3.4 Thermal stability of the Mg/Co and Mg/Co/Zr multilayers

We have studied the thermal stability of the Mg/Co and Mg/Co/Zr multilayers up to an annealing temperature equal to 200°C. The evolution, as a function of the annealing temperature, of the reflectivity of the Mg/Co and Mg/Co/Zr multilayers measured in the short spectral range at 45 and 50° of grazing incidence is presented in Fig. 5. For both angles (even if this effect is more pronounced at 50°), as the annealing temperature increases, the Bragg peak position is slightly shifted towards higher wavelengths. This shift away from the Mg L edge may have for consequence the slight reflectivity increase observed for both samples at 50°. Since the peak position is related to the period of the stack, the peak shift towards higher wavelengths would correspond to a slight period increase (period dilatation) with the annealing temperature. Since we have not performed XRR measurements on the annealed multilayers, we cannot follow the evolution of the period value as a function of the annealing temperature. The values of the peak reflectivity and background measured at 45° of grazing incidence in the wide spectral range (20.7–31.0 nm) are presented in Table 6 as a function of the annealing temperature.

For both the bi- and tri-layered structures, the reflectivity slightly increases with the temperature. At 45° of grazing incidence and considering the samples annealed at 200°C, the peak reflectivity value is at 25.1 nm equal to 44.1% for

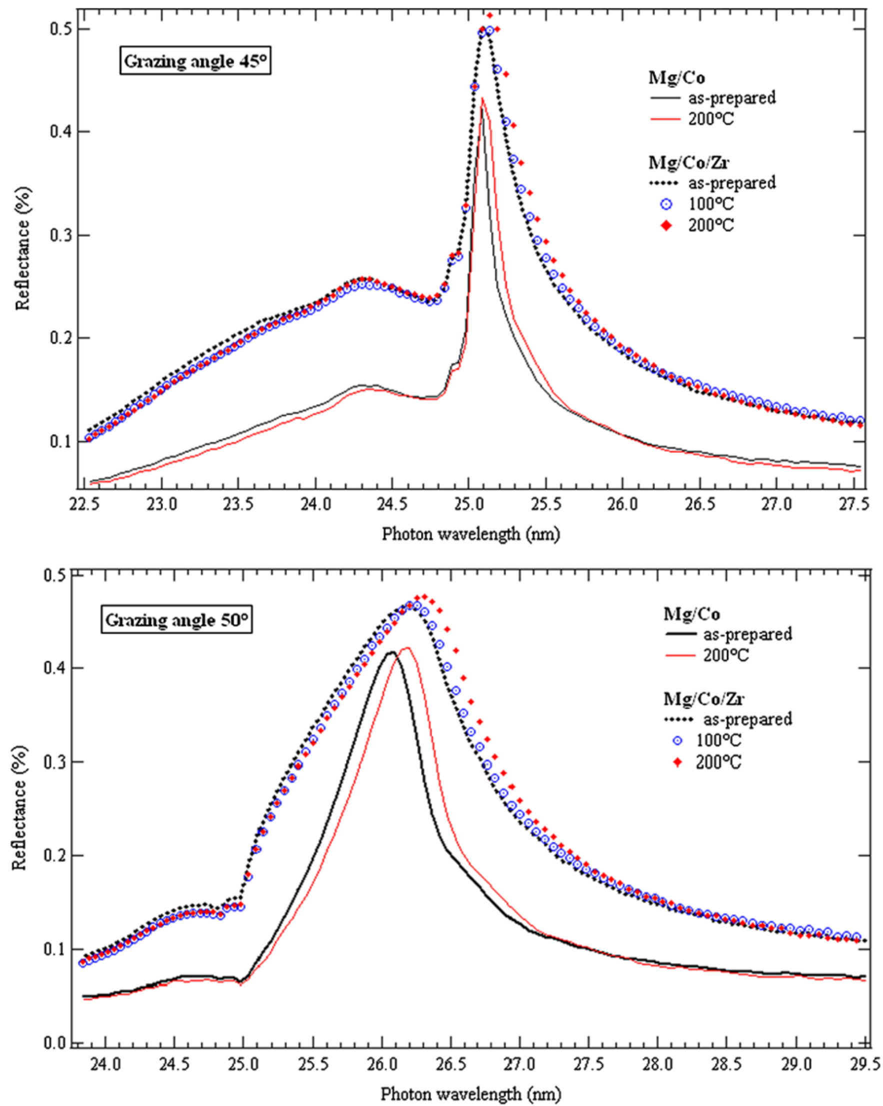

Fig. 5 Evolution, as a function of the annealing temperature, of the Mg/Co and Mg/Co/Zr EUV reflectivity spectrum measured at 45 and 50° of grazing incidence in the short spectral range

Table 6 Evolution as a function of the annealing temperature of the values, at 45° of grazing incidence, of the peak reflectivity and background measured in the wide spectral range (20.7–31.0 nm)

Multilayer	Mg/Co		Mg/Co/Zr	
	Peak reflectivity	Background	Peak reflectivity	Background
As-prepared	42.4% @ 25.1 nm	6.0% @ 25.1 nm	50.0% @ 25.1 nm	6.9% @ 25.1 nm
100°C	–	–	49.6% @ 25.1 nm	6.8% @ 25.1 nm
200°C	44.1% @ 25.1 nm	5.6% @ 25.1 nm	51.3% @ 25.1 nm	7.0% @ 25.1 nm

Mg/Co and 51.3% for Mg/Co/Zr. This latter value constitutes a promising result as far as the parameters during the multilayer deposition can be optimized.

4 Conclusion

We have presented the comparative analysis of the EUV optical quality of bi-, tri- and quadri-layered structures based on Mg, Co and Zr. The stack structural parameters and EUV optical performances have been estimated through X-ray and EUV reflectometry measurements, respectively. The addition of Zr at the only Mg–on–Co interface has proven to be an efficient combination to enhance the reflectance. The analysis of the measured EUV reflectance of tri- and quadri-layered systems has allowed us to validate the model of Larruquert predicting the order of the materials introduced within the structure. A reflectance slightly higher than 50% at 25.1 nm is reported for the Mg/Co/Zr system annealed at 200°C. Nevertheless it would be pertinent to perform complementary analysis, such as X-ray reflectometry, to inves-

tigate the slight period dilatation upon annealing. Given the compromise between the high reflectance at the application wavelength and the relatively high background, stress is laid on the use of these multilayers for imaging purpose through astrophysics applications for example.

References

1. H. Maury, P. Jonnard, K. Le Guen, J.-M. André, Z. Wang, J. Zhu, J. Dong, Z. Zhang, F. Bridou, F. Delmotte, C. Hecquet, N. Mahne, A. Giglia, S. Nannarone, Eur. Phys. J. B **64**, 193 (2008)
2. P. Jonnard, H. Maury, K. Le Guen, J.-M. André, N. Mahne, A. Giglia, S. Nannarone, Surf. Sci. **604**, 1015 (2010)
3. K. Le Guen, M.-H. Hu, J.-M. André, P. Jonnard, S.K. Zhou, H.Ch. Li, J.T. Zhu, Z.S. Wang, C. Meny, J. Phys. Chem. C **114**, 6484 (2010)
4. J. Zhu, S. Zhou, H. Li, Q. Huang, Z. Wang, K. Le Guen, M.-H. Hu, J.-M. André, P. Jonnard, Appl. Opt. **49**, 3922 (2010)
5. P. Boher, L. Hennet, Ph. Houdy, in *Advanced X-Ray/EUV Radiation Sources and Applications*, ed. by J.P. Knaueur, G.K. Shenoy. Proc. SPIE, vol. 1345 (SPIE Press, Bellingham, 1990), p. 198
6. M. Singh, J.J.M. Braat, Appl. Opt. **39**, 2189 (2000)
7. J.I. Larruquert, J. Opt. Soc. Am. A **18**, 1406 (2001)
8. J.I. Larruquert, J. Opt. Soc. Am. A **19**, 391 (2002)
9. J. Gautier, F. Delmotte, M. Roulliay, F. Bridou, M.-F. Ravet, A. Jérome, Appl. Opt. **44**, 384 (2005)
10. E. Meltchakov, C. Hecquet, M. Roulliay, S. De Rossi, Y. Ménesguen, A. Jérome, F. Bridou, F. Varniere, M.-F. Ravet-Krill, F. Delmotte, Appl. Phys A **98**, 111 (2010)
11. J.I. Larruquert, J. Opt. Soc. Am. A **18**, 2617 (2001)
12. M.-H. Hu, K. Le Guen, J.-M. André, P. Jonnard, S.K. Zhou, H.Ch. Li, J.T. Zhu, Z.S. Wang, AIP Conf. Proc. **1221**, 56 (2010)
13. S. Nannarone, F. Borgatti, A. DeLuisa, B.P. Doyle, G.C. Gazzadi, A. Giglia, P. Finetti, N. Mahne, L. Pasquali, M. Pedio, G. Selvaggi, G. Naletto, M.G. Pelizzo, G. Tondello, AIP Conf. Proc. **708**, 450 (2004)
14. J.I. Larruquert, J. Opt. Soc. Am. A **19**, 385 (2002)

Observation of an asymmetrical effect when introducing Zr in Mg/Co multilayers

K. Le Guen,[1,a)] M.-H. Hu,[1] J.-M. André,[1] S. K. Zhou,[2] H. Ch. Li,[2] J. T. Zhu,[2] Z. S. Wang,[2] C. Meny,[3] A. Galtayries,[4] and P. Jonnard[1]
[1]*Laboratoire de Chimie Physique—Matière et Rayonnement, CNRS UMR 7614, UPMC Univ Paris 06, 11 rue Pierre et Marie Curie, F-75231 Paris Cedex 05, France*
[2]*Institute of Precision Optical Engineering, Department of Physics, Tongji University, Shanghai 200092, People's Republic of China*
[3]*CNRS UMR 7504, Institut de Physique et Chimie des Matériaux de Strasbourg, 23 rue du Loess, BP 43, F-67034 Strasbourg Cedex 2, France*
[4]*Laboratoire de Physico-Chimie des Surfaces, CNRS UMR7045, Ecole Nationale Supérieure de Chimie de Paris (Chimie ParisTech), 11 rue Pierre et Marie Curie, F-75231 Paris Cedex 05, France*

(Received 24 March 2011; accepted 30 May 2011; published online 21 June 2011)

We have developed Mg/Co, Mg/Zr/Co, Mg/Co/Zr, and Mg/Zr/Co/Zr periodic multilayers and measured at 25.1 nm a reflectivity (R) highly sensitive to the material order within the period. To understand why Mg/Co/Zr is a more efficient mirror (R=50%) than Mg/Zr/Co and Mg/Zr/Co/Zr (~40%), we have probed the interface quality through time-of-flight secondary ion mass spectrometry and nuclear magnetic resonance measurements. The Zr-on-Co interface is found quite sharp while a strong intermixing process is evidenced between the upper Co and lower Zr layers, responsible for the decrease in optical contrast and subsequent R loss. *© 2011 American Institute of Physics*. [doi:10.1063/1.3601859]

We have developed Mg/Co, Mg/Zr/Co, Mg/Co/Zr, and Mg/Zr/Co/Zr nanometric periodic multilayers to build efficient mirrors for applications in the extreme ultraviolet (EUV) range.[1,2] For *s*-polarized light, the experimental peak reflectivity at 25.1 nm and 45° of grazing incidence for Mg/Co, Mg/Zr/Co, Mg/Co/Zr, and Mg/Zr/Co/Zr is equal to 42.4%, 41.4%, 50.0%, and 40.6%, respectively. Introducing a Zr layer at one or at the other interface or at both interfaces of Mg/Co does not induce an equivalent effect on the optical performances.[2] We are interested in understanding this asymmetrical "behavior" by correlating the mirror reflectivity to the quality of its interfaces. Sharp interfaces are required to ensure the highest reflectance, but the choice of the material combination is highly important as well as the order of the sequence within a period, for multilayers made of more than two materials.[3]

To describe the interface composition and structure, we have performed time-of-flight secondary ion mass spectrometry (ToF-SIMS) to get information about the chemical and elemental distribution, and nuclear magnetic resonance (NMR) spectroscopy to probe the chemical state of the magnetic Co atoms. To check the reliability of the stack structure reconstructed from ToF-SIMS and NMR analysis, we compare, for a given multilayer, the simulated EUV reflectivity curve to that measured at the ELETTRA synchrotron.[2] In a previous work based on X-ray emission spectroscopy (XES),[1] the chemical state of the Mg atoms within Mg/Co was found to be the same as in Mg metal: no noticeable interaction between the Mg and Co layers was evidenced. We have checked that the same result remains valid for Mg/Zr/Co, Mg/Co/Zr, and Mg/Zr/Co/Zr.

All multilayers were deposited using magnetron sputtering.[2] Each sample consists of 30 periods and exhibits a 3.5-nm-thick B_4C capping layer to prevent oxidation. In the following list, the first mention concerns the first layer deposited onto the Si substrate and the thickness is expressed in nm: Mg (14.45)/Co (2.55); Mg (13.20)/Zr (1.50)/Co (2.50); Mg (13.20)/Co (2.50)/Zr (1.50); Mg (12.00)/Zr (1.50)/Co (2.00)/Zr (1.50).

Depth elemental distributions are measured using ToF-SIMS working in the dual beam mode: both Bi^+ primary and Cs^+ sputtering ion beams are aligned to analyze secondary ions from the center of the sputtered crater. Here, we present only the Co^- ion depth profile since the Mg^- ion yield is very low and the Zr layers are too thin to provide Zr^- profiles exhibiting clear periodic oscillations. As a consequence, in the following we will not discuss the quality of the Mg-on-Zr and Zr-on-Mg interfaces. However, our XES analysis concluded that there was no significant interaction between Mg and Zr layers (unpublished). As sputtering yields can vary drastically, the sputtering time scale is not converted into a thickness scale and the profile intensity is not related to the number of atoms. The sample is analyzed from the surface down to the substrate.

The multilayers are analyzed using zero field NMR spectroscopy operating a broadband spectrometer working at 4.2 K. The NMR spectra depict the Co atom distribution as a function of their resonance frequency.[4,5] Since the presence of alien atoms as nearest neighbor of Co atoms shifts the resonance frequency, this technique is powerful to probe the Co local environment. All spectra are normalized to the sample surface area. The NMR intensity is therefore proportional to the thickness of ferromagnetic Co atoms in each frequency range.

Figure 1 presents the comparison of the Co^- profile for the four samples from period five to period ten as counted from the surface. It is striking that the shape of the Co^- profile is nearly symmetrical for Mg/Co and Mg/Co/Zr while

[a)]Author to whom correspondence should be addressed. Electronic mail: karine.le_guen@upmc.fr. Dr Karine Le Guen Laboratoire de Chimie Physique—Matière et Rayonnement 11 rue Pierre et Marie Curie F-75231 Paris Cedex 05, France. Tel.: 33 (0)1 44 27 66 08. FAX: 33 (0)1 44 27 62 26.

 © 2011 American Institute of Physics

Author complimentary copy. Redistribution subject to AIP license or copyright, see http://apl.aip.org/apl/copyright.jsp

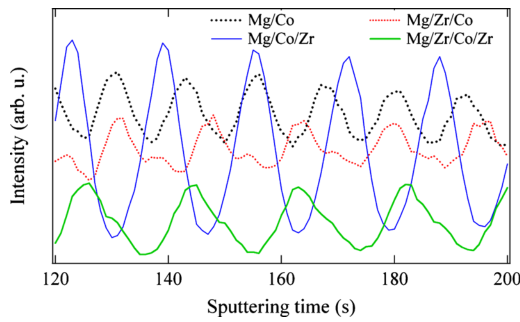

FIG. 1. (Color online) Evolution over five periods of the Co^- ToF-SIMS depth profile.

it is asymmetrical for Mg/Co/Zr and Mg/Zr/Co/Zr where it exhibits a main peak and an intense shoulder toward higher sputtering times.

For a given period, we define the contrast as the profile amplitude divided by the profile minimum. On the 130–150 s region, the contrast values are 0.34, 0.35, 2.10, and 0.87 for Mg/Co, Mg/Zr/Co, Mg/Co/Zr, and Mg/Zr/Co/Zr, respectively. By compiling the qualitative (symmetry) and quantitative (contrast) information on the Co^- profile shape, we can draw some conclusions about the interfaces. In Mg/Co, the symmetrical profile and our previous results[1] allow us to exclude intermixing between layers. The low value of the contrast could be due to a 0.5–0.6 nm interfacial roughness. Mg/Co/Zr presents the best profiles in terms of both symmetry and contrast. This indicates well-defined Co-on-Mg and Zr-on-Co interfaces. For Mg/Zr/Co, the splitting of the profile could reveal intermixing at the Co-on-Zr interface only. As a consequence, the interfaces in Mg/Zr/Co/Zr are asymmetrical: no intermixing at the Zr-on-Co interface (as in Mg/Co/Zr) while intermixing occurs at the Co-on-Zr interface (as in Mg/Zr/Co).

The NMR spectra of all samples are presented in Fig. 2. On one hand, the Mg/Co and Mg/Co/Zr spectra are both characterized by a well-defined and intense line at 226 MHz due to bulk hcp Co and a shoulder at 156 MHz related to the Co/Mg interface. In the spectrum of Mg/Co/Zr, we note the additional presence of a shoulder at 180 MHz corresponding to the Co/Zr interface. On the other hand, the 226 MHz line is no more observed in the spectra of Mg/Zr/Co and Mg/Zr/Co/Zr: they are solely made of a wide and flat feature covering the whole frequency domain.

From this distinction, we can deduce that (i) the Co layers and related interfaces are well-defined in Mg/Co and Mg/Co/Zr, giving evidence in this latter case that the Zr-on-Co interface is sharp in agreement with ToF-SIMS results and (ii) no more pure Co layers remain within Mg/Zr/Co and

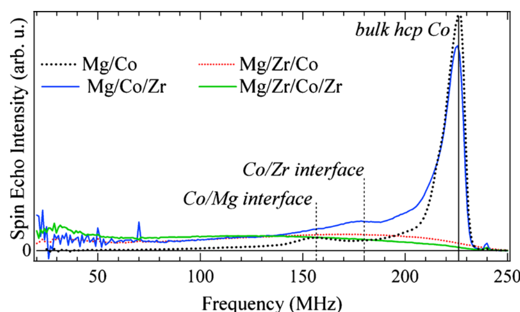

FIG. 2. (Color online) NMR spectra of the Mg/Co, Mg/Zr/Co, Mg/Co/Zr, and Mg/Zr/Co/Zr multilayers.

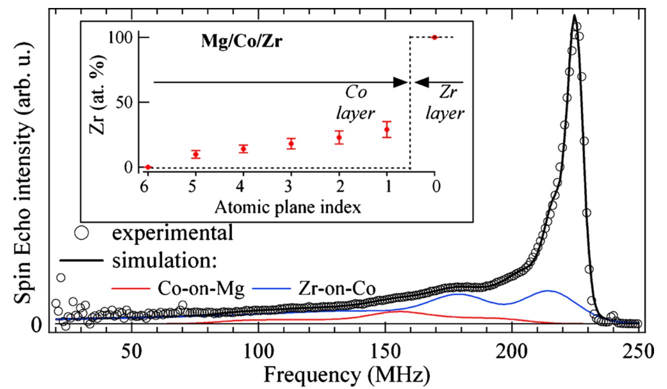

FIG. 3. (Color online) For Mg/Co/Zr, comparison of the experimental and simulated NMR spectra, the simulated spectrum being divided into the respective contributions of Co-on-Mg and Zr-on-Co interfaces. The Zr concentration profile at the Zr-on-Co interface is shown in inset compared to an "ideal" interface (dotted line).

Mg/Zr/Co/Zr as a consequence of an intermixing between upper Co and lower Zr layers at the Co-on-Zr interface.

However, a careful look at the Mg/Co/Zr and Mg/Co spectra shows significant differences: lower amplitude and broadening of the hcp Co bulk line and larger intensity in the low-frequency range. This suggests that the Zr-on-Co interface in Mg/Co/Zr is not as sharp as the Co-on-Mg interface in Mg/Co. Thus we have simulated the Mg/Co/Zr NMR spectrum. Two interface models are available: the step model which considers a perfectly flat interface with only step defects of monoatomic heights and the diffuse model where the interface is a succession of two dimensional random alloys, the fitting parameter being the concentration profile at the interface.[4]

The step interface model used for Mg/Co[1] cannot be implemented for Mg/Co/Zr as its intensity for frequencies lower than 200 MHz is significantly larger. However, since a feature similar to the one observed for the Co/Mg multilayer can still be observed (156 MHz), we assumed that the Mg/Co interfaces are similar to the interfaces of the Co/Mg multilayers and that the additional interfacial mixing that is observed arises solely from the Co/Zr interfaces. The simulated spectrum in Fig. 3, assuming a Co-on-Mg step interface and a Zr-on-Co diffuse interface, reproduces the experimental one. In the inset, the interfacial concentration profile at the Zr-on-Co interface shows that the intermixing region extends over five atomic planes with a concentration of Zr atoms into the Co layer limited to (29 ± 6) at. %. To give an order of magnitude, a 2.55-nm-thick hcp Co layer corresponds to ~12 atomic planes.

Given the drastic differences between the NMR spectra of Mg/Co/Zr and Mg/Zr/Co in Fig. 2, we assume that the Zr-on-Co interface in Mg/Co/Zr is sharp. The distinctions between the two sets of samples (on one hand Mg/Co and Mg/Co/Zr and on the other hand, Mg/Zr/Co and Mg/Zr/Co/Zr) are in agreement with ToF-SIMS results and with our recent studies.[1,2] From the point of view of thermodynamics, this asymmetrical behavior could be explained by a surfactant effect, i.e., an atomic exchange at the frontier induced by the minimization of the surface energy leading to the formation of the Co_xZr_y compound, rather than by a chemical effect accounting for a strong chemical affinity between Co and Zr.[9] In their study of a series of Au/Si bilayers exhibiting different period values but a constant thickness ratio, Labat

Author complimentary copy. Redistribution subject to AIP license or copyright, see http://apl.aip.org/apl/copyright.jsp

TABLE I. Structural parameters used to build the Mg/Co/Zr and Mg/Zr/Co systems and simulate their respective EUV reflectivity curves.

Sample	Mg/Co/Zr	Mg/Zr/Co
Period (nm)	17.1	17.2
Intermixing	—	At the Co-on-Zr interface
Structure	Trilayered stack Mg/Co/Zr	Bilayered stack $Mg/(Co_{0.78}Zr_{0.22})$
Layer thickness (nm)	Mg: 13.2 Zr: 1.5 Co: 2.4	Mg: 13.2 $Co_{0.78}Zr_{0.22}$: 4.0
Layer density (g cm^{-3})	Mg: 1.6 Zr: 6.5 Co: 8.8	Mg: 1.6 $Zr_{0.22}Co_{0.78}$: 8.4
Interfacial roughness (nm)	Co-on-Zr=0.6 Mg-on-Co=0.6 Zr-on-Mg=0.7	Mg-on-$(Co_{0.78}Zr_{0.22})$=1.4

et al.[6] reported a large asymmetry between the Au-on-Ni and Ni-on-Au interfaces. They correlated the intermixing evidenced at the Ni-on-Au interface to the surfactant effect of Au atoms leading to a subsequent accommodation of the lattice parameters. In our case, this "dynamic segregation" mechanism[7] relies on vertical exchanges on a microscopic scale between lower Zr and upper Co atoms, responsible for the formation of a diffuse Co-on-Zr interface as a consequence of the surfactant effect of Zr atoms.

We are now able to propose a reliable description of each multilayer. As a test of validity, the simulated EUV reflectivity curve is compared to the experimental one. We simulate the EUV reflectivity curves at 50° of grazing angle.[2] We restrict our simulations to the Mg/Co/Zr and Mg/Zr/Co trilayered systems.

In Mg/Co/Zr, all layers and interfaces are well-defined. The corresponding structural parameters (thickness, roughness, and density of all layers) are those extracted from the fit of the x-ray reflectivity curve measured at 0.154 nm.[2]

As a consequence of the intermixing taking place at the Co-on-Zr interface, Mg/Zr/Co cannot be considered as a trilayered system anymore. But, given the high peak reflectivity of this sample, a sufficiently high optical contrast and thus a layered structure still exist between the materials present in this sample. For these reasons, we model Mg/Zr/Co as a $Mg/(Co_xZr_y)$ bilayered stack where x and y are the relative number of Co and Zr atoms, respectively. The values of x and y, estimated from the number of Co and Zr atoms within the Co and Zr layers in Mg/Zr/Co, are found equal to 0.78 and 0.22, respectively. This compound could be ascribed to Co_4Zr ($Co_{23}Zr_6$ in the literature) present in the Zr–Co binary phase diagram.[8] Its density, calculated as the weighted sum of the Co and Zr densities, is estimated to 8.4 g cm^{-3}. In addition to the structural parameters describing the stack, we also take into account the fact that, in the EUV range, the available refractive indices[9] are not known with high accuracy. Therefore, in a second step, we introduce the possibility of varying the indices (directly or indirectly through the density). All simulation parameters are collected in Table I. The corresponding simulated reflectivity curves are presented in Fig. 4, in comparison with the one measured.

In the case of Mg/Co/Zr, the agreement between measurement and simulation becomes reasonable provided that the values of the refractive indices are slightly changed

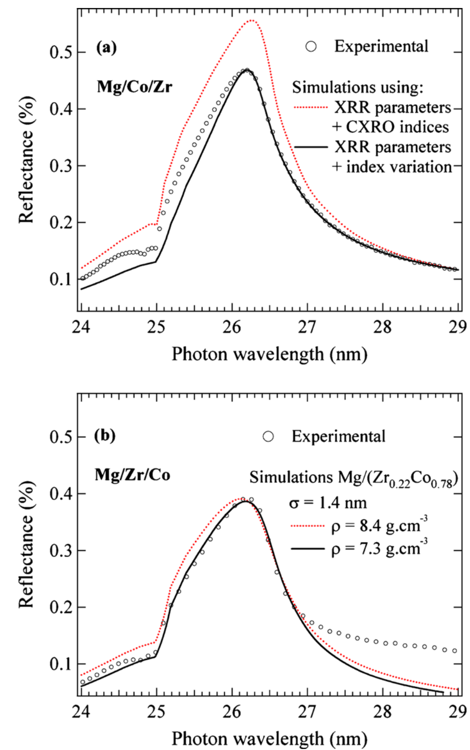

FIG. 4. (Color online) Comparison of the experimental and simulated reflectivity curves at 50° of grazing incidence of Mg/Co/Zr (a) and Mg/Zr/Co (b). Simulations are performed without (dotted line) and with (plain line) modification of the CXRO refractive indices.

(±15% maximum).[2] For Mg/Zr/Co, taking also into account an indirect variation in the EUV indices through a decrease of 13% of the $Co_{0.78}Zr_{0.22}$ density while keeping constant that of Mg, the simulated curve satisfactorily reproduces the experimental one up to 27 nm.

In conclusion, we have found a correlation between the optical performances of Mg/Co/Zr and the high structural quality of the interfaces within this stack. On the contrary, at the Co-on-Zr interface within Mg/Zr/Co, we have observed an intermixing process leading to the formation of $Co_{0.78}Zr_{0.22}$ and hence ruled out the preservation of the trilayered structure.

This work was funded by ANR-10-INTB-902-01 and supported by the European Community through the FP6 program under Contract No. RII3-CT-2004-506008 (IA-SFS).

[1]K. Le Guen, M.-H. Hu, J.-M. André, P. Jonnard, S. K. Zhou, H. Ch. Li, J. T. Zhu, Z. S. Wang, and C. Meny, J. Phys. Chem. C **114**, 6484 (2010).
[2]K. Le Guen, M.-H. Hu, J.-M. André, P. Jonnard, S. K. Zhou, H. Ch. Li, J. T. Zhu, Z. S. Wang, N. Mahne, A. Giglia, and S. Nannarone, Appl. Phys. A: Mater. Sci. Process. **102**, 69 (2011).
[3]J. I. Larruquert, J. Opt. Soc. Am. A **19**, 391 (2002); J. I. Larruquert, *ibid.* **18**, 2617 (2001).
[4]C. Meny and P. Panissod, in *Modern Magnetic Resonance*, edited by G. Webb (Springer, Heidelberg, 2006).
[5]P. Panissod and C. Meny, Appl. Magn. Reson. **19**, 447 (2000).
[6]S. Labat, P. Gergaud, O. Thomas, B. Gilles, and A. Marty, Appl. Phys. Lett. **75**, 914 (1999).
[7]D. L. Beke, C. Cserháti, Z. Erdélyi, and I. A. Szabó, in *Nanoclusters and Nanocrystals*, edited by H. S. Nalwa (American Scientific Publ., Stevenson Ranch California, USA, 2003), pp. 242–243.
[8]B. Predel, *Phase Equilibria, Crystallographic and Thermodynamic Data of Binary Alloys*, Landolt-Börnstein, New Series, Group IV, Vol. 5, edited by O. Madelung (Springer, Berlin 1991).
[9]CXRO database http://www-cxro.lbl.gov.

Author complimentary copy. Redistribution subject to AIP license or copyright, see http://apl.aip.org/apl/copyright.jsp

Chapitre 4 :

Etude des multicouches Al/SiC, Al/W/SiC et Al/Mo/SiC

4.1 Introduction

Dans ce chapitre nous présentons les performances de multicouches basées sur le système Al/SiC. Elles sont développées pour travailler dans la région spectrale entre 15 et 35 nm, en incidence normale. Dans cette gamme, de nombreuses multicouches sont étudiées telle Mo/Si (utilisé pour la mission STEREO par exemple) qui présente dans le domaine spectral 25-35 nm une réflectivité comprise entre 15% et 20% [20-22]. Le système Si/SiC a montré une réflectivité de 16,7% à 32,8 nm [23]. Le système Mg/SiC présente une réflectivité expérimentale de 42% à 30,4 nm [24].

L'étude des systèmes Al/SiC, Al/W/SiC et Al/Mo/SiC se déroule dans le cadre de l'ANR blanc ATTOMIX, un projet de caractérisation des multicouches développées pour réaliser les optiques de sources «attoseconde». Le projet a été accepté en 2007 avec l'institut d'Optique comme coordinateur et le LCPMR comme partenaire. L'intérêt des sources «attoseconde» est de permettre la mise en phase d'un spectre large d'harmoniques XUV avec une efficacité élevée. La génération d'impulsions ultra-brèves à l'échelle du temps attoseconde (10^{-18} s) ouvre le vaste champ d'exploration des phénomènes à dynamique ultra-rapide. Le projet propose d'utiliser l'interférométrie XUV pour avoir un accès direct aux constantes optiques des matériaux en miroirs multicouches. L'objectif de ce projet est donc de concevoir, réaliser et caractériser des miroirs de phase pour impulsions attosecondes, en s'appuyant sur des mesures fiables des indices des matériaux en couches minces et en combinant des analyses optiques et physico-chimiques des matériaux et de leurs interfaces. Le but de l'étude des matériaux est d'améliorer leurs valeurs de réflectivité dans la gamme EUV.

Notre équipe a déjà développé une méthodologie non destructive pour caractériser les miroirs multicouches périodiques [7]. J'ai été chargée d'appliquer cette méthodologie alliant réflectométrie XRR et EUV et XES aux systèmes Al/SiC, Al/W/SiC et Al/Mo/SiC. Les résultats ont été complétés par ceux obtenus par ToF-SIMS et XPS.

4.1 Introduction

Le choix des matériaux intéressants pour notre gamme spectrale est avant tout dicté par leurs propriétés optiques et notamment par leur absorption. Nous nous sommes donc tournés dans un premier temps vers les matériaux qui possèdent un seuil d'absorption dans notre gamme spectrale et qui, par conséquent, sont peu absorbants pour réaliser des miroirs. Nous avons donc choisi de travailler sur le dépôt d'aluminium qui possède un seuil d'absorption à 17 nm, et qui est donc compatible avec les structures bi-bandes visées. Comme la longueur d'onde de 30,4 nm a un rôle important, nous nous sommes également intéressés à l'étude des miroirs à cette longueur d'onde. Les difficultés attendues a priori pour cette étude sont d'une part la forte réactivité de l'aluminium avec l'oxygène et d'autre part sa facilité à cristalliser et donc à former des interfaces rugueuses. Le choix de SiC est dû à ses propriétés optiques et la stabilité de ses liaisons chimiques.

Nous nous sommes concentrés dans un premier temps sur les multicouches Al/SiC. Dans les simulations de réflectivité, une multicouche «idéale» (ni rugosité, ni réaction chimique aux interfaces) est considérée. Des simulations indiquent en effet que la structure multicouche idéalement optimisée pour les longueurs d'onde de 30,4 nm et 17,5 nm, présente une réflectivité théorique de 40% et 60%, à incidence normale et en polarisation s.

Les performances optiques de Al/SiC dépendent de la qualité des interfaces entre les différentes couches de l'empilement. Par ailleurs, au contact de l'air, la surface de ces empilements peut s'oxyder ce qui peut aussi affecter de façon non négligeable les performances des multicouches. La densité des couches et la rugosité géométrique affectent les propriétés optiques à la longueur d'onde d'application et peuvent diminuer la réflectance. Pour les longueurs d'onde de 17,5 nm, ces multicouches possèdent une réflectivité expérimentale de 37% à 10° de l'incidence normale en polarisation s. Nous avons montré que c'est bien l'interface Al sur SiC qui semble la plus problématique en terme de rugosité ~1,2 nm. Nous avons pu quantifier les pertes de réflectivité dues à l'oxydation et la rugosité géométrique.

Nous avons ajouté un nouveau matériau à cette interface afin de réduire la rugosité et développer les systèmes de tri-couches. Nous sommes intéressés à l'étude des multicouches périodiques à trois matériaux afin d'augmenter la réflectivité pour les longueur d'onde de 30,4 nm et 17,5 nm. Les matériaux que nous avons utilisés sont W et Mo. Les résultats montrent que dans tous les cas, l'ajout d'un troisième matériau permet d'augmenter la réflectivité, si la

séquence des matériaux est dans le bon ordre. Par exemple, dans le système Al/Mo/SiC [25], la simulation optimisée pour la longueur d'onde de 30,4 nm et 17,5 nm, présente les réflectivités théoriques de 44,4% et 66,2%. Une réflectivité de 32,4% à 30,4 nm et 53,4% à 17,5 nm, pour l'incidence quasi-normale a été mesurée avec le rayonnement synchrotron sur un composant optique réel. C'est le premier rapport d'une réflectivité expérimentale supérieure à 50% autour de 17 nm. La rugosité de Al/SiC avec W et Mo est ~0,6 nm pour l'interface Al sur SiC. Il est étonnant de constater que l'introduction d'un troisième matériau W ou Mo dans l'empilement Al/SiC conduit à la réduction de la rugosité à toutes les interfaces. Ce doit être la raison de leur réflectivité augmentée par rapport à Al/SiC.

La comparaison des valeurs théorique et expérimentale de réflectivité est discutée. La différence entre les valeurs simulée et mesurée est attribuée à l'oxydation de la couche de SiC, une réduction de la densité de Mo et les rugosités entre les différentes couches.

Dans ce chapitre, nous allons présenter les résultats du système Al/SiC avec ou sans la troisième couche (article **4-[1] et A-[5]**) et puis le système Al/Mo/SiC (article **4-[2] et A-[6]**).

4.2 Principales publications

4-[1]

P. Jonnard, K. Le Guen, M.–H. Hu, J.-M. André, E. Meltchakov, C. Hecquet, F. Delmotte : **Optical, chemical and depth characterization of Al/SiC periodic multilayers,** *Proc. SPIE 7360, O1-9 (2009)*

4-[2]

M.–H. Hu, K. Le Guen, J.-M. André, P. Jonnard, E. Meltchakov, F. Delmotte, A. Galtayries :

Structural properties of Al/Mo/SiC multilayers with high reflectivity for extreme ultraviolet light, *Optics Express, Vol. 18, Issue 19, pp. 20019-20028 (2010)*

Optical, chemical and depth characterization of Al/SiC periodic multilayers

P. Jonnard *[a], K. Le Guen [a], M.-H. Hu [a], J.-M. André [a], E. Meltchakov[b], C. Hecquet[b], F. Delmotte[b], A. Galtayries[c]

[a]Laboratoire de Chimie Physique – Matière et Rayonnement, Université Pierre et Marie Curie, CNRS UMR 7614, 11 rue Pierre et Marie Curie, F-75231 Paris Cedex 05, France

[b]Laboratoire Charles Fabry de l'Institut d'Optique, CNRS, Univ Paris-Sud, Campus Polytechnique, RD128, F-91127 Palaiseau cedex, France

[c]Laboratoire de Physico-Chimie des Surfaces, ENSCP, CNRS UMR 7045, 11 rue Pierre et Marie Curie, F-75231 Paris Cedex 05, France

ABSTRACT

We present the characterization of Al/SiC periodic multilayers designed for optical applications. In some samples, a thin layer of W or Mo is added at the SiC-on-Al interfaces. We use x-ray reflectivity (XRR) in order to determine the parameters of the stacks, *i.e.* thickness and roughness of all the layers. We have performed x-ray emission spectroscopy (XES) to identify the chemical state of the Al and Si atoms present within the structure from an analysis of the shape of the Al Kβ and Si Kβ emission bands. Finally, time of flight secondary ion mass spectrometry (ToF-SIMS) is used to obtain the depth profile of the different elements present within the studied stacks. A fit of the XRR curves shows that the Al/SiC multilayer present large interfacial roughness (up to 2.8 nm), which is decreased considerably (down to 1 nm or less) when the refractory metal layers are introduced in the periodic structure. The combination of XES and ToF-SIMS allows us to conclude that in these systems the roughness is a purely geometrical parameter and not related to chemical interfacial reactions.

Keywords: periodic multilayer, x-ray emission, x-ray reflectivity, time of flight secondary ion mass spectrometry

* philippe.jonnard@upmc.fr, phone 33 1 44 27 63 03, fax 33 1 44 27 62 26, www.lcpmr.upmc.fr/

1. INTRODUCTION

The Al/SiC system is promising for optical application in the 18-80 nm photon energy range. However, Al/SiC periodic multilayers are hampered by large interfacial roughness that leads to much lower experimental reflectivity compared to that of an ideal multilayer without roughness and interdiffusion. Particularly, x-ray reflectivity (XRR) measurements have shown that the Al-on-SiC and SiC-on-Al interfaces present rather different values of interfacial roughness. In order to improve the optical properties of this system, a thin layer of refractory metal, W or Mo, is added to the periodic structure. As deduced from optical simulations, the introduction of the thin metal layer would increase the multilayer reflectivity at the wavelength of application in the extreme UV (EUV) range. Preliminary experiments performed with synchrotron radiation around 30 nm have confirmed the reflectivity increase of the three-component multilayers with respect to the bi-layer system.

In this paper, we report on the study Al/SiC multilayers with and without additional W or Mo layers by combining different techniques:

- X-ray reflectivity to evaluate the thickness and roughness of the various layers in the stacks;
- X-ray emission spectroscopy (XES), to elucidate the chemical state of the Si and Al atoms within the multilayers and to show the possible presence of an interfacial compound if any;

E V and X- ay ptics: Synergy bet een aboratory and Space, edited by en udec, adislav Pina,
Proc. of SPIE Vol. 7360, 73600 · © 2009 SPIE · CCC code: 0277-786X/09/$18 · doi: 10.1117/12.820913

- Time of flight secondary ion mass spectrometry (ToF-SIMS) to determine the depth distribution of various elements present within the stacks.

To our knowledge there is presently no published study of the Al/SiC system performed neither by XRR, XES nor by ToF-SIMS techniques. However, some periodic multilayers, made of metallic or semi-conducting layers or designed for optical applications, have already been studied by XES [1-7] and by dynamic SIMS as well as ToF-SIMS [2,8-11].

2. METHODOLOGY

2.1 Sample preparation

The samples were prepared using magnetron sputtering in an apparatus described elsewhere [12]. The sputtering gas was Ar. Samples were deposited on Si polished wafers. The sputtering targets (99.995% or higher purity) were SiC, and Al with 1.5 wt% Si. Indeed, it has been shown by XRR that aluminum thin films prepared with a small amount of silicon are smoother (≈1 nm *rms* roughness) than those produced from pure Al targets (≈2 nm *rms* roughness).

The Al/Si multilayer consists of 40 bilayers, the thickness of the Al and SiC layers being 13.4 and 4.0 nm, respectively. The top layer is SiC. Two other multilayers were prepared with a thin refractory metal layer added at the SiC-on-Al interface. This interface was chosen because it has been shown by calculations that an introduction of a W or Mo in the multilayer period provides for a better XUV reflectivity if it is deposited in the above-mentioned order. The addition of the third material would also make an influence on the conditions of the layers growth and the interfaces formation. The W/SiC and Mo/SiC systems are known for their low interfacial roughness, so a smoothing effect was expected for the multilayers with Al. The simulations show that in case of the three-component multilayer, the number of periods needed to achieve the maximum of reflectivity is smaller than that of the two-component system. Thus, the reduced number of periods considerably limits the cumulative increasing of the roughness. The resulting structures consist of 15 periods of: Al(10.6 nm) / W(1.9 nm) / SiC(3.6 nm) and Al(11.5 nm) / Mo(1.3 nm) / SiC(3.6 nm).

2.2 X-ray reflectivity

The multilayers were analyzed by x-ray specular reflectivity measurements at 0.154 nm (Cu Kα emission at 8048 eV) performed with a grazing-incidence reflectometer working in the θ-2θ mode [13]. The angular resolution is 5/1000°. The detector is a gas-filled counter with the signal dynamics of seven orders of magnitude achieved by using calibrated absorption filters. The reflectivity curves are presented on a logarithmic scale.

2.3 X-ray emission spectroscopy

XES measurements were performed using a high spectral resolution wavelength dispersive spectrometer. We have measured the Al Kβ and Si Kβ emission bands resulting from the Al and Si 3p-1s electron transitions, respectively. These emissions describe the occupied valence states having the Al 3p and Si 3p character, respectively. Their shape is sensitive to the chemical state of the Al and Si emitting atoms, respectively. Following the ionization of the atoms present in the sample, characteristic x-rays were emitted [14], then dispersed by a $(10\bar{1}0)$ quartz (for Al Kβ emission) or (111) InSb (for Si Kβ emission) bent crystal. The radiation was detected in a gas-flux counter working in the Geiger regime. The spectral resolution E/ΔE is estimated to be ≈5000 in the Al Kβ range and ≈3000 in the Si Kβ range.

X-rays were produced upon electron excitation. The energy of the incident electrons has been chosen to be higher than the threshold of the studied emission: in the present case, 1560 and 1840 eV for the Al 1s and Si 1s binding energies, respectively. In the case of the Si emission, the electron energy was chosen sufficiently low in order that the incident electrons had not enough energy to produce Si 1s ionizations within the substrate. This way, the Si Kβ emission originated only from the multilayer stack and not from its substrate. The shape and intensity of the studied emission were checked to remain unchanged during the experiments.

In the following, emission spectra are presented, normalized with respect to their maximum and after a linear background subtraction. This background corresponds to the Bremsstrahlung radiation. The spectra of the multilayers are compared to these of thin films of Al(Si 1.5 wt%) and amorphous SiC, both prepared by magnetron sputtering.

2.4 Time of flight secondary ion mass spectrometry

The time of flight SIMS measurements were performed using the ToF SIMS 5 apparatus (ION-TOF Gmbh). The working pressure in the chamber was about 3 10^{-7} Pa. The total primary ion flux was below 10^{12} ions.cm^{-2} to ensure static conditions. The depth profiles were measured using the instrument in dual beam mode. A 25 keV primary Bi^+ ion source (LMIG) at a DC current of 15 nA (high mass resolution mode), rastered over a scan area of 100 µm x 100 µm was used as the analysis beam. The sputtering was performed using a 1 keV Cs^+ ion beam at a current of 50 nA and rastered over an area of 500 µm x 500 µm. Both ion beams were impinging the sample surface under an angle of 45° with respect to the surface normal and were aligned in such a way that the analyzed ions were taken from the middle of the sputtered crater.

The secondary ions following the Bi^+ sputtering come from the outermost surface (depth resolution of about 1 nm). Both positive and negative ions were recorded. However, in this work, only positive SIMS spectra are discussed, as the sputtering yields of the various species of each layer are sufficiently high to provide convenient data. Negative SIMS spectra have allowed to follow the diffusion of oxygen: this showed that oxygen impurities are present in the contamination layer (the outermost atoms which have reacted with atmosphere) and also incorporated within the Al layers (not shown here).

The profiles are presented on a sputtering time scale because the sputtering yields of the various layers are different. In order to increase the intensity of the W and Mo profiles, the intensities of W and Mo three isotopes have been added. The profiles are presented on a linear scale and with their maximum normalized to unity in order to show the relative contrast of the ion signals. The contrast is defined here as the difference between the maximum and minimum intensities with respect to the maximum intensity. The ToF-SIMS depth profiles presented in this work show three periods of the multilayers. It was possible to analyze in depth the total 15 periods, down to the Si substrate. The contamination layer (the first 150-200 s) is omitted in the figures. The depth resolution was examined as a function of the sputtering time. Within the experimental uncertainties, there is no systematic trend of a loss of intensity, whatever the element. This shows that in our experimental conditions, the sputtering does not induce significant roughness within the samples**.**

3. RESULTS AND DISCUSSION

The XRR curves obtained at 0.154 nm of the three studied multilayers are presented in Figure 1. With the Al/SiC multilayer, only 4 Bragg peaks are seen up to 1°, whereas up to 9 Bragg peaks are observed over the whole scanned angle range (2.6°) for the multilayers with W or Mo layers. It is also observed that the decrease of the background is much steeper for Al/SiC with respect to Al/W/SiC or Al/Mo/SiC. The differences between Al/W/SiC and Al/Mo/SiC are less pronounced. In fact only 7 Bragg peaks are observed with Al/Mo/SiC instead of 9 with Al/W/SiC and the decrease of the background is slightly more pronounced in the case of Al/Mo/SiC.

The different shapes of the curves, with and without W or Mo interlayers, give evidence that the introduction of the refractory metals improves the structural quality of the multilayers. This is expected to be related to the interfacial roughness and more particularly to the SiC-on-Al interfacial roughness. It is known that the interfacial roughness in Mg/SiC multilayers (≈2 nm) is quite large [5] with respect to that (less than 1 nm) of conventional multilayers for x-ray and EUV optics.

Thus, the XRR curves were fitted in order to determine the parameters of the stacks: the thickness and roughness of their various layers. A simple model of the stack is used for this purpose, *i.e.* without considering the possible formation of interfacial layers: succession of bilayers for the Al/SiC system and trilayers for Al/W/SiC and Al/Mo/SiC systems. The thicknesses have already been given in the methodology section (Cf. § 2) and then Table 1 summarizes the roughness of each layer in the stacks. For the Al/SiC multilayers, the roughness at the Al-on-SiC interface is more than twice the one determined at the SiC-on-Al interface. When W or Mo layers are introduced, the interfacial roughnesses decrease, the more striking values being obtained at the Al-on-SiC interface. In this case, a decrease by a factor 4.7 occurs, leading to

Al-on-SiC interface to be the smoothest one, within the experimental uncertainty. When comparing the Al/W/SiC and Al/Mo/SiC systems, it is observed that all layers have similar roughnesses, however the average roughness is slightly lower with W than with Mo.

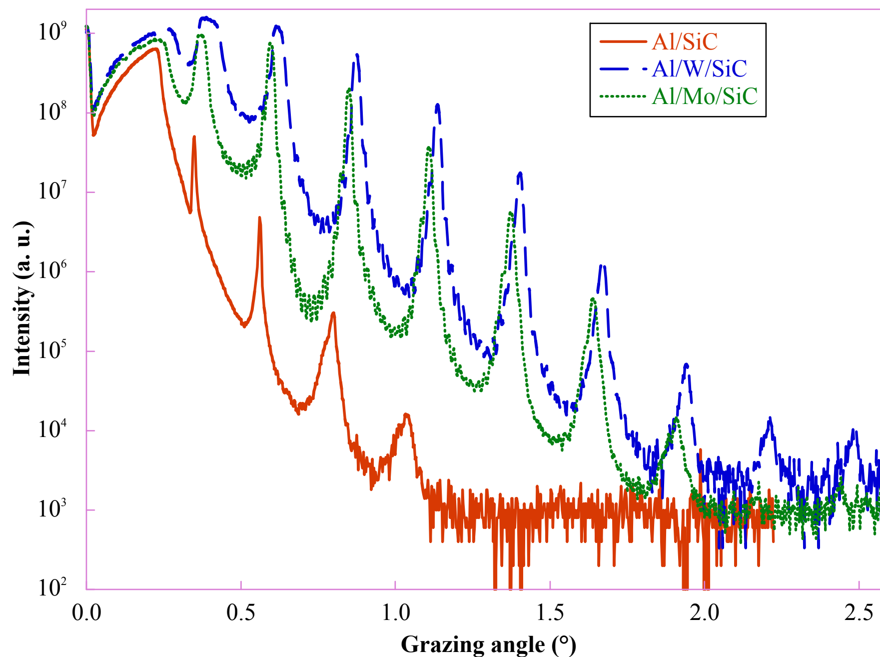

Figure. 1. X-ray reflectivity curves measured at 0.154 nm of Al/SiC, Al/W/SiC and Al/Mo/SiC multilayers.

Table 1. Roughness of the different layers of the Al/SiC, Al/W/SiC and Al/Mo/SiC multilayers. The values are given ±0.2 nm. "Roughness Al" refers to the SiC-on-Al interface for the two-component multilayer and to the W(Mo)-on-Al interface for the three-component systems; "Roughness SiC" refers to the Al-on-SiC interface; "Roughness W(Mo) refers to the SiC-on-W(Mo) interface for the three component system.

Multilayer	Roughness Al (nm)	Roughness W or Mo (nm)	Roughness SiC (nm)
Al/SiC	1.2	-	2.8
Al/W/SiC	0.8	1.0	0.6
Al/Mo/SiC	0.9	1.1	0.6

Figure 2 presents the Al Kβ and Si Kβ emission bands of all the samples except the Si K band of the Al/W/SiC multilayer. In this last case, a strong emission from tungsten (W Mβ emission, $4f_{5/2} - 3d_{3/2}$ electron transition) interferes with the silicon emission. The emission band of Al(Si 1.5 wt%) is identical to that of pure Al. The low Si concentration does not disturb the Al electronic structure [15]. The Al band presents a large peak, about 10 eV wide, with a sharp discontinuity marking the Fermi level at 1559.3 eV. The background is lower for photon energies beyond the Fermi level because of the strong self-absorption of the emitted photons in this range. The wide and faint structure around 1540 eV corresponds to a satellite emission. The Si band presents a large peak about 10 eV wide, with a shoulder located around 1828 eV. This shoulder is due to the hybridization between the Si p and C s valence states.

The formation of some interfacial compound, within the multilayers, would lead to the observation of a spectrum being the combination of the reference (due to the atoms that have not reacted) and the compound (due to the interfacial reaction) spectra. In addition to that, a strong variation in the shape of the emission band would be expected between two different compounds. As an illustration, the Al Kβ spectra of the Al(Si 1.5 wt%) and of a pressed powder of Al_4C_3

(possibly resulting from an interfacial reaction between Al and C atoms [16]) is shown in Figure 3. Both spectra exhibit different positions of their maximum, different bandwidths and also different secondary structures. Taking into account the x-ray emission spectroscopy sensitivity, an interfacial compound can be detected if it contributes to the intensity of the multilayer spectrum by more than 10%. In other words, an Al-containing interfacial compound thicker than about 1 nm and/or a Si-containing interfacial compound thicker than about 0.5 nm could be detected if occurring. This was the case with previous Mo/Si multilayers, where molybdenum silicide interfacial layers between 0.5 and 1.5 nm thick could be detected, depending on the preparation and treatment of the samples [2,3,6,7].

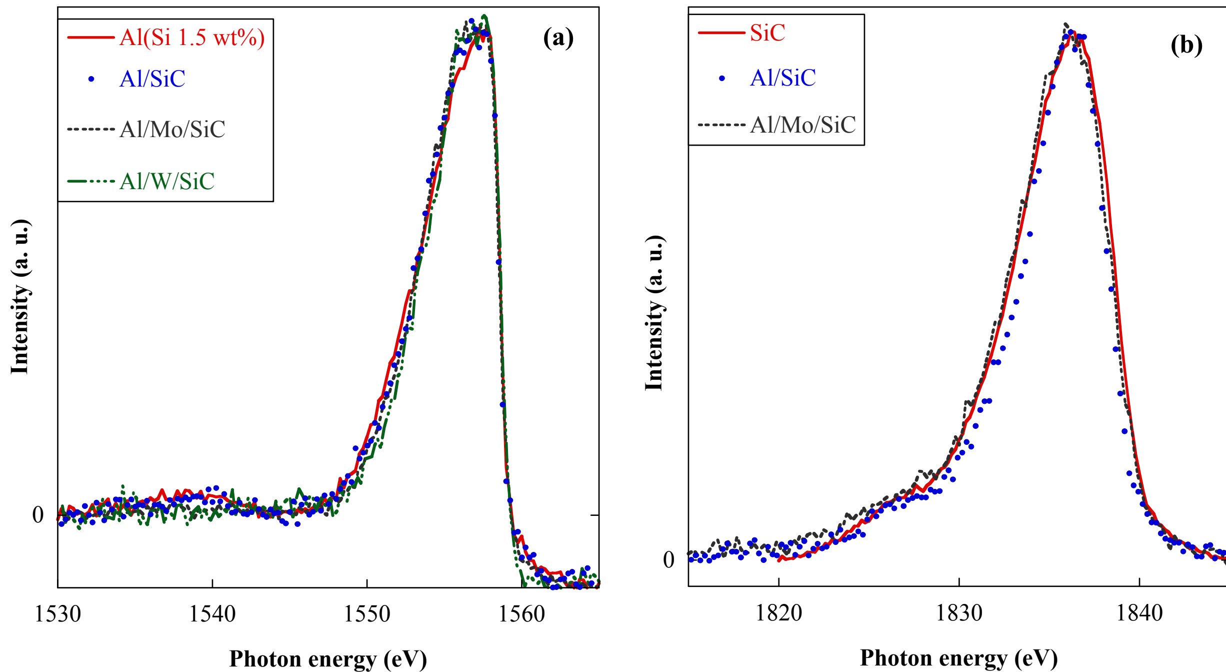

Figure. 2. Al Kβ (a) and Si Kβ (b) emission bands of Al/SiC, Al/W/SiC and Al/Mo/SiC compared to those of thin films of Al(Si 1.5 wt%) and amorphous SiC prepared by magnetron sputtering.

In spite of of slight variations of the bandwidth, there is no significant difference between the emission spectra of the multilayers and those of the reference thin films. This means that within the sample, Al atoms are in the same chemical state as Al atoms in Al(Si 1.5 wt%) and Si atoms are in the same chemical state as Si atoms in SiC, *i.e.* within the experimental uncertainties, there is no interaction between the Al(Si 1.5 wt%) and SiC layers leading to the formation of an interfacial compound.

In the case of the Al/W/SiC sample, the chemical state of the Si atoms was examined through the Si Kα atomic line (2p – 1s electron transition, not shown here). This atomic line is less sensitive to the chemical state than the Si Kβ emission band, however it has also shown that the Si atoms are in a SiC-like environment.

Figure 4 presents the depth profiles of the Al, Si, C, Mo and W positive ions obtained by ToF-SIMS for the three studied samples. Due to the low intensity (sputter yield) of the SiC^+ ions, the SiC information is given by both Si^+ and C^+ ions. Indeed, the C^+ profile closely follows the Si^+ line (Figure 4a). This was repeated with all samples. Thus, for the sake of clarity, only the Si^+ profiles are presented. The periodic modulations of the profiles clearly show the periodic structure of the stacks. For the Al/SiC multilayer (Figure 4a), the Al^+ profile is in opposite phase with respect to the Si^+ and C^+ profiles. For the Al/W/SiC multilayer (Figure 4b), the maximum of each profile is well separated from the other, leading to a clear determination of the succession of the layers. However, it is noted that the maximum of W^+ line corresponds to the minimum of Al^+, whereas the maximum of Si^+ is on the decreasing edge of the Al^+ profile. The same trend is observed for the Al/Mo/SiC sample (Figure 4c), with the difference that the maxima of the Mo^+ and Si^+ profiles are much closer than the ones of W^+ and Si^+. In this case the Mo and Si profiles are only slightly shifted.

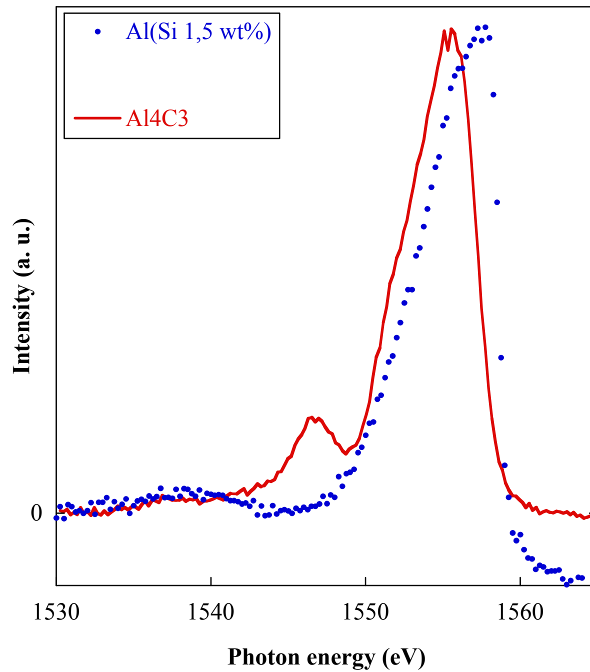

Figure. 3. Al Kβ emission bands of an Al(Si 1.5 wt%) thin film and an Al_4C_3 pressed powder.

It is possible to observe that the contrast of the amplitude of the profiles have different behaviors. For Al^+, whatever the sample, the contrast is almost the same, within the experimental uncertainty. This can be attributed to the large thickness of the Al layers with respect to the roughness values (Table 1). For Si^+ (and C^+), the contrast increases when W or Mo is introduced in the multilayer. There is no significant difference of the Si contrast between the Al/W/SiC and Al/Mo/SiC multilayers.

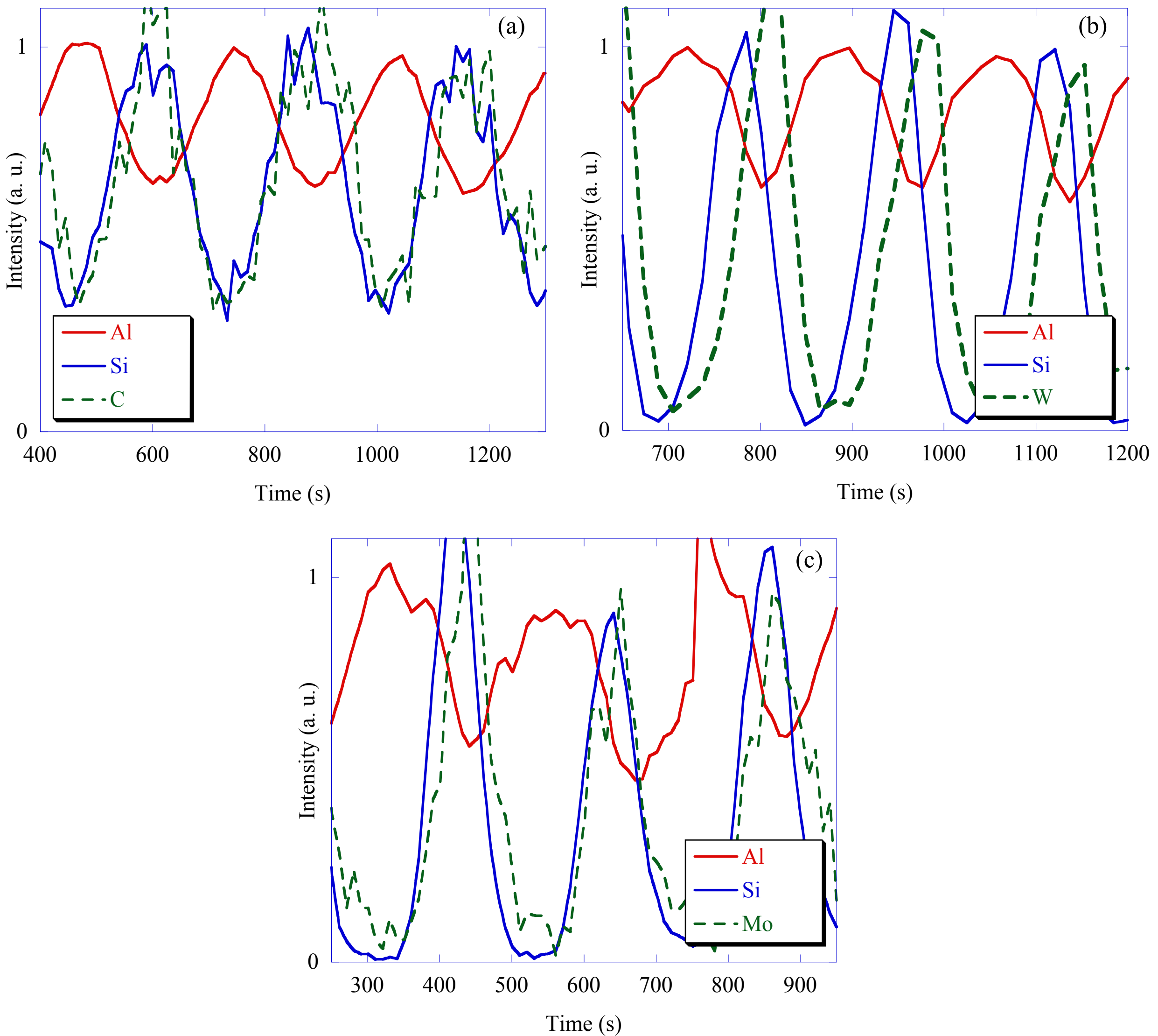

Figure. 4. Depth profiles of the Al, Si, C, Mo and W positive ions in the Al/SiC (a), Al/W/SiC (b) and Al/Mo/SiC (c) multilayers.

Figure 5 presents the comparison of the profile of only one element, Al or Si, for the three samples. The profiles have been shifted in time in order to align one of their maximum and only one period is presented. The shapes of the Al and Si profiles of the Al/SiC stack are nearly symmetrical and present gentle positive and negative slopes. The shape of the Si profiles of Al/W/SiC and Al/Mo/SiC is also quite symmetrical but the slopes are much steeper than those of Al/SiC. This leads to well defined Al and SiC layers, showing that the interfaces are more abrupt in the presence of the refractory metal in the multilayer structure. This can be due to:

- geometrical or mechanical roughness, as a result of small random variations of the thickness of various layers;
- chemical roughness, as a result of the diffusion of one element to the neighboring layers.

The second assumption can be ruled out because the Si and C profiles are strongly correlated, whereas if diffusion occurs, one should expect different gradients of chemical potentials for Si and C. This should induce one of these two species to diffuse more than the other one. Then, different profiles would be observed for Si^+ and C^+. The fact that no

significant chemical roughness is observed by ToF-SIMS is in good agreement with XES measurements, which did not show any evidence of the presence of interfacial compound. This is also in good agreement with the XRR measurements, showing that it is not necessary to take into account some interfacial layers to fit the reflectivity curves and that the interfacial roughness decreases when introducing the refractory metal within the multilayer.

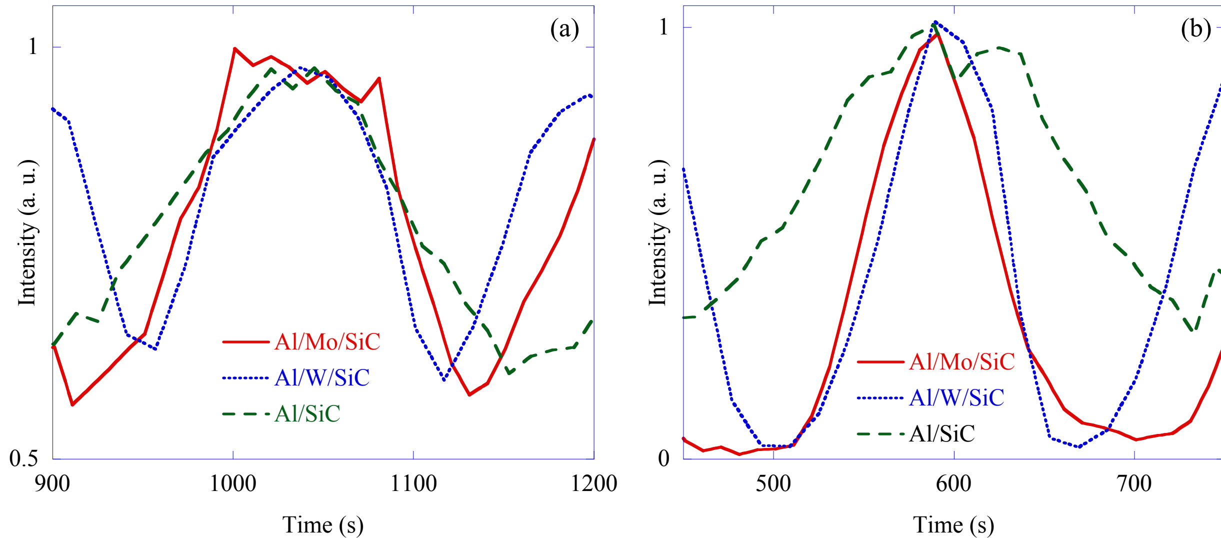

Figure. 5. Depth profiles of the Al^{+} (a) and Si^{+} (b) ions for the Al/SiC, Al/W/SiC and Al/Mo/SiC multilayers.

Regarding the Si^{+} profile of Al/W/SiC, we note that its negative slope is steeper than that of the Al/Mo/SiC system. This might indicate that the SiC-on-W interface is more abrupt than its counterpart SiC-on-Mo. Thus it would be better to introduce thin W layers instead of the Mo ones in order to reduce the interfacial roughness. This could also explain why the W and SiC layers in the Al/W/SiC multilayer (Figure 4b) are better resolved than the Mo and SiC layers in the Al/Mo/SiC multilayer (Figure 4c).

4. CONCLUSION

Periodic Al/SiC multilayers were studied by combining various experimental techniques, which provide valuable information on their optical characteristics (XRR), chemical properties (XES) and depth elemental/layer distribution of the elements (ToF-SIMS) within the stacks. The effect resulting from addition of thin layers of refractory metal, W or Mo, at the SiC-on-Al interfaces has been observed. This introduction considerably decreases the interfacial roughness and improves the structural quality of the multilayer stack (XRR). The formation of sharper interfaces is confirmed by the ToF-SIMS experiments. XES does not show any chemical reaction between the Al and SiC layers and thus confirms that here the roughness is a purely geometrical parameter and not a chemical one. It is possible to attribute a small differences between XRR curves and ToF-SIMS profiles of the Al/W/SiC and Al/Mo/SiC stacks to lower interfacial roughness when W is present. The difference could also be related to the crystalline or amorphous state of the refractory metal layers.

ACKNOWLEDGMENTS

Part of this work was funded by the ANR project 07-BLAN-0150. Pr. Z. Wang is thanked for providing us with the SiC thin film. The authors would like to thanks Pr. S. Nanaronne, Dr. A. Giglia and Dr. N. Mahne at synchrotron Trieste for their assistance during synchrotron radiation measurements. All multilayer depositions have been carried out on the deposition machine at CEMOX (Centrale d'Elaboration et de Métrologie des Optiques X).

REFERENCES

[1] Muramatsu, Y., Takenaka, H., Ueno, Y., Gullikson, E. M. and Perera, R. C. C., "Chemical bonding state analysis of silicon carbide layers in Mo/SiC/Si multilayer mirrors by soft x-ray emission and absorption spectroscopy," Appl. Phys. Lett. 77, 2653-2655 (2000).

[2] Maury, H., Jonnard, P., André, J.-M., Gautier, J., Roulliay, M., Bridou, F., Delmotte, F., Ravet, M.-F., Jérome, A. and Holliger, P., "Non destructive study of the interphases in Mo/Si and Mo/B_4C/Si/B_4C multilayers," Thin Solid Films 514, 278-286 (2006).

[3] Maury, H., Jonnard, P., André, J.-M., Gautier, J., Bridou, F., Delmotte, F. and Ravet, M.-F., "Interface characteristics of Mo/Si and B4C/Mo/Si multilayers using non-destructive x-ray techniques," Surf. Sci. 601, 2315-2322 (2007).

[4] Shulakhov, A. S., Bukin, S. V., Zdanchuk, E. V. and Tveryanovich, S. Y., "X-ray emission spectroscopy of solids in the depth-resolution mode : investigation of *a*-Si/Al/*c*-Si nanolayers," Bull. Russ. Acad. Sci. Phys. 72, 434-438 (2008).

[5] Maury, H., Jonnard, P., Le Guen, K., André, J.-M., Wang, Z., Zhu, J., Dong, J., Zhang, Z., Bridou, F., Delmotte, F., Hecquet, C., Mahne, N., Giglia, A. and Nannaronne, S., "Thermal cycles, interface chemistry and optical performance of Mg/SiC multilayers," Eur. Phys. J. B64, 193-199 (2008).

[6] Maury, H., André, J.-M., Le Guen, K., Mahne, N., Giglia, A., Nannarone, S., Bridou, F., Delmotte, F. and Jonnard, P., "Analysis of Mo/Si multilayers: influence of the Mo thickness," Surf. Sci. 603, 407-411 (2009).

[7] Maury, H., Jonnard, P., Le Guen, K. and André, J.-M., "Formation of silicides in annealed periodic multilayers," Proc. SPIE 7360.

[8] Maury, H., Holliger, P., Farès, B., Gautier, J., Roulliay, M., Bridou, F., Delmotte, F., Ravet, M.-F., André, J.-M. and Jonnard, P., "Analysis of a B_4C / Mo / Si multilayer interferential mirror by SIMS : influence of the sputtering ion," Surf. Interf. Anal. 38, 781-783 (2006).

[9] Cwil, M., Konarski, P. and Ciosek, J. "Ion mass interferences and matrix effects on SIMS depth profiling of thin Ti/Si multilayer films induced by hydrogen, carbon and oxygen contaminations," Int. J. Mass Spectrom. 263, 54-58 (2007).

[10] Kim, K. J., Simons, D. and Gillen, G., "Quantitative depth profiling of an alternating Pt/Co multilayer and a Pt–Co alloy multilayer by SIMS using a Buckminsterfullerene (C60) source," Appl. Surf. Sci. 253, 6000-6005 (2007).

[11] Chakraborty, P., "Ultra-high depth resolution SIMS for the interface analysis of complex low-dimensional structures," Nucl. Instrum. Meth. Phys. Res. B 266, 1858-1865 (2008).

[12] Gautier, J., Delmotte, F., Roulliay, M., Bridou, F., Ravet, M.-F. and Jérome, A., "Study of normal incidence of three-component multilayer mirrors in the range 20-40 nm," Appl. Opt. 44, 384-390 (2005).

[13] Névot, L., Pardo, B. and Corno, J., "Characterization of X-UV multilayers by grazing-incidence reflectometry," Rev. Phys. Appl. 23, 1675-1686 (1988).

[14] Bonnelle, C, "X-ray spectroscopy," Ann. Rep. Prog. Chem., Sect. C: Phys. Chem. 84, 201-272 (1987).

[15] Jonnard, P., Le Guen, K., Gauvin, R. and Le Berre, J.-F., "Characterization of Al and Mg alloys from their emission bands," Microscopy & Microanalysis 15, 36-45 (2009).

[16] Gröbner, J., Lukas, H. L. and Aldinger, F., "Thermodynamic calculation of the ternary system Al-Si-C," Calphad 20, 247-254 (1996).

Structural properties of Al/Mo/SiC multilayers with high reflectivity for extreme ultraviolet light

Min-Hui Hu,[1] Karine Le Guen,[1] Jean-Michel André,[1] Philippe Jonnard,[1,*] Evgueni Meltchakov,[2,4] Franck Delmotte,[2] and Anouk Galtayries[3]

[1]*Laboratoire Chimie Physique – Matière Rayonnement, UPMC Univ Paris 06, CNRS UMR 7614, 11 rue Pierre et Marie Curie, F-75005 Paris, France*
[2]*Laboratoire Charles Fabry de l'Institut d'Optique, CNRS UMR 8501, Université Paris-Sud, F-91127 Palaiseau, France*
[3]*Laboratoire de Physico-Chimie des Surfaces, École Nationale Supérieure de Chimie de Paris (Chimie ParisTech), CNRS UMR 7045, F-75005 Paris, France*
[4]*Now at Institut d'Astrophysique Spatiale, Université Paris-Sud, France*
** philippe.jonnard@upmc.fr*

Abstract: We present the results of an optical and chemical, depth and surface study of Al/Mo/SiC periodic multilayers, designed as high reflectivity coatings for the extreme ultra-violet (EUV) range. In comparison to the previously studied Al/SiC system, the introduction of Mo as a third material in the multilayer structure allows us to decrease In comparison to the previously studied Al/SiC system with a reflectance of 37% at near normal incidence around 17 nm, the introduction of Mo as a third material in the multilayer structure allows us to decrease the interfacial roughness and achieve an EUV reflectivity of 53.4%, measured with synchrotron radiation. This is the first report of a reflectivity higher than 50% around 17 nm. Time-of-flight secondary ion mass spectrometry (ToF-SIMS) and x-ray photoelectron spectroscopy (XPS) measurements are performed on the Al/Mo/SiC system in order to analyze the individual layers within the stack. ToF-SIMS and XPS results give evidence that the first SiC layer is partially oxidized, but the O atoms do not reach the first Mo and Al layers. We use these results to properly describe the multilayer stack and discuss the possible reasons for the difference between the measured and simulated EUV reflectivity values.

©2010 Optical Society of America

OCIS codes: (340.7480) X-rays, soft x-rays, extreme ultraviolet (EUV); (230.4170) Multilayers; (230.1480) Bragg reflectors; (240.6675) Surface photoemission and photoelectron spectroscopy.

References and links

1. T. W. Barbee, Jr., S. Mrowka, and M. C. Hettrick, "Molybdenum-silicon multilayer mirrors for the extreme ultraviolet," Appl. Opt. **24**(6), 883–886 (1985).
2. K. Skulina, C. Alford, R. Bionta, D. Makowiecki, E. Gullikson, R. Soufli, J. Kortright, and J. Underwood, "Molybdenum/beryllium multilayer mirrors for normal incidence in the extreme ultraviolet," Appl. Opt. **34**(19), 3727–3730 (1995).
3. S. Bajt, H. N. Chapman, N. Nguyen, J. Alameda, J. C. Robinson, M. Malinowski, E. Gullikson, A. Aquila, C. Tarrio, and S. Grantham, "Design and performance of capping layers for extreme-ultraviolet multilayer mirrors," Appl. Opt. **42**(28), 5750–5758 (2003).
4. M. G. Pelizzo, M. Suman, G. Monaco, P. Nicolosi, and D. L. Windt, "High performance EUV multilayer structures insensitive to capping layer optical parameters," Opt. Express **16**(19), 15228–15237 (2008).
5. S. A. Yulin, F. Schaefers, T. Feigl, and N. Kaiser, "Enhanced reflectivity and stability of Sc/Si multilayers," Proc. SPIE **5193**, 155–163 (2004).
6. A. Aquila, F. Salmassi, Y. Liu, and E. M. Gullikson, "Tri-material multilayer coatings with high reflectivity and wide bandwidth for 25 to 50 nm extreme ultraviolet light," Opt. Express **17**(24), 22102–22107 (2009).
7. P. Jonnard, K. Le Guen, M.-H. Hu, J.-M. André, E. Meltchakov, C. Hecquet, F. Delmotte, and A. Galtayries, "Optical, chemical and depth characterization of Al/SiC periodic multilayers," Proc. SPIE **7360**, O1–O9 (2009).
8. A. Galtayries, M.-H. Hu, K. Le Guen, J.-M. André, P. Jonnard, E. Meltchakov, C. Hecquet, and F. Delmotte, "Nanometer designed Al/SiC periodic multilayers: characterization by a multi-technique approach," Surf. Interface Anal. **42**(6-7), 653–657 (2010).

#131948 - $15.00 USD Received 19 Jul 2010; revised 26 Aug 2010; accepted 26 Aug 2010; published 3 Sep 2010

9. : J. Gautier, F. Delmotte, M. Roulliay, F. Bridou, M.-F. Ravet, and A. Jérome, "Study of normal incidence of three-component multilayer mirrors in the range 20-40 nm," Appl. Opt. **44**(3), 384–390 (2005).
10. S. Nannarone, F. Borgatti, A. DeLuisa, B. P. Doyle, G. C. Gazzadi, A. Giglia, P. Finetti, N. Mahne, L. Pasquali, M. Pedio, G. Selvaggi, G. Naletto, M. G. Pelizzo, and G. Tondello, "The BEAR beamline at ELETTRA," AIP Conf. Proc. **705**, 450–453 (2004).
11. A. Galtayries, S. Wisniewski, and J. Grimblot, "Formation of thin oxide and sulphide films on polycrystalline molybdenum foils: characterization by XPS and surface potential variations," J. Electron Spectrosc. Relat. Phenom. **87**(1), 31–44 (1997).
12. K. Domen, and T. J. Chuang, "Laser-induced photodissociation and desoprtion. 1. CH_2I_2 adsorbed on Al_2O_3," J. Chem. Phys. **90**(6), 3318–3331 (1989).
13. Y. Mizokawa, K. M. Geib, and C. W. Wilmsen, "Characterization of β-SiC surfaces and the Au/SiC interface," J. Vac. Sci. Technol. A **4**(3), 1696–1700 (1986).
14. M. Yuan, J.-T. Lu, and G. Kong, "Effect of SiO_2:Na_2O molar ratio of sodium silicate on the corrosion resistance of silicate conversion coatings," Surf. Coat. Tech. **204**(8), 1229–1235 (2010).
15. S. Tanuma, C. J. Powell, and D. R. Penn, "Calculations of electron inelastic mean free paths. V. Data for 14 organic compounds over the 50-2000 eV range," Surf. Interface Anal. **21**(3), 165–176 (1994).
16. J. H. Scofield, "Hartree-Slater subshell photoionization cross-sections at 1254 and 1487 eV," J. Electron Spectrosc. Relat. Phenom. **8**(2), 129–137 (1976).
17. D. L. Windt, "IMD - Software for modeling the optical properties of multilayer films," Comput. Phys. **12**(4), 360–370 (1998).
18. E. Meltchakov, C. Hecquet, M. Roulliay, S. Rossi, Y. Menesguen, A. Jérome, F. Bridou, F. Varniere, M.-F. Ravet-Krill, and F. Delmotte, "Development of Al-based multilayer optics for EUV," Appl. Phys., A Mater. Sci. Process. **98**(1), 111–117 (2010).
19. P. Jonnard, K. Le Guen, M.-H. Hu, J.-M. André, E. Meltchakov, C. Hecquet, F. Delmotte, and A. Galtayries, "Optical, chemical and depth characterization of Al/SiC periodic multilayers", Proc. SPIE **7360**, 7360O1–7360–O9 (2009).

1. Introduction

In the extreme ultra-violet (EUV) spectral range, the performances of multilayer mirrors are usually limited by material absorption, interfacial roughness and/or surface oxidation. The first experimental reflectivity higher than 50% has been reported by Barbee *et al.* 25 years ago with Mo/Si multilayers near the Si L edge [1]. Since then, a lot of improvements have been made. In fact, most of the high reflectivity multilayer coatings, as Mo/Si, Mo/Be, Mo_2C/Si, Ru/Be, have been developed for the 11 to 14 nm range, mainly for EUV lithography application [2–4]. Nevertheless, only few results with reflectivity higher than 50% have been reported at higher wavelengths: Sc/Si at 45.9 nm [5] and more recently Mg/Sc/SiC multilayers at 28.4 nm [6]. It is thus required to study new material combinations in order to improve multilayer coating performances in the whole EUV range.

Optical simulations indicate that the Al/SiC material combination could be valuable for applications in the EUV range from 15 to 35 nm. However, Al/SiC periodic multilayers have a large interfacial roughness that leads to low experimental reflectivity. No significant interdiffusion between the layers could be observed using x-ray emission spectroscopy [7,8]. An addition of a thin Mo layer to only the SiC-on-Al interfaces decreases the interfacial roughness and thus improves the optical performances of this system. Moreover, the introduction of a third material in a periodic multilayer structure can increase the peak reflectivity in the EUV range [9].

In this paper, we combine different complementary experimental techniques to study the material distribution within the Al/Mo/SiC multilayers of short and long periods. X-ray reflectivity (XRR) measurements at 0.154 nm (Cu Kα emission at 8048 eV) allowed us to obtain the thicknesses of individual layers and estimate the values of interfacial roughness within the stacks. The optical performances of the new multilayers in the EUV range were tested with synchrotron radiation. Time-of-flight secondary ion mass spectrometry (ToF-SIMS) was performed both to determine the depth distribution (depths profiles) of various elements and identify the chemical composition of a region close to the surface of the samples. We applied the X-ray photoelectron spectroscopy (XPS) in order to determine the chemical state of the outermost 10 nm-thick depth of the stack. A chemical modification of the top SiC layer was of particular interest as this can be responsible for the reflectivity loss in the EUV range.

2. Experiment

Sample preparation and characterization by XRR at 0.154 nm

The Al/Mo/SiC multilayers were prepared by magnetron sputtering in an apparatus described elsewhere [9]. We use a 2 mTorr argon plasma in dc mode for deposition of Mo and rf mode for SiC and Al. All the samples are deposited onto Si polished wafers. The sputtering targets (99.95% or higher purity) are Mo, SiC and Al with 1.5 wt% Si. Indeed, it has been shown by XRR that aluminum thin films including a small amount of silicon are smoother (≈1 nm *rms* roughness) than those produced from pure Al targets (≈2 nm *rms* roughness). We have selected the multilayers of a short (8.8 nm) and a long (16.6 nm) period with a different number of trilayers. The parameters and the names assigned to the two samples are given below:

Al/Mo/SiC_15: Si / $[Al(11.5\ nm)/Mo(1.3\ nm)/SiC(3.8\ nm)]_{15}$;

Al/Mo/SiC_25: Si / $[Al(6.4\ nm)/Mo(1.4\ nm)/SiC(1.1\ nm)]_{25}$ / SiC(1.1 nm).

The Al layers are polycrystalline and the Mo ones are amorphous. Due to the thinness of the SiC layer of Al/Mo/SiC_25, an additional SiC capping layer was added on top of the multilayer. Then, in both samples, the top SiC layer was relatively thick, 3.8 or 2.2 nm, in order to protect the underlying layers from oxidation. The samples were stored in a clean room at 20°C for three months prior to their analysis.

The samples were analyzed by XRR measurements at 0.154 nm (Cu Kα emission at 8048 eV) performed with a grazing-incidence reflectometer working in the θ-2θ mode. The angular resolution is 5/1000°. The dynamic range of a gas-filled detector equipped with calibrated absorption filters is about six orders of magnitude. The XRR curves were fitted in order to determine the parameters of the stacks: the thickness and roughness of their various layers. A simple model of the stack was used for this purpose, *i.e.* without considering the possible formation of interfacial layers. Since the thicknesses have already been given above, Table 1 summarizes the interfacial roughness of each layer in the stacks.

Table 1. Interfacial roughness values at the three interfaces of the Al/Mo/SiC multilayers derived from the fit of the reflectivity curves measured at 0.154 nm. The values are given ± 0.2 nm

Multilayer	roughness (nm) Mo-on-Al	roughness (nm) SiC-on-Mo	roughness (nm) Al-on-SiC
Al/Mo/SiC_15	0.7	0.9	0.7
Al/Mo/SiC_25	0.5	0.8	0.6

EUV reflectivity

The EUV reflectivity measurements were performed on the BEAR beamline [10] of Elettra synchrotron facility. The reflectivity curves were measured at near normal incidence (80° glancing incidence) using *s*-polarized light. The absolute uncertainty of the reflectivity values is less than 0.5%. The photon energy is calibrated with respect to the absorption edges of metal filters installed in the beamline. The intensities of incident and reflected radiation were measured with a solid state photodiode. Incoming photon flux was also monitored by using a gold mesh inserted in the beam path, whose drain current was used for normalization.

ToF-SIMS

ToF-SIMS measurements were performed using a ToF-SIMS 5 apparatus (ION-TOF Gmbh). The working pressure in the chamber was about 3 10^{-7} Pa. The total primary ion flux was below 10^{12} ions.cm^{-2} to ensure static conditions. The depth profiles were measured with the instrument working in the dual beam mode. The sputtering was performed using a 1 keV Cs^+ ion beam at a current of 50 nA and rastered over an area of 250 µm × 250 µm. A 25 keV

#131948 - $15.00 USD Received 19 Jul 2010; revised 26 Aug 2010; accepted 26 Aug 2010; published 3 Sep 2010
(C) 2010 OSA

primary Bi^+ ion source (LMIG) at a DC current of 14 nA (high mass resolution mode) rastered over a scan area of 100 µm × 100 µm constitutes the analysis beam. Both ion beams were impinging the sample surface forming an angle of 45° with the surface normal and were aligned in such a way that the analyzed ions are taken from the centre of the sputtered crater.

Since the sputtering yields are not well-known and can vary drastically from one type of ion to another, all profiles are presented as a function of the sputtering time. Only, negative ions were recorded in our measurements. Their signals are intense and rather different from each other. Consequently these profiles are presented on a logarithmic scale. For a given profile, the contrast is defined as the difference between the higher and lower signals with respect to the maximum intensity.

XPS

For XPS characterization, the Si 2p, Al 2p, O 1s, C 1s and Mo $3d_{3/2,5/2}$ core level spectra were recorded using Thermo ESCALAB 250 x-ray photoelectron spectrometer working with a monochromatised focused Al Kα radiation (1486.6 eV) at a pass energy of 20 eV and a take-off angle of 90°. The binding energy scale was calibrated using the binding energies of clean Cu, Ag and Au samples as references. With this calibration, the binding energy of adventitious hydrocarbon contamination is 285.0 eV. The core level spectra were processed with the help of the Avantage program, provided by Thermo Electron Corporation. From the intensities obtained by peak decomposition, equivalent thicknesses of the detected layers were estimated, based on the intensity attenuation (Beer Lambert law) of the XPS signals (see details of the calculation below).

3. Results and discussion

EUV reflectivity

In Fig. 1 we present the EUV reflectivity curves measured at near normal incidence of the two studied samples. High peak reflectivity values are measured: 32.4% at 30.4 nm for Al/Mo/SiC_15 and 53.4% at 17.5 nm for Al/Mo/SiC_25. To our knowledge, this is the first time that such a high reflectivity is reported at this wavelength. They are compared to simulated reflectivity curves expected for ideal stacks, *i.e.* without roughness and interdiffusion. The high experimental reflectance demonstrated in Fig. 1 indicates the good structural quality of the samples.

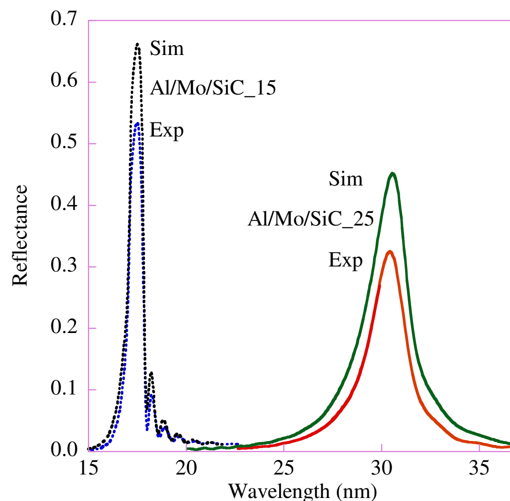

Fig. 1. Experimental (bottom lines) and simulated (top lines) EUV reflectivity curves of the Al/Mo/SiC multilayers: Al/Mo/SiC_15 (dotted lines) Al/Mo/SiC_25 (solid lines).

#131948 - $15.00 USD Received 19 Jul 2010; revised 26 Aug 2010; accepted 26 Aug 2010; published 3 Sep 2010
(C) 2010 OSA

Analysis of the layers within the stack

Figure 2(a) displays a schematic representation of the two ultimate periods of the studied stacks. From this scheme, one can understand that ToF-SIMS experiments start with period 1. The depth profile of the Al/Mo/SiC_15 multilayer, which has been sputtered down to the substrate, are shown in Fig. 2(b). For the sake of clarity, we do not show the SiC^- and C^- profiles since they follow closely the Si^- profile. Also, the Mo^- profile is not shown at this point and will be discussed later.

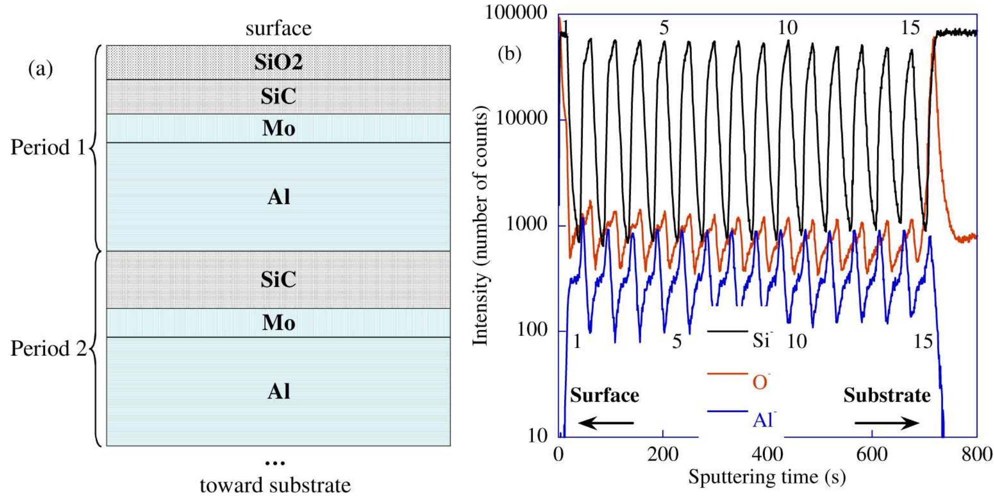

Fig. 2. (a)– Schematic representation of the two ultimate periods of the multilayered stack. (b)– the Si^-, O^- and Al^- ion depth profiles (ToF-SIMS) of the Al/Mo/SiC_15 sample. The numbers 1, 5, 10 and 15 above and below the profiles refer to the Al/Mo/SiC trilayer period as counted from the surface.

The important result is that the 15 different periods of the stack are clearly identified from the periodic modulations of the three selected signals, Si^-, Al^- and O^-. However, the relative concentrations cannot be deduced from the intensities as the ToF-SIMS technique is not quantitative (different sputtering yields are expected with the nature of the elements and the matrix composition). The presence of oxygen is observed at the air/stack and substrate/stack interfaces. The former is most probably due to the atmospheric contamination of the outermost surface layers during transfer and storage in air and the latter corresponds to the native oxide on the silicon substrate. The oxygen within the multilayer, in phase with the Si signals, most probably comes from impurities present in the SiC target. The concentration of oxygen within the samples is very low and this does not impact the optical performances.

In Fig. 3, we present the depth profiles of the Si^-, Al^- and Mo^- ions from the second, third and fourth periods of the Al/Mo/SiC_15 sample. As previously mentioned, the SiC^- follows the Si^- profile and is not presented. Only a limited number of periods is considered in order to zoom on the bulk of the stack and to clearly distinguish the shape of the signals. All three profiles have almost the same shape: at the start of a given period, the number of counts increases, then reaches a plateau increases up again to a maximum and decreases toward the start of the following period. Due to the logarithmic scale, the plateau of Si^- seems almost as high as the maximum; for Mo^-, the plateau is almost seen as a secondary maximum.

As mentioned above, the asymmetrical shape of the SIMS profiles is most probably due to a matrix effect and does not correspond to a gradient of concentration within one period. Due to the thickness of the layers (ultra-thin layers), it is not possible to reach a steady sputtering regime before the end of the period. Large variations of the sputtering yields occur at interfaces (change of matrix) and this leads for example to the sharp maximum of the Al^- profile. It is possible to identify the following sequence (from the surface): Si (SiC layer), Mo and Al, thus we have the experimental proof of the expected order of the layers. It is also

#131948 - $15.00 USD   Received 19 Jul 2010; revised 26 Aug 2010; accepted 26 Aug 2010; published 3 Sep 2010
(C) 2010 OSA

worth stating that the depth resolution (expected below 1 nm) allows a satisfactory detection of the Mo layer. By considering that the center of a layer corresponds to the end of the plateau, we can express the position of the layers for period 3 as a sputtering time: 102 s for Si, 108 s for Mo, 130 s for Al.

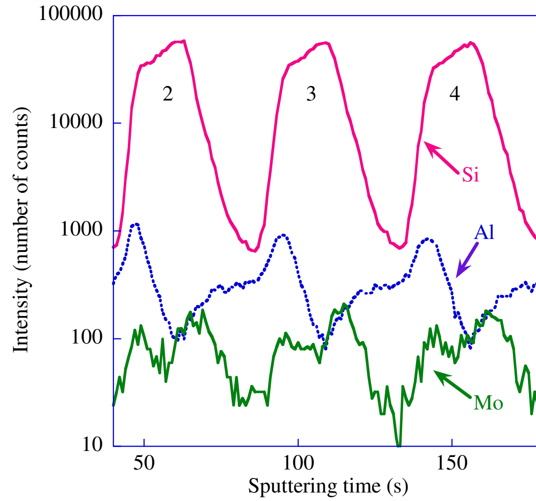

Fig. 3. The Si^-, Al^- and Mo^- ion depth profiles (ToF-SIMS) of the second, third and fourth periods of Al/Mo/SiC_15. The Mo^- profile intensity has been multiplied by a factor 4 for comparison. The numbers 2, 3 and 4 refer to the Al/Mo/SiC trilayer period as counted from the air/surface interface.

The depth profiles of the second, third and fourth periods of the Al/Mo/SiC_25 are shown in Fig. 4 for the Si^-, Al^- and Mo^- ions. Compared to Al/Mo/SiC_15, the contrasts are smaller because of the lower thickness of the layers (closer to the depth resolution). This time, the Al^- profile has a sawtooth shape and the Si^- and Mo^- profiles are rather symmetrical. However, still considering that the maxima are due to an enhancement of the ion signals at the interfaces (matrix effect) and then estimating the position of the center of the layers not at the plateau (not resolved any more) but in the ascending part of the profiles, we recover the expected order of the layers.

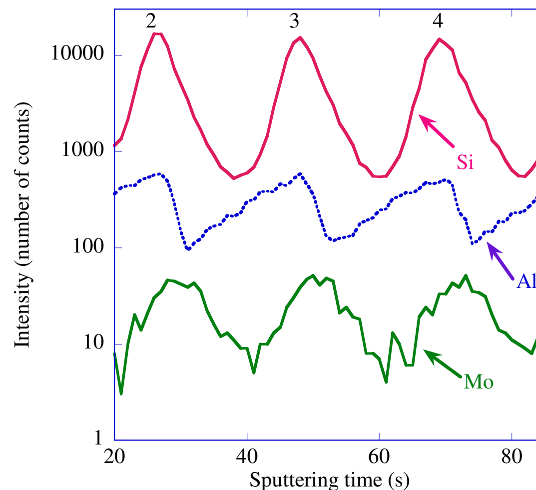

Fig. 4. The Si^-, Al^- and Mo^- ion depth profiles (ToF-SIMS) of the second, third and fourth periods of Al/Mo/SiC_25. The numbers 2, 3 and 4 refer to the Al/Mo/SiC trilayer period as counted from the surface.

#131948 - $15.00 USD Received 19 Jul 2010; revised 26 Aug 2010; accepted 26 Aug 2010; published 3 Sep 2010
(C) 2010 OSA

Analysis of the superficial layers

The depth profiles of the SiC^-, Al^-, Mo^-, O^- and SiO_2^- ions for the two ultimate periods of the Al/Mo/SiC_25 are presented in Fig. 5. Within the first 5 seconds, the SiC^- signal reaches a non-negligible intensity. This is most probably due to the formation of an oxide layer on top of the SiC layer. Indeed, in the same set of 5 seconds, the SiO_2^- and O^- signals are intense, immediately followed by a SiO_2^- intensity drastic decrease down to the noise level after the first period. The O^- profile confirms the SiO_2^- intensity variations: the O atoms remain in the upper part of the SiC top layer. Between 10 and 25 s of sputtering, the intensity of the O^- profile remains nearly constant except the small increase periodically occurring in the frame of the SiC layer (oxygen impurities from the target). We also note that the intensity drop of the O^- profile (6 seconds) occurs while the Mo^- profile reaches its first plateau. Thus, the oxygen diffusion can be limited by the presence of the Mo layer, which acts as a diffusion barrier. This point can be checked with the XPS results. Similar variations were observed with the Al/Mo/SiC_15 sample.

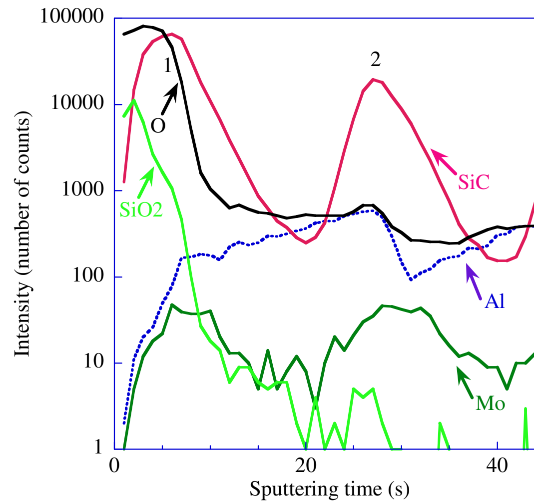

Fig. 5. The O^-, SiC^-, Al^-, Mo^- and SiO_2^- ion depth profiles (ToF-SIMS) of the first and second periods of Al/Mo/SiC_25. The numbers 1 and 2 refer to the Al/Mo/SiC trilayer period as counted from the surface.

The XPS spectra are performed with the Al/Mo/SiC_15 sample having the thicker SiC superficial layer. Figure 6 displays the core level spectra corresponding to the main elements of the system. The first important result is that it is possible to probe a complete period (period 1) by XPS, until the aluminum layer. The only unexpected element present on the surface is Cs (see the Cs 3d core level on the high binding energy (BE) side of the Al 2p core level). This surface contamination can be explained by a Cs implantation during the ToF-SIMS depth profiling (performed before the XPS analysis).

#131948 - $15.00 USD Received 19 Jul 2010; revised 26 Aug 2010; accepted 26 Aug 2010; published 3 Sep 2010
(C) 2010 OSA

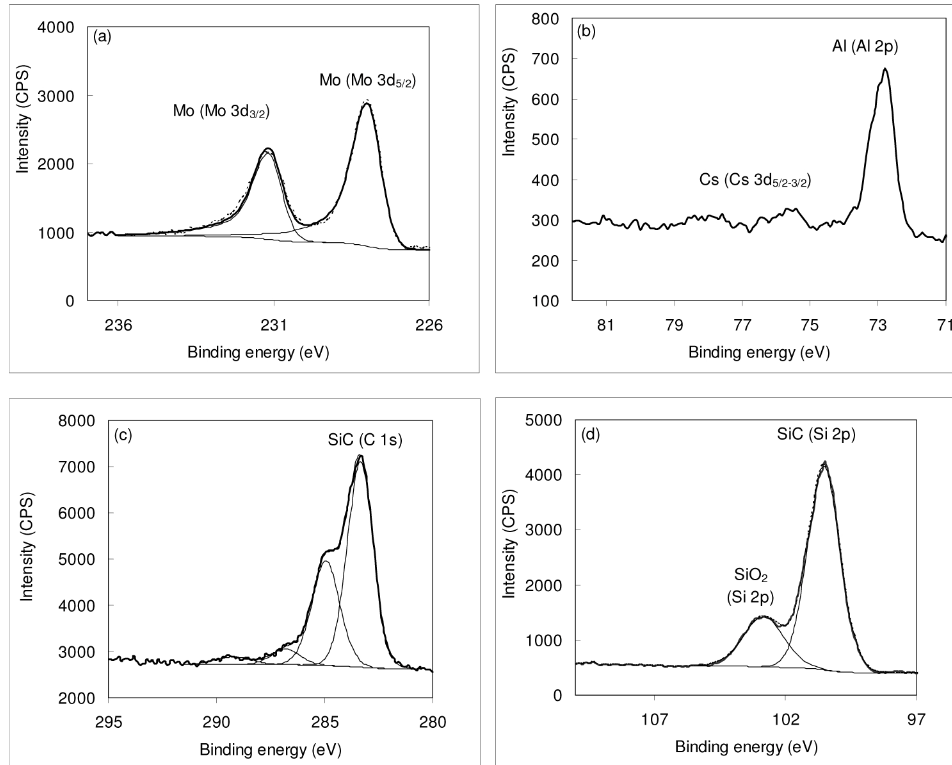

Fig. 6. Surface characterization (XPS) of Al/Mo/SiC_15. Solid bold line: experiment; solid lines: components obtained from the decomposition of the core level; dashed line: recomposed signal.

By a careful examination of the core level spectra, it is possible to state on the chemical states of the elements present in the more external period (period 1). As regards the Mo $3d_{5/2}$ core level [Fig. 6(a)], both its shape (asymmetry of Doniach-Sunjic type) and its BE (227.9 ± 0.1 eV), unambiguously correspond to the Mo metal [11]. This is an important result here to confirm that Mo is not oxidized. The Al 2p core level [Fig. 6(b)] presents only one unresolved doublet (Al $2p_{3/2-1/2}$) of low intensity, located at 72.8 ± 0.1 eV, characteristic of metallic aluminum [12]. The C 1s core level [Fig. 6(c)] presents two main chemical states: the more intense one, located at a BE of 283.3 ± 0.1 eV, is related to carbon in SiC [13] and the second one, located at 285.0 ± 0.1 eV is due to adventitious hydrocarbon surface contamination. Two other contributions of minor intensities (located at 286.8 ± 0.1 eV and 289.2 ± 0.1 eV) are also attributed to surface contamination, corresponding to carbon bound once or twice to oxygen atoms. The Si 2p core level [Fig. 6(d)] exhibits two chemical states. The first component, located at a BE of 100.5 ± 0.1 eV corresponds to bulk SiC [13]. The second one is located at 102.8 ± 0.1 eV and assigned to oxidized silicon SiO_x (non stoichiometric silica) and/or silicates [14]. As regards the O 1s core level (not shown) a symmetrical peak is observed with a maximum at 532.6 ± 0.1 eV that can be attributed to SiO_x.

Taking into account the multilayer described in Fig. 2(a), confirmed by the ToF-SIMS depth profiles and assuming a stoichiometric SiO_2 in the outermost layer (instead of SiO_x), we have calculated the thickness of the SiO_2, SiC, Mo and Al layers in the first period of the stack. Based on the XPS intensity attenuation of the Al 2p intensity, the equations used for the calculations are given in Table 2. The calculations (considering a 10% of uncertainty) give d_{Mo} = 1.5 ± 0.2 nm, d_{SiC} = 6.3 ± 0.6 nm and d_{SiO2} = 1.6 ± 0.2 nm. These values are in satisfactory agreement with the expected thicknesses. The values of d_{SiC} and d_{SiO2} are probably slightly over-evaluated ; this may come from an interface layer with a gradient of SiO_x and

#131948 - $15.00 USD Received 19 Jul 2010; revised 26 Aug 2010; accepted 26 Aug 2010; published 3 Sep 2010
(C) 2010 OSA

SiC, the density of which being difficult to estimate (as well as the corresponding inelastic mean free path).

Table 2. Equations of the XPS equivalent thicknesses of the layers in the first period multilayer (period 1) where λ represents the inelastic mean free path (calculated from the TPP-2M formula [15]), θ the take-off angle, N the atomic density; σ the photoemission cross section [16] and I the peak intensity

$$d_{Mo} = \lambda_{Mo}^{Mo}.\sin\theta.\ln\left[1+\frac{N_{Al}^{Al}.\lambda_{Al}^{Al}.\sigma_{Al\,2p}}{N_{Mo}^{Mo}.\lambda_{Mo}^{Mo}.\sigma_{Mo\,3d_{5/2}}}\cdot\frac{I_{Mo}^{Mo}}{I_{Al}^{Al}}\right]$$

$$d_{SiC} = \lambda_{Si}^{SiC}.\sin\theta.\ln\left[1+\frac{N_{Al}^{Al}.\lambda_{Al}^{Al}.\sigma_{Al\,2p}}{N_{Si}^{SiC}.\lambda_{Si}^{SiC}.\sigma_{Si\,2p}}\cdot\frac{I_{Si}^{SiC}}{I_{Al}^{Al}}\cdot\exp\left(\frac{-d_{Mo}}{\lambda_{Al}^{Mo}.\sin\theta}\right)\right]$$

$$d_{SiO_2} = \lambda_{Sii}^{SiO_2}.\sin\theta.\ln\left[1+\frac{N_{Al}^{Al}.\lambda_{Al}^{Al}.\sigma_{Al2p}}{N_{Si}^{SiO_2}.\lambda_{Si}^{SiO_2}.\sigma_{Si2p}}\cdot\frac{I_{Si}^{SiO_2}}{I_{Ni}^{all}}\cdot\exp\left(\frac{-d_{Mo}}{\lambda_{Al}^{Mo}.\sin\theta}\right)\cdot\exp\left(\frac{-d_{SiC}}{\lambda_{Al}^{SiC}.\sin\theta}\right)\right]$$

Modelling of the stacks

Theoretical EUV reflectivity curves were calculated using the IMD software [17]. Starting from "ideal" multilayers (no interfacial roughness and no interdiffusion), we modified step by step the modelling of the stack by introducing three effects presented below in order to decrease the simulated reflectivity value toward the measured value. Those three effects are the following:

(1) For the interfacial roughness between the different layers, we use the interfacial roughness values presented in Table 1 and obtained at 0.154 nm.

(2) A 10% reduction of the density of Mo layers is introduced. Indeed, in the reflectivity simulations of Al/Mo/SiC multilayers in Ref [18], such a density reduction has been taken into account for the difference between crystalline and amorphous Mo layers.

(3) The oxidation of the SiC top layer is confirmed by XPS and ToF-SIMS measurements. The present simulations consider for both samples the formation of a 1.6 nm-thick SiO_2 layer at the top of the multilayer stack as a result of oxidation:

Al/Mo/SiC_15*:* Si / [Al(11.5 nm)/Mo(1.3 nm)/SiC(3.8 nm)]$_{14}$

/ [Al(11.5 nm)/Mo(1.3 nm)/SiC(2.2 nm)] / SiO_2(1.6 nm);

Al/Mo/SiC_25*:* Si / [Al(6.4 nm)/Mo(1.4 nm)/SiC(1.1 nm)]$_{24}$

/ [Al(6.4 nm)/Mo(1.4 nm)/SiC(0.6 nm)] / SiO_2 (1.6 nm).

We do not consider the formation of an interfacial compound at the Al/Mo interface since we have demonstrated [19] that the Al chemical state is the same in the Al/SiC and Al/Mo/SiC systems, indicating that no strong interaction between the Al and SiC layers or between the Al and Mo layers.

To quantify the effect on the reflectivity value of each of the three phenomena listed above, the reflectivity simulations are first carried out considering either the development of interfacial roughness (1), or the reduced density of Mo (2), or the formation of SiO_2 top layer (3). Then, the combined effect of the three modifications (1) + (2) + (3) is calculated. The reflectivity value resulting from each simulation case is presented in Table 3.

#131948 - $15.00 USD Received 19 Jul 2010; revised 26 Aug 2010; accepted 26 Aug 2010; published 3 Sep 2010
(C) 2010 OSA

Table 3. Comparison of experimental and simulated reflectivity values (R) for Al/Mo/SiC_15 and Al/Mo/SiC_25. Simulation results from individual or combined simulation case (see text for details)

sample	Al/Mo/SiC_15	Al/Mo/SiC_25
wavelength (nm)	30.4	17.5
R (%) exp	32.4	53.4
R (%) "ideal"	44.4	66.2
R (%) / (1)	39.0	61.0
R (%) / (2)	40.3	62.7
R (%) / (3)	43.4	64.6
R (%) / (1) + (2) + (3)	34.8	56.9

The results show that the development of interfacial roughness (1) drastically alters the reflectivity value of the "ideal" multilayer. The Mo density reduction (2) and the introduction of a SiO_2 top layer (3) have less effect on the reflectivity value. Finally, the simulated reflectivity is close to the experimental value when the three effects (1) + (2) + (3) are combined.

4. Conclusion

Periodic Al/Mo/SiC multilayers were studied by combining various experimental techniques providing valuable information on (i) the structural parameters (XRR), (ii) the reflectivity value at the application wavelength (EUV reflectivity), (iii) the depth elemental distribution within the stack (ToF-SIMS) and (iv) the chemical state and distribution of the elements present at the surface (XPS and ToF-SIMS). EUV reflectivity measurements show the excellent optical performance of the multilayers (about 53% at 17 nm). ToF-SIMS depth profiles show the regular succession of the various layers. The XPS analysis demonstrates that SiC in surface of the multilayers is oxidized (about 1.6 nm of SiO_x). This oxidation remains limited in depth and the O atoms do not reach neither the first Mo nor Al layers. A model taking into account the interfacial roughness, the density of Mo thin layer lower than that of crystalline Mo and the 1.6 nm-thick silicon oxidized surface layer, gives EUV reflectivity values close to the experimental ones.

Acknowledgments

Part of this work was funded by the ANR project 07-BLAN-0150. Authors are thankful to Pr. Nanaronne and Drs. Mahne and Giglia from the BEAR beamline for their help during the synchrotron measurements and to Dr. E. Quesnel form CEA for helpful discussion. Multilayer depositions have been carried out on the deposition machine at CEMOX (Centrale d'élaboration et de métrologie des optiques X).

#131948 - $15.00 USD Received 19 Jul 2010; revised 26 Aug 2010; accepted 26 Aug 2010; published 3 Sep 2010
(C) 2010 OSA

Conclusion et perspectives

Ce travail de thèse a porté sur la caractérisation physico-chimique et optique des mirois multicouches conçus pour fonctionner dans le domaine EUV. De nombreux miroirs multicouches ont été étudiés et optimisés: Mg/Co, Mg/Co/Zr, Al/SiC, Al/Mo/SiC, ... L'étude de ces multicouches et de leurs interfaces a permis des développements dans le domaine de l'optique multicouche EUV. L'amélioration de la réflectivité des miroirs multicouches dans ce domaine constitue une motivation importante pour nos recherches. Nous avons appliqué notre méthodologie de caractérisation physico-chimique et optique combinant la réflectométrie X et EUV, XES, RMN, ToF-SIMS, XPS, FIB et STEM-EELS pour étudier les multicouches.

Dans le cas des systèmes Mg/Co, nous avons conçu le nouveau système et ses possibles tri- ou quatre-couches à partir de simulations. Les mesures de réflectivité de la multicouche Mg/Co à la longueur d'onde de 25 nm et de 30,4 nm sont de 46 % et 40 % respectivement. Les mesures XES et RMN indiquent que les interfaces entre les couches Mg et Co ne présentent pas d'interdiffusion et la seule rugosité géométrique explique la différence entre les valeurs de réflectance simulée et mesurée. Nous avons également étudié l'effet de l'insertion de couches de B_4C ou Zr aux interfaces. Les mesures de réflectivité montrent que l'introduction de la multicouche B_4C dégrade considérablement, conduisant à une valeur inférieure à 1%. À partir de mesures XES et RMN, la faible réflectance est due à la fois à une forte interdiffusion aux interfaces. Les mesures montrent que Mg/Co/Zr est plus efficace (50% de réflectivité) que Mg/Zr/Co et Mg/Zr/Co/Zr (~40%). Pour comprendre ce comportement asymétrique, nous avons étudié la qualité de l'interface par ToF-SIMS et RMN et nous avons attribué cette différence à un processus interdiffusion quand les couches Co sont déposées sur des couches Zr. Afin de comprendre comment se développe la rugosité et se forment les éventuels composés interfaciaux aux interfaces des multicouches Mg/Co nous avons entrepris une étude en fonction du recuit jusqu'à 400°C. Les mesures montrent que la stabilité thermique de Mg/Co jusqu'à 300°C. A partir de 300°C, un fort changement dans la morphologie de l'échantillon se produit qui explique la perte de réflectivité. Les études de la stabilité thermique de Mg/Co/Zr montrent que la réflectivité atteint à 51% quand il a été recuit à 200°C.

Dans le cas des systèmes Al/SiC, les simulations indiquent en effet que la structure multicouche idéalement optimisée pour les longueurs d'onde de 30,4 nm et 17,5 nm, présente

une réflectivité théorique de 40% et 60%. Pour les longueurs d'onde de 17,5 nm, ces multicouches possèdent une réflectivité expérimentale de 37%. Nous avons montré que c'est bien l'interface Al sur SiC qui semble la plus problématique en terme de rugosité ~1.2 nm. Nous avons pu quantifier les pertes de réflectivité dues à l'oxydation et la rugosité géométrique. Nous avons donc ajouté un nouveau matériau à cette interface afin de réduire la rugosité et développer les systèmes de tri-couches. Dans le système Al/Mo/SiC, la simulation optimisée pour la longueur d'onde de 30,4 nm et 17,5 nm, présente les réflectivités théoriques de 44,4% et 66,2%. Pour les longueurs d'onde de 17,5 nm, ces multicouches possèdent une réflectivité expérimentale de 53,4%. C'est le premier rapport d'une réflectivité expérimentale supérieure à 50% autour de 17 nm. L'introduction d'un troisième matériau W ou Mo dans l'empilement Al/SiC conduit à la réduction de la rugosité à toutes les interfaces. La rugosité de Al/SiC avec W et Mo est ~0.6 nm pour l'interface Al sur SiC. Enfin, la différence entre les valeurs simulée et mesurée est attribuée à l'oxydation de la couche de SiC, une réduction de la densité de Mo et les rugosités entre les différentes couches.

Les multicouches Mg/Co et Al/SiC sont prometteuses pour des applications dans le domaine EUV. Un prolongement de ce travail pourrait être l'étude du matériau Y (yttrium) comme couche interfaciale dans la multicouche Mg/Co. Les simulations effectuées montrent que, avec la polarisation s de la lumière incidente à 45°, la reflectance atteint une valeur maximale égale à 61% autour de 25 nm de longueur d'onde lorsque nous avons introduit le couche Y à l'interface Co-sur-Mg (article **3-[1]**). Les échantillons futurs envisagés sont des tri- et quadri-couches avec de Y dont on espère obtenir des performances optiques supérieures à celles obtenues avec les systèmes avec Zr. Nous pouvons aussi envisager de refaire des mesures sur les systèmes avec ou sans Zr pour lesquels on aurait optimisé les épaisseurs. On s'attend à une augmentation de plus de 10% de la réflectance théorique. Si on observe la même augmentation sur la réflectance mesurée, on atteindrait presque 60% ce qui serait très performant. Cependant, pour ces échantillons, je pense qu'il se produirait les mêmes effets aux interfaces que ceux que nous venons d'analyser. L'intérêt de leur analyse par émission X ou RMN serait alors moindre.

Pour le système Mg/Co, il serait intéressant d'étudier le profil d'aimantation dans les couches Co par effet magnéto-optique dans les rayons X mous. Cela permet de détecter une couche de transition dont l'épaisseur peut être près d'une monocouche. L'équipe a fait la première mesure au synchrotron Elettra. Le profil d'aimantation des couches Co est mesurée

avec des photons d’énergie voisine du seuil d'absorption Co L_3 (778 eV) pour deux rayonnements de polarisation circulaire opposée (article **A-[3]**). Les mesures ne montrent pas l'interaction entre les couches Co et Mg dans les multicouches.

La méthodologie développée au cours de cette thèse constitue un outil original d’analyse des structures multicouches. Son utilisation peut être généralisée à d’autres types de multicouches. Elle nous a permis d'une part de progresser dans la compréhension de la physique des empilements multicouches EUV et d'autre part de développer de nouveaux composants pour cette gamme spectrale. A plus long terme, on peut imaginer introduire d’autres types de matériau dans les optiques EUV. Nous sommes intéressés à optimiser et déposer les nouveaux systèmes. Nous pouvons calculer les épaisseurs des couches qui optimisent la réflectivité à une longueur d’onde donnée. Nous pourrions aussi l’introduction d’un troisième matériau pour accroître la réflectivité. Ensuite par les différentes mesures que nous pouvons étudier la caractérisation physico-chimique et optique de miroirs multicouches pour le domaine EUV. Une continuation de nos études permettrait une avancée notable dans la compréhension des phénomènes inhérents aux systèmes multicouches.

Références

[1] B. Henke, E. Gullikson, and J. Davis, "X-ray interactions: Photoabsorption, scattering, transmission, and reflection at e = 50-30,000 eV, z = 1-92", Atomic Data and Nuclear Data Tables, 1993, vol. 54, pp. 181–342.

[2] http://www.cxro.lbl.gov/optical_constants/pert_form.html

[3] E. Spiller, "Low-Loss Reflection Coatings Using Absorbing Materials", Appl. Phys. Lett,1972, 20, 365.

[4] D. L. Windt, "IMD—Software for modeling the optical properties of multilayer films", Comput. Phys, 1998, 12, 360.

[5] J. Gautier, F. Delmotte, M. Roulliay, F. Bridou, M.-F. Ravet, and A. Jérome, "Study of normal incidence of three-component multilayer mirrors in the range 20-40 nm", Appl. Opt. 2005, 44, 384.

[6] Z.-S. Wang, S.-M. Zhang, W.-J. Wu, J.-T. Zhu, H.-C. Wang, C.-X. Li, Y. Xu, F.-L. Wang, Z. Zhang, L.-Y. Chen, H.-J. Zhou, and T.-L. Huo, "B4C/Mo/Si high reflectivity multilayer mirror at 30.4 nm", Chin. Opt. Lett. 2006, 4, 611.

[7] H. Maury, "Relations entres les caractéristiques structurales de miroirs multicouches et leurs propriétés optiques dans le domaine X-UV", Thèse de l'Université Paris VI, 2007.

[8] D.L. Windt, S. Donguy, J. Seely, B. Kjornrattanawanich, "Experimental Comparison of Extreme-Ultraviolet Multilayers for Solar Physics", Appl. Opt. 2004, 9, 1835 .

[9] C. Bonnelle, F. Vergand, P. Jonnard, J.-M. André, P. Avila, P. Chargelègue, M.-F. Fontaine, D. Laporte, P. Paquier, A. Ringuenet, B. Rodriguez, "Instrument for research on interfaces and surfaces (IRIS) ", Rev. Sci. Instrum.1994, 65, 3466.

[10] D. Drouin, A. R. Couture, D. Joly, X. Tastet, V. Aimez, R. Gauvin, "CASINO V2.42 - A Fast and Easy-to-use Modeling Tool for Scanning Electron Microscopy and Microanalysis Users", Scanning, 2007, 29, 92 .

[11] H. H. Johann, "Die Erzeugung lichtstarker Röntgenspektren mit Hilfe von Konkavkristallen", Z. Phys. 1931, 69, 185.

[12] C. F. Hague, D. Laporte, "Spectrometer for soft x-ray emission studies of liquid metals and metallic vapors", Rev. Sci. Instrum.1980, 51, 624.

[13] F. Borgatti, A. Deluisa, B. P. Doyle, A. Giglia, N. Mahne, L. Pasquali, M. Pedio, G. Selvaggi, S. Nannarone, G. Naletto, M. G. Pelizzo, and G. Tondello, "The new bear beamline : a short presentation", Elettra News 47 - September 30, 2003.

[14] C. Meny, and P. Panissod, “Nuclear Magnetic Resonance in Ferromagnetic Multilayers and Nanocomposites : Investigations of Their Structural and Magnetic Properties In Modern Magnetic Resonance”, G. Webb, Ed., Springer, Heidelberg, 2006.

[15] P. Panissod, and C. Meny, “Nuclear magnetic resonance investigations of the structure and magnetic properties of metallic multilayers and nanocomposites”, Applied Magnetic Resonance. 2000, 19, 447.

[16] Thomson, J.J., “Rays of positive electricity”, Phil.Mag. 1910, 20, 752.

[17] Castaing, R., and Slodzian, G. J., “Optique corpusculaire—premiers essais de microanalyse par emission ionique secondaire”, Microscopie 1, 1962, 395.

[18] Maury, H., Jonnard, P., Le Guen, K., Andre´, J.-M., Wang, Z., Zhu, J., Dong, J., Zhang, Z., Bridou, F., Delmotte, F., Hecquet, C., Mahne, N., Giglia, A., Nannarone, S., “Thermal cycles, interface chemistry and optical performance of Mg/SiC multilayers”, Eur. Phys. J. B 2008, 64, 193.

[19] A. E. Rosenbluth, “Computer search for layer materials that maximize the reflectivity of x-ray multilayers”, Revue Phys. Appl. 23, 1988, 1599-1621.

[20] I. Yoshikawa, M. Nakamura, M. Hirahara, Y. Takizawa, K. Yamashita, H. Kunieda, T. Yamazaki, K. Misaki, and A. Yamaguchi, “Observation of He II emission from the plasmasphere by a newly developed EUV telescope on board sounding rocket S-520-19”, J. Geophys. Res., 1997, 102, A9.

[21] P. Jonnard, I. Jarrige, R. Benbalagh, H. Maury, J.-M. André, Z. Dankhazi, G. Rolland, “Physico-chemical and X-ray optical characterizations of a Mo/Si multilayer interferential mirror upon annealing”, Surf. Sci. 2005, 589, 164.

[22] H. Maury, P. Jonnard, J.-M. André, J. Gautier, F. Bridou, F. Delmotte, M.-F. Ravet, “Interface characteristics of Mo/Si and B_4C/Mo/Si multilayers using non-destructive X-ray techniques”, Surf. Sci. 2007, 601, 2315.

[23] D. L. Windt, S. Donguy, J. Seely, B. Kjornattanawanich., “Experimental comparison of extreme-ultraviolet multilayers for solar physics”, Appl. Opt. 2004, 43, 1835.

[24] H. Maury, P. Jonnard, K. Le Guen, J.-M. André, Z. Wang, J. Zhu, J. Dong, Z. Zhang, F. Bridou, F. Delmotte, C. Hecquet, N. Mahne, A. Giglia, S. Nannarone, “Thermal cycles, interface chemistry and optical performance of Mg/SiC multilayers”, Eur. Phys. J. B , 2008,64, 193.

[25] E. Meltchakov, C. Hecquet, M. Roulliay, S. De Rossi, Y. Ménesguen, A. Jérome, F. Bridou, F. Varniere, M.-F. Ravet-Krill, F. Delmotte, “Development of Al-based multilayer optics for EUV”, Appl. Phys A, 2010, 98, 111.

Liste des publications :

3-[1] M.–H. Hu, K. Le Guen, J.-M. André, P. Jonnard, S. K. Zhou, H. Ch. Li, J. T. Zhu, Z. S. Wang, “Co/Mg/X multilayer mirrors for the EUV range”, X-RAY OPTICS AND MICROANALYSIS：AIP Conference Proceedings, 2010, Volume 1221, pp. 56-58.

3-[2] K. Le Guen, M.-H. Hu, J.-M. André, P. Jonnard, S. K. Zhou, H. Ch. Li, J. T. Zhu, Z. S. Wang, C. Meny, “Development and interfacial characterization of Co/Mg periodic multilayers for the EUV range”, The Journal of Physical Chemistry C (ACS Publications), 2010, 114 (14), pp 6484–6490.

3-[3] J. T. Zhu, S. K. Zhou, H. Ch. Li, Q. Sh. Huang, Z. S. Wang, K. Le Guen, M.-H. Hu, J.-M. André, P. Jonnard, “Comparison of Mg-based multilayers for solar He-II radiation at 30.4 nm wavelength”, Applied Optics, 2010, Vol. 49, No. 20, pp. 3922-3925.

3-[4] M.-H. Hu, K. Le Guen, J.-M. André, S. K. Zhou, H. Ch. Li, J. T. Zhu, Z. S. Wang, C. Meny, N. Mahne, A. Giglia, S. Nannarone, I. Estève, M. Walls, P. Jonnard, “Investigation on the thermal stability of Mg/Co periodic multilayers for EUV applications”, Appl Phys A: Materials Science & Processing, 2011, in press.

3-[5] K. Le Guen, M.-H. Hu, J.-M. André, P. Jonnard, S.K. Zhou, H.C. Li, J.T. Zhu, Z.S. Wang, N. Mahne, A. Giglia, S. Nannarone, “Introduction of Zr in nanometric periodic Mg/Co multilayers”, Appl Phys A: Materials Science & Processing, 2011, Volume 102, Number 1, 69-77.

3-[6] K. Le Guen, M.-H. Hu, J.-M. André, S. K. Zhou, H. Ch. Li, J. T. Zhu, Z. S. Wang, C. Meny, A. Galtayries and P. Jonnard, “Observation of an asymmetrical effect when introducing Zr in Mg/Co multilayers”, Applied Physics Letters, 2011, 98, 251909.

4-[1] P. Jonnard, K. Le Guen, M.–H. Hu, J.-M. André, E. Meltchakov, C. Hecquet, F. Delmotte, “Optical, chemical and depth characterization of Al/SiC periodic multilayers”, Proc. SPIE 7360, 2009, O1-9.

4-[2] M.–H. Hu, K. Le Guen, J.-M. André, P. Jonnard, E. Meltchakov, F. Delmotte, A. Galtayries, “Structural properties of Al/Mo/SiC multilayers with high reflectivity for extreme ultraviolet light”, Optics Express, 2010, Vol. 18, Issue 19, pp. 20019-20028.

A-[1] M.-H. Hu, K. Le Guen, J.-M. André, P. Jonnard, S. K. Zhou, H. Ch. Li, J. T. Zhu, Z. S. Wang, N. Mahne, A. Giglia, S. Nannarone, “Thermal properties, optical and interface characterization of Mg/Co multilayers for the EUV range’, Proc. SPIE 7995, 2010, 79950P.

A-[2] K. Le Guen, M.-H. Hu, J.-M. André, P. Jonnard, S. K. Zhou, H. Ch. Li, J. T. Zhu, Z. S. Wang, N. Mahne, A. Giglia, S. Nannarone, “Introduction of Zr in Mg/Co nanometric periodic multilayers”, Proc. SPIE 7995, 2010, 799525.

Références

A-[3] P. Jonnard, K. Le Guen, M.-H. Hu, J.-M. André, S. K. Zhou, H. Ch. Li, J. T. Zhu, Z. S. Wang,N. Mahne, A. Giglia, S. Nannarone, A. Verna, C. Meny, A. Galtayries, I. Estève and M. Walls, "Optical, chemical, depth and magnetic characterization of Mg/Co-based nanometric periodic multilayers", Proc. SPIE 8168, 816818 (2011).

A-[4] Jingtao Zhu, Sika Zhou, Haochuan Li, Zhanshan Wang, Philippe Jonnard, Karine Le Guen, Min-Hui Hu, Jean-Michel André, Hongjun Zhou and Tonglin Huo, "Thermal stability of Mg/Co multilayer with B_4C, Mo or Zr diffusion barrier layers", Optics Express, Vol. 19, Issue 22, pp. 21849-21854 (2011).

A-[5] A. Galtayries, M.–H. Hu, K. Le Guen, J.-M. André, P. Jonnard, E. Meltchakov, C. Hecquet, F. Delmotte, "Nanometer designed Al/SiC periodic multilayers: characterization by a multi-technique approach", Surface and Interface Analysis, 2010, Volume 42, Issue 6-7, 653–657.

A-[6] K. Le Guen, M.-H Hu, J.-M. André, P. Jonnard, Z. Wang, J. Zhu, A. Galtayries, C. Meny, E. Meltchakov, C. Hecquet and F. Delmotte, "Characterization of EUV periodic multilayers", X-RAY Spectrometry, 2011, Volume 40, Issue 5, pp. 338–342.

Annexes: Autres publications

A-[1]

M.-H. Hu, K. Le Guen, J.-M. André, P. Jonnard, S. K. Zhou, H. Ch. Li, J. T. Zhu, Z. S. Wang, N. Mahne, A. Giglia, S. Nannarone : **Thermal properties, optical and interface characterization of Mg/Co multilayers for the EUV range,** *Proc. SPIE 7995, 79950P (2010)*

A-[2]

K. Le Guen, **M.-H. Hu,** J.-M. André, P. Jonnard, S. K. Zhou, H. Ch. Li, J. T. Zhu, Z. S. Wang, N. Mahne, A. Giglia, S. Nannarone : **Introduction of Zr in Mg/Co nanometric periodic multilayers,** *Proc. SPIE 7995, 799525 (2010)*

A-[3]

P. Jonnard, K. Le Guen, **M.-H. Hu,** J.-M. André, S. K. Zhou, H. Ch. Li, J. T. Zhu, Z. S. Wang,N. Mahne, A. Giglia, S. Nannarone, A. Verna, C. Meny, A. Galtayries, I. Estève and M. Walls : **Optical, chemical, depth and magnetic characterization of Mg/Co-based nanometric periodic multilayers**, *Proc. SPIE 8168, 816818 (2011)*

A-[4]

Jingtao Zhu, Sika Zhou, Haochuan Li, Zhanshan Wang, Philippe Jonnard, Karine Le Guen, **Min-Hui Hu**, Jean-Michel André, Hongjun Zhou and Tonglin Huo : **Thermal stability of Mg/Co multilayer with B_4C, Mo or Zr diffusion barrier layers**, *Optics Express, Vol. 19, Issue 22, pp. 21849-21854 (2011)*

A-[5]

A. Galtayries, **M.–H. Hu,** K. Le Guen, J.-M. André, P. Jonnard, E. Meltchakov, C. Hecquet, F. Delmotte : **Nanometer designed Al/SiC periodic multilayers: characterization by a multi-technique approach,** *Surface and Interface Analysis, Volume 42, Issue 6-7, 653–657 (2010)*

A-[6]

K. Le Guen, **M.-H Hu,** J.-M. André, P. Jonnard, Z. Wang, J. Zhu, A. Galtayries, C. Meny, E. Meltchakov, C. Hecquet and F. Delmotte : **Characterization of EUV periodic multilayers**, *X-RAY Spectrometry, Volume 40, Issue 5, pp. 338–342 (2011)*

Thermal properties, optical and interface characterization of Mg/Co multilayers for the EUV range

M.-H. Hu[a*], K. Le Guen[a], J.-M. André[a], P. Jonnard[a], S. K. Zhou[b], H. Ch. Li[b], J. T. Zhu[b], Z. S. Wang[b], N. Mahne[c], A. Giglia[c], S. Nannarone[c]
[a]Laboratoire Chimie Physique - Matière Rayonnement, UPMC CNRS UMR 7614, Paris, France
[b]Institute of Precision Optical Engineering, Tongji University, Shanghai, China
[c]Istituto Officina dei Materiali IOM-CNR Laboratorio TASC, Trieste, Italy

ABSTRACT

We present the results of the thermal stability of Mg/Co multilayers in the EUV range. The annealing study is performed up to a temperature of 400°C. The X-ray reflectivity at 0.154 nm is used in order to determine the structural parameters (thickness, roughness and density) of the layers. The measurements of the EUV reflectivity around 25 nm show that the reflectivity decreases when the annealing temperature increases above 300°C. X-ray emission spectroscopy is performed to determine the chemical state of the Mg atoms within the Mg/Co multilayer. The results show a small oxidation after annealing at 305°C, which increases greatly at 400°C. Scanning electron microscopy images of cross sections of the multilayer show a change of the surface morphology above 305°C. This large change of morphology and the oxidation explain the large reflectivity loss.

Keywords: interface, multilayer, annealing, Co, Mg, x-ray reflectivity, EUV reflectivity, x-ray emission, scanning electron microscopy

1. INTRODUCTION

In the extreme ultraviolet (EUV) range, highly efficient periodic multilayers are widely used in many fields such as X-ray space telescopes, EUV lithography or X-ray laser facilities. The previous measurements of the optical and interface properties of the Mg/Co multilayer show that this multilayer is promising for future applications at wavelength close to the Mg L edge around 25 nm[1], as well as for the 30.4 nm wavelength (He II radiation). In this paper, we combine different complementary experimental techniques to study the thermal properties, the optical and interface characterization of Mg/Co multilayers for the EUV range.

The Mg/Co multilayer samples were prepared by magnetron sputtering and their structural quality checked by X-ray reflectivity (XRR) at 0.154 nm. The annealing study is performed up to a temperature of 400°C, under ultra-high vacuum. EUV reflectivity measurements around 25 nm are made to control the optical properties of the multilayer at the application wavelength. X-ray emission spectroscopy (XES) is performed to determine the chemical state of the Mg atoms.

2. SAMPLES

The studied periodic Mg/Co multilayers were prepared using a calibrated ultra-high vacuum direct current magnetron sputtering system (JGP560C6, SKY Inc., China) with targets of Co (purity 99.95%) and Mg (purity 99.98%). The multilayers were all deposited onto ultra-smooth polished Si substrates. The description of the designed structure of each multilayered sample is summarized in Table 1. Each sample is made of 30 bilayers. The first layer on the substrate is the Mg one. A 3.50 nm-thick capping layer made of B_4C is deposited at the surface of each sample in order to prevent oxidation. The sample Mg/Co_1 characterized by a short period is dedicated to the XES analysis. The sample Mg/Co_2 is dedicated to the XRR measurement in the EUV range[2].

* Email: dancerhh@hotmail.com

Seventh International Conference on Thin Film Physics and Applications,
edited by Junhao Chu, Zhanshan Wang, Proc. of SPIE Vol. 7995, 79950P
© 2011 SPIE · CCC code: 0277-786X/11/$18 · doi: 10.1117/12.888261

Downloaded from SPIE Digital Library on 23 Mar 2011 to 222.66.175.218. Terms of Use: http://spiedl.org/terms

Table 1: Designed structure of the Mg/Co multilayers.

Multilayer	Sample Name	Period d (nm)	d_{Co} (nm)	d_{Mg} (nm)	d_{B4C} (nm)	Simulated Reflectivity
Mg/Co	Mg/Co_1	8.00	2.55	5.45	-	-
	Mg/Co_2	17.00	2.55	14.45	-	56.5% @ 25.2 nm

The structural parameters of the Mg/Co multilayer, deduced from the fit of the XRR curve obtained at 0.154 nm, show a good agreement between the aimed and effective thicknesses of the layers and an interfacial roughness of about 0.6 nm. In order to check the thermal stability of the multilayer, annealing is performed at 280°C, 305°C and 400°C in a vacuum of 10^{-8} mbar during 1 hour.

3. EXPERIMENTS AND RESULTS

3.1 EUV reflectivity

The measurement of the reflectivity curves in the EUV domain is performed on the BEAR beamline[3] at the Elettra synchrotron centre using *s*-polarization. Impinging and reflected photon intensities are measured using a solid state photodiode. The overall accuracy on the absolute reflectivity values is estimated to be about 1%. We show in Figure 1 the reflectivity curves as a function of the annealing temperature, measured in the 42-52 eV energy range at 50° of grazing incidence. The structure around 50 eV is due to the presence of the Mg L edge (L_2 and L_3 edges at 49.8 and 49.6 eV respectively).

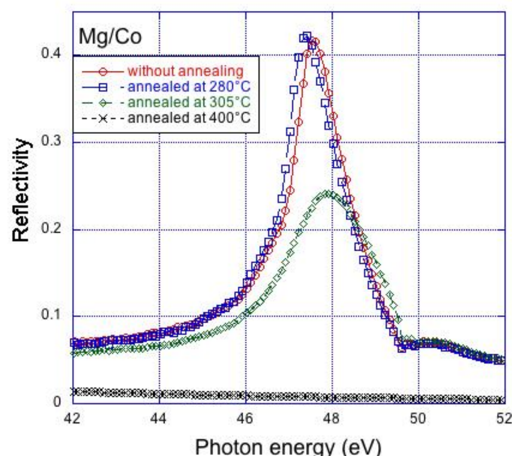

Figure 1: Evolution, as a function of the annealing temperature, of the Mg/Co_2 EUV reflectivity curve obtained at 50° of grazing incidence.

The reflectivity slightly increases between room temperature and annealing at 280°C. A slight shift of the peak is also observed. At 305°C, a reflectivity drop of nearly 45% is observed as well as a peak shift (+0.4 eV) towards higher photon energies. At 400°C, the reflectivity can be considered as zero. The structural parameters of the stack deduce from fit of the reflectivity curves are collected in Table 2. From the results we can see that the interfacial roughness increase quite a lot for the Mg/Co annealed at 305°C.

3.2 X-ray emission spectroscopy

The X-ray emission analysis is performed in a high-resolution wavelength dispersive soft X-ray spectrometer. The Mg Kß coming from the magnesium atoms present in the Mg/Co multilayered samples are analyzed. These emissions correspond to the Mg 3p - 1s transitions respectively and are related to the occupied valence states having the Mg 3p character. These emissions are sensitive to the physico-chemical state of the magnesium atoms respectively[4,5]. We present the Mg Kß emission band of the Mg/Co_1 sample as a function of the annealing temperatures compared with Mg/Co sample without annealing in Figure 2. We also make the comparison with the spectrum of MgO.

Downloaded from SPIE Digital Library on 23 Mar 2011 to 222.66.175.218. Terms of Use: http://spiedl.org/terms

Table 2: Parameter values extracted from the fit of the Mg/Co reflectivity curve measured at EUV range. σ stands for the interfacial roughness. The density ratio (%) is defined as the density of the layer divided by the density of the bulk.

Multilayer	d (nm)	dco (nm) dMg (nm)	σ (nm)
Mg/Co Without annealing	16.9	Co: 2.6 Mg: 14.3	Co/Mg = 0.5 Mg/Co = 0.6
Mg/Co Annealed at 280°C	16.98	Co: 2.86 Mg: 14.12	Co/Mg = 0.5 Mg/Co = 0.6
Mg/Co Annealed at 305°C	16.9	Co: 3.95 Mg: 12.95	Co/Mg = 1.0 Mg/Co = 2.7

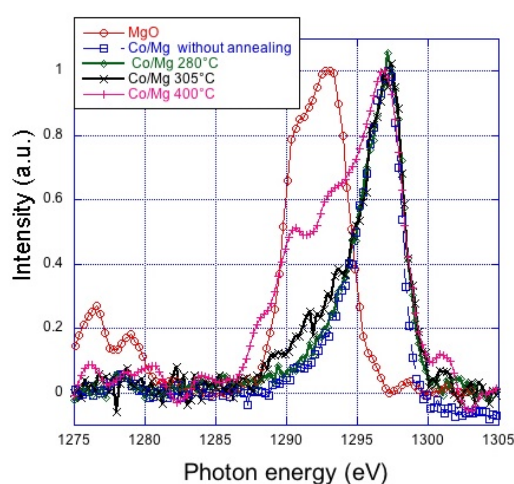

Figure 2: The Mg Kß emission band of Mg/Co_1 sample annealed at different temperatures and its comparison with the MgO spectrum.

The spectrum of the sample annealed at 280°C is close to the spectrum of Mg/Co_1 without annealing. As we already know that the Mg atoms in Mg/Co without annealing are in the same state as in Mg metal[1], we can say that within the sample annealed at 280°C, the Mg atoms are in a physico-chemical state close to that of Mg atoms in the Mg metallic state. The spectra of Mg/Co_1 samples annealed at 305°C and 400°C differ from that of Mg/Co without annealing toward the low photon energies. A shoulder appears in the region of the MgO maximum (1288-1295 eV). As the shoulder intensity increases with the temperatures increasing, a small contribution of oxidized Mg atoms is observed that increases at 400°C. Because of the annealing conditions, we think that the oxidation takes place when the sample is returned to the air.

3.3 Scanning electron microscopy images (SEM)

The Mg/Co lamellae were cut out by Focused Ion Beam. Then the surface and cross section were observed by SEM (Scanning Electron Microscope). The thickness is the lamella about 50 nm. The Mg/Co multilayers without annealing and annealed at 280°C have smooth surfaces and clear multilayer structures. The Mg/Co multilayer annealed at 305°C and 400°C have serious cracks on the surface and within the multilayer structure. A loss of adherence (probably due to relaxation of the mechanical stress) happened during the annealing. The highest annealing temperature image presents the more serious changes. Figure 3 shows the multilayer structures of Mg/Co multilayer annealed at 305°C and 400°C. The figures show the cracks between multilayer and substrate for both of them. For the multilayer annealed at 400°C, cracks exist also between the layers. Because of the cracks, the multilayer is no more flat and so its reflectivity decrease. The cracks facilitate the introduction of oxygen within the multilayer. This also explains the oxidation observed in XES.

Downloaded from SPIE Digital Library on 23 Mar 2011 to 222.66.175.218. Terms of Use: http://spiedl.org/terms

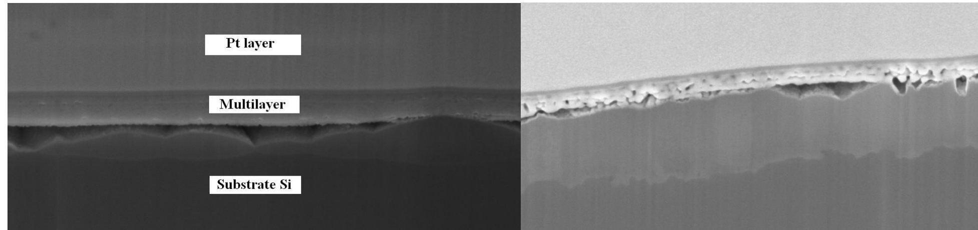

Figure 3: Images of Mg/Co multilayer annealed at 305°C (left) and 400°C (right).

4. CONCLUSION

We present the results of the thermal stability of the Mg/Co multilayers designed for the EUV range, by experiments of EUV reflectivity around 25 nm, X-ray emission spectroscopy and scanning electron microscopy images. EUV reflectivity measurements show that the reflectivity slightly increases with the temperature till 280°C. At 305°C, a reflectivity drop of nearly 45% is observed. At 400°C, the reflectivity can be considered as zero. The XES results show that a small oxidation of the sample is observed after annealing at 305°C. This oxidation should explain a part of the observed reflectivity loss. The SEM images show a change of the surface morphology and the serious cracks within the multilayer structure above 305°C. This large change of morphology explains the large reflectivity loss. In the future, we plan to do more experiments such as nuclear magnetism resonance (NMR), in order to study the chemical state of the (magnetic) Co atoms. Transmission electron microscopy (TEM) images will give direct evidence of the possible formation of interfacial compounds, the quality of the layers as well as their roughness.

REFERENCES

[1] K. Le Guen, M.-H. Hu, J.-M. André, P. Jonnard, S. K. Zhou, H. Ch. Li, J. T. Zhu, Z. S. Wang, C. Meny, “Development and interfacial characterization of Mg/Co periodic multilayers for the EUV range”, J. Phys. Chem. C, 2010, 114, 6484.
[2] M.-H. Hu, K. Le Guen, J.-M. André, P. Jonnard, S. K. Zhou, H. Ch. Li, J. T. Zhu, Z. S. Wang, “Mg/Co/X Multilayer Mirrors For the EUV Range”, AIP Conf. Proc., 1221, 56-58 (2010).
[3] Nannarone, S.; Borgatti, F.; DeLuisa, A.; Doyle, B. P.; Gazzadi, G. C.; Giglia, A.; Finetti, P.; Mahne, N.; Pasquali, L.; Pedio, M.; Selvaggi, G.; Naletto, G.; Pelizzo, M. G.; Tondello, G., AIP Conference Proceedings 2004, 708, 450.
[4] Maury, H.; Jonnard, P.; Le Guen, K.; André, J.-M.; Wang, Z.; Zhu, J.; Dong, J.; Zhang, Z.; Bridou, F.; Delmotte, F.; Hecquet, C.; Mahne, N.; Giglia, A.; Nannarone, S. European Physical Journal B 2008, 64, 193.
[5] Jonnard, P.; Vergand, F.; Bonnelle, C.; Orgaz, E.; and Gupta, M., Physical Review B 1998, 57, 12111.

Downloaded from SPIE Digital Library on 23 Mar 2011 to 222.66.175.218. Terms of Use: http://spiedl.org/terms

Introduction of Zr in Mg/Co nanometric periodic multilayers

Karine Le Guen[*a], Min-Hui Hu[a], Jean-Michel André[a], Philippe Jonnard[a], Sika Zhou[b], Haochuan Li[b], Jingtao Zhu[b], Zhanshan Wang[b], Nicola Mahne[c], Angelo Giglia[c], Stefano Nannarone[c] and Christian Meny[d]

[a]Laboratoire de Chimie Physique – Matière et Rayonnement, UPMC Univ Paris 06, CNRS UMR 7614, 11 rue Pierre et Marie Curie, F-75231 Paris cedex 05, France;

[b]Institute of Precision Optical Engineering, Department of Physics, Tongji University, Shanghai 200092, P.R. China;

[c]Istituto Officina dei Materiali IOM-CNR Laboratorio TASC, s.s. 14, km 163.5 in Area Science Park, I-34012 Trieste, Italy;

[d]Institut de Physique et Chimie des Matériaux de Strasbourg, CNRS UMR 7504, 23 rue du Loess, BP 43, F-67034 Strasbourg cedex 2, France

ABSTRACT

We study the introduction of Zr as a third material within a nanometric periodic Mg/Co structure designed to work as optical component in the EUV range. Mg/Co, Mg/Zr/Co, Mg/Co/Zr and Mg/Zr/Co/Zr multilayers are designed, then characterized in terms of structural quality and optical performances through X-ray and EUV reflectometry measurements respectively. For the Mg/Co/Zr structure, the reflectance value is reported to be 50% at 25.1 nm and 45° of grazing incidence. Nuclear Magnetic Resonance (NMR) measurements are performed to study the nearest neighbour local environment around the Co atoms.

Keywords: multilayer, interface, extreme UV, roughness, interdiffusion, reflectometry, nuclear magnetic resonance

1. INTRODUCTION

We are interested in the design, development and characterization of multilayered mirrors exhibiting high reflectance values in the extreme ultraviolet (EUV) range[1-4]. To that purpose, we explore different ways as for instance the introduction of a third material within a bilayered structure. Multilayers made of more than two materials have already proven to be efficient optical systems[5-10]. Such multilayered mirrors can be used as optical components in various applications owing to the high peak reflectivity at the wavelength of interest which is enhanced with respect to the neighbouring wavelengths although the spectral purity is not assured. They can be used as monochromators at 45° in synchrotron centres, in telescopes for imaging purposes even if telescopes are generally operated at normal incidence. We have recently shown that Co/Mg multilayers exhibit a reflectance value equal to 42.6% at 25.1 nm[3]. To enhance the performance of this latter system, in this paper we present the comparative analysis of the optical performances in the EUV spectral range of bi-, tri- and quadri-layered structures based on Mg, Co and Zr. X-ray and EUV reflectivity measurements are performed to access the structural parameters of the stack and estimate the EUV optical performances respectively. In order to investigate on possible interdiffusion through the interface between layers, Nuclear Magnetic Resonance (NMR) measurements are performed to study the nearest neighbour local environment around the Co atoms.

2. EXPERIMENT

2.1 Multilayer deposition

Mg/Co, Mg/Zr/Co, Mg/Co/Zr and Mg/Zr/Co/Zr periodic multilayers were prepared using a calibrated ultra-high vacuum direct current magnetron sputtering system (JGP560C6. SKY Inc. China) with targets of Mg, Co, and Zr (purity 99.5%

[*] karine.le_guen@upmc.fr; phone 33 (0)1 44 27 66 08; fax 33 (0)1 44 27 62 26; lcpmr.upmc.fr

Seventh International Conference on Thin Film Physics and Applications,
edited by Junhao Chu, Zhanshan Wang, Proc. of SPIE Vol. 7995, 799525
© 2011 SPIE · CCC code: 0277-786X/11/$18 · doi: 10.1117/12.888193

Downloaded from SPIE Digital Library on 23 Mar 2011 to 222.66.175.218. Terms of Use: http://spiedl.org/terms

or higher) in Ar gas. The base pressure was 5.10^{-5} Pa and the working pressure was 1.10^{-1} Pa of Ar gas. The power applied on the Co, Mg and Zr targets was set to 20, 15 and 20 W respectively. Multilayers were deposited onto ultra-smooth polished Si substrates with *rms* surface roughness of 0.3 nm. Each sample is made of 30 periods. The first layer on the substrate is the first layer given in the sample name. A 3.50 nm-thick B_4C capping layer is deposited at the surface of each sample to prevent oxidation. Materials and layer thicknesses are optimized to get the highest reflectance at 45° of incidence. At 45°, the Bragg peak is very close to the Mg L absorption edge (24.9 nm for $2p_{1/2}$ and 25.0 nm for $2p_{3/2}$) and consequently its shape is asymmetrical.

2.2 X-ray reflectivity at 0.154 nm

The quality of the multilayers was controlled through x-ray reflectometry using the Cu Kα emission line (0.154 nm or 8048 eV). Measurements are made using a grazing incidence X-ray reflectometer (D1 system. Bede Ltd) operated in the θ-2θ mode. The angular resolution is 5/1000°. The fit of the XRR curves performed with IMD was used to determine the structural parameters of the stacks (see Table 1). The density ratio (%) is defined as the density of the layer divided by the density of the bulk. In each structure, the layer thickness is close to the aimed value, the roughness is around 0.6 nm whatever the interface and the layer density is close to the value of the bulk material. In addition, the reflectivity values simulated at 45° considering an "ideal" structure (no roughness, no interdiffusion) are also given.

Table 1. Structural parameters extracted from the fit of the XRR curves measured at 0.154 nm and values of the simulated reflectivity considering an "ideal" stack (no roughness, no interdiffusion).

Multilayer	d (nm)	d_{co} (nm) d_{Mg} (nm) d_{Zr} (nm)	σ (nm)	Density ratio (%) Co Mg Zr	R_{sim} (%) $\lambda = 25.2$ nm $\theta = 45°$
Mg/Co	16.9	Co: 2.6 Mg: 14.3	$\sigma_{Co/Mg} = 0.5$ $\sigma_{Mg/Co} = 0.6$	100 96	56.7
Mg/Zr/Co	17.3	Co: 2.3 Mg: 13.5 Zr: 1.5	$\sigma_{Co/Zr} = 0.6$ $\sigma_{Zr/Mg} = 0.6$ $\sigma_{Mg/Co} = 0.7$	96 100 94	54.6
Mg/Co/Zr	17.1	Co: 2.4 Mg: 13.2 Zr: 1.5	$\sigma_{Zr/Co} = 0.6$ $\sigma_{Co/Mg} = 0.6$ $\sigma_{Mg/Zr} = 0.7$	100 95 98	62.7
Mg/Zr/Co/Zr	17.0	Co: 2.0 Zr: 1.5 Mg: 12.0 Zr: 1.5	$\sigma_{Zr/Co} = 0.7$ $\sigma_{Co/Zr} = 0.7$ $\sigma_{Zr/Mg} = 0.5$ $\sigma_{Mg/Zr} = 0.6$	99 100 100 100	47.1

2.3 EUV reflectivity

The measurement of the reflectivity curves in the EUV domain is performed on the BEAR beamline at the Elettra synchrotron centre using *s*-polarized light. The photon energy is carefully calibrated using the Pt $4f_{7/2}$ feature and the Si L absorption edge. The goniometer angular resolution is 1/100°. Impinging and reflected photon intensities are measured using a photodiode. Incident intensities are monitored using an Au mesh inserted in the beam path whose drain current is used for normalization. The overall accuracy on the absolute reflectivity values is estimated to be about 1%.

2.4 Nuclear Magnetic Resonance (NMR) spectroscopy

Zero field NMR has been performed with a homemade automated broadband NMR spectrometer. For the sake of sensitivity all the samples were measured at 4.2 K since the NMR signal increases as the inverse of the measurement temperature. All spectra have been recorded for different values of radiofrequency field strengths allowing correcting the NMR intensities with a frequency dependent enhancement factor. Therefore the NMR spectra represent the distribution of Co atoms versus their resonance frequency[11,12]. The NMR resonance frequency is sensitive to the local environment of

Downloaded from SPIE Digital Library on 23 Mar 2011 to 222.66.175.218. Terms of Use: http://spiedl.org/terms

the probed atoms: nearest neighbor local structure and/or local chemical environment. Bulk reference samples consisting in 1% Zr and 1% Mg into Co have been measured to check the influence of the Zr and Mg neighborhood on the Co resonance frequency (hyperfine field).

3. RESULTS AND DISCUSSION

3.1 EUV reflectometry

The EUV reflectivity spectra of the Mg/Co, Mg/Zr/Co, Mg/Co/Zr and Mg/Zr/Co/Zr multilayers measured at 45° of grazing incidence are presented in Figure 1. The asymmetric shape of the curves originates from the presence of the Mg L edge. For each multilayer, the Bragg peak stands onto a background corresponding to the total reflection and diffuse scattering. In the following, we will distinguish the values (in %) at the application wavelength of the peak reflectivity, the background and the net reflectivity, this latter being the difference between the two previous quantities. The background height at the application wavelength is estimated considering the 20.7-31.0 nm range. All these values are collected in Table 2.

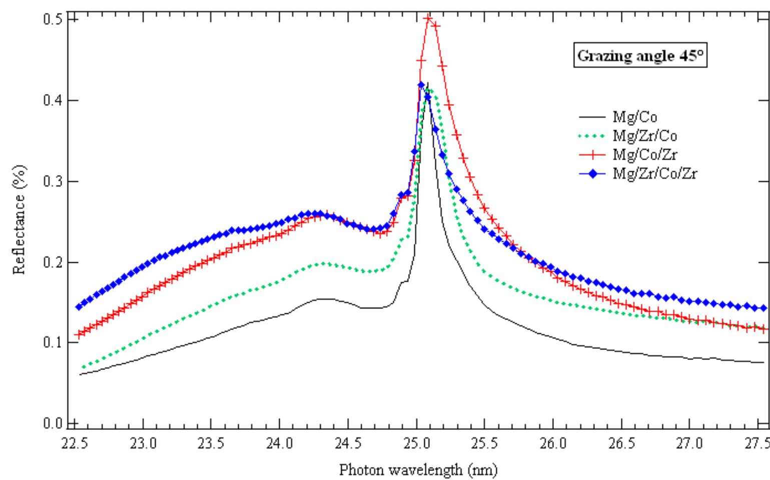

Figure 1. EUV reflectivity spectra of the Mg/Co, Mg/Zr/Co, Mg/Co/Zr and Mg/Zr/Co/Zr multilayers measured at 45° of grazing incidence.

With respect to the bi-layered Mg/Co structure (42.4%), the addition of a third component in the stack leads to a higher peak reflectivity (50.0%) if Zr is introduced at the Mg-on-Co interface while a lower value (41.4%) is measured when Zr is introduced at the Co-on-Mg interface. The presently studied quadri-layer leads to the lowest reflectance (40.6%) as expected from the simulations. The background value is the highest for the quadri-layered system. Among the tri-layered structures, although Mg/Co/Zr exhibits the highest background, its net reflectivity remains the best.

Table 2. Values of the reflectivity and background measured at 45° of grazing incidence in the 20.7-31.0 nm range. R_{exp} and R_{sim} stand for measured and simulated reflectance respectively.

Multilayer	λ (nm)	Peak reflectivity (%)	Background (%)	Net reflectivity (%)	R_{exp}/R_{simul}
Mg/Co	25.1	42.4	5.5	36.9	0.75
Mg/Zr/Co	25.1	41.4	5.2	36.2	0.76
Mg/Co/Zr	25.1	50.0	6.4	43.6	0.80
Mg/Zr/Co/Zr	25.1	40.6	6.9	33.7	0.86

In spite of the relatively high background, since the reflectance at the wavelength of interest is enhanced with respect to the neighbouring wavelengths, these multilayers (particularly Mg/Co/Zr) could be efficiently used for imaging purposes

Downloaded from SPIE Digital Library on 23 Mar 2011 to 222.66.175.218. Terms of Use: http://spiedl.org/terms

in astrophysics applications for instance. As an illustration, Mg-based multilayers (Co/Mg, SiC/Mg, B_4C/Mg and Si/Mg) operated at near normal incidence have been very recently developed for solar He-II radiation at 30.4 nm[4]. On the contrary, their use for spectroscopic purpose may be inadequate since in that case high spectral purity is required.

3.2 NMR analysis

NMR spectra obtained for the Mg/Co, Mg/Co/Zr, Mg/Zr/Co and Mg/Zr/Co/Mg/Zr multilayers are presented in Figure 2. To compare the shape of the spectra, their total surface area is normalized to unity. The Mg/Co and Mg/Co/Zr samples show a well-defined line at 226 MHz that is the fingerprint of bulk hcp Co. The Co atoms are mainly situated in pure Co layers and the intermixing at the Co/Mg interfaces is limited. The shoulder around 155 MHz originates from the Co/Mg interfaces. This suggests that the Mg/Co and Mg/Co/Zr multilayers present sharp interfaces.

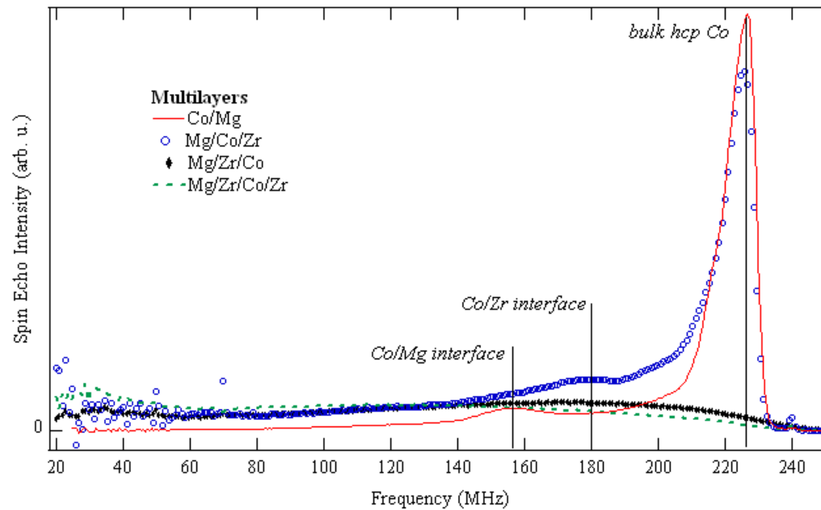

Figure 2. NMR spectra of Co/Mg, Mg/Zr/Co, Mg/Co/Zr and Mg/Zr/Co/Zr multilayers. The spectra surface areas are normalized to the same area.

In contrast, the shape of the Mg/Zr/Co and Mg/Zr/Co/Zr spectra is very different. No Co bulk line is observed anymore. This shows that the Co layers are not pure but that alien atoms (Mg or Zr) are mixed with Co. Since the present NMR analysis indicates that the Mg/Co multilayers show sharp interfaces, which is confirmed by previous X-ray emission spectroscopy (XES) data[3], the mixing is likely to originate from the Co/Zr interfaces. These Co atoms are most probably situated into non-ferromagnetic phases and therefore give no NMR signal.

4. CONCLUSION

We have presented the comparative analysis of the EUV optical quality of bi-, tri- and quadri-layered structures based on Mg, Co and Zr. The stack structural parameters and EUV optical performances have been estimated through X-ray and EUV reflectometry measurements respectively. The addition of Zr at the only Mg-on-Co interface has proven to be an efficient combination to enhance the reflectance. Given the compromise between the high reflectance at the application wavelength and the relatively high background, stress is laid on the use of these multilayers for imaging purpose through astrophysics applications for example. NMR spectra give evidence for a strong intermixing between Co and Zr layers in both Mg/Zr/Co and Mg/Zr/Co/Zr while the interfaces remain sharp within Mg/Co and Mg/Co/Zr.

Downloaded from SPIE Digital Library on 23 Mar 2011 to 222.66.175.218. Terms of Use: http://spiedl.org/terms

REFERENCES

[1] Maury, H., Jonnard, P., Le Guen, K., André, J.-M., Wang, Z., Zhu, J., Dong, J., Zhang, Z., Bridou, F., Delmotte, F., Hecquet, C., Mahne, N., Giglia, A. and Nannarone, S., Eur. Phys. J. B 64, 193-199 (2008).
[2] Jonnard, P., Maury, H., Le Guen, K., André, J.-M., Mahne, N., Giglia, A. and Nannarone, S., Surf. Science 604, 1015-1021 (2010).
[3] Le Guen, K., Hu, M.-H., André, J.-M., Jonnard, P., Zhou, S. K., Li, H. Ch., Zhu, J., Wang, Z. and Meny, C., J. Phys. Chem. C 114, 6484-6490 (2010).
[4] Zhu, J., Zhou, S.K., Li, H. Ch.; Huang, Q., Wang, Z., Le Guen, K., Hu, M.-H., André, J.-M. and Jonnard, P., Appl. Opt. 49, 3922-3925 (2010).
[5] Boher, P., Hennet, L. and Houdy, Ph., [Advanced X-Ray/EUV Radiation Sources and Applications], J. P. Knaueur and G. K. Shenoy eds., Proc. SPIE 1345**,** 198-212 (1990)
[6] Singh, M. and Braat, J. J. M., Appl. Opt. 39**,** 2189-2197 (2000).
[7] Larruquert, J.I., J. Opt. Soc. Am. A 18, 1406-1414 (2001).
[8] Larruquert, J.I., J. Opt. Soc. Am. A 19, 391-397 (2002).
[9] Gautier, J., Delmotte, F., Roulliay, M., Bridou, F., Ravet, M.-F. and Jérome, A., Appl. Opt. 44, 384-390 (2005).
[10] Meltchakov, E., Hecquet, C., Roulliay, M., De Rossi, S., Ménesguen, Y., Jérome, A., Bridou, F., Varnière, F., Ravet-Krill, M.-F. and Delmotte, F., Appl. Phys A 98, 111-117 (2010).
[11] Meny, C. and Panissod, P., [Modern Magnetic Resonance], G. Webb, Ed., Springer, Heidelberg (2006).
[12] Panissod, P. and Meny, C., Appl. Magn. Reson. 19, 447-460 (2000).

Downloaded from SPIE Digital Library on 23 Mar 2011 to 222.66.175.218. Terms of Use: http://spiedl.org/terms

Optical, chemical, depth and magnetic characterization of Mg/Co-based nanometric periodic multilayers

P. Jonnard[1], K. Le Guen[1*], M.-H. Hu[1], J.-M. André[1], S. K. Zhou[2], H. Ch. Li[2], J. T. Zhu[2], Z. S. Wang[2], N. Mahne[3], A. Giglia[3], S. Nannarone[3], A. Verna[3], C. Meny[4], A. Galtayries[5], I. Estève[6] and M. Walls[7]

[1]Laboratoire de Chimie Physique – Matière Rayonnement, UPMC Univ Paris 06, CNRS UMR 7614
11 rue Pierre et Marie Curie, F-75231 Paris cedex 05, France

[2]Institute of Precision Optical Engineering, Department of Physics, Tongji University, Shanghai 200092, P.R. China

[3]Istituto Officina dei Materiali IOM-CNR Laboratorio TASC
S.S.14. km 163.5 in Area Science Park, I-34012 Trieste, Italy

[4]Institut de Physique et Chimie des Matériaux de Strasbourg, CNRS UMR 7504
23 rue du Loess, BP 43, F-67034 Strasbourg cedex 2, France

[5]Laboratoire de Physico-Chimie des Surfaces, Ecole Nationale Supérieure de Chimie de Paris (Chimie ParisTech), CNRS UMR7045, 11 rue Pierre et Marie Curie, F-75231 Paris cedex 05, France

[6]Institut de Minéralogie et de Physique des Milieux Condensés, Univ Paris 06 et 07, CNRS UMR 7590, 4 place Jussieu, F-75252 Paris cedex 05, France

[7]Laboratoire de Physique des Solides, CNRS UMR 8502, Univ Paris Sud, F-91405 Orsay, France

ABSTRACT

We have developed and elaborated a series of Mg/Co-based periodic multilayers to build efficient mirrors for the extreme ultraviolet (EUV) range. For *s*-polarized light and at 45° of grazing incidence, the reflectivity of as-deposited Mg/Co is 42.6% at 25.1 nm. X-ray emission spectroscopy and nuclear magnetic resonance measurements do not indicate any noticeable interdiffusion at the interfaces between layers. Scanning transmission electronic microscopy images attest the high structural quality of the stack. X-ray reflectivity (XRR) curves in the hard x-ray and EUV domains confirm this description and estimate a weak interfacial roughness (~ 0.5 nm). Taking advantage of the magnetic character of Co, we have performed resonant magnetic reflectivity measurements by scanning the photon energy around the Co L absorption edge for opposite circular polarizations. The magnetization profile of the Co layers within Co/Mg determined with an expected depth resolution of one monolayer confirms the interface abruptness. Scanning electron microscopy images and XRR curves give evidence of the thermal stability of Mg/Co up to 300 °C. From that value, a strong change in the sample morphology due to the delamination of the multilayer from the substrate occurs. This should account for the

[*] Corresponding author: Dr. Philippe Jonnard, Laboratoire de Chimie Physique – Matière et Rayonnement, 11 rue Pierre et Marie Curie, F-75231 Paris Cedex 05, France; tel: 33 1 44 27 63 03; fax: 33 1 44 27 62 26; philippe.jonnard@upmc.fr

drastic reflectivity drop observed above this temperature. Starting from Mg/Co, we have inserted a Zr layer at one or at the other interface or at both interfaces to estimate the effect of the introduction of a third material within the period. We have found that Mg/Co/Zr is more efficient (50% of reflectivity) than Mg/Zr/Co and Mg/Zr/Co/Zr (~ 40%). Through time-of-flight secondary ion mass spectrometry depth profiling and NMR measurements, we have assigned this difference to an intermixing process when Co layers are deposited onto Zr layers.

Keywords: periodic multilayer, cobalt, magnesium, zirconium, reflectance, interface, annealing

1 INTRODUCTION

A series of multilayers, in which Mg/Co is the starting point, is studied according to three main axes. The first one focuses on the as-prepared Mg/Co multilayers and by combining different techniques such as x-ray reflectivity (XRR) in the hard and EUV (extreme ultra-violet) ranges, magneto-optical Kerr effect in the EUV range, x-ray emission and nuclear magnetic resonance spectroscopies (XES and NMR), scanning and transmission electron microscopies (SEM and STEM) and time of flight secondary ion mass spectrometry (ToF-SIMS). Second, the thermal resistance of Mg/Co upon annealing up to 400 °C is investigated. Indeed, the consequence of a high thermal load of this kind of mirrors has to be evaluated since these samples could be used as optical components in synchrotron beamlines or for astrophysics purposes. The third thematic intends to examine the effect of the introduction of a third material, namely Zr, within the two-material Mg/Co structure in terms of gain or loss of reflectivity

2 SAMPLES AND EXPERIMENTS

Following their deposition by direct current magnetron sputtering, all the multilayers were characterized in terms of thickness, roughness and density of layers using XRR at 0.154 nm and subsequent data fitting. Whatever the sample, the roughness value varies between 0.5 and 0.7 nm. The number of periods in each sample is equal to 30. Table 1 presents the value of the period and layer thickness of the as-deposited samples as determined by XRR.

Table 1: Values of period and layer thickness in the as-deposited multilayers extracted from the fit of the XRR curves.

Sample	Mg/Co	Mg/Zr/Co	Mg/Co/Zr	Mg/Zr/Co/Zr
d (nm)	16.9	17.3	17.1	17.0
d_{Mg} (nm)	14.3	13.5	13.2	12.0
d_{Co} (nm)	2.6	2.3	2.4	2.0
d_{Zr} (nm)	-	1.5	1.5	1.5

EUV reflectometry measurements were carried out at the Elettra synchrotron facility using *s*-polarized radiation at 45° of grazing incidence, in order to estimate the optical properties of the multilayers at their application wavelength, around 25 nm [1-3].

To identify the chemical state of the atoms within the multilayers (as-deposited and annealed Mg/Co as well as Mg/Co/Zr, Mg/Zr/Co and Mg/Zr/Co/Zr) and thus evidence a possible interdiffusion, the choice of the experimental technique is directly related to the probed element itself. For Mg atoms, XES measurements are suited since the shape of the Mg Kβ emission band is very sensitive to the local environment of the Mg atoms. On the other hand, we have taken advantage of the magnetic nature of the Co atoms to perform NMR spectroscopy at 4.2 K to probe the possible presence of alien atoms as nearest neighbours of Co atoms. Details about the operating conditions during XES and NMR measurements are described elsewhere [1,4]. To go beyond the detection limit of the XES and NMR methodologies and be able to detect a transition layer which thickness could be close to one monolayer, we have probed the magneto-optical effect within Mg/Co on the BEAR beamline at the Elettra synchrotron centre. The magnetization profile of the Co layers is measured by scanning the photon energy around the Co L_3 absorption edge (778 eV) for opposite circularly-polarized radiations.

To probe the structural quality and the composition of the layers and interfaces, two main techniques were implemented: one based on electron microscopies, the other on depth profiling. First, we have analyzed the morphology of the as-deposited Mg/Co multilayer through scanning transmission electronic microscopy (STEM) while the evolution of the

Mg/Co multilayer morphology as a function of the annealing temperature was controlled using scanning electronic microscopy (SEM) on cross sections prepared by focused ion beam [3]. Secondly, in the case of Mg/Co, Mg/Co/Zr, Mg/Zr/Co and Mg/Zr/Co/Zr samples, we have performed time-of-flight secondary ion mass spectrometry (ToF-SIMS) depth profiling to measure the elemental and chemical distributions as a function of depth [4.].

3 RESULTS AND DISCUSSION

3.1 The Mg/Co system

In order to study the interface composition within the multilayer-two sets of measurements are carried out. First, the chemical state of the Mg atoms is investigated by comparing the shape of the Mg Kβ emission band originating from the Mg atoms present within Mg/Co to that of Mg atoms from two reference samples, namely Mg metal and MgO. As presented in Figure 1(a), we can exclude any reaction involving the Mg atoms of the multilayer since the physico-chemical environment of these latter is identical (at the limit of resolution of XES) to that in pure Mg.

Secondly, the chemical state of the Co atoms present within Mg/Co is examined by studying the distribution of their NMR resonance frequency. In Figure 1(b), only two features are observed: the more intense one related to bulk *hcp* Co atoms and the weak peak to Co atoms having Mg atoms for nearest neighbours. This attests that the Co atoms have not reacted and that the morphology of the stack is of high quality (well-defined Co layers as well as abrupt interfaces).

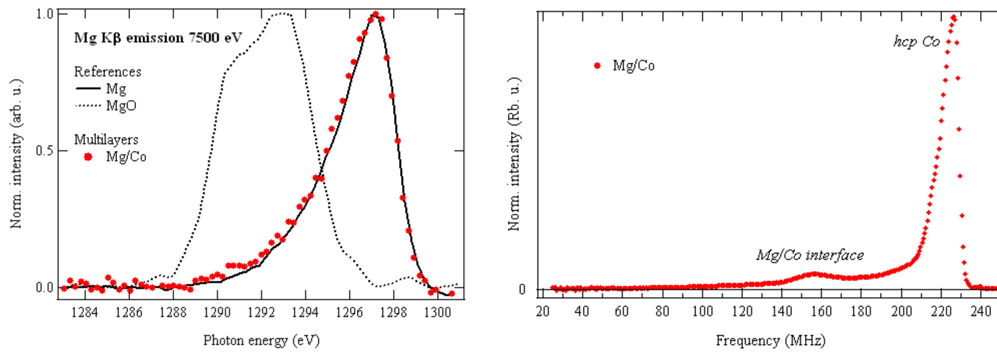

Figure 1: (a) Mg Kβ emission band from Mg/Co compared to that of Mg and MgO references; (b) NMR spectrum of Mg/Co.

The XES and NMR sets of data allow us to exclude any reaction between Mg and Co atoms within the Mg/Co sample. Measurements of the magneto-optical effects within Mg/Co enable us to go beyond these limits and even access a resolution close to one monolayer. Thus, we have recorded around the Bragg peaks a 3D map showing the reflectivity distribution as a function of the grazing angle and the photon energy values. The position of the Bragg peaks had been previously determined from reflectivity measurements. The incident photon beam is circularly polarized and its energy is varied along the Co L_3 edge. As an example, we give in Figure 2 the spectra obtained around the first and third Bragg peaks. In each case, the 3D map is obtained for two opposite sample magnetizations and the dichroic signal is taken as their difference.

From the observation of the maps, it can be seen that the variation of the reflectance with the grazing angle and the photon energy is complex: there is no single peak as expected for non-magnetic materials; secondary maximum is also observed for the Co/Mg multilayer. The 3D dichroic maps obtained around the first and second (not shown) present negative values contrary to the one obtained around the third Bragg peak. The first analysis of these maps, made by comparing them to maps simulated from multilayers taking into account a dead magnetic zone at the interfaces, do not give evidence of an interaction between the Co and Mg layers within the stack.

The good quality of the periodic structure is evidenced in the STEM image presented in Figure 3 of the cross-section from a ~30 nm-thick lamella excavated from Mg/Co using a focused ion beam (FIB). The 30 periods are clearly seen between the protective Pt layer on top of the sample and the Si substrate (bottom). The zoom on the thinnest part of the sample shows that both Co and Mg layers are crystallized.

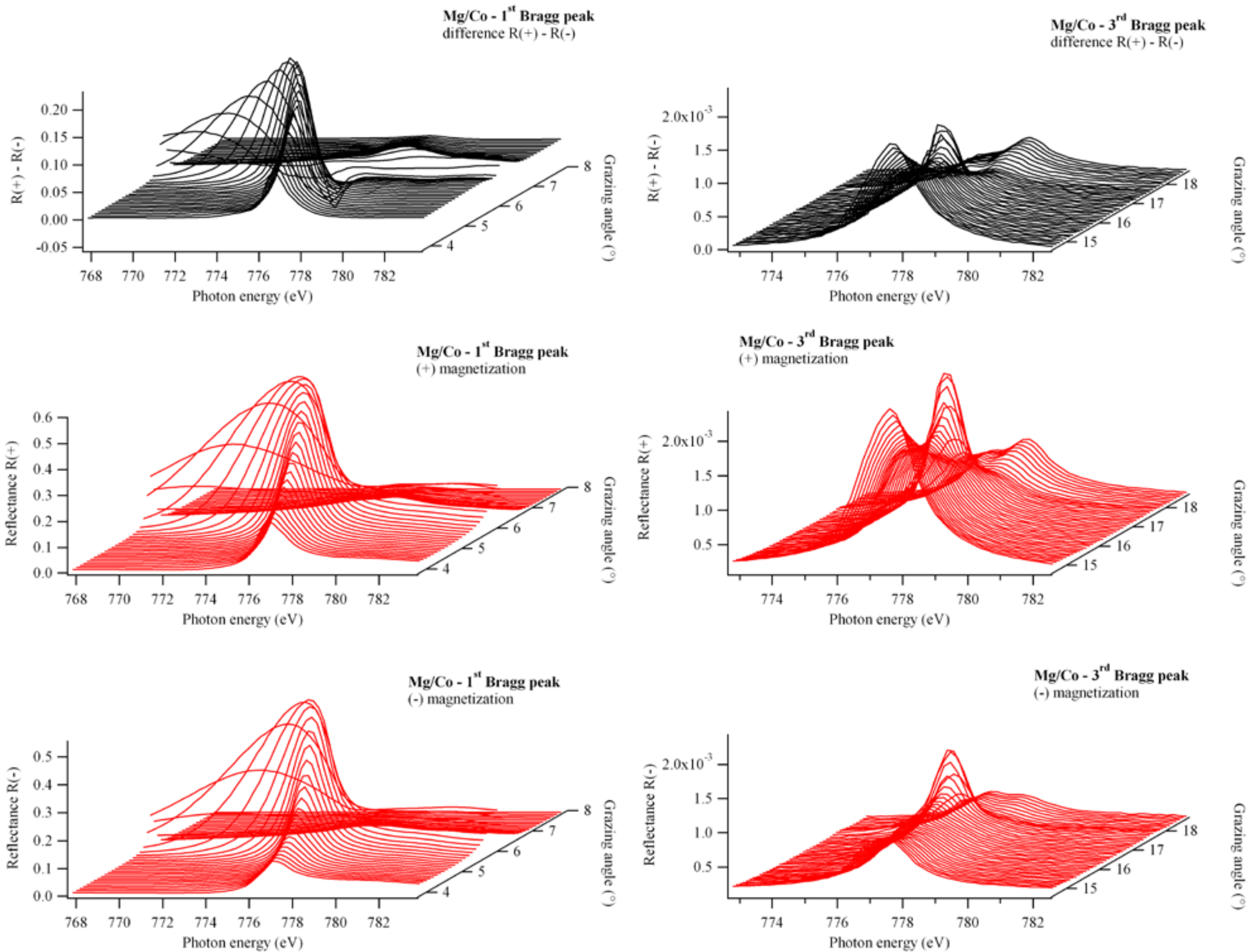

Figure 2: Evolution of the reflectivity curves as a function of the photon energy (around the Co L_3 edge) and the grazing angle around the 1st (left) and 3rd (right) Bragg peaks, for two opposite sample magnetizations (bottom and middle) using a given circular polarization. The top spectrum is the dichroic signal and represents the difference between the middle and bottom spectra.

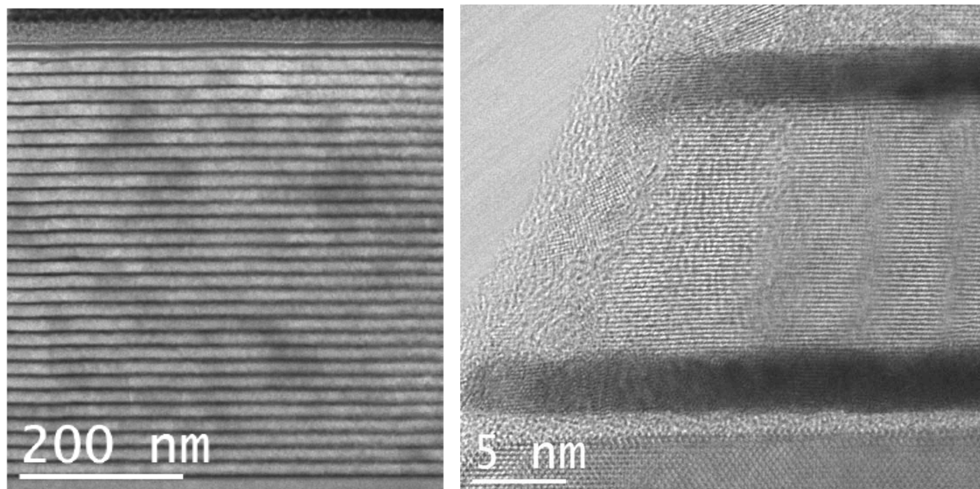

Figure 3: Left: STEM image of the cross-section from a ~30 nm-thick lamella excavated from Mg/Co by FIB. The Pt layer on top of the sample aims to protect the surface from ion beam damages during the preparation of the cross section. Right: Zoom on the thinnest part of the sample: bottom is the silicon substrate; dark regions are the Co layers; bright region between the Co layers is the Mg layer.

3.2 Annealing of Mg/Co up to 400 °C

Figure 4 presents the evolution of the reflectivity (R) of Mg/Co as a function of the annealing temperature at a grazing incidence equal to 45°. Starting from R = 42.4% at 25.1 nm for the as-deposited multilayer, R increases up to 45.0% in the case of Mg/Co annealed at 280°C. Then, carry on annealing at higher temperature results at 305°C in a drastic drop of R down to 26.2% and at the same time a slight shift of the Bragg peak (25.0 nm). At 400°C, R vanishes.

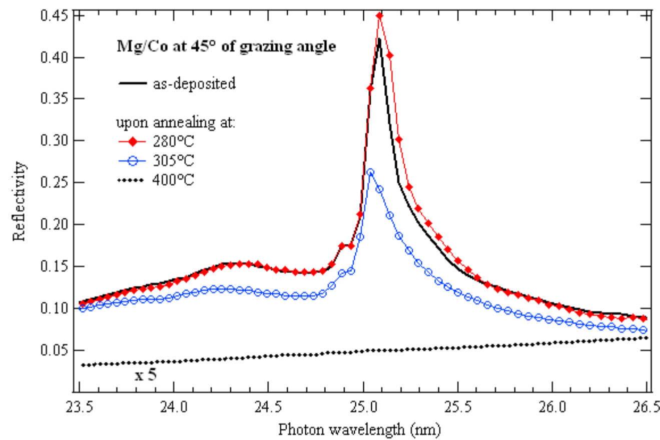

Figure 4: EUV reflectivity spectra of the as-deposited and annealed Mg/Co samples measured at 45° of grazing incidence.

The fit of the EUV reflectivity curves (not shown) indicates that the layer thickness and roughness remain constant up to 280 °C while from 305 °C their values vary strongly. To get higher insight on the evolution of the stack morphology as a function of the annealing temperature, a series of SEM images has been recorded.

Figure 5 presents the comparison between the SEM images of the samples annealed at 280 and 305°C. It is clearly seen that the multilayer does not resist to temperatures higher than 305 °C since from that limit the stack comes unstuck from the substrate and the interfaces are not flat anymore. This loss of flatness from 305°C is responsible for the reflectivity drop to ~42% with respect to Mg/Co annealed at 280°C. At 400°C (not shown), the defects are more pronounced and a delamination between the layers of the stack is even observed. In the same way, the analysis of the NMR spectra measured for this set of as-deposited and annealed samples (not shown) lead to the conclusion that from 305°C the Co thin layers are clustering into large Co grains [3]. This is responsible for the drastic change of morphology of the sample from that temperature.

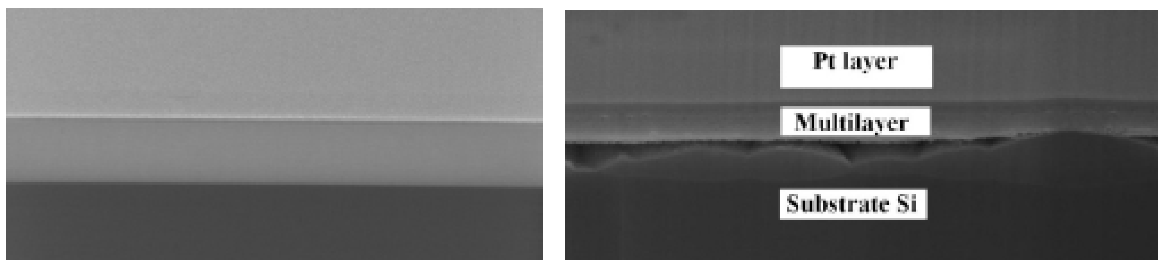

Figure 5: SEM image of the cross-section from Mg/Co annealed at 280 (left) and 305°C (right).

3.3 Study of a three- and four-material systems: introduction of Zr into Mg/Co

The EUV reflectivity spectra of Mg/Co, Mg/Zr/Co, Mg/Co/Zr and Mg/Zr/Co/Zr measured at 45° of grazing incidence are presented in Figure 6. With respect to Mg/Co (42.4%), the addition of a third component in the stack leads to a higher reflectivity (50.0%) if Zr is introduced at the Mg-on-Co interface and a lower value (41.4%) when Zr is introduced at the Co-on-Mg interface. The quadri-layer is characterized by the lowest reflectance (40.6%) and presents

the highest background. Thus, introducing a Zr layer at one or the other interface or at both interfaces of Mg/Co is not equivalent.

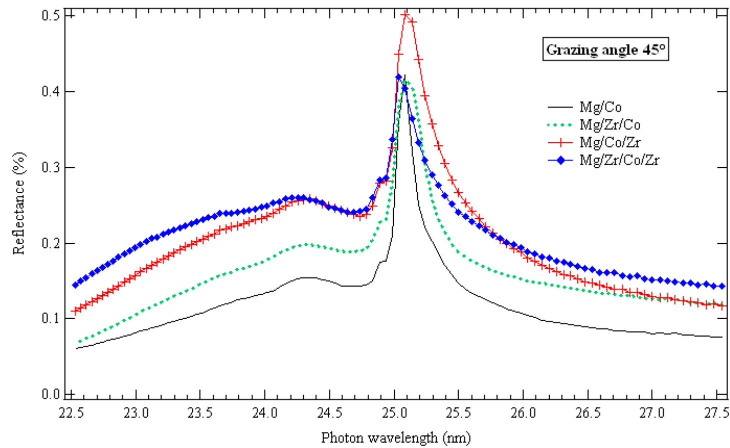

Figure 6: EUV reflectivity curves of Mg/Co, Mg/Zr/Co, Mg/Co/Zr and Mg/Zr/Co/Zr measured at 45° of grazing incidence.

We also resort to ToF-SIMS depth profiling to study the interface structure within these samples. Figure 7 presents the comparison, over about 5 periods, of the Co^- profile for Mg/Co, Mg/Zr/Co, Mg/Co/Zr and Mg/Zr/Co/Zr. The profile shape is almost symmetrical for Mg/Co and Mg/Co/Zr while asymmetrical for Mg/Co/Zr and Mg/Zr/Co/Zr. In addition, if for a given period we define the contrast as the profile amplitude divided by the profile minimum, its value is estimated to 0.34, 0.35, 2.10 and 0.87 for Mg/Co, Mg/Zr/Co, Mg/Co/Zr and Mg/Zr/Co/Zr respectively. In summary, among all samples, Mg/Co/Zr presents the best profiles in terms of symmetry and contrast, signature of well-defined Co-on-Mg and Zr-on-Co interfaces. On the contrary, in Mg/Zr/Co and Mg/Zr/Co/Zr the profile splitting could be related to intermixing occurring at the Co-on-Zr interface. This is in good agreement with the optical performances of Mg/Co/Zr, Mg/Zr/Co and Mg/Zr/Co/Zr.

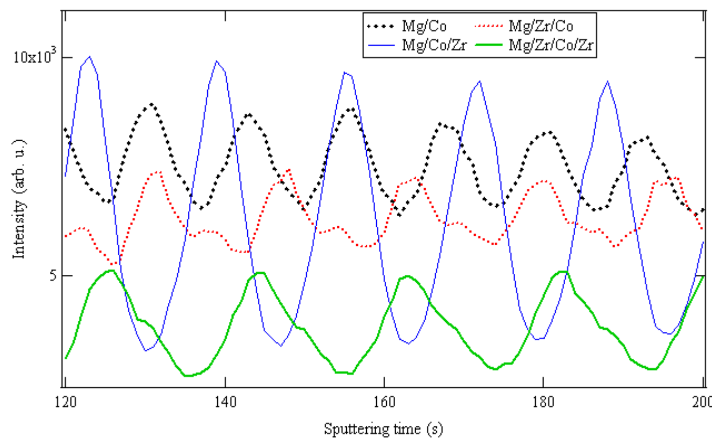

Figure 7: Evolution over 5 periods of the Co ToF-SIMS depth profiles of Mg/Co, Mg/Zr/Co, Mg/Co/Zr and Mg/Zr/Co/Zr stacks.

NMR measurements allow refining the description of the interfaces within Mg/Co, Mg/Zr/Co, Mg/Co/Zr and Mg/Zr/Co/Zr multilayers as presented in Figure 8. The Mg/Co and Mg/Co/Zr spectra are both characterized by a well-defined and intense line assigned to bulk hcp Co (226 MHz) and a shoulder related to the Co/Mg interface (156 MHz). An additional shoulder corresponding to the Co/Zr interface (180 MHz) is observed for Mg/Co/Zr. The spectra of Mg/Zr/Co and Mg/Zr/Co/Zr consist in a wide and flat feature covering the whole frequency range (no more line at 226 MHz). To synthesize these results, the Co layers and Co-on-Zr interfaces within Mg/Co/Zr are rather well defined whereas no more pure Co layers remain within the Mg/Zr/Co and Mg/Zr/Co/Zr multilayers as a consequence of intermixing at the Zr-on-Co interface. This mechanism relies on vertical exchanges on a microscopic scale between lower Zr and upper Co atoms and is the consequence of the surfactant effect of Zr atoms [4].

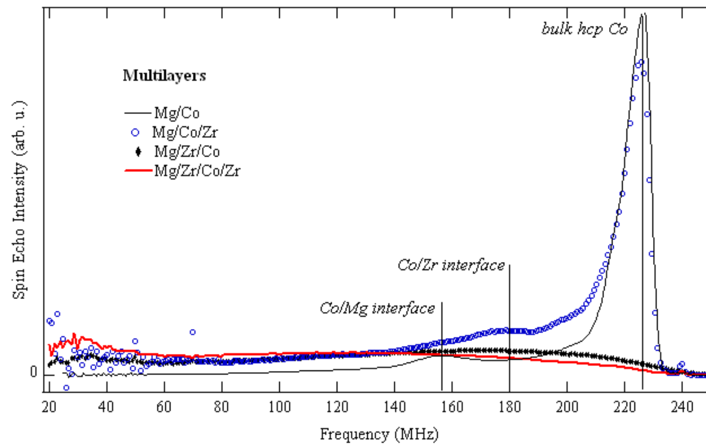

Figure 8: NMR spectra of Mg/Co, Mg/Zr/Co, Mg/Co/Zr and Mg/Zr/Co/Zr stacks.

4 CONCLUSION

Mg/Co-based periodic multilayers prove to be efficient multilayers in the EUV range as an experimental reflectance of 50% as been obtained at 45° of incidence at 25 nm with *s*-polarized light when thin Zr layers are introduced at the Mg-on-Co interfaces. These multilayers have also proven their efficiency around 30 nm [5]. The system is stable up to a temperature of 300°C. These good properties are the consequence of the sharp interfaces existing between the Co and Mg layers of the stacks as determined from the combination of various spectroscopic and microscopic techniques. However, when Zr layers are introduced at the Co-on-Mg interface the reflectance decreases owing to the formation of a diffuse Co-on-Zr interface.

ACKNOWLEDGMENTS

Parts of this work have been funded by the grants COBMUL ANR 2010-INTB-902-01, NSFC 11061130549 and supported by the European Community - Research Infrastructure Action under the FP6 “Structuring the European Research Area” Programme (through the Integrated Infrastructure Initiative “Integrating Activity on Synchrotron and Free Electron Laser Science”) under contract RII3-CT-2004-506008 (IA-SFS).

REFERENCES

[1] K. Le Guen, M.-H. Hu, J.-M. André, P. Jonnard, S. K. Zhou, H. Ch. Li, J. T. Zhu, Z. S. Wang and C. Meny, “Development and interfacial characterization of Co/Mg periodic multilayers in the EUV range”, J. Phys. Chem. C, **114**, 6484-6490 (2010).

[2] K. Le Guen, M.-H. Hu, J.-M. André, P. Jonnard, S. K. Zhou, H. Ch. Li, J. T. Zhu, Z. S. Wang, N. Mahne, A. Giglia and S. Nannarone, “Introduction of Zr layers in Mg/Co multilayers for EUV applications”, Appl. Phys. A **102**, 69-77 (2011).

[3] M.-H. Hu, K. Le Guen, J.-M. André, P. Jonnard, S. K. Zhou, H. Ch. Li, J. Zhu, Z. Wang, C. Meny, N. Mahne, A. Giglia, S. Nannarone, I. Estève and M. Walls, “Investigation of the thermal stability of Mg/Co periodic multilayers for EUV applications”, submitted to Appl. Phys. A.

[4] K. Le Guen, M.-H. Hu, J.-M. André, S. K. Zhou, H. Ch. Li, J.T. Zhu, Z.S. Wang, C. Meny, A. Galtayries and P. Jonnard, “Observation of asymmetry when introducing Zr in Mg/Co multilayers”, Appl. Phys. Lett. **98**, 251909 (2011).

[5] J. Zhu, S. Zhou, H. Li, Q. Huang, Z. Wang, K. Le Guen, M.-H. Hu, J.-M. André, P. Jonnard, “Comparison of Mg-based multilayers for solar He II radiation at 30.4 nm wavelength”, Appl. Opt. **49**, 3922-3925 (2010).

Thermal stability of Mg/Co multilayer with B_4C, Mo or Zr diffusion barrier layers

Jingtao Zhu,[1] Sika Zhou,[1] Haochuan Li,[1] Zhanshan Wang,[1,*] Philippe Jonnard,[2] Karine Le Guen,[2] Min-Hui Hu,[2] Jean-Michel André,[2] Hongjun Zhou,[3] and Tonglin Huo[3]

[1]*Department Institute of Precision Optical Engineering, Department of Physics, Tongji University, Shanghai 200092, China*

[2]*Laboratoire de Chimie Physique – Matière Rayonnement, UPMC Univ Paris 06, CNRS UMR 7614, 11 rue Pierre et Marie Curie, F-75231 Paris cedex 05, France*

[3]*National Synchrotron Radiation Laboratory, University of Science and Technology of China, Hefei 230029, China*

[*]*wangzs@tongji.edu.cn*

Abstract: The efficiency of B_4C, Mo and Zr barrier layers to improve thermal stability of Mg/Co multilayer up to 400 °C is investigated. Multilayers were deposited by direct current magnetron sputtering and characterized using X-ray and extreme ultraviolet reflection. The results suggest that B_4C barrier layer is not effective due to drastic diffusion at Mg-B_4C interface. Although introducing Mo barriers improves the thermal stability from 200 to 300 °C, it increases the interface roughness and thus degrades the optical performances. On the contrary, Zr barriers can significantly increase the thermal stability of Mg/Co up to 400 °C without optical performance degradation. Thus, Mg/Zr/Co/Zr is suitable for EUV applications requiring both optimal optical performances and heat resistance.

©2011 Optical Society of America

OCIS codes: (340.7480) X-rays, soft x-ray, extreme ultraviolet (EUV); (230.4170) Multilayers; (340.6720) Synchrotron radiation.

References and links

1. Y. Kondo, T. Ejima, H. Takatsuka, and M. Watanabe, "Microscopic ultraviolet photoelectron spectroscopy using He-I and He-II resonance lines," Surf. Rev. Lett. **9**(1), 521–527 (2002).
2. N. Dudovich, O. Smirnova, J. Levesque, Y. Mairesse, M. Yu. Ivanov, D. M. Villeneuve, and P. B. Corkum, "Measuring and controlling the birth of attosecond XUV pulses," Nat. Phys. **2**(11), 781–786 (2006).
3. D. L. Windt, S. Donguy, J. Seely, B. Kjornrattanawanich, E. M. Gullikson, C. C. Walton, L. Golub, and E. DeLuca, "EUV multilayers for solar physics," Proc. SPIE **5168**, 1–11 (2004).
4. M. Suman, M. G. Pelizzo, D. L. Windt, and P. Nicolosi, "Extreme-ultraviolet multilayer coatings with high spectral purity for solar imaging," Appl. Opt. **48**(29), 5432–5437 (2009).
5. Y. Y. Platonov, D. Broadway, B. DeGroot, B. Verman, B. Kim, G. Gutman, J. Wood, J. Rodriguez, and N. Grupido, "Deposition of X-Ray Multilayers on Long Size Substrates for Synchrotron Applications," Proc. SPIE **3152**, 231–239 (1997).
6. T. Ejima, A. Yamazaki, T. Banse, K. Saito, Y. Kondo, S. Ichimaru, and H. Takenaka, "Aging and thermal stability of Mg/SiC and Mg/Y_2O_3 reflection multilayers in the 25-35 nm region," Appl. Opt. **44**(26), 5446–5453 (2005).
7. J. T. Zhu, Z. S. Wang, Z. Zhang, F. L. Wang, H. C. Wang, W. J. Wu, S. M. Zhang, D. Xu, L. Y. Chen, H. J. Zhou, T. L. Huo, M. Q. Cui, and Y. D. Zhao, "High reflectivity multilayer for He-II radiation at 30.4 nm," Appl. Opt. **47**(13), C310–C314 (2008).
8. J. Zhu, S. Zhou, H. Li, Q. Huang, Z. Wang, K. L. Guen, M.-H. Hu, J.-M. André, and P. Jonnard, "Comparison of Mg-based multilayers for solar He II radiation at 30.4 nm wavelength," Appl. Opt. **49**(20), 3922–3925 (2010).
9. K. Le Guen, M.-H. Hu, J.-M. André, P. Jonnard, S. K. Zhou, H. Ch. Li, J. T. Zhu, Z. S. Wang, and C. Meny, "Development and interfacial characterization of Co/Mg periodic multilayers for the EUV range," J. Phys. Chem. C **114**(14), 6484–6490 (2010).
10. H. Maury, P. Jonnard, K. Le Guen, J.-M. André, Z. Wang, J. Zhu, J. Dong, Z. Zhang, F. Bridou, F. Delmotte, C. Hecquet, N. Mahne, A. Giglia, and S. Nannaronne, "Thermal cycles, interface chemistry and optical performance of Mg/SiC multilayer," Eur. Phys. J. B **64**(2), 193–199 (2008).
11. A. Aquila, F. Salmassi, Y. Liu, and E. M. Gullikson, "Tri-material multilayer coatings with high reflectivity and wide bandwidth for 25 to 50 nm extreme ultraviolet light," Opt. Express **17**(24), 22102–22107 (2009).

#153768 - $15.00 USD Received 30 Aug 2011; revised 29 Sep 2011; accepted 6 Oct 2011; published 20 Oct 2011

12. A. A. Nayeb-Hashemi and J. B. Clark, "The Mg-Zr (Magnesium-Zirconium) System," Bull. Alloy Phase Diagrams **6**(3), 246–250 (1985).
13. T. Bottger, D. C. Meyer, P. Paufler, S. Braun, M. Moss, H. Mai, and E. Beyer, "Thermal stability of Mo/Si multilayers with boron carbide interlayers," Thin Solid Films **444**(1-2), 165–173 (2003).
14. P. Jonnard, H. Maury, K. Le Guen, J.-M. André, N. Mahne, A. Giglia, S. Nannarone, and F. Bridou, "Effect of B_4C diffusion barriers on the thermal stability of Sc/Si periodic multilayers," Surf. Sci. **604**(11-12), 1015–1021 (2010).
15. A. A. Nayeb-Hashemi and J. B. Clark, *Phase Diagrams of Binary Magnesium Alloys* (ASM International, 1988), pp 204–205.
16. K. Le Guen, M.-H. Hu, J.-M. André, P. Jonnard, S. K. Zhou, H. C. Li, J. T. Zhu, Z. S. Wang, N. Mahne, A. Giglia, and S. Nannarone, "Introduction of Zr layers in Mg/Co multilayers for EUV applications," Appl. Phys., A Mater. Sci. Process. **102**, 69–77 (2011).
17. K. Le Guen, M.-H. Hu, J.-M. André, S. K. Zhou, H. Ch. Li, J. T. Zhu, Z. S. Wang, C. Meny, A. Galtayries, and P. Jonnard, "Observation of an asymmetrical effect when introducing Zr in Mg/Co multilayers," Appl. Phys. Lett. **98**(25), 251909 (2011).
18. M. Wormington, C. Panaccione, K. Matney, and D. Bowen, "Characterization of structures from X-rayscattering data using genetic algorithms," Philos. Trans. R. Soc. Lond. A **357**(1761), 2827–2848 (1999).

1. Introduction

High reflective multilayer mirrors are widely used as optical elements for applications such as extreme ultraviolet (EUV) microspectroscopy [1], high harmonic femtosecond chemistry [2], solar astrophysics imaging [3,4], and synchrotron radiation [5]. Mg-based multilayers, such as Mg/SiC, Mg/Y_2O_3 and Mg/Co are promising in the 25-40nm wavelength range, the Mg L3 absorption edge being located at 25nm [6–10]. Mg/SiC obtained a peak reflectance of 44% at 31.2nm at 10° of incidence [6]. Mg/Co has a peak reflectance of 40.3% at 30.5nm at 10° [8]. Tri-material Mg/Sc/SiC reported has a peak reflectivity of 48.7% at 36.8 nm [11].

Multilayers mirrors usually endured a high flux of incident light or high heat loads in applications such as synchrotron radiation and solar imaging. However, Mg is known to have a low melting point (650 °C) [12], making it difficult to improve the thermal stability of Mg-based multilayers. Previous studies demonstrated that Mg/SiC and Mg/Y_2O_3 are thermally stable below the temperature of 200 °C, but deteriorate drastically at higher temperatures [6,10]. According to previous research, Mg/Co can be stable at 200 °C [8]. Further investigation on the heat resistance of this new multilayer has not been reported. Compared with Mg/SiC, Mg/Y_2O_3 and Mg/Sc/SiC, Mg/Co has narrower bandwidth which produced better spectral resolution [8], making it more attractive for applications requiring a narrow spectral bandwidth, such as monochromatic solar imaging. Thus, it is important to investigate and improve the thermal stability of Mg/Co for such practical applications.

To improve the thermal stability, diffusion barrier layers can be inserted between the Mg and Co layers. B_4C is a stable ceramic and also a common diffusion barrier layer. The efficiency of B_4C barrier layer has been demonstrated for some multilayers. B_4C diffusion barriers with thicknesses between 0.3 and 1.0 nm increased the thermal stability from 150 up to 400 °C for Mo/Si [13] and from 100 up to 200 °C for Sc/Si [14]. Mo and Zr barriers are expected to be efficient to prevent diffusion in Mg/Co multilayer, since both Mo and Zr have high melting point and do not chemical react with Mg or Co below 650 °C [12,15]. Moreover, the introduction of barrier layer in Mg/Co can also improve reflectance when the order of the materials within a period is correctly chosen [16,17]. Thus, in this paper, we investigate the thermal stability of Mg/Co multilayer and then, that of Mg-Co based multilayers where B_4C, Mo and Zr barriers have been introduced to enhance thermal stability.

2. Experimental

Four sets of multilayer samples with a gamma value of 0.83 ($d_{Mg}/(d_{Mg} + d_{Co})$) have been prepared, including Mg/Co, Mg/B_4C/Co/B_4C, Mg/Mo/Co/Mo and Mg/Zr/Co/Zr. The number of period is 30, and the period thickness is near 17.0 nm. All the samples were deposited onto polished silicon wafers (100) with a size of 30×30 cm^2 using direct current (DC) magnetron sputtering method. A 3.5 nm-thick B_4C capping layer was deposited onto the surface of each

#153768 - $15.00 USD Received 30 Aug 2011; revised 29 Sep 2011; accepted 6 Oct 2011; published 20 Oct 2011
(C) 2011 OSA

sample to prevent oxidation. Following deposition, each sample was cut into nine equal small pieces of 10×10 cm^2 for heat resistance study. The small samples were mounted on a plate heated by a wire-wound furnace in a vacuum chamber with a base pressure of 3×10^{-4} Pa. The samples were heated from room temperature to 300, 350 or 400°C, respectively, and held for 1 hour. The temperature was monitored by a thermocouple gauge attached the back of plate.

X-ray and EUV reflectometry measurements were carried out to test the changes in the multilayers before and after annealing. Grazing incident X-ray reflection (GIXR) measurements were made in the θ-2θ reflection geometry mode, using an X-ray diffractometer working at Cu Kα line (0.154nm). The fit of the GIXR curves performed with Bede Refs software was used to determine individual layer thickness, interface roughness, and layer density [18]. EUV reflectance measurements were made at 45°, using the reflectometer operating on the Spectral Radiation Standard and Metrology Beamline and Station (U26) at the National Synchrotron Radiation Laboratory (NSRL), China. The details on deposition and measurement procedure have been described elsewhere [8].

3. Results and discussion

3.1 Thermal stability of Mg/Co multilayer

The measured X-ray and EUV reflectance curves of Mg/Co multilayers before and after annealing are shown in Fig. 1. MgCo_1, MgCo_2, MgCo_3 and MgCo_4 stand for the as-deposited sample and those annealed at 300, 350 and 400°C, respectively. The period thickness of MgCo_1 MgCo_2 and MgCo_3 are 16.9, 16.7 and 16.7nm respectively.

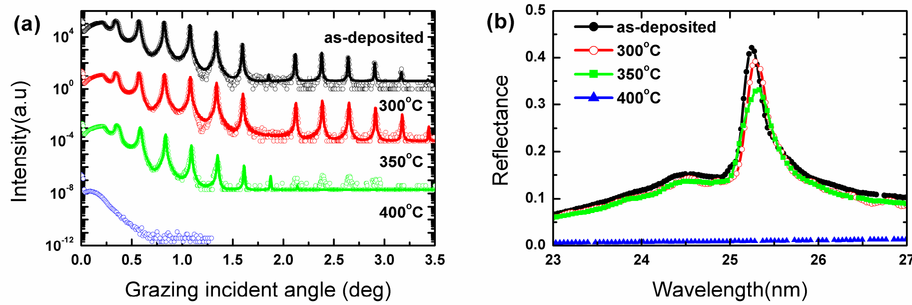

Fig. 1. (Color online) Measured GIXR (a) and EUV (b) reflectance curves of Mg/Co multilayers: as-deposited, 300, 350 and 400 °C, respectively. In (a), each curve was shifted vertically by 4 orders of magnitude for better discrimination; scatter and solid lines represent measured and fitted GIXR curves, respectively.

As shown in Fig. 1(a), upon annealing at 300 °C, the high-order Bragg peaks become broadened and slightly shift towards higher angle, which correspond to a slight period thickness contraction and inter-diffusion increase. The structure of MgCo_3 encountered significant degradation upon 350 °C annealing, as the high Bragg orders are not well-defined any more. Interface roughness values derived from GIXR curves were 0.4, 0.5 and 1.2nm for MgCo_1, MgCo_2 and MgCo_3, respectively. Following 400 °C annealing, the multilayer structure of MgCo_4 is completely destroyed since no Bragg peak is presented in corresponding curve. Consistent with GIXR measurements, the measured EUV reflectance in Fig. 1(b) shows slight reflectance decrease at 300 °C and then, notable decline at 350 °C, while no reflectance is obtained upon 400 °C annealing. Previous work has demonstrated that Mg/Co multilayer was stable up to 200 °C annealing [8]. However, at higher temperatures, its structure changed and optical performances degraded. Hence, interface engineering such as barrier introduction is required to improve the thermal property of Mg/Co.

#153768 - $15.00 USD Received 30 Aug 2011; revised 29 Sep 2011; accepted 6 Oct 2011; published 20 Oct 2011
(C) 2011 OSA

3.2 Mg/Co multilayer with B_4C barrier layers

Figure 2(a) presents the GIXR curves of $Mg/B_4C/Co/B_4C$ and Mg/Co both made of 10 periods. The thickness of B_4C layer is 0.9 nm. The period thickness of Mg/Co multilayer and $Mg/B_4C/Co/B_4C$ is 8.0 and 9.8 nm, respectively. The results suggest that the quality of $Mg/B_4C/Co/B_4C$ is worse than that of Mg/Co. To identify which interface, Co-B_4C or Mg-B_4C, was responsible for the poor performance of the $Mg/B_4C/Co/B_4C$, Mg/B_4C and Co/B_4C multilayers were prepared and characterized by GIXR measurements. Figure 2(b) shows the GIXR curve of a 120 bi-layered Co/B_4C multilayer with a period thickness of 3.6 nm. The well-defined and intense Bragg peaks indicate abrupt interfaces in Co/B_4C. According to the fit of the experimental curve, the thicknesses of Co and B_4C are estimated to be 1.8 and 1.7nm, respectively, while the interface widths (σ) is 0.6 nm for $\sigma_{B4C\text{-}on\text{-}Co}$ and $\sigma_{Co\text{-}on\text{-}B4C}$. As already reported in our previous work [8], Mg/B_4C multilayer had a peak reflectivity of only 0.2% at 30.4nm: it is a direct consequence of its poor structural quality resulting from significant inter-diffusion at the interfaces. Chemical reaction at Mg-B_4C interface, if any, is not clear in this work and will be investigated in a forthcoming study. Therefore, the stable B_4C ceramic, though effective in other multilayers as a diffusion barrier layer [13,14], is not suitable for Mg/Co, mainly due to the poor structural quality of Mg-B_4C interface.

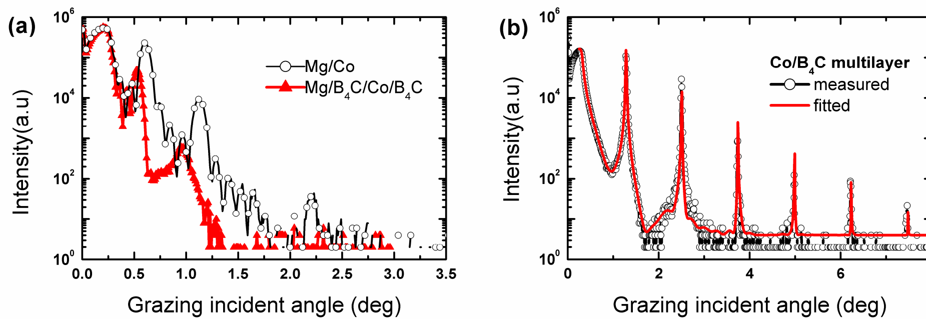

Fig. 2. (Color online) GIXR curves: (a) Mg/Co and $Mg/B_4C/Co/B_4C$ multilayers; (b) Co/B_4C multilayer for interface study.

3.3 Mg/Co multilayer with Mo barriers

Figure 3(a) shows the GIXR measurement of Mg/Mo/Co/Mo multilayer. Mg/Mo/Co/Mo_1, _2, _3 and _4 stand for the as-deposited sample and annealed at 300, 350 and 400 °C, respectively. Their periods are 17.2, 17.2, 17.8 and 17.8 nm, respectively. No significant structural changes are observed for Mg/Mo/Co/Mo_2 upon annealing at 300 °C. Following annealing at 350 °C, the Bragg peaks of Mg/Mo/Co/Mo_3 are broadened and their positions are significantly shifted towards smaller angle: this suggests increase of both inter-diffusion and period thickness. Upon 400 °C annealing, less Bragg peaks are now observed, indicating that the structure quality becomes worse. Thus, the introduction of Mo as barrier layer improves the thermal resistance of Mg/Co multilayer from 200 up to 300°C. According to the fit of the experimental reflectivity curve, the interface roughness is 0.7 nm for both MgMoCoMo_1 and _2. It was not possible to fit Mg/Mo/Co/Mo_3 and _4 reflectivity curve: given their poor interface quality, a multilayer model cannot be introduced for fitting purpose. Corresponding changes can be observed in the EUV reflectance measurements shown in Fig. 3(b). The EUV peak reflectance decreased while the peak position shifts towards longer wavelength upon 350 and 400 °C annealing. The peak reflectance of Mg/Mo/Co/Mo (34.6%) is lower than that of as-deposited Mg/Co (42.2%) for two reasons: the high absorption of Mo and the increased interface roughness. Moreover, the full width at half maximum (FWHM) of Mg/Mo/Co/Mo (5.5nm) is much larger than that of Mg/Co (0.4nm).

#153768 - $15.00 USD Received 30 Aug 2011; revised 29 Sep 2011; accepted 6 Oct 2011; published 20 Oct 2011
(C) 2011 OSA

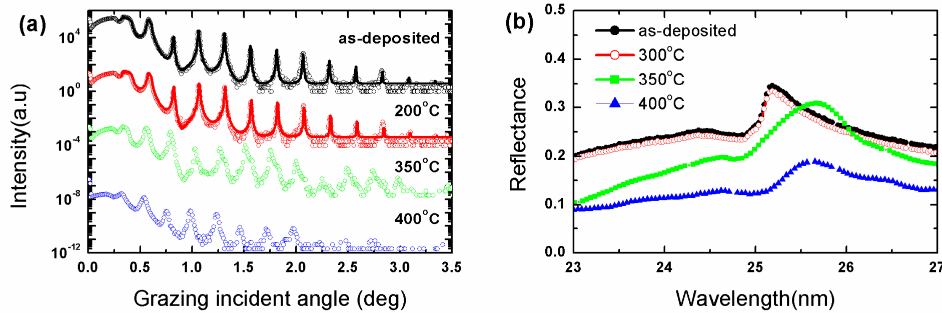

Fig. 3. (Color online) GIXR curves (a) and EUV reflectance (b) curves of Mg/Mo/Co/Mo multilayers: as-deposited, 300, 350 and 400 °C, respectively. In (a), each curve has been shifted vertically by 4 orders of magnitude for better discrimination; scatter and solid lines represent measured and fitted GIXR curves, respectively.

3.4 Mg/Co multilayer with Zr barrier layers

Figure 4 presents the experimental X-ray and EUV reflectivity curves of as-deposited and annealed Mg/Zr/Co/Zr multilayers. It can be seen that Mg/Zr/Co/Zr multilayer remains almost stable upon temperature increase. When annealing up to 400 °C, the EUV peak reflectance only decreases slightly, while no significant structural change can be deduced from the analysis of the GIXR curves. This slight change of reflectance can be attributed to the slight differences of samples. The interface roughness value extracted from the fit of the experimental curves of Fig. 4(a) is 0.5 nm for the four samples. In addition to its good thermal stability, Mg/Zr/Co/Zr is characterized by a high EUV reflectivity (44.5%) close to that of Mg/Co (42.6%). Thus, Zr is a suitable barrier layer for Mg/Co multilayer, since its introduction at both interfaces improves the thermal stability from 200 to 400 °C, without reducing EUV reflectance.

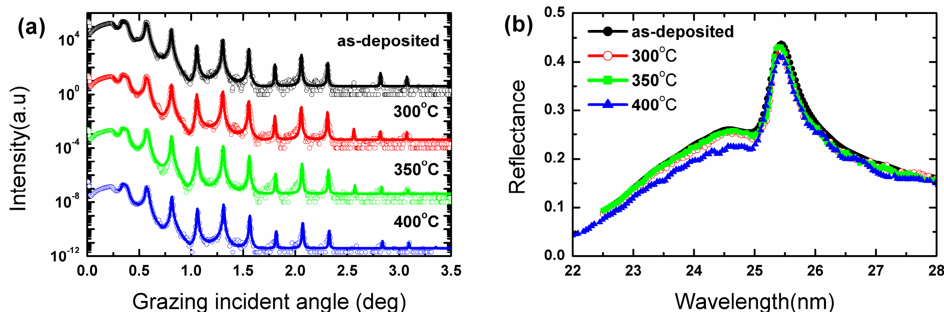

Fig. 4. (Color online) GIXR curves (a) and EUV reflectance (b) curves of Mg/Zr/Co/Zr multilayers: as-deposited, 300, 350 and 400 °C, respectively. In (a), each curve has been shifted vertically by 4 orders of magnitude for better discrimination; scatter and solid lines represent measured and fitted GIXR curves, respectively.

For comparison, Fig. 5 shows the evolution, as a function of the annealing temperature, of the normalized EUV reflectance decrease (NRD) measured for the Mg/Co, Mg/Mo/Co/Mo and Mg/Zr/Co/Zr multilayers. The value of NRD, defined as:

#153768 - $15.00 USD Received 30 Aug 2011; revised 29 Sep 2011; accepted 6 Oct 2011; published 20 Oct 2011
(C) 2011 OSA

$$NRD(T) = \frac{R(T)}{R_{as-deposited}} \quad (1)$$

is calculated using the experimental values extracted from Figs. 1(b), 3(b) and 4(b), respectively. As mentioned above, the Mg/Mo/Co/Mo is stable up to 300 °C but is not efficient anymore for higher temperatures. On the contrary, Mg/Zr/Co/Zr can resist heat treatment up to 400 °C. Thus, introducing Zr as diffusion barriers can successfully improve the thermal stability of Mg/Co multilayer.

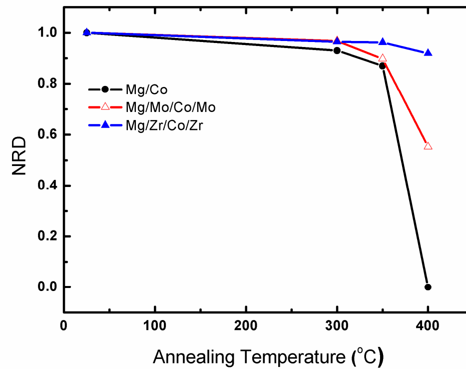

Fig. 5. (Color online) Evolution, as a function of the annealing temperature, of the normalized EUV reflectance decrease (NRD) of the Mg/Co, Mg/Mo/Co/Mo and Mg/Zr/Co/Zr multilayers.

4. Conclusion

According to our investigations, the optical performances of Mg/Co multilayer remain stable if the multilayer is not annealed higher than 200°C. In order to enhance this temperature limit, barrier layers made of B_4C, Mo and Zr are introduced into Mg/Co. From the analysis of the evolution, as a function of the annealing temperature, of the X-ray and EUV reflectivity curves, B_4C is not suitable for Mg/Co multilayer, since inter-diffusion may take place at Mg-B_4C interface. The introduction of Mo improves thermal stability up to 300 °C but is accompanied of a loss of EUV reflectivity. The introduction of Zr significantly improves the thermal stability of Mg/Co (up to 400°C) without degrading EUV reflectance. In conclusion, the introduction of Zr barrier layer constitutes an efficient method to upgrade the thermal stability of Mg/Co multilayer for EUV applications. This thermal resistance is mandatory for applications such as astronomical observation and synchrotron radiation where high thermal charges are encountered.

Acknowledgments

This work is supported by the National Natural Science Foundation of China (Grant No. 10825521, 11061130549 and 10905042), and by 973 program (Grant No. 2011CB922203) and by Agence Nationale de la Recherche (Grant No. 2010-INTB-902-01).

#153768 - $15.00 USD Received 30 Aug 2011; revised 29 Sep 2011; accepted 6 Oct 2011; published 20 Oct 2011
(C) 2011 OSA

SURFACE and INTERFACE ANALYSIS

Received: 12 October 2009 Revised: 9 March 2010 Accepted: 9 March 2010 Published online in Wiley Interscience: 22 April 2010

(www.interscience.wiley.com) DOI 10.1002/sia.3393

Nanometer-designed Al/SiC periodic multilayers: characterization by a multi-technique approach†

A. Galtayries,[a]* M.-H. Hu,[b] K. Le Guen,[b] J.-M. André,[b] P. Jonnard,[b] E. Meltchakov,[c] C. Hecquet[c] and F. Delmotte[c]

Nanometer-thick Al/SiC periodic multilayers, designed for the Extreme Ultra Violet (EUV) range, have been characterized by different techniques dedicated to such thin multilayers (each between 4 and 10 nm thick). In order to decrease the roughness and to improve the optical performances of the stacks, an ultrathin (2 nm) refractory metal layer has also been introduced, thus making Al/W/SiC and Al/Mo/SiC multilayer systems with three layers in period.

The samples are deposited by magnetron sputtering. The stacks have a period ranging between 16 and 18 nm. Time-of-Flight SIMS (ToF-SIMS) is used here to determine the depth profiles of the different elements present within the multilayers. It is observed that the interfaces of the Al/W/SiC and Al/Mo/SiC multilayers are sharper than those of the Al/SiC system. X-ray emission spectroscopy (XES) is used to identify the chemical state of the Al and Si atoms within the multilayers and to check if there is any interfacial compound. The results show that there is no interaction between the Al and SiC layers leading to the formation of an interfacial compound. The results are confirmed by X-ray reflectivity (XRR) measurements. They show that the Al/SiC multilayers present large interfacial roughnesses, but the Al/W/SiC and Al/Mo/SiC multilayers have the lower roughness values. **Copyright © 2010 John Wiley & Sons, Ltd.**

Keywords: multilayer; interface; Al; SiC; ToF-SIMS; X-ray emission; X-ray reflectivity

Introduction

Nanometer-designed Al (<10 nm)/SiC (∼4 nm) systems are promising for optical application in the 18–80 nm photon energy range. However, Al/SiC multilayers are hampered by large interfacial roughness that leads to much lower experimental reflectivity compared to that of an ideal multilayer. Large roughness has already been reported for the Mg/SiC system[1]. In order to improve the optical properties of the Al/SiC system, an ultrathin layer of refractory metal (about 2 nm thick), W or Mo, is added to the periodic structure. From optical simulations, the introduction of the ultrathin metal layer would increase the reflectivity of the system. The simulations also show that with three-component multilayers, the number of periods needed to achieve the maximum of reflectivity is smaller than that with two-component systems. Thus, the number of periods is reduced to limitate the cumulative increase of the roughness. The W/SiC and Mo/SiC systems are known for their low interfacial roughness, so a smoothing effect is expected for the multilayers with Al.

Once prepared, the challenge is to characterize such nanometer-thick periodic multilayers designed as optical components for the X-ray or Extreme Ultra Violet (EUV) ranges. Indeed, different phenomena such as diffusion, chemical reaction, and roughness development can occur at the interfaces. Thus, it is necessary to use complementary techniques to determine the thickness and roughness of all the layers as well as any possible interfacial compounds.

The study of Al/SiC periodic multilayers with and without additional W or Mo layers is reported, by combining different techniques:

- Time-of-Flight SIMS (ToF-SIMS) to determine the depth distribution of various elements present within the stacks,
- X-ray Emission Spectroscopy (XES) to elucidate the chemical state of the Si and Al atoms within the multilayers and to detect the presence of an interfacial compound,
- X-ray reflectivity (XRR) to evaluate the thickness and roughness of the various layers in the stacks.

Some periodic multilayers made of metallic or semi-conducting layers, or designed for optical applications, have already been studied by XES[2–7] and by dynamic SIMS as well as ToF-SIMS,[3,8–11] but none concerning the Al/SiC system, to the best of our knowledge.

* Correspondence to: A. Galtayries, Laboratoire de Physico-Chimie des Surfaces, École Nationale Supérieure de Chimie de Paris, CNRS UMR 7045, 11 rue Pierre et Marie Curie, F-75231 Paris Cedex 05, France.
E-mail: anouk-galtayries@chimie-paristech.fr

† Paper published as part of the ECASIA 2009 special issue.

a Laboratoire de Physico-Chimie des Surfaces, École Nationale Supérieure de Chimie de Paris, CNRS UMR 7045, 11 rue Pierre et Marie Curie, F-75231 Paris Cedex 05, France

b Laboratoire de Chimie Physique – Matière et Rayonnement, Université Pierre et Marie Curie, CNRS UMR 7614, 11 rue Pierre et Marie Curie, F-75231 Paris Cedex 05, France

c Laboratoire Charles Fabry de l'Institut d'Optique, CNRS, Université de Paris-Sud, Campus Polytechnique, RD128, F-91127 Palaiseau cedex, France

Copyright © 2010 John Wiley & Sons, Ltd.

Experimental Details

Multilayers

The samples are prepared using magnetron sputtering in an apparatus described elsewhere.[12] Samples are deposited at room temperature on Si polished wafers using Ar as the sputtering gas. The high-purity sputtering targets (99.95% or higher) are SiC, Mo and Al with 1.5 wt% Si. In that latter case, XRR measurements have demonstrated that the average roughness value of an Al thin film prepared with a small amount of silicon is about 1 nm, *i.e.* approximately two times smaller than that of a pure Al thin film. The sputtering process is run under an Ar pressure of 2 mTorr, in RF mode for Al and SiC targets and DC mode (0.06 A) for the Mo target. The applied power was 150 W for all targets.

The Al/Si multilayer consists of 40 bilayers, the top layer being SiC. Two other multilayers are prepared with an ultrathin W or Mo layer added at the SiC-on-Al interface (15 periods).

Techniques

The ToF-SIMS measurements are performed using the ToF SIMS.5 spectrometer (ION-TOF Gmbh). The working pressure in the chamber is ~3 10^{-7}Pa. The total primary ion flux is below 10^{12} ions.cm^{-2} to ensure static conditions. The depth profiles are measured using the instrument in dual beam mode. A 25 keV primary Bi^+ ion source (LMIG) at a DC current of 15 nA (high mass resolution mode), rastered over a scan area of 100 µm × 100 µm was used as the analysis beam. The sputtering was performed using a 1 keV Cs^+ ion beam at a current of 50 nA and rastered over an area of 500 µm × 500 µm. Both ion beams are impinging the sample surface under an angle of 45° and are centered so that the analyzed area corresponds to the middle of the sputtered crater.

The secondary ions following the Bi^+ sputtering come from the outermost surface (depth resolution of 1 nm). In this work, only positive SIMS spectra are presented, as the sputtering yields of the various species of each layer are sufficiently high to provide convenient data. In order to increase the intensity of the W^+ and Mo^+ profiles, the intensities of ^{182}W (26%), ^{184}W (31%) and ^{186}W (29%) as well as ^{95}Mo (16%), ^{96}Mo (17%) and ^{98}Mo (24%) isotopes, respectively, have been added. The profiles are displayed on a linear scale, with their maximum normalized to unity in order to show the relative contrast of the ion signals. The contrast is defined here as the difference between the maximum and minimum intensities with respect to the maximum intensity.

It was possible to analyze in depth the total 15 periods, down to the Si substrate, but only 3 periods are presented. The contaminated and chemically modified layer corresponding to the first 150–200 s of sputtering is purposely omitted here (it will be the subject in another paper). The depth resolution was examined as a function of the sputtering time. Within the experimental uncertainties, there is no systematic trend of a loss of intensity, whatever the element. This shows that in our experimental conditions, the sputtering does not induce significant roughness within the samples.

XES measurements are performed using a wavelength-dispersive spectrometer.[13] The Al K_β and Si K_β emission bands were measured, resulting from the Al and Si 3p-1s electron transitions, respectively. These emissions describe the occupied valence states having the Al 3p and Si 3p characters, respectively. Their shape is sensitive to the chemical state of the Al and Si-emitting atoms.[14–16] Following the ionization of the atoms present in the sample, characteristic X-rays are emitted, then dispersed by bent crystals: (10$\bar{1}$0) quartz for Al K_β emission and (111) InSb for Si K_β emission. The spectral resolution $\Delta E/E$ is a few thousands in the Al and Si K_β ranges. The radiation is detected in a gas-flux counter working in the Geiger regime. X-rays are produced upon electron excitation. The energy of the incident electrons has been chosen to be higher than the threshold of the studied emission, i.e. higher than the Al 1s and Si 1s binding energies, respectively. The current density of the electrons reaching the sample is set to less than 1 mA.cm^{-2} to avoid any change in the sample.

The emission spectra are normalized with respect to their maximum and after a linear background subtraction (Bremsstrahlung radiation). The spectra of the multilayers are compared to those of thin films of Al (Si 1.5 wt%) and amorphous SiC.

The multilayers are analyzed by X-ray specular reflectivity measurements at 0.154 nm, performed with a grazing-incidence reflectometer working in the $\theta-2\theta$ mode.[17] The angular resolution is 5/1000°. The detector is a gas-filled counter with the signal dynamics of seven orders of magnitude achieved by using calibrated absorption filters.

Results and Discussion

Figure 1 presents the depth profiles of the Al, Si, C, Mo and W positive ions obtained by ToF-SIMS for the three studied samples. Due to the low intensity of SiC^+, the SiC information is given by both Si^+ and C^+ ions. The C^+ profile closely follows the Si^+ line (Fig. 1(a)). Thus, in the following, only the Si^+ profiles are presented. For the Al/SiC multilayer (Fig 1(a)), the Al^+ profile is in opposite phase with respect to the Si^+ and C^+ profiles. For the Al/W/SiC multilayer (Fig. 1(b)), the maximum of each profile is well separated from the other, leading to a clear determination of the

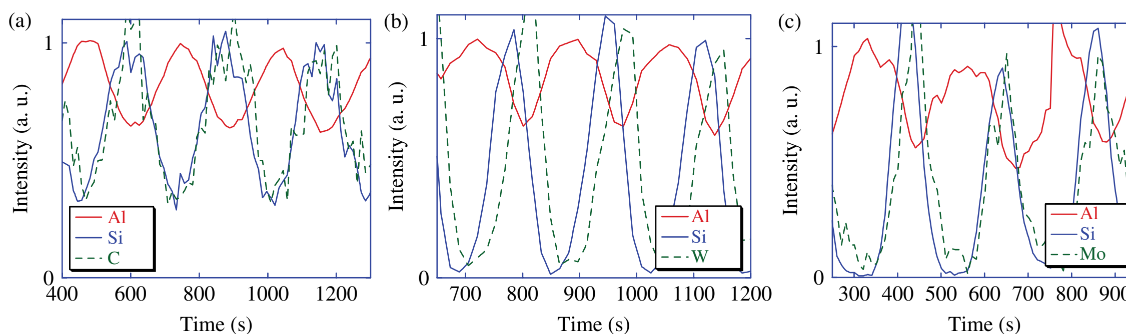

Figure 1. Depth profiles of the Al^+, Si^+, C^+, Mo^+ and W^+ ions in the Al/SiC (a), Al/W/SiC (b) and Al/Mo/SiC (c) multilayers.

Copyright © 2010 John Wiley & Sons, Ltd.

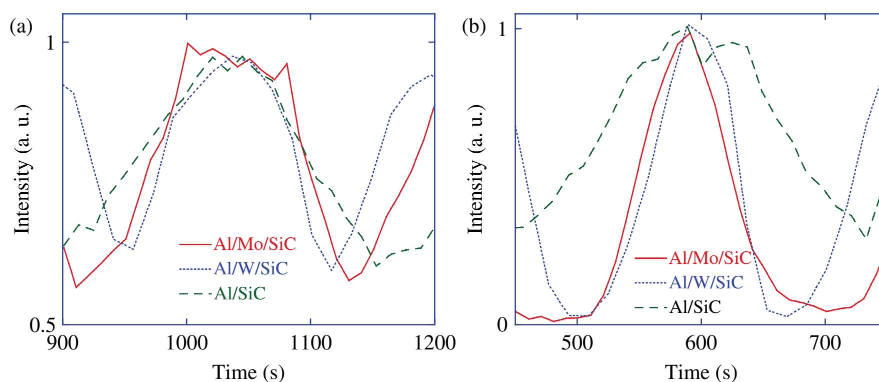

Figure 2. Depth profiles of the Al^+ (a) and Si^+ (b) ions for the Al/SiC, Al/W/SiC and Al/Mo/SiC multilayers.

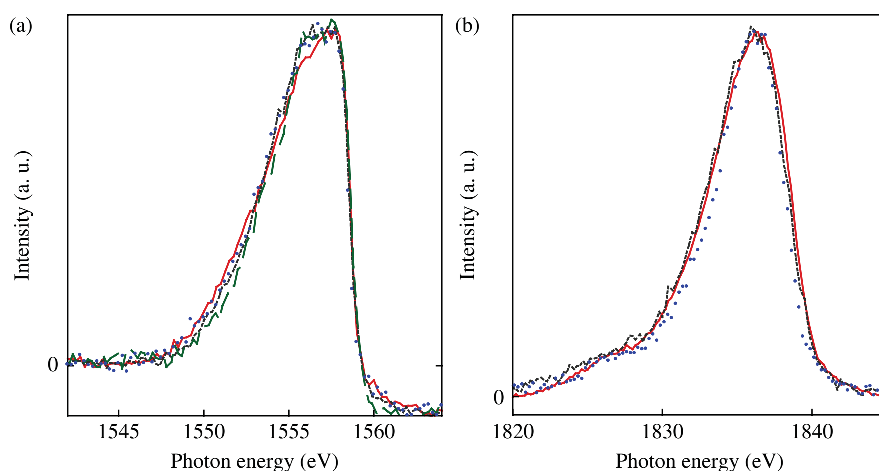

Figure 3. Al Kβ (a) and Si Kβ (b) emission bands of Al/SiC (dots), Al/W/SiC (dashed line) and Al/Mo/SiC (dotted line) compared to those of reference thin films (solid lines) of Al(Si 1.5 wt%) and amorphous SiC prepared by magnetron sputtering.

succession of the layers. It is noted that the maxima of the W^+ and Si^+ profiles coincide with the minimum of Al^+. The same trend is observed for the Al/Mo/SiC sample (Fig. 1(c)), except that the maxima of the Mo^+ and Si^+ profiles are closer than the ones of W^+ and Si^+.

The amplitude contrasts of the profiles have different behaviors. For Al^+, the contrast is almost the same for all samples. This can be attributed to the large thickness of the Al layers with respect to the roughness values. For Si^+ and C^+, respectively, the contrast increases when W or Mo is introduced in the multilayer. There is no significant difference of the Si contrast between the Al/W/SiC and Al/Mo/SiC multilayers.

Figure 2 presents the profile comparison of only one element, Al or Si, for all samples. The profiles have been shifted in time in order to align one of their maximum, and only one period is presented. The shapes of the Al and Si profiles of the Al/SiC stack are nearly symmetrical and present gentle positive and negative slopes. The shape of the Si profiles of Al/W/SiC and Al/Mo/SiC is also quite symmetrical, but the slopes are much steeper than those of Al/SiC. This leads to well-defined Al and SiC layers, showing that the interfaces are sharper in the presence of the refractory metal in the multilayer structure. This can be due to

- Geometrical or mechanical roughness, as a result of small random variations of the thickness of various layers,
- Chemical roughness, as a result of the diffusion of one element to the neighboring layers.

The second assumption can be ruled out in the case of a diffusion of SiC into Al. If such diffusion occurs, one should expect different chemical potentials for Si and C, inducing one of these two species to diffuse more, thus different Si^+ and C^+ profiles, whereas the Si and C profiles are observed strongly correlated.

Figure 3 presents the Al K_β and Si K_β emission bands of samples except the Si K_β band of the Al/W/SiC multilayer. The emission band of Al (Si 1.5 wt%) is identical to that of pure Al, i.e. the low Si concentration does not disturb the Al electronic structure.[14] The Al band presents a large peak, ∼10 eV wide, with a sharp discontinuity marking the Fermi level at 1559.3 eV. The background is lower for photon energies beyond the Fermi level because of the strong self-absorption of the emitted photons in this range. The Si band presents a large peak ∼10 eV wide, with a shoulder located ∼1828 eV. This shoulder is due to the hybridization between the Si p and C s valence states.

If an interfacial compound was formed within the multilayers, the resulting spectrum would correspond to a linear combination of the reference (due to the atoms that have not reacted) and the compound (due to the interfacial reaction) spectra. In addition, a strong variation in the shape of the emission band would be expected between two different compounds. This was the case with previous Mo/Si multilayers, where molybdenum silicide interfacial layers between 0.5 and 1.5 nm thick could be detected, depending on the preparation and treatment of the samples.[2–3,6–7] In spite of slight variations in the bandwidth, there

Copyright © 2010 John Wiley & Sons, Ltd.

is no significant difference here between the emission spectra of the multilayers and those of the reference thin films. This means that within the sample, Al atoms are in the same chemical state as Al atoms in Al (Si 1.5 wt%), and Si atoms are in the same chemical state as Si atoms in SiC, i.e. there is no interaction between the Al (Si 1.5 wt%) and SiC layers leading to the formation of an interfacial compound.

The Si K_β spectrum of the Al/W/SiC sample is not presented in Fig. 2(a), because in this photon energy range, the W M_β emission ($4f_{5/2}-3d_{3/2}$ transition) overlaps the Si K_β emission band. Thus, the chemical state of the Si atoms is examined through the Si $K_{\alpha 1,2}$ atomic line ($2p_{3/2,1/2}-1s$ electron transition). The shape of this atomic line is not sensitive to the chemical state of the emitting atoms unlike the position of its maximum.[18–19] Thus, two Lorentzian curves, separated by the spin-orbit splitting and with an intensity ratio of 2, fit the $K\alpha_{1,2}$ doublet.

The positions (energies) of the maximum intensity of the $K_{\alpha 1}$ component of the doublet are 1740.20 ± 0.05 eV for Al/W/SiC, 1740.00 ± 0.05 eV for crystalline Si, and 1740.23 ± 0.05 eV for a thin amorphous film of SiC and for Al/Mo/SiC. The maximum energy shifts toward higher photon energies with the electronegativity of the ligand. Hence, with respect to crystalline silicone, a shift of ∼0.40 eV is measured for Si_3N_4 and 0.55 eV for SiO_2.[20] The comparison of the position of the different maxima clearly shows that the Si atoms of the Al/W/SiC multilayer are in a SiC-like environment. The same result is obtained for the Al/Mo/SiC multilayer in agreement with the analysis of the Si K_β emission band shape.

The XRR curves obtained at 0.154 nm of the studied multilayers are presented in Fig. 4. With the Al/SiC multilayer, only 4 Bragg peaks are seen up to 1°, whereas up to 9 Bragg peaks are observed over the whole scanned angle range (2.6°) for the multilayers with W or Mo layers. It is also observed that the background decrease is steeper for Al/SiC with respect to Al/W/SiC or Al/Mo/SiC. The differences between Al/W/SiC and Al/Mo/SiC are less pronounced. In fact, only 7 Bragg peaks are observed with Al/Mo/SiC instead of 9 with Al/W/SiC, and the background decrease is slightly more pronounced in the case of Al/Mo/SiC.

The different shapes of the curves, with and without W or Mo interlayers, give evidence that the introduction of the refractory metals improves the structural quality of the multilayers. This is related to the interfacial roughness, and more particularly to the SiC-on-Al interfacial roughness. It is known that the interfacial roughness in Mg/SiC multilayers (≈2 nm) is quite large[1] with respect to that (less than 1 nm) of conventional multilayers for X-ray and EUV optics.

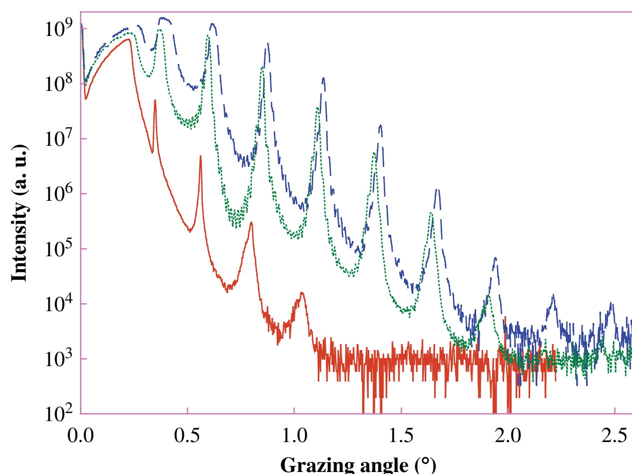

Figure 4. X-ray reflectivity curves measured at 0.154 nm of Al/SiC (solid line), Al/W/SiC (dashed line) and Al/Mo/SiC (dotted line) multilayers.

Table 1. Parameters of the studied multilayers. 'Roughness Al' refers to the SiC-on-Al interface for the Al/SiC multilayer and to the W(Mo)-on-Al interface for the Al/W/SiC and Al/Mo/SiC multilayers; 'Roughness SiC' refers to the Al-on-SiC interface; 'Roughness W/Mo' refers to the SiC-on-W(Mo) interface for the Al/W/SiC and Al/Mo/SiC multilayers.

Multilayer	Number of periods	Thickness Al (nm) Roughness Al (nm)	Thickness W/Mo (nm) Roughness W/Mo (nm)	Thickness SiC (nm) Roughness SiC (nm)
Al/SiC	40	13.4	–	4.0
		1.2		2.8
Al/W/SiC	15	10.6	1.9	3.6
		0.8	1.0	0.6
Al/Mo/SiC	15	11.5	1.3	3.6
		0.9	1.1	0.6

The XRR curves are fitted using IMD software[21] in order to determine the parameters of the stacks: thickness and roughness of the various layers.

A simple model of the stack is used for this purpose, i.e. without considering the possible formation of interfacial layers: succession of bilayers for the Al/SiC system and trilayers for Al/W/SiC and Al/Mo/SiC systems. Table 1 summarizes the thickness and roughness of each layer in the stacks. For the Al/SiC multilayers, the roughness at the Al-on-SiC interface is more than twice the one determined at the SiC-on-Al interface. When W or Mo layers are introduced, the interfacial roughnesses decrease, the major evolution being obtained at the Al-on-SiC interface. In this case, a decrease by a factor 4.7 occurs, leading to Al-on-SiC interface to be the smoothest one. When comparing the Al/W/SiC and Al/Mo/SiC systems, it is observed that all layers have similar roughnesses, however, the average roughness is slightly lower with W than with Mo. The fact that it is not necessary to take into account some interfacial layers to fit the reflectivity curves, and that the interfacial roughness decreases when introducing the refractory metal within the multilayer is in agreement with the ToF-SIMS and XES measurements.

Conclusion

Periodic nanometer-thick Al/SiC multilayers were studied by combining various complementary techniques, which provide valuable information on the depth elemental/layer distribution of the elements (ToF-SIMS) within the stacks, their chemical (XES) as well as their optical properties (XRR). The addition of ultrathin layers of refractory metal, W or Mo, at the SiC-on-Al interfaces considerably decreases the interfacial roughness and improves the structural quality of the multilayer stack (XRR). The formation of sharper interfaces is confirmed by the ToF-SIMS experiments. XES does not show any chemical reaction between the Al and SiC layers, and thus confirms that here, the roughness is a purely geometrical parameter and not a chemical one.

Copyright © 2010 John Wiley & Sons, Ltd.

Acknowledgments

This work was partly funded by the ANR Project 07-BLAN-0150. All multilayer depositions have been carried out on the deposition machine at CEMOX (Centrale d'Elaboration et de Métrologie des Optiques X).

References

[1] H. Maury, P. Jonnard, K. Le Guen, J.-M. André, Z. Wang, J. Zhu, J. Dong, Z. Zhang, F. Bridou, F. Delmotte, C. Hecquet, N. Mahne, A. Giglia, S. Nannaronne, *Eur. Phys. J.* **2008**, *B64*, 193.
[2] Y. Muramatsu, H. Takenaka, Y. Ueno, E. M. Gullikson, R. C. C. Perera, *Appl. Phys. Lett.* **2000**, *77*, 2653.
[3] H. Maury, P. Jonnard, J.-M. André, J. Gautier, M. Roulliay, F. Bridou, F. Delmotte, M.-F. Ravet, A. Jérome, P. Holliger, *Thin Solid Films* **2006**, *514*, 278.
[4] H. Maury, P. Jonnard, J.-M. André, J. Gautier, F. Bridou, F. Delmotte, M.-F. Ravet, *Surf. Sci.* **2007**, *601*, 2315.
[5] A. S. Shulakhov, S. V. Bukin, E. V. Zdanchuk, S. Y. Tveryanovich, *Bull. Russ. Acad. Sci. Phys.* **2008**, *72*, 434.
[6] H. Maury, J.-M. André, K. Le Guen, N. Mahne, A. Giglia, S. Nannarone, F. Bridou, F. Delmotte, P. Jonnard, *Surf. Sci.* **2009**, *603*, 407.
[7] P. Jonnard, K. Le Guen, M.-H. Hu, J.-M. André, E. Meltchakov, C. Hecquet, P. Delmotte, A. Galtayries, *Proc. SPIE 7360 O1–9*, **2009**.
[8] H. Maury, P. Holliger, B. Farès, J. Gautier, M. Roulliay, F. Bridou, F. Delmotte, M.-F. Ravet, J.-M. André, P. Jonnard, *Surf. Interf. Anal.* **2006**, *38*, 781.
[9] M. Cwil, P. Konarski, J. Ciosek, *Int. J. Mass Spectrom.*, **2007**, *263*, 54.
[10] K. J. Kim, D. Simons, G. Gillen, *Appl. Surf. Sci.* **2007**, *253*, 6000.
[11] P. Chakraborty, *Nucl. Instrum. Meth. Phys. Res.* **2008**, *B 266*, 1858.
[12] J. Gautier, F. Delmotte, M. Roulliay, F. Bridou, M.-F. Ravet, A. Jérome, *Appl. Opt.* **2005**, *44*, 384.
[13] C. Bonnelle, F. Vergand, P. Jonnard, J.-M. André, P. Avila, P. Chargelègue, M.-F. Fontaine, D. Laporte, P. Paquier, A. Ringuenet, B. Rodriguez, *Rev. Sci. Instrum.* **1994**, *65*, 3466.
[14] P. Jonnard, K. Le Guen, R. Gauvin, J.-F. Le Berre, *Microscopy and Microanalysis* **2009**, *15*, 36.
[15] F. Vergand, P. Jonnard, C. Bonnelle, *Europhysics Letters* **1989**, *10*, 67.
[16] I. Jarrige, P. Jonnard, N. Frantz-Rodriguez, K. Danaie, A. Bosseboeuf, *Surf. Interf. Anal.* **2002**, *34*, 694.
[17] L. Névot, B. Pardo, J. Corno, *Rev. Phys. Appl.* **1988**, *23*, 1675.
[18] D. E. Day, *Nature 200*, **1963**, 649.
[19] P. Jonnard, J. P. Morreeuw, H. Bercegol, *Eur. Phys. J. Appl. Phys.* **2003**, *21*, 147.
[20] J. Hasegawa, T. Tada, Y. Oguri, M. Hayashi, T. Toriyama, T. Kawabata, K. Masai, *Rev. Sci. Instrum.* **2007**, *78*, 073105.
[21] F. Bridou, B. Pardo, *J. Opt.* **1990**, *21*, 183.

Copyright © 2010 John Wiley & Sons, Ltd.

Received: 15 June 2010 Accepted: 1 May 2011 Published online in Wiley Online Library: 26 July 2011

(wileyonlinelibrary.com) DOI 10.1002/xrs.1350

Characterization of EUV periodic multilayers

K. Le Guen,[a*] M.-H. Hu,[a] J.-M. André,[a] P. Jonnard,[a] Z. Wang,[b] J. Zhu,[b] A. Galtayries,[c] C. Meny,[d] E. Meltchakov,[e] C. Hecquet[e] and F. Delmotte[e]

Nanometric Co/Mg, Co/Mg/B_4C, Al/SiC and Al/Mo/SiC periodic multilayers deposited by magnetron sputtering are studied in order to correlate their optical performances in the extreme ultraviolet (EUV) range to their structural quality. To that purpose, our recently developed methodology based on high-resolution X-ray emission spectroscopy (XES) and X-ray and EUV reflectometry is now extended to nuclear magnetic resonance (NMR) spectroscopy and time-of-flight secondary ions mass spectrometry (ToF-SIMS). The analysis of the Co L$\alpha\beta$ and Mg Kβ emission spectra shows that the Co and Mg atoms within the multilayers are in a chemical state equivalent to that of the atoms in the pure Co and Mg references, respectively. But NMR spectra give evidence for a reaction between Co atoms and B and/or C atoms from B_4C. The Al and Si Kβ emission spectra do not reveal the formation of an interfacial compound in Al/SiC and Al/Mo/SiC. Only the roughness limits the optical quality of Al/SiC. The comparative analysis of the ToF-SIMS spectra of Al/SiC and Al/Mo/SiC indicates that the structural quality is enhanced when Mo is introduced within the stack. **Copyright © 2011 John Wiley & Sons, Ltd.**

Introduction

Nanometric periodic multilayers are used as optical components in the X-rays and extreme UV (EUV) spectral ranges for applications such as spatial telescopes, X-rays microscopes, EUV photolithography or synchrotron beamlines. Their optical performances highly depend on the quality of the interfaces between the different layers within the stack. Both interdiffusion and geometrical roughness modify the optical properties at the application wavelength and therefore can lower the reflectance.

The aim of the present paper is to propose a way to disentangle interdiffusion and geometrical roughness in order to correlate the multilayer optical performances to its structural quality. To that purpose, we have recently developed a methodology coupling high-resolution X-ray emission spectroscopy (XES) and X-ray and EUV reflectometry.[1–4] Nevertheless, in the case of the Co/Mg, Co/Mg/B_4C, Al/SiC and Al/Mo/SiC multilayers, the sensitivity limit of this methodology appears to be reached, which does not allow us to firmly conclude. Complementary investigations are thus required. We have explored alternative experimental techniques, namely nuclear magnetic resonance (NMR) spectroscopy and time-of-flight secondary ions mass spectrometry (ToF-SIMS), to refine the stack structural description initiated by the XES and reflectivity measurements.

Experiment

Multilayer deposition

All the periodic multilayers were prepared using magnetron sputtering working with Ar gas. The samples were deposited onto ultra-smooth polished Si substrates with rms surface roughness of 0.3 nm. The Co/Mg and Co/Mg/B_4C multilayers were deposited at the IPOE in Shanghai with targets of Co (purity 99.95%), Mg (purity 99.98%) and B_4C (purity 99.5%) in Ar gas (99.999%). The power applied on the Co, Mg and B_4C targets was 25, 15 and 80 W, respectively. The Al/SiC and Al/Mo/SiC multilayers were prepared at the Institut d'Optique in Palaiseau. The sputtering targets (99.95% or higher purity) are Mo, SiC and Al with 1.5 wt% Si. The Al and SiC targets were operated in rf-mode with applied power of 150 W and the Mo target was utilized in dc-mode (0.05 A). The name assignment and description of all the samples are given below:

1. Co/Mg: Si substrate/[Co (2.55 nm)/Mg (14.45 nm)]$_{30}$/B_4C (3.50 nm)
2. Co/Mg/B_4C: Si substrate/[Co (2.55 nm)/Mg (14.45 nm)/B_4C (0.90 nm)]$_{30}$/B_4C (2.60 nm)
3. Al/SiC: Si substrate/[Al (13.4 nm)/SiC (4.0 nm)]$_{40}$
4. Al/Mo/SiC: Si substrate/[Al (11.2 nm)/Mo (1.7 nm)/SiC (3.5 nm)]$_{15}$

The role of the B_4C (SiC) top layer in the Co/Mg and Co/Mg/B_4C (Al/SiC and Al/Mo/SiC) multilayers is to prevent, or at least minimize, the oxidation process. The choice of the Al target doped with 1.5 wt% Si was done with the purpose to decrease the roughness of the Al layers.[5] The effective layer thicknesses of the deposited multilayers are controlled through X-ray reflectometry (XRR) using the Cu Kα emission (0.154 nm or 8048 eV) and performed with a grazing-incidence reflectometer working in the $\theta-2\theta$ mode. The fit of these reflectivity curves allows the estimation of the stack structural parameters (thickness, roughness

* Correspondence to: K. Le Guen, Laboratoire de Chimie Physique - Matière et Rayonnement, UPMC CNRS UMR 7614, Paris, France.
E-mail: karine.le_guen@upmc.fr

a Laboratoire de Chimie Physique - Matière et Rayonnement, UPMC CNRS UMR 7614, Paris, France

b Institute of Precision Optical Engineering, Department of Physics, Tongji University, Shanghai, PR China

c Laboratoire de Physico-Chimie des Surfaces, Ecole Nationale Supérieure de Chimie de Paris (Chimie Paris Tech), CNRS UMR 7045, Paris, France

d Institut de Physique et Chimie des Matériaux, CNRS UMR 7504, Strasbourg, France

e Laboratoire Charles Fabry de l'Institut d'Optique, CNRS, Univ Paris-Sud, Palaiseau, France

 Copyright © 2011 John Wiley & Sons, Ltd.

and density of each layer). The rms roughness values are collected in Table 1.

In Co/Mg, the two interfaces appear to be symmetrical. The fit results of the Co/Mg/B_4C X-ray curve are not presented in Table 1 since only five intense and well-defined Bragg peaks are measured. It is striking that the introduction of Mo as a third material into the Al/SiC multilayer basic design has resulted in decreasing roughness at all interfaces (by a factor 4.7 at the Al-on-SiC interface and by a factor 1.3 at the SiC-on-Mo interface) although Mo is introduced only at the SiC-on-Al interface.

EUV reflectivity

The EUV reflectivity curves are measured on the BEAR beamline[6] at the Elettra synchrotron source using s-polarized light. The photon energy is carefully calibrated using the Pt $4f_{7/2}$ feature and the Si L edge. The goniometer angular resolution is 1/100°. The intensities of incident and reflected light are measured with a solid state photodiode. The incoming photon flux is also monitored by measuring the drain current of an Au mesh inserted in the beam path. The overall accuracy of the absolute reflectivity values is estimated to be about 1%.

X-ray emission spectroscopy

XES is performed using a high-resolution wavelength dispersive soft X-ray spectrometer.[7] The measured emissions are:

1. the Co $L\alpha\beta$ ($3d-2p_{3/2}$ and $3d-2p_{1/2}$ transitions) and Mg $K\beta$ (Mg 3p–1s transition) emissions originating respectively from the cobalt and magnesium atoms present in the Co/Mg and Co/Mg/B_4C;
2. the Si $K\beta$ (Si 3p–1s transition) and Al $K\beta$ (Al 3p–1s transition) emissions originating respectively from the silicon and aluminum atoms present in the Al/SiC and Al/Mo/SiC.

The Co $L\alpha\beta$, Mg $K\beta$, Si $K\beta$ and Al $K\beta$ emission spectra, respectively, correspond to the distribution of the occupied valence states of the Co, Mg, Si and Al atoms present within the stack. As valence electrons are the most weakly bound, the emission band is very sensitive to the physico-chemical environment of the emitting atoms.

The core holes are created by an electron beam coming from a Pierce gun. The energy of the incident electrons is set to 7.5 and 3.5 keV for the Mg $K\beta$ and the Co $L\alpha\beta$ emissions respectively, and 7 keV for the Si and Al $K\beta$ emissions respectively. Following the ionization of the atoms present in the sample, characteristic X-rays are emitted,[8,9] then dispersed by a (0 0 1) TlAP (Co $L\alpha\beta$ emission), $(1 0 \bar{1} 0)$ beryl (Mg $K\beta$ emission), (1 1 1) InSb (Si $K\beta$ emission) or $(1 0 \bar{1} 0)$ quartz (Al $K\beta$ emission) bent crystal and detected in a gas-flux counter working in the Geiger regime. The current density of the electrons reaching the sample is set to less than 1 mA cm^{-2} to ensure that the shape and intensity of the studied emission band remain constant throughout the measurements.

Each emission spectrum is normalized with respect to its maximum and a linear background corresponding to the Bremsstrahlung contribution is subtracted. To determine the composition of the multilayer (especially to identify possible interfacial compounds), its emission spectrum is compared to that of reference compounds. This methodology is now routinely used to study complex materials, particularly various thin films and nanometric multilayers.[10–17]

Nuclear magnetic resonance spectroscopy

The Co/Mg and Co/Mg/B_4C multilayers are analyzed by zero field NMR spectroscopy at 4.2 K using a homemade automated broadband spectrometer. The NMR spectra represent the distribution of the Co atoms as a function of their resonance frequency, that is to say the hyperfine field experienced by the Co nuclei.[18,19] The NMR resonance frequency is sensitive to the local environment of the probed (magnetic) atoms: nearest neighbor local structure and/or local chemical environment. Bulk references consisting in 1% B and 1% Mg into Co are measured to check the influence of the B and Mg neighborhood on the Co resonance frequency (hyperfine field), giving rise to NMR lines at 117 and 170 MHz, respectively. For each spectrum, the total surface area of the sample is normalized to unity.

Time-of-flight secondary ion mass spectrometry

The depth distribution of the Al/SiC and Al/Mo/SiC multilayers is measured using ToF-SIMS with the instrument working in the dual beam mode. The sputtering is performed using a 1 keV Cs^+ ion beam (current equal to 50 nA) scanning a 250 × 250 µm area. The analysis beam consists in a 25 keV primary Bi^+ ion source (current equal to 14 nA) scanning a 100 × 100 µm area. Both ion beams are aligned in such a way that the analyzed ions originate from the center of the sputtered crater. Both positive and negative ions are recorded. We have to keep in mind that the sputtering yields are not well known and can vary drastically: (1) from one element to another and (2) for a given element, from a chemical environment to another (e.g. from the center of a layer to the interface with the neighboring layer). Consequently, (1) the sputtering time scale cannot be easily converted into a thickness scale and (2) the intensity of the profile cannot be related to the number of atoms.

Table 1. Values of the rms roughness extracted from the fit of the XRR curves

σ (nm)	Mg-on-Co	B_4C-on-Mg	Co-on-B_4C	Co-on-Mg
Co/Mg	0.4	–	–	0.4
Co/Mg/B_4C	–	–	–	–
	SiC-on-Al	Mo-on-Al	SiC-on-Mo	Al-on-SiC
Al/SiC	1.2	–	–	2.8
Al/Mo/SiC	–	1.1	0.9	0.6

Results and Discussion

EUV reflectometry

The comparison between measured and simulated EUV peak reflectivity values is presented in Table 2 for the four multilayers. IMD reflectivity simulations[20] are performed assuming an 'ideal' multilayer (neither roughness nor chemical reaction at the interfaces) and using s-polarized light incoming at 45° for Co/Mg and Co/Mg/B_4C and 10° from normal incidence for the Al/SiC and Al/Mo/SiC.

The discrepancy between the measured and simulated values can be ascribed to the interfacial roughness and/or the formation of interfacial compounds. To disentangle these two possible origins, in the next section, we present the analysis of the XES spectra. If no chemical reaction at the multilayer interfaces can be evidenced, only the interfacial roughness is responsible for the reflectivity loss.

Copyright © 2011 John Wiley & Sons, Ltd.

Table 2. Comparison of measured and simulated peak reflectivity values

Multilayer	Grazing incidence (°)	R_{exp}	R_{ideal}
Co/Mg	45	42.6% @ 25.1 nm	56.5% @ 25.2 nm
Co/Mg/B_4C	45	0.7% @ 25.1 nm	53.5% @ 25.8 nm
Al/SiC	80	7.4% @ 31.6 nm	34.2% @ 31.8 nm
Al/Mo/SiC	80	28.5% @ 30.2 nm	42.4% @ 30.2 nm

In IMD simulations, an 'ideal' multilayer (neither roughness nor chemical reaction at the interfaces) is considered.

XES: Co/Mg, Co/Mg/B_4C, Al/SiC and Al/Mo/SiC multilayers

Figure 1(a) and (b) presents the Co L$\alpha\beta$ and Mg Kβ emission bands of the Co/Mg and Co/Mg/B_4C multilayers, while Fig. 1(c) and (d) shows the Si and Al Kβ emission bands of the Al/SiC and Al/Mo/SiC multilayers, respectively. In all the cases, the multilayer emission band is compared to that of a reference sample: a Co thin film for the Co L$\alpha\beta$ emission, the Mg metal for the Mg Kβ emission, an amorphous SiC thin film for the Si Kβ emission and an Al (1.5 wt% Si) thin film for the Al Kβ emission.

The Co L$\alpha\beta$ and Mg Kβ emission bands of the Co/Mg and Co/Mg/B_4C multilayers are discussed into details in Ref. [21] and that of the Si and Al Kβ emission bands in Ref. [22]. In summary, in Fig. 1(a), the Co L$\alpha\beta$ emission bands of the Co/Mg and Co/Mg/B_4C multilayers are close to that of the Co reference. For the Mg Kβ emission, Fig. 1(b), the multilayers spectra are similar to that of the Mg metal. In Fig. 1(c), the Si Kβ emission band of the Al/SiC and Al/Mo/SiC multilayers closely resembles that of the SiC reference while the Al Kβ emission band of the Al (1.5 wt% Si) reference in Fig. 1(d) is quite identical to that of the Al/SiC and Al/Mo/SiC multilayers.

In our recent study of Al–Mg alloys,[23] the presence of at least 10 wt% of Al (Mg) into Mg (Al) is enough to significantly change the shape of the Mg Kβ (Al Kβ) emission band and to allow the identification of an intermetallic compound (Al_3 Mg_2 or Al_{12} Mg_{17}) formed within the alloy. Moreover, in our studies of the Mo/Si multilayers[2,3] and of the annealing of the Mg/SiC multilayers,[24] the analysis of the shape of the Si Kβ emission band allowed us to evidence the formation of an interfacial compound which thickness is equal or lower than 1 nm. Thus, for the Mg, Al and Si Kβ emissions, the sensitivity of the technique toward the p valence states is high.

These results enable us draw the following conclusions: (1) in Co/Mg and Co/Mg/B_4C, the Mg atoms are in a physico-chemical state close to that of the Mg atoms in pure Mg metal and (2) in Al/SiC and Al/Mo/SiC the Si and Al atoms are in a physico-chemical state close to that of the Si and Al atoms in the SiC and Al with 1.5 wt% of Si references, respectively. Thus, the interdiffusion can be unambiguously excluded in Al/SiC and Al/Mo/SiC while in Co/Mg and Co/Mg/B_4C, we can only assert that the Mg atoms have not reacted. Indeed, the sensitivity of our XES analysis toward the Co 3d states appears to be limited and prevents us from stating any firm conclusion concerning a possible reaction of the Co atoms. This limitation certainly originates from the localization of the d state wavefunction in the vicinity of the nucleus. Complementary

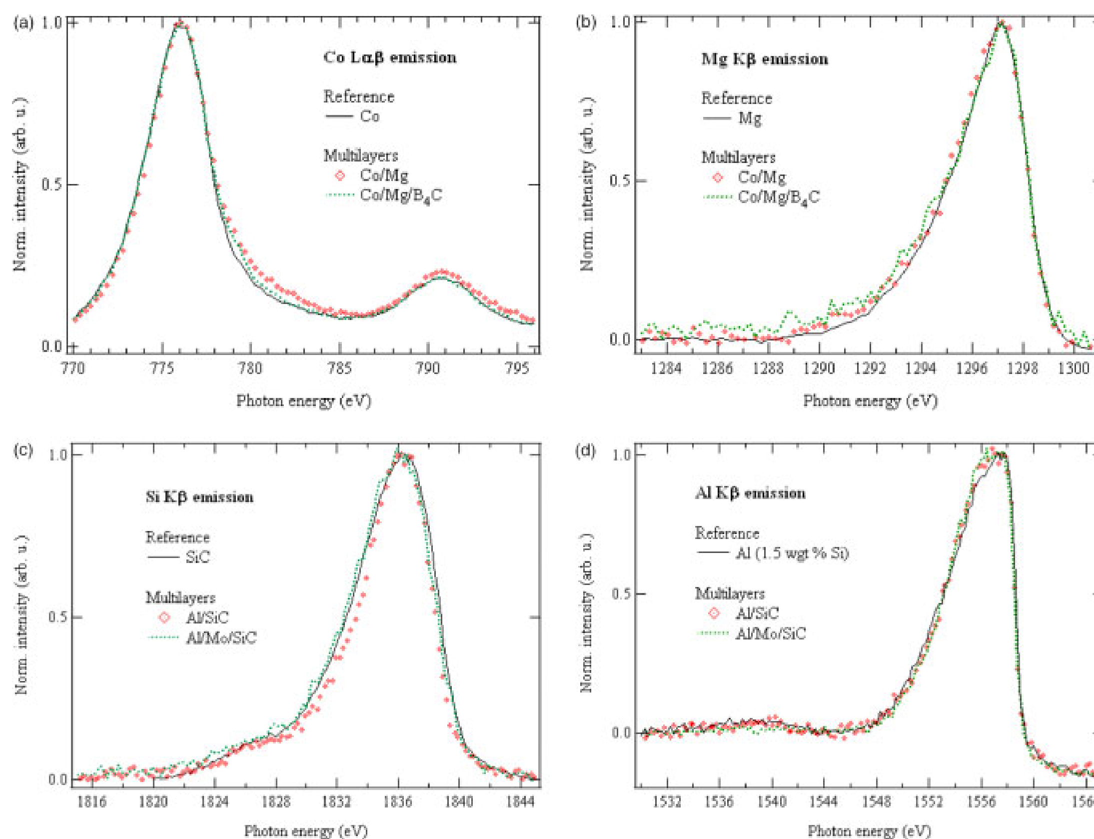

Figure 1. Emission bands originating from multilayers and reference compounds: (a) Co L$\alpha\beta$ emission, (b) Mg Kβ emission, (c) Si Kβ emission and (d) Al Kβ emission.

Copyright © 2011 John Wiley & Sons, Ltd.

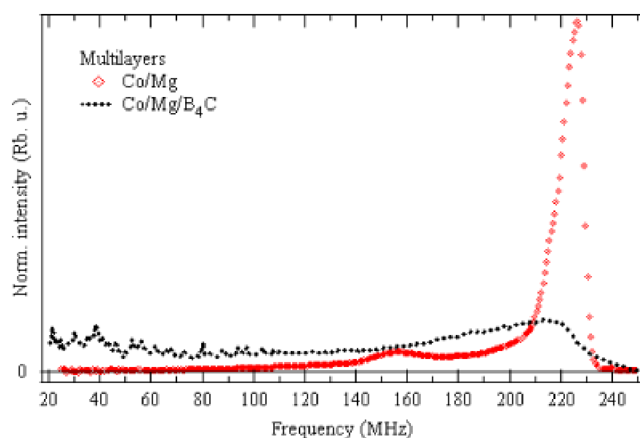

Figure 2. Co/Mg and $Co/Mg/B_4C$ NMR spectra.

experimental techniques are required to rule on the physico-chemical state of the Co atoms and also to understand the higher reflectance of Al/Mo/SiC with respect to Al/SiC.

Co/Mg and $Co/Mg/B_4C$ multilayers: NMR spectroscopy

NMR spectra of the Co/Mg and $Co/Mg/B_4C$ multilayers are presented in Fig. 2. The Co/Mg sample exhibits a well-defined line at 226 MHz which is the signature of the bulk hcp Co. Therefore, the Co atoms are mainly situated in pure Co layers and the intermixing at the interfaces remains limited. The additional line observed at 156 MHz cannot be related to the 1% Mg into Co reference sample (170 MHz) which most probably corresponds to Co in a Co_2 Mg phase. Therefore the 156 MHz NMR line is likely to arise from Co situated at well-defined Co/Mg interfaces. In the $Co/Mg/B_4C$ spectrum, no Co bulk line is observed anymore. The Co layers are not pure and alien atoms (Mg, B or C) are mixed with Co atoms. As, from the XES analysis, no compound is formed at the Co/Mg interface, the mixing in $Co/Mg/B_4C$ multilayers originates from the Co/B_4C interface. This intermixing is strong: the absolute integral intensity of the $Co/Mg/B_4C$ spectra is three times smaller than the intensity of the Co/Mg spectra, meaning that two-thirds of the total Co atoms included in the sample are not observed in the $Co/Mg/B_4C$ NMR spectra.

These Co atoms are most probably into a nonferromagnetic phase with a large content of B and/or C atoms and therefore do not contribute to the NMR signal. The difference between the experimental and simulated reflectivity values in Co/Mg can be ascribed only to the interfacial roughness because no compound formation is evidenced. In contrast, in $Co/Mg/B_4C$, it is observed that the Co atoms react with the B or C atoms of the carbide layers to form an interfacial compound, while the Mg atoms remain undisturbed. Therefore, the low reflectance originates from both interdiffusion and roughness. Fitting the corresponding X-ray curve, it turns out that a three-layer model fails to describe this stack. Concerning the Co $L\alpha\beta$ emission band of $Co/Mg/B_4C$ (Section 'XES: Co/Mg, $Co/Mg/B_4C$, Al/SiC and Al/Mo/SiC Multilayers'), the sensitivity limit of the XES technique to the Co 3d states did not allow us to evidence this intermixing.

Al/SiC and Al/Mo/SiC multilayers: ToF-SIMS measurements

The depth distribution of the Si^- and Al^- ions originating from the Al/Mo/SiC multilayer, analyzed down to the substrate, is shown on a logarithmic scale in Fig. 3(a). The italic numbers from 1 to 15 refer to the trilayer order counted from the surface. For sake of clarity, we do not show the C^- profile since it is observed that it closely follows that of SiC^-. The 15 periods of the stack are clearly identified from the signal periodic oscillations.

In Fig. 3(b), we present on a linear scale the SiC^-, Al^- and Mo^- ion depth profiles from the second, third and fourth periods of Al/Mo/SiC. The asymmetrical shape of the profile (particularly in the case of Al^- and Mo^-) cannot be related to a gradient of the atom number within the layer. In fact, as the layer thickness is small, a steady sputtering regime has not enough time to be established before the end of the layer erosion. In addition, as mentioned above, large variations of the sputtering yield occur at interfaces leading, for example, to the sharp maximum of the Al^- profile. Thus, in a given profile, if we consider that the center of a layer corresponds approximately to the end of the plateau just before the intensity maximum, the right order of the layers is found, that is, from the substrate: Al, Mo, and then SiC.[25]

The comparison of the Si^+ ion depth distribution in the Al/SiC and Al/Mo/SiC multilayers is presented in Fig. 4.

Both positive and negative slopes of the profile in Al/Mo/SiC are much steeper than those in Al/SiC. The same effect is reported for Al^+ (not shown).[22] The steeper is the slope, the more abrupt is the interface. This gives evidence for better defined Al and SiC layers and more abrupt interfaces when Mo is introduced as a third material within the multilayer structure, in good agreement with the XRR measurements.

Conclusions

We have performed X-ray emission and reflectivity measurements to access the structural description of the Co/Mg, $Co/Mg/B_4C$, Al/SiC and Al/Mo/SiC multilayers. As the sensitivity of the XES analysis restricts us to draw firm conclusions, we have resorted to complementary characterization techniques, namely NMR spectroscopy and ToF-SIMS.

Concerning the Co/Mg and $Co/Mg/B_4C$ systems, a reflectivity value of 42.6 and 0.7% respectively is measured at 45° of incidence at 25.1 nm. The analysis of the Co $L\alpha\beta$ and Mg $K\beta$ emission spectra shows that the Co and Mg atoms within the multilayers are in a chemical state equivalent to that of the atoms in the pure Co and Mg references respectively. However, the NMR spectra give evidence of a reaction between Co atoms and B and/or C atoms from B_4C. In Co/Mg, the interfaces do not present any interdiffusion and only the roughness is responsible for the difference between the measured and simulated reflectance values. In $Co/Mg/B_4C$, the low reflectance originates from both interdiffusion and roughness.

In the case of the Al/SiC system, the introduction of a third layer material (Mo) reduces the roughness at all interfaces, leading to a reflectivity value equal to 28.5% at quasi-normal incidence at 30.2 nm. The Al and Si $K\beta$ emission spectra do not reveal the formation of an interfacial compound in Al/SiC and Al/Mo/SiC. Thus we suppose that the geometrical roughness mainly limits the optical quality of Al/SiC. The comparative analysis of the ToF-SIMS spectra of Al/SiC and Al/Mo/SiC indicates that the structural quality is enhanced when Mo is introduced within the stack.

Acknowledgements

S. Nannarone, A. Giglia and N. Mahne from the BEAR beamline at the ELETTRA synchrotron are thanked for their help during

Copyright © 2011 John Wiley & Sons, Ltd.

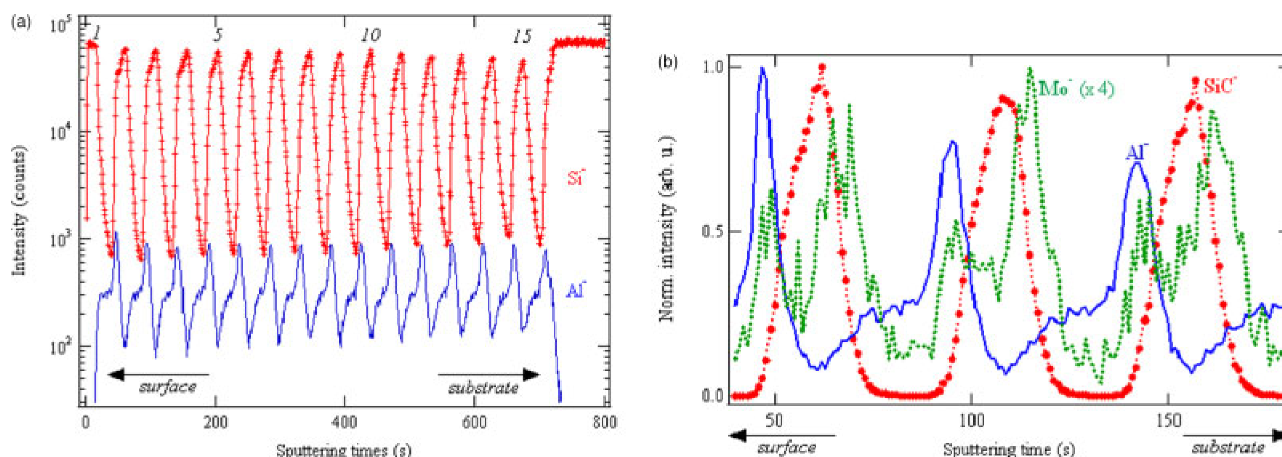

Figure 3. (a) Al^- and Si^- ion depth distribution of the Al/Mo/SiC multilayer; (b) SiC^-, Al^- and Mo^- ion depth distributions of the 2nd, 3rd and 4th periods of Al/Mo/SiC. For the sake of comparison, the Mo^- profile intensity has been multiplied by a factor 4.

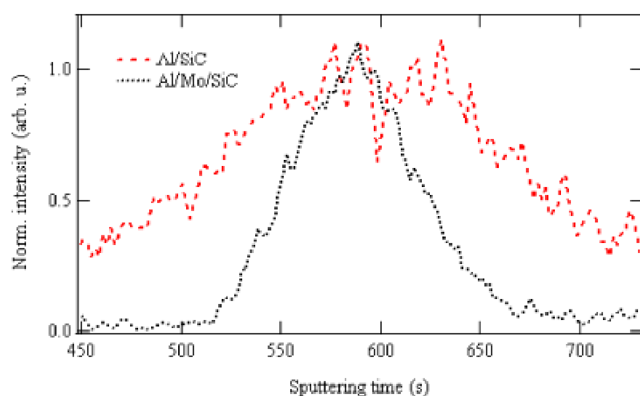

Figure 4. Comparison of the Si^+ ion depth distribution in the Al/SiC and Al/Mo/SiC multilayers. The profiles have been shifted in time in order to align their respective maximum and only one period is presented.

the measurements of EUV reflectivity. The authors from Tongji University are indebted to the National Natural Science Foundation of China (Grant No. 10825521). The work dealing with Al/SiC and Al/Mo/SiC was funded by the ANR project 07-BLAN-0150. The deposition of Al/SiC and Al/Mo/SiC has been carried out on the deposition machine of CEMOX (Centrale d'élaboration et de métrologie des optiques X) implemented at the Institut d'Optique by PRaXO (Pôle d'optique des Rayons X d'Orsay).

References

[1] P. Jonnard, I. Jarrige, R. Benbalagh, H. Maury, J.-M. André, Z. Dankhazi, G. Rolland, *Surf. Sci.* **2005**, *589*, 164.
[2] H. Maury, P. Jonnard, J.-M. André, J. Gautier, M. Roulliay, F. Bridou, F. Delmotte, M.-F. Ravet, A. Jérome, P. Holliger, *Thin Solids Films* **2006**, *514*, 278.
[3] H. Maury, P. Jonnard, J.-M. André, J. Gautier, F. Bridou, F. Delmotte, M.-F. Ravet, *Surf. Sci.* **2007**, *601*, 2315.
[4] K. Le Guen, H. Maury, J.-M. André, H. Wang, J. Zhu, Z. Wang, P. Jonnard, *Appl. Surf. Sci.* **2007**, *253*, 8443.
[5] E. Meltchakov, C. Hecquet, M. Roulliay, S. De Rossi, Y. Menesguen, A. Jérôme, F. Bridou, F. Varnière, M.-F. Ravet-Krill, F. Delmotte, *Appl. Phys. A* **2010**, *98*, 111.
[6] S. Nannarone, F. Borgatti, A. DeLuisa, B. P. Doyle, G. C. Gazzadi, A. Giglia, P. Finetti, N. Mahne, L. Pasquali, M. Pedio, G. Selvaggi, G. Naletto, M. G. Pelizzo, G. Tondello, *AIP Conf. Proc.* **2004**, *708*, 450.
[7] C. Bonnelle, F. Vergand, P. Jonnard, J.-M. André, P. F. Staub, P. Avila, P. Chargelègue, M.-F. Fontaine, D. Laporte, P. Paquier, A. Ringuenet, B. Rodriguez, *Rev. Sci. Instrum.* **1994**, *65*, 3466.
[8] L. V. Azaroff, *X-ray Spectroscopy*, McGraw-Hill Inc.: New York, **1974**.
[9] C. Bonnelle, *Annu. Rep. Prog. Chem., Sect. C, Phys. Chem.* **1987**, *84*, 201.
[10] M. Iwami, M. Kusaka, M. Hirai, R. Tagami, H. Nakamura, H. Watabe, *Appl. Surf. Sci.* **1997**, *117*, 434.
[11] E. Z. Kurmaev, V. R. Galakhov, S. N. Shamin, *Crit. Rev. Solid State Mater. Sci.* **1998**, *23*, 65.
[12] N. Miyata, S. Ishikawa, M. Yanagihara, M. Watanabe, *Jpn. J. Appl. Phys. Part 1 – Regular Papers Short Notes Rev. Papers* **1999**, *38*, 6476.
[13] I. Jarrige, P. Jonnard, N. Frantz-Rodriguez, K. Danaie, A. Bosseboeuf, *Surf. Interf. Anal.* **2002**, *34*, 694.
[14] V. R. Galakhov, *X-Ray Spectrom.* **2002**, *31*, 203.
[15] M. Salou, S. Rioual, J. Ben Youssef, D. T. Dekadjevi, S. P. Pogossian, P. Jonnard, K. Le Guen, G. Gamblin, B. Rouvellou, *Surf. Interf. Anal.* **2008**, *40*, 1318.
[16] K. Le Guen, G. Gamblin, P. Jonnard, M. Salou, J. Ben Youssef, S. Rioual, B. Rouvellou, *Eur. Phys. J. Appl. Phys.* **2009**, *45*, 20502.
[17] H. Maury, J.-M. André, K. Le Guen, N. Mahne, A. Giglia, S. Nannarone, F. Bridou, F. Delmotte, P. Jonnard, *Surf. Sci.* **2009**, *603*, 407.
[18] C. Meny, P. Panissod, in *Modern Magnetic Resonance* (Ed.: G. Webb), Springer: Heidelberg, **2006**.
[19] P. Panissod, C. Meny, *Appl. Magn. Res.* **2000**, *19*, 447.
[20] D. L. Windt, *Comput. Phys.* **1998**, *12*, 360.
[21] K. Le Guen, M.-H. Hu, J.-M. André, P. Jonnard, S. K. Zhou, H. Ch. Li, J. T. Zhu, Z. S. Wang, C. Meny, *J. Phys. Chem. C* **2010**, *114*, 6484.
[22] P. Jonnard, K. Le Guen, M.-H. Hu, E. Meltchakov, C. Hecquet, F. Delmotte, A. Galtayries, *Proc. SPIE* **2009**, *7360*, O1.
[23] P. Jonnard, K. Le Guen, R. Gauvin, J.-F. Le Berre, *Microsci. Microanal.* **2009**, *15*, 36.
[24] H. Maury, P. Jonnard, K. Le Guen, J.-M. André, Z. Wang, J. Zhu, J. Dong, Z. Zhang, F. Bridou, F. Delmotte, C. Hecquet, N. Mahne, A. Giglia, S. Nannarone, *Eur. Phys. J. B* **2008**, *64*, 193.
[25] M.-H. Hu, K. Le Guen, J.-M. André, P. Jonnard, E. Meltchakov, F. Delmotte and A. Galtayries, *Opt. Express* **2010**, *18*, 20019.

Copyright © 2011 John Wiley & Sons, Ltd.

Caractérisation physico-chimique et optique de miroirs multicouches pour le domaine EUV

Le domaine du rayonnement extrême ultraviolet (EUV) offre de grandes possibilités scientifiques et technologiques en photolithographie, en astrophysique, en spectrométrie de photoélectron, etc. Ainsi, de nombreux miroirs multicouches sont développés pour fonctionner dans ce domaine spectral, qui joue un rôle important pour les applications optiques.

L'objectif de ce travail est de concevoir, réaliser, caractériser et proposer des multicouches (Mg/Co, Al/SiC, ...). Puis le but est d'appliquer une méthode capable de distinguer entre interdiffusion et rugosité géométrique afin de corréler les performances optiques de la multicouche à sa qualité structurale. Nous proposons de caractériser les miroirs multicouches en employant une méthodologie combinant plusieurs techniques (Spectroscopie d'émission X, Réflectométrie EUV, ...). La combinaison de ces méthodes permet d'obtenir une description chimique et structurale de l'empilement multicouche et de comprendre les phénomènes prenant place aux interfaces. Il est en effet important de connaître les phénomènes interfaciaux, comme la formation de composés ou le développement de la rugosité, car ils gouvernent les propriétés optiques des multicouches.

MOTS-CLES

Optique des rayons X et extrême ultraviolet, multicouches, interfaces, diffusion, rugosité, recuit, Spectroscopie d'Emission X (XES), Réflectométrie X durs (XRR), Réflectométrie EUV, Spectroscopie de Résonance Magnétique Nucléaire (RMN), Spectrrométrie de Masse d'Ions Secondaires par Temps de Vol (ToF-SIMS), Faisceau d'Ions Focalisés (FIB), Microscopie Electronique à Balayage en Transmission (STEM), Spectroscopie de Perte d'Energie des Electrons (EELS).

Physico-chemical and optical characterization of multilayer mirrors for the EUV domain

The radiation domain of extreme ultraviolet (EUV) has great potential in science and technology in photolithography, astrophysics, photoelectron spectroscopy, etc.. Indeed, many multilayer mirrors have been developed to operate in this spectral range, which is important for optical applications.

The objective of this work is to design, deposit, characterize and propose the multilayers (Mg/Co, Al/SiC, ...). Then the aim is to apply a method to distinguish between interdiffusion and geometric roughness in order to correlate the optical performance to the multilayer structural quality. We propose to characterize the multilayer mirrors using a methodology combining several techniques (X-ray emission spectroscopy, EUV reflectivity, ...). The combination of these methods provides a chemical and structural description of the multilayer and necessary to understand the phenomena taking place at the interfaces. It is important to know the interfacial phenomena, such as the formation of compounds or the development of roughness, as they govern the optical properties of multilayers.

KEYWORDS

EUV and X-ray Optics, multilayers, interfaces, diffusion, roughness, annealing, X-ray Emission Spectroscopy (XES), X-ray and EUV Reflectivity, Nuclear Magnetism Resonance Spectroscopy (NMR), Time-of-Flight Secondary Ion Mass Spectrometry (ToF-SIMS), Focused Ion Beam (FIB), Scanning Transmission Electron Microscopy (STEM), Electron Energy Loss Spectroscopy (EELS).

LABORATOIRE DE CHIMIE PHYSIQUE MATIERE ET RAYONNEMENT

Université Pierre et Marie Curie & Unité Mixte de Recherche du CNRS (UMR 7614)

11 Rue Pierre et Marie Curie,75231 Paris Cedex 05